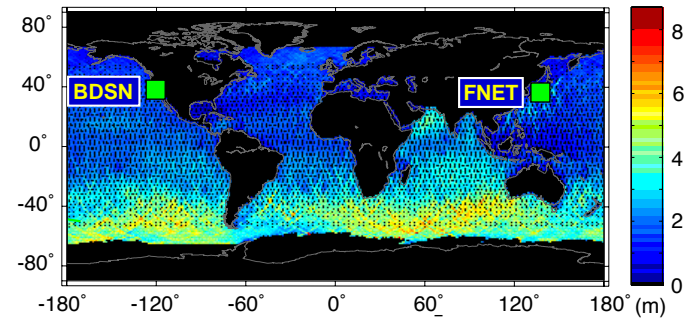
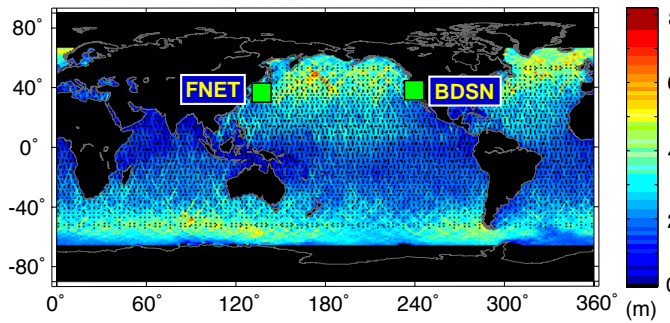
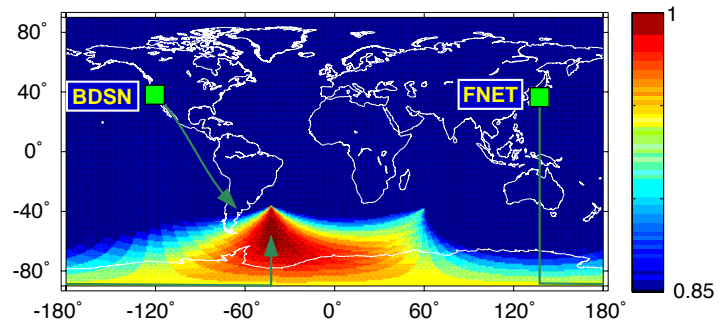
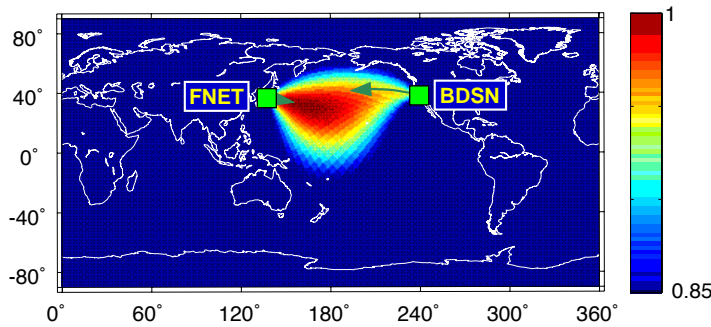


Berkeley Seismological Laboratory

WINTER

SUMMER



Annual Report
July 2003 - June 2004

Contents

- 1 Director’s Report 4**
 - 1. Background and Facilities 5
 - 2. Highlights of 2003-2004 6
 - 3. Acknowledgements 9
 - 4. Glossary of Common Acronyms 10

- 2 California Integrated Seismic Network 12**
 - 1. Introduction 12
 - 2. CISN Background 12
 - 3. 2003-2004 Activities 13
 - 4. Acknowledgements 21
 - 5. References 21

- 3 Berkeley Digital Seismic Network 22**
 - 1. Introduction 22
 - 2. BDSN Overview 22
 - 3. 2003-2004 Activities 25
 - 4. Acknowledgements 30
 - 5. References 30

- 4 Northern Hayward Fault Network 34**
 - 1. Introduction 34
 - 2. NHFN Overview 34
 - 3. 2003-2004 Activities 36
 - 4. Acknowledgements 41
 - 5. References 41

- 5 Parkfield Borehole Network 43**
 - 1. Introduction 43
 - 2. HRSN Overview 43
 - 3. 2003-2004 Activities 47
 - 4. Acknowledgements 52
 - 5. References 54

- 6 Bay Area Regional Deformation Network 55**
 - 1. Introduction 55
 - 2. 2003-2004 Activities 59
 - 3. Data Analysis and Results 60
 - 4. Real-Time Processing 62
 - 5. Acknowledgements 63
 - 6. References 63

7	Plate Boundary Deformation Project	64
1.	Introduction	64
2.	Mini-PBO Station Configuration	64
3.	Broadband Deformation Data	66
4.	Acknowledgements	68
8	Data Acquisition and Quality Control	70
1.	Introduction	70
2.	McCone Hall Facilities	70
3.	Data Acquisition	71
4.	Seismic Noise Analysis	72
5.	Sensor Testing Facility	73
6.	Acknowledgements	76
7.	References	76
9	Northern California Earthquake Monitoring	77
1.	Introduction	77
2.	Northern California Management Center	77
3.	2003-2004 Activities	78
4.	Routine Earthquake Analysis	83
5.	Acknowledgements	88
6.	References	88
10	Northern California Earthquake Data Center	90
1.	Introduction	90
2.	NCEDC Overview	90
3.	2003-2004 Activities	90
4.	Data Collections	91
5.	Data Quality Control	97
6.	User Interface Development	97
7.	Database Development	99
8.	Data Distribution	100
9.	Acknowledgements	100
11	Outreach and Educational Activities	101
1.	Introduction	101
2.	Outreach Overview	101
3.	2003-2004 Activities	102
4.	Acknowledgements	102
12	Research Studies	103
1.	Periodic Earthquake Rate Variations on the San Andreas Fault	105
2.	Finite-Source Modeling of the 22 December 2003 San Simeon Earthquake	108
3.	Coseismic Slip Distribution of the 22 December 2003 San Simeon Earthquake	111
4.	Measuring and Modeling Fluid Movements in Volcanoes: Insights from Continuous Broadband Seismic Monitoring at Galeras Volcano, Colombia	114
5.	The Orinda Earthquake Sequence	116
6.	Non-Double-Couple Earthquakes in the Long Valley Volcanic Region	118
7.	Observations of Infragravity Waves at the Monterey Ocean Bottom Broadband Station (MOBB)	120
8.	Slicing up the San Francisco Bay Area: Block Kinematics from GPS-derived Surface Velocities	122
9.	Active Tectonics of Northeast Asia: Using GPS Velocities and Block Modeling to Test Okhotsk Plate Motion Independent from North America	125
10.	The Spatial Pattern of Active Uplift in Eastern Taiwan	127

11.	Crustal Deformation Along the Northern San Andreas Fault System	129
12.	The Adriatic Region: An Independent Microplate within the Africa-Eurasia Collision Zone	131
13.	Bayesian Inference of Lower-Crustal Viscosity Near the Kunlun Fault Based on Geologic, Geomorphic, and Geodetic Data	133
14.	Observations and Modeling of Microseisms in the Santa Clara Valley, California	136
15.	Excitation of Earth's Incessant Free Oscillations by Atmosphere-Ocean-Seafloor Coupling	138
16.	Episodic Tremor and Slip in the Southern Cascadia Subduction Zone	140
17.	A Three Dimensional Radially Anisotropic Model of Shear Velocity in the Whole Mantle	141
18.	High Resolution Anisotropic Structure of the North American Upper Mantle from Inversion of Body and Surface Waveform Data	143
19.	Tests of Normal Mode Asymptotic Approximations against Computation Using the Spectral Element Method	145
20.	Finite Boundary Perturbation Theory for the Elastic Equation of Motion	147
21.	Sharp lateral Boundaries in the D'' Region	149
22.	Hemispherical Transition of Seismic Attenuation at the Top of the Earth's Inner Core	152

13 Appendices

154

Chapter 1

Director's Report

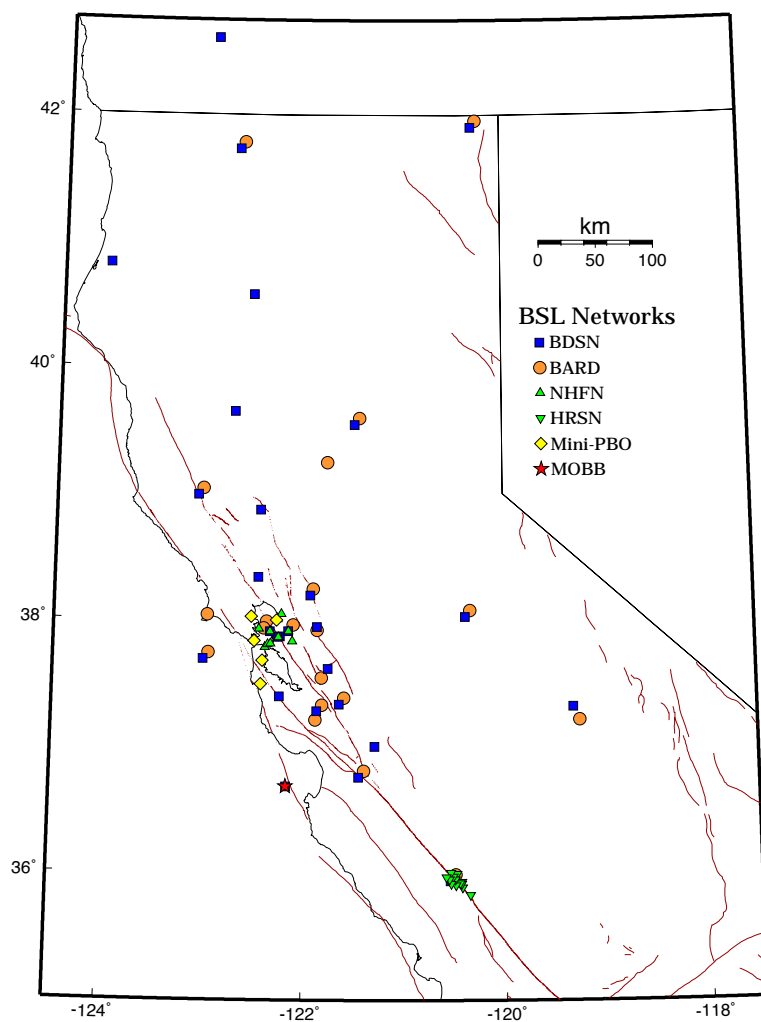


Figure 1.1: Map illustrating the distribution of stations in the BDSN, NHFN, HRSN, BARD, and Mini-PBO networks in northern and central California. A star indicates the location of the MOBB deployment.

1. Background and Facilities

The Berkeley Seismological Laboratory (BSL), formerly the Berkeley Seismographic Station (BSS), is the oldest Organized Research Unit (ORU) on the U. C. Berkeley campus. Its mission is unique in that, in addition to research and education in seismology and earthquake-related science, it is responsible for providing timely information on earthquakes (particularly those that occur in northern and central California) to the UC Berkeley constituency, the general public, and various local and state government and private organizations. The BSL is therefore both a research center and a facility/data resource, which sets it apart from most other ORUs. A major component of our activities is focused on developing and maintaining several regional observational networks, and participating, along with other agencies, in various aspects of the collection, analysis, archival and distribution of data pertaining to earthquakes, while maintaining a vigorous research program on earthquake processes and Earth structure. In addition, the BSL staff spends considerable time with public relations activities, including tours, talks to public groups, responding to public enquiries about earthquakes and, more recently, World-Wide-Web presence (<http://www.seismo.berkeley.edu/seismo/>).

U.C. Berkeley installed the first seismograph in the Western Hemisphere at Mount Hamilton (MHC) in 1887. Since then, it has played a leading role in the operation of state-of-the-art seismic instruments and in the development of advanced methods for seismic data analysis and interpretation. Notably, the installation, starting in 1927, of Wood-Anderson seismographs at 4 locations in northern California (BKS, ARC, MIN and MHC) allowed the accurate determination of local earthquake magnitude (M_L) from which a unique historical catalog of regional earthquakes has been maintained to this day, providing crucial input to earthquake probabilities studies.

Over the years, the BSS continued to keep apace of technological improvements. The first centrally telemetered network using phone lines in an active seismic region was installed by BSS in 1960. The BSS was the first institution in California to operate a 3-component "broadband" system (1963). Notably, the BSS played a major role in the early characterization of earthquake sources using "moment tensors" and source-time functions, and made important contributions to the early definitions of detection/discrimination of underground nuclear tests and to earthquake hazards work, jointly with UCB Engineering. Starting in 1986, the BSS acquired 4 state-of-the-art broadband instruments (STS-1), while simultaneously developing PC-based digital telemetry, albeit with limited resources. As the telecommunication and computer technology made rapid progress, in parallel with broadband instrument development, paper record reading could be completely abandoned in favor of largely

automated digital data analysis.

The current modern facilities of BSL have been progressively built over the last 13 years, initiated by significant "upgrade" funding from U.C. Berkeley in 1991-1995. The BSL currently operates and acquires data, continuously and in real-time, from over 60 regional observatories, housing a combination of broadband and strong motion seismic instrumentation installed in vaults, borehole seismic instrumentation, permanent GPS stations of the BARD network, and electromagnetic instrumentation. The seismic data are fed into the BSL real-time processing and analysis system and are used in conjunction with data from the USGS NCSN network in the joint earthquake notification program for northern California, started in 1996. This program capitalizes on the complementary capabilities of the networks operated by each institution to provide rapid and reliable information on the location, size and other relevant source parameters of regional earthquakes. In recent years, a major emphasis in BSL instrumentation has been in densifying the state-of-the-art seismic and geodetic networks, while a major on-going emphasis in research has been the development of robust methods for quasi-real time automatic determination of earthquake source parameters and predicted strong ground motion, using a sparse network combining broadband and strong motion seismic sensors, as well as permanent geodetic GPS receivers.

The backbone of the BSL operations is a regional network of 25+ digital broadband and strong motion seismic stations, the Berkeley Digital Seismic Network (BDSN), with continuous telemetry to UC Berkeley. This network provides the basic regional data for the real-time estimation of location, size and rupture parameters for earthquakes of M 3 and larger in central and northern California, within our Rapid Earthquake Data Integration (REDI) program and is the Berkeley contribution to the California Integrated Seismic Network (CISN). It also provides a fundamental database for the investigation of three-dimensional crustal structure and its effects on regional seismic wave propagation, ultimately crucial for estimating ground shaking for future earthquakes. Most stations also record auxiliary temperature/pressure channels, valuable in particular for background noise quality control. Complementing this network is a 25 station "high-resolution" network of borehole seismic sensors located along the Hayward Fault (HFN) and under the Bay Area bridges, operated jointly with the USGS/Menlo Park and linked to the Bridge Safety Project of the California Department of Transportation (Caltrans). The latter has facilitated the installation of sensor packages at 15 bedrock boreholes along 5 east-bay bridges in collaboration with LLNL. A major science goal of this network is to collect high signal-to-noise data for micro-earthquakes along the Hayward Fault to gain insight into the physics that govern fault rupture and its nucleation. The BSL is

also involved in the operation and maintenance of the 13 element Parkfield borehole seismic array (HRSN), which is yielding enlightening results on quasi-periodic behavior of micro-earthquake clusters and important new constraints on earthquake scaling laws and is currently playing an important role in the characterization of the site for the future San Andreas Fault Observatory at Depth (SAFOD). Since April 2002, the BSL is also involved in the operation of a permanent broadband ocean bottom station, MOBB, in collaboration with MBARI (Monterey Bay Aquarium Research Institute).

In addition to the seismic networks, the BSL is involved in data archival and distribution for the permanent geodetic BARD (Bay Area Regional Deformation) Network as well as the operation and maintenance, and data processing of 22 out of its 70+ sites. Whenever possible, BARD sites are collocated with BDSN sites in order to minimize telemetry costs. In particular, the development of analysis methods combining the seismic and geodetic data for the rapid estimation of source parameters of significant earthquakes has been one focus of BSL research.

Finally, two of the BDSN stations (PKD, SAO) also share data acquisition and telemetry with 5-component electromagnetic sensors installed with the goal of investigating the possibility of detection of tectonic signals. In 2002-2003, an automated quality control software was implemented to monitor the electromagnetic data.

Archival and distribution of data from these and other regional networks is performed at the Northern California Earthquake Data Center (NCEDC), operated at the BSL in collaboration with USGS/Menlo Park. The data reside on a mass-storage device (4.5+ Terabyte capacity), and are accessible "on-line" over the Internet (<http://www.quake.geo.berkeley.edu>). Among others, data from the USGS Northern California Seismic Network (NCSN), are archived and distributed through the NCEDC. The NCEDC also maintains, archives and distributes the ANSS/CNSS earthquake catalog.

Core University funding to our ORU has suffered from permanent budget cuts to research programs from the State of California, and currently provides salary support for 2 field engineers, one computer expert, 2 data analysts, 1 staff scientist and 2 administrative staff. This supports a diminishing portion of the operations of the BDSN and provides seed funding for our other activities. All other programs are supported through extramural grants primarily from the USGS and NSF, and in the past three years, the Governor's Office of Emergency Services (OES). We acknowledge valuable recent contributions from other sources such as Caltrans, the CLC program, PEER, as well as our Earthquake Research Affiliates.

2. Highlights of 2003-2004

2.1 Infrastructure and Earthquake Notification

In 2003-2004, BSL's activities have centered around two major projects: the continuation of CISN and the deployment in California of the *BigFoot* component of USArray/Earthscope. In this context, we have continued our efforts to expand the northern California broadband network while trying to reduce the costs of operation, in the wake of significant cuts to our University funding. In addition, we have continued the installation of the remaining "mini-PBO" sites and the expansion of the NCEDC database, and have taken the first steps towards designing an integrated telemetry link from Parkfield, CA, in particular in anticipation of our collecting and archiving data from the San Andreas Fault Observatory at Depth (SAFOD) program of Earthscope. The M 6.5 San Simeon earthquake of 12/22/03 was an opportunity to test the capabilities of CISN as well as those of the HRSN, and those of recently developed research tools, as will be described in the Research Section.

The main goal of the CISN (Chapter 2) is to ensure a more uniform system for earthquake monitoring and reporting in California. The highest priority, from the point of view of emergency responders in California, is to improve the robustness of statewide real-time notification and to achieve a uniform interface across the State to the California OES and other emergency responders. This represents a major challenge, as the CISN started as a heterogeneous collection of networks with disparate instrumentation, software systems and culture. Therefore, in the past year, as previously, the emphasis has been on software development. Notably, we have made significant progress on merging the USGS/Menlo Park and BDSN networks in northern California. We note also, that the coordinated software development across CISN partners over the last 3 years is bearing its fruits: for example, we now have a pool of staff members in the northern and southern processing centers that have a sufficient knowledge of each other's software to be in a position to help each other or serve as back-up in the case of a failure. This contributes to the improvement in the robustness of the statewide system.

Another goal of the CISN program is to improve the seismic infrastructure in northern California. Because funding is limited, this goal is continued at a slower pace. Nevertheless, we have started the construction of two new broadband/strong motion stations in 2003-2004 (Alder Springs and Marconi). These sites should be completed by the end of 2004, in spite of considerable delays due to the shortage of personnel.

BSL staff continue to spend considerable efforts in organizational activities for CISN, notably by participating in the CISN Project Management Group (Gee),

which includes weekly 2 hour phone conferences, and the Standards Committee (Neuhauser-chair, Gee, Lombard), which strives to define and coordinate software development tasks. Romanowicz and Gee continue to serve on the CISN Steering Committee. The CISN also represents California as a designated region of ANSS (Advanced National Seismic System) and the BSL is actively involved in planning activities for the ANSS.

In the last two years, a major component of our activities has been coordinating with IRIS on the deployment in northern California of 50 temporary broadband stations of the BigFoot array of Earthscope. The BSL will contribute many (15+) of its existing sites to this effort and is involved in the joint siting of 10 new sites. These sites will be permitted by BSL and constructed by US-Array. When BigFoot leaves California in 2007, these sites will be available for permanent BSL installation, provided funding is found for the seismic instrumentation. In 2003-04, we have helped permit one station in the vicinity of the epicenter of the San Simeon earthquake. This station (located at the Hastings Reserve) is now operational. We are currently pursuing the permitting of other sites.

This past year has seen progress towards the completion of the *Mini-PBO* project (Chapter 7), a project supported partly by a grant from the NSF/MRI program, in collaboration with CIW, UCSD and USGS/Menlo Park, with matching from participating institutions (including UCB) as well as Caltrans (http://www.seismo.berkeley.edu/seismo/bdsn/mpbo_overview.html). This project's focus is the installation of a network of multi-parameter stations in the San Francisco Bay Area to monitor the evolution of tectonic strain in time and space - a pilot project for the Plate Boundary Observatory (PBO) component of Earthscope (a national infrastructure program funded by NSF within its Major Research Equipment program). The installation of the 5 borehole strainmeters and seismometers, as well as auxiliary sensors (pore pressure, temperature and tilt) was completed in 2002-03, but 3 of the sites lacked GPS receivers as well as continuous telemetry to UC Berkeley for distribution through the NCEDC. Four sites are completed, while the remaining one is in the final stages of the installation of power and communications systems.

The *MOBB* (Monterey Ocean bottom Broad Band observatory) is a collaborative project between the BSL and MBARI and builds upon the experience gained in 1997 through the MOISE project, which involved the temporary deployment of a broadband ocean bottom system in Monterey Bay. *MOBB* is now a permanent installation and comprises a broadband seismic package (Guralp CMG-1), a battery and recording package, as well as auxiliary sensors: a current-meter and a DPG (differential Pressure Gauge). The system was assembled and tested

at BSL in early 2002, and successfully deployed in April 2002 (Chapter 3). Extensive testing of seismometer insulation procedures, which were developed at Byerly Vault on the UCB campus prior to *MOBB* deployment (Chapter 8) have now been applied to three similar systems destined for the KECK project (Juan de Fuca plate), in collaboration with University of Washington at Seattle. In February 2004, we experienced the failure of one of our horizontal components. Thanks to the availability of one of the Keck instruments and the willingness of the MBARI crew, we were able to swap the seismic package in May 2004 and send it for repair. It has now been successfully reinstalled. The *MOBB* is scheduled to be hooked up to the MARS cable which will be installed in Monterey Bay in the Fall of 2005.

The BSL has continued to be involved in the coordination of site characterization for the SAFOD drilling project in the Parkfield area (Chapter 5). In particular, the HRSN has played a key role in providing seismic waveform data for a series of active source experiments conducted to characterize the SAFOD drilling site. These high quality waveform data are complementary to those, by nature more noisy, recorded by temporary deployments at the surface. Efforts have continued to reduce noise levels at the borehole sites to increase the detection level of magnitude -1.0 and lower earthquakes. The occurrence of the M6.5 San Simeon earthquake on 12/22/03, with its numerous aftershocks, has both significantly complicated the routine data processing task for HRSN and provided an opportunity to rethink the traditional processing schemes implemented more than 15 years ago.

The NHFN network project has focused on the development of new algorithms to lower the detection threshold of microseisms along the Hayward Fault (Chapter 4). This includes a pattern recognition approach, a phase coherence method and a phase onset time detector. Completion of the Bay Bridge sites has been hampered by the shortage of personnel, concurrent with the necessity to concentrate our efforts on the highly visible HRSN network and the intensive efforts in preparation for the SAFOD drilling.

The NCEDC (Chapter 10), continues archiving and distribution of on-line of data from expanding BDSN, NHFN, HRSN, BARD, Mini-PBO, and other networks and data collections in northern California and Nevada. A major accomplishment in the last year is making the entire collection of NCSN waveform data available (1984-2003) through the NCEDC archive (including instrument responses for all NSCN stations). These waveform data can now also be retrieved by a query based on event-id. There have also been notable enhancements in the *BREQ_FAST* and *NetDC* data retrieval interfaces, that now provide access to NCSN waveform data in SEED format.

The BSL continues to collaborate with the USGS/Menlo Park in the generation of ShakeMap for northern California and to develop and implement successive upgrades to this system, integrated within the REDI environment (Chapter 9). ShakeMap is calculated routinely for magnitude 3.5 and larger events in northern California. Any magnitude 5.0 or larger will now also trigger the finite-fault processing. The 12/22/03 M6.5 San Simeon earthquake provided an opportunity to demonstrate the capabilities of the automatic finite fault processing system, which is triggered for M 5.0 and larger earthquakes.

Finally, through Dr Lind Gee's efforts, BSL has been actively involved in the preparation of UC Berkeley's participation in the commemoration activities of the centennial anniversary of the 1906 earthquake (Chapter 11). These activities include a joint SSA/EERI/DRC conference to be held in San Francisco in April 2006 as well as many exhibits, classes, and public lectures on the UC Berkeley Campus.

2.2 Research Accomplishments

Chapter 12 documents the main research contributions of the past year. Research at the BSL spans a broad range of topics, from the study of microseismicity at the local scale to global deep earth structure, and includes the use of seismological, geodetic and remote sensing (InSAR) techniques.

The M6.5 San Simeon earthquake of 12/22/03 was an ideal opportunity to demonstrate the power of several approaches that have been pioneered at BSL over the last few years. The finite source modeling technique, developed by Dreger and his students to obtain directivity information for large regional earthquakes using a sparse set of regional distance broadband stations, provides information on the regional distribution of shaking, as well as on the the source process. The corresponding algorithm was implemented into the BSL real time analysis system two years ago, just in time to capture the San Simeon earthquake (12.2.) for which it provided significant information, since this event occurred in an area poorly covered by seismic, and particularly strong motion, stations. The combination of seismic and geodetic constraints, another approach in which BSL is a leader, provided a robust model for the corresponding slip distribution on the causative fault, confirming the marked south east progression of the rupture (12.3.). BSL researchers continue to study regional earthquakes and volcanic processes using broadband seismic data (12.4., 12.6.), microseismicity using data from our borehole networks (12.1., 12.5.), as well as regional deformation in California (12.8., 12.11.) and elsewhere in the world (12.9., 12.10., 12.12., 12.13.) using GPS and InSAR data.

We note an increasing interest in the study of seismic

background noise, which, it turns out, contains valuable information on 3D shallow structure, such as that of sedimentary basins (12.14.). At low frequencies, a fascinating component of the background noise is the Earth's "hum", discovered 6 years ago by Japanese scientists. A highlight of this past year's work at BSL is the development of an array-based method that has allowed us to locate the primary source of the "hum" in the oceans. This main source moves from the northern oceans in the northern hemisphere winter to the southern oceans in the summer, as wind-generated waves grow stronger in the winter in the respective hemispheres. This study has been published in Nature and received considerable media attention (12.15.). The existence of the BDSN which its regional distribution of very broadband STS-1 seismometers in high quality installations has been instrumental in this study. Indeed, BDSN is one of only two such suitable regional arrays in the world for which data have been continuously available for several years (the other one is in Japan). Data from our ocean floor MOBB station in Monterey Bay are also proving valuable, in conjunction with ocean buoy data, to investigate how short period ocean wave energy is converted into long period elastic waves (12.7.). Another area where "digging into the noise" has proven useful, is the discovery by Japanese and Canadian scientists of deep strain events along subduction zones manifested by signals in GPS associated with seismic tremors. Such signals appear to be present also in California, at the southern end of the northwest Pacific subduction zone (12.16.).

In the last year, we have sustained our investigations of global earth structure. Notably, we developed the first whole mantle radially anisotropic model, showing, in particular, the predominance of horizontal shear in the D'' region near the core-mantle boundary, a study published in Science (12.17.). The anisotropic formalism developed over the last few years is being extended to more detailed studies at the continental scale, with the inclusion of azimuthal anisotropy (12.18.). Concurrently, we continue our efforts in the modeling of wave propagation in 3D structure at the global scale, using numerical and analytical approaches (12.21., 12.20., 12.19.). We also maintain an active program in the study of inner core structure, this year documenting the presence of large scale lateral variations in temperature at the top of the inner core (12.22.).

I am happy to announce the completion of two Ph.D theses in this past year: Matt d'Alessio has started a Mendenthal Postdoctoral fellowship at the USGS in Menlo Park, CA, while Mark Panning will stay as a post-doc at BSL for the next year. In the summer of 2003, post-doc and former student Yuancheng Gung returned to Taiwan where he joined the faculty at the National University of Taiwan, while visiting scientist Nozomu Takeuchi has returned to his post at the Earthquake Re-

search Institute in Tokyo. Post-doc George Hilley will join the faculty at Stanford University in January 2005.

3. Acknowledgements

I wish to thank our technical and administrative staff, scientists and students for their efforts throughout the year and their contributions to this annual report. Individual contributions to activities and report preparation are mentioned in the corresponding sections, except for the Appendix section, prepared by Christina Jordan and Eleanor Blair.

I also wish to specially thank the individuals who have regularly contributed to the smooth operation of the BSL facilities: André Basset, Sierra Boyd, Rich Clymer, Doug Dreger, John Friday, Lind Gee, Wade Johnson, Bill Karavas, Pete Lombard, Rick McKenzie, Mark Murray, Bob Nadeau, Doug Neuhauser, Charley Paffenbarger, David Rapkin, Bob Uhrhammer, and Stephane Zuzlewski. I particularly want to thank Doug Dreger for serving as Associate Director of the BSL.

To our regret, David Rapkin had to leave BSL in Fall of 2003. He now works for the Institute of Transportation Studies. André Basset and Wade Johnson left in the Spring of 2004 and, as employees of UNAVCO, they have joined the technical crews responsible for the deployment of PBO. We welcome the addition of Cédric de la Beaujardière, who joined the BSL staff in June 2004, assisting Mark Murray and Lind Gee in the data management and processing of BARD and BDSN data.

In 2003-2004, there have been some changes in the BSL administrative office. Eleanor Blair, Myriam Cotton and Christina Jordan continue to provide critical support to the administration of our lab. They have been assisted by part-time student employees Patty Villa and Loan Pham. In May 2004, Yolanda Andrade joined our staff as administrative assistant for the BSL.

I also wish to thank our undergraduate assistants Charles Chiau, Alex Goines, Edwin Kwan, and Gabe Treves for their contributions to our research and operational activities.

As every year, I am particularly thankful to Lind Gee and Christina Jordan for their help in putting together this Annual Report.

The Annual Report of the Berkeley Seismological Laboratory is available on the WWW at http://www.seismo.berkeley.edu/seismo/annual_report/.

Barbara Romanowicz
October 15, 2004

4. Glossary of Common Acronyms

Table 1.1: Standard abbreviations used in this report.

Acronym	Definition
AGU	American Geophysical Union
ANSS	Advanced National Seismic System
BARD	Bay Area Regional Deformation
BDSN	Berkeley Digital Seismic Network
BSL	Berkeley Seismological Laboratory
BSS	Berkeley Seismographic Station
CISN	California Integrated Seismic Network
CGS	California Geological Survey
CLC	Campus Laboratory Collaboration
CNSS	Council of the National Seismic System
CSRC	California Spatial Reference Center
DRC	Disaster Resistent California
EM	Electromagnetic
EPRI	Electric Power Research Institute
EERI	Earthquake Engineering Research Institute
FBA	Force Balance Accelerometer
FIR	Finite Impulse Response
FRAD	Frame Relay Access Device
GPS	Global Positioning System
HFN	Hayward Fault Network
HRSN	High Resolution Seismic Network
IGS	International Geodetic Service
IMS	International Monitoring System
InSAR	Interferometric Synthetic Aperture Radar
IRIS	Incorporated Research Institutions for Seismology
ISC	International Seismological Center
ISTAT	Integrating Science, Teaching, and Technology
JPL	Jet Propulsion Laboratory
LBNL	Lawrence Berkeley National Laboratory
LLNL	Lawrence Livermore National Laboratory
MBARI	Monterey Bay Aquarium Research Institute
MHH	Murdoch, Hutt, and Halbert
MOBB	Monterey Ocean Bottom Broadband observatory
MOISE	Monterey Bay Ocean Bottom International Seismic Experiment
MPBO	Mini-Plate Boundary Observatory
MRI	Major Research Initiative
MRE	Major Research Equipment
MT	Magnetotelluric
NCEDC	Northern California Earthquake Data Center
NCSN	Northern California Seismic Network
NEHRP	National Earthquake Hazards Reduction Program
NEIC	National Earthquake Information Center
NHFN	Northern Hayward Fault Network
NGS	National Geodetic Survey
NSF	National Science Foundation
NSN	National Seismic Network
OES	Office of Emergency Services
ORU	Organized Research Unit
PBO	Plate Boundary Observatory

continued on next page

Table 1.1: *continued*

Acronym	Definition
PEER	Pacific Earthquake Engineering Center
PH	Pilot Hole
PPE	Parkfield Prediction Experiment
PREM	Preliminary Reference Earth Model
PSD	Power Spectral Density
REDI	Rapid Earthquake Data Integration
SAF	San Andreas Fault
SAFOD	San Andreas Fault Observatory at Depth
SAR	Synthetic Aperture Radar
SCEC	Southern California Earthquake Center
SCEDC	Southern California Earthquake Data Center
SCIGN	Southern California Integrated GPS Network
SEED	Standard for the Exchange of Earthquake Data
SEM	Spectral Element Method
SHFN	Southern Hayward Fault Network
SIO	Scripps Institutions of Oceanography
SNCL	Station Network Channel Location
SSA	Seismological Society of America
STP	Seismogram Transfer Program
UCB	University of California at Berkeley
UNAVCO	University NAVSTAR Consortium
UrEDAS	Urgent Earthquake Detection and Alarm System
USGS	United States Geological Survey

Chapter 2

California Integrated Seismic Network

1. Introduction

Advances in technology have made it possible to integrate separate earthquake monitoring networks into a single seismic system as well as to unify earthquake monitoring instrumentation. In California, this effort was initiated under the TriNet Project in southern California, where Caltech, the then California Division of Mines and Geology, and the USGS combined their efforts to create a unified seismic system for southern California. With major funding provided by FEMA, OES, and the USGS, the TriNet project provided the opportunity to upgrade and expand the monitoring infrastructure, combining resources in federal, state, university partnership. More recently, the California Geological Survey, Caltech, UC Berkeley, USGS Menlo Park, and the USGS Pasadena have agreed to cooperate on a statewide basis because of the obvious benefit to the state.

In the 2000-2001 Annual Report, we described the initial efforts to create this collaboration through the establishment of a memorandum of agreement and the development of the CISN strategic and implementation plans. The CISN is now in its fourth year of collaboration and its third year of funding from the California Governor's Office of Emergency Services.

2. CISN Background

2.1 Organization

The core CISN institutions (California Geological Survey, Caltech, UC Berkeley, USGS Menlo Park, and USGS Pasadena) and OES have signed a MOA (included in the 2000-2001 Annual Report) that describes the CISN organizational goals, products, management, and responsibilities of member organizations. To facilitate coordination of activities among institutions, the CISN has formed three management centers:

- Southern California Management Center: Caltech/USGS Pasadena
- Northern California Management Center: UC Berkeley/USGS Menlo Park

- Engineering Strong Motion Data Center: California Geological Survey/USGS National Strong Motion Program

A goal of the CISN is for the Northern and Southern California Management Centers to operate as twin statewide earthquake processing centers while the Engineering Strong Motion Data Center has the responsibility for producing engineering data products and distributing them to the engineering community.

The Steering Committee oversees CISN projects and is comprised of two representatives from each core institution and a representative from OES. The position of chair rotates among the institutions; Mike Riechle is the current chair of the Steering Committee.

An external Advisory Committee, representing the interests of structural engineers, seismologists, emergency managers, industry, government, and utilities, has been formed for review and oversight. The Advisory Committee is chaired by Bruce Clark of the California Seismic Safety Commission, although in the past year, Ron Tognazinni of LA Department of Water and Power has served as acting chair. The Advisory committee last met in September 2003 and the next meeting is planned for October 2004.

The Steering Committee has formed other committees, including a Program Management Group to address planning and coordination, a Strong Motion Working Group to focus on issues related to strong-motion data, and a Standards Committee to resolve technical design and implementation issues.

In addition to the core members, several organizations contribute data that enhances the capabilities of the CISN. Contributing members of the CISN include: University of California, Santa Barbara; University of California, San Diego; University of Nevada, Reno; University of Washington; California Department of Water Resources; Lawrence Livermore National Lab; and Pacific Gas and Electric.

2.2 CISN and ANSS

The USGS Advanced National Seismic System (ANSS) is being developed along a regionalized model. 8 regions have been organized, with the CISN representing California. David Oppenheimer of the USGS serves as the CISN representative to the ANSS National Implementation Committee.

Over the last 5 years, ANSS funding in California has been directed primarily to the USGS Menlo Park to expand the strong-motion instrumentation in the San Francisco Bay Area. As a result, instruments at over 100 sites have been installed or upgraded, significantly improving the data available for ShakeMaps.

As the ANSS moves forward, committees and working groups are being established to address issues of interest. In the last year, Lind Gee joined the Technical Integration Committee (TIC), which oversees technical issues for the ANSS. Other BSL faculty and staff have been involved in several TIC working groups, including Doug Dreger, Pete Lombard, Doug Neuhauser, Bob Uhrhammer, and Stephane Zuzlewski.

2.3 CISN and OES

The California Governor's Office of Emergency Services has had a long-term interest in coordinated earthquake monitoring. The historical separation between northern and southern California and between strong-motion and weak-motion networks resulted in a complicated situation for earthquake response.

OES has been an advocate of increased coordination and collaboration in California earthquake monitoring and encouraged the development of the CISN Strategic and Implementation Plans. In FY01/02, Governor Gray Davis requested support for the CISN, to be administered through OES. Funding for the California Geological Survey, Caltech and UC Berkeley was made available in spring 2002, officially launching the statewide coordination efforts.

Following the first year of funding, OES support led to the establishment of 3-year contracts to the UC Berkeley, Caltech, and the California Geological Survey for CISN activities. Although at a reduced level of support from the previous year, these funds are critical to continued efforts in statewide integration.

3. 2003-2004 Activities

The CISN funding from OES facilitated a number of activities at the BSL during the past year. However, the late award of the funding (the amended contract was received by UC Berkeley on May 13, 2004) complicated some aspects of the BSL activities, particularly those related to station installations and the development of the earthquake information distribution system.

3.1 San Simeon Earthquake

The December 22, 2003, San Simeon earthquake provided the first significant test of CISN capabilities since the initiation of the statewide collaboration. The event highlighted some known issues and illuminated some areas where additional effort is required, particularly with respect to ShakeMaps. The PMG report (*Gee et al.*, 2004a) documents the CISN response in detail.

Overall, the CISN performance for the distribution of information following the San Simeon earthquake was good. Automatic information about the location was available within 30 seconds and a final location with a reliable magnitude was released about 4.5 minutes after the event. The first ShakeMap was issued 8 minutes after origin time and distributed to OES and multiple Web servers. During the next 24 hours, additional information about aftershock probabilities, the fault rupture, and seismological/engineering aspects of interest were made available by the CISN.

However, one of the most challenging aspects of this event was the lack of modern stations with communication capabilities in the vicinity of the earthquake. This compromised the quality of the ShakeMaps for the mainshock and aftershocks and posed limitations in our ability to obtain reliable locations and magnitudes for the smaller events. Although the greater Los Angeles area and the San Francisco Bay region are approaching sufficient station density to provide data-driven ShakeMaps, significant portions of California lack the necessary coverage.

More information about the San Simeon earthquake is available in Chapter 9 on Northern California earthquake monitoring and in Chapter 12 in research contributions 12.2. and 12.3.

3.2 Expanded Instrumentation

In 2001-2002, the BSL purchased equipment for 5 BDSN stations, including STS-2 seismometers, Episenors, and Q4120 data loggers, and initiated efforts to identify potential sites, considering such factors as the current distribution of stations, private versus public property, location of power and telecommunications, and geologic materials. This equipment allowed the BSL to add two broadband stations in 2002-2003 (PACP and MNRC, Figure 3.1).

In the past year, the BSL initiated the installation of a site at Alder Springs (GASB), California. This site has been under discussion for a number of years, initially as part of the National Tsunami Hazards Program. The efforts for site preparation and installation are more fully described in Chapter 3.

In the fall of 2004, the BSL will install a site near Pt. Reyes, at the Marconi Conference Center. This site will be partially funded by IRIS (part of the permanent component of USArray) and OES.

3.3 Network Operations

As part of the CISN project, the BSL purchased 23 upgrade kits for their Q4120 data loggers with the goal of improving remote diagnostic capabilities last year. Three different kits were purchased – power board only, calibration board only, and combined power and calibration boards – in order to ensure that every Q4120 has a power board and that every 8-channel Q4120 also has a calibration board. The power boards provide the capability to monitor battery voltage, allowing staff to discriminate between power and telemetry problems remotely. The calibration boards provide the capability to monitor mass position as well as allow remote calibration of the seismic sensors. Both boards also record data logger temperature.

Successful upgrade of the dataloggers requires a site visit to remove the datalogger and bring it back to the lab, installation of the boards, replacement of lattices on the CPU board, construction of new cables to transmit the mass position signals, and redeployment of the datalogger in the field. Of the 23 kits purchased, all but three have been installed as of June 30th, although a few sites still require new cables or replacement of the lattices.

3.4 Collaboration with USArray

In late 2003, the CISN concluded a memorandum of agreement with the Incorporated Research Institutions in Seismology (IRIS) covering the duration of the USArray project in California. In early 2004, Caltech and the BSL completed agreements with IRIS for the contribution of their stations to USArray. As a result 19 stations operated by the BSL and 41 stations operated by Caltech are part of USArray during its California deployment.

Both Caltech and the BSL needed to modify some aspects of their station operation in order to meet the USArray specifications. In particular, USArray calls for BH data sampling at 40 Hz, rather than the 20 Hz rate that has been standard in California. In the case of the BSL, all surface broadband stations were converted to 40 Hz over June 15-16th. The collaboration between the BSL and USArray is discussed more fully in Chapters 3 and 8.

3.5 Statewide Communications

One of the major accomplishments in FY01/02 was the design and initial implementation of a CISN communications infrastructure. Doug Neuhauser of the BSL took the lead in investigating options and the CISN partners decided to establish a "ring" of T1 communication links (Figure 2.1) with dual routers at each node.

As described last year, the CISN ring is up and operational. It is being used to transmit seismic waveform data and parametric data, including strong motion parameters, between the management centers and to distribute

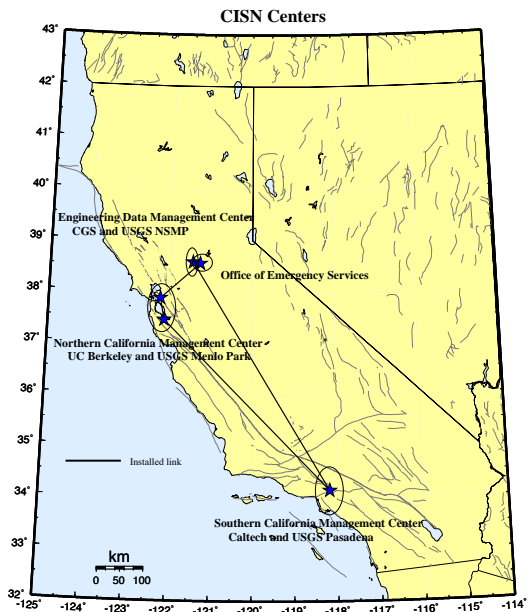


Figure 2.1: Map showing the geographical distribution of the CISN partners and centers. The communications "ring" is shown schematically with installed links (solid lines).

ShakeMaps to OES. It is also used to support mirroring of the CISN Web server.

During the last year, the CISN performed a test to verify the failover and redundancy capabilities of the CISN ring. The goals of the test were to 1) verify that if a single segment of the CISN ring fails, the backbone routers will detect the outage in a timely fashion and will reroute traffic to all CISN sites around the remaining CISN ring segments, and 2) verify that if a site is completely disconnected from the CISN ring, the backbone routers will detect the outage in a timely fashion and will reroute traffic to/from that site over the backup Internet tunnels between the disconnected site and all other CISN sites.

The test conducted demonstrated that the CISN routers and ring are performing according to design. However, the CISN OES routers do NOT have public Internet connections yet, so they have no Internet tunnel connections. If the CISN T1 circuits were to go down at OES, OES would be completely isolated from the CISN network and all CISN partners. This continues to be an issue of major concern.

The CISN intends to test the failover capabilities of the ring regularly. The full report of the May 21 test is available at the CISN Web site, under the reports of the Standards Committee.

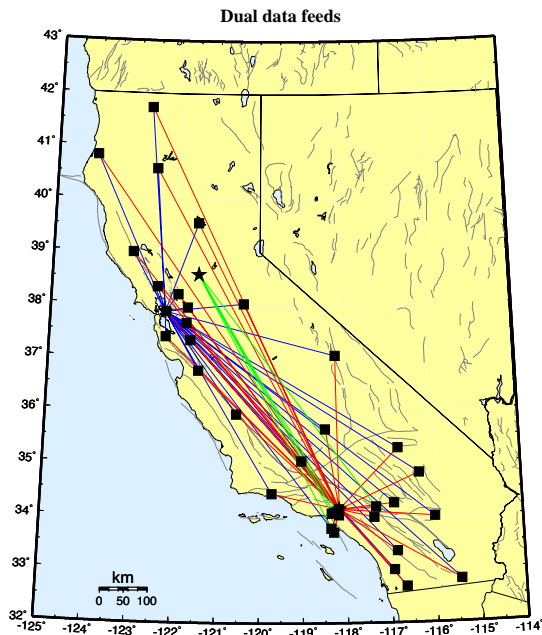


Figure 2.2: Map showing the 30 stations selected to send data directly to the Northern and Southern California processing centers, and the 5 stations that send data directly to the Engineering Data Center and the Southern California processing center.

3.6 Northern California Management Center

As part of their effort within the CISON, the BSL and the USGS Menlo Park have begun to plan for the next generation of the northern California joint notification system. Chapter 9 describes the operations of the existing Management Center and reports on design discussions.

Communications Infrastructure

In order to move ahead with plans for restructuring the northern California earthquake monitoring system, the USGS Menlo Park and BSL have been working to improve their communications infrastructure.

At present, the BSL and the USGS Menlo Park are connected by two dedicated T1 circuits. One circuit is a component of the CISON ring, while the second circuit was installed last year (Figure 2.3) to support the anticipated level of dedicated traffic between Berkeley and Menlo Park above and beyond that associated with the CISON.

The installation of the second dedicated T1 between Berkeley and Menlo Park freed up a frame-relay connection deployed by the BSL as part of the CalREN project in mid-1990s. In the past year, the BSL has been reconfiguring the frame-relay circuit to serve as a second data acquisition link. The plan is to distribute the BDSN data

acquisition between the two frame-relay T1 circuits, eliminating what had been a single point of failure. A second component of the plan is to establish an additional Permanent Virtual Circuit (PVC) at each BDSN site so that each station has connections to both T1s. This configuration will allow the BSL to migrate acquisition from one T1 to the other if a failure occurs. These changes (which are still underway and will be completed in the fall of 2004) will improve the robustness of the BSL operations.

In the long term, the BSL and USGS Menlo Park hope to have a high-bandwidth microwave or satellite connection in addition to the current land lines. Unfortunately, we have not been able to obtain funding for this additional communication link at this time.

3.7 Statewide Integration

BSL staff are involved in many elements of the statewide integration effort. The Standards Committee continues to define and prioritize projects necessary to develop a prototype system and establish working groups to address them (see the minutes from meetings and conference calls at <http://www.cisn.org/standards/meetings.html>).

Dual Station Feeds

One of the major accomplishments in the first few years has been the establishment of "dual station feeds" at 30 stations (15 in northern California and 15 in southern California) (Figure 2.2). To achieve this, the BSL and Caltech both ordered the DLCIs (data link connection identifier) that allow the 2nd center to establish a PVC (permanent virtual circuit) to each station using the frame-relay network.

The Northern California Management Center is using data from the Southern California stations to estimate magnitudes on a routine basis. A subset of these stations are being used for the moment tensor inversions, a computation that is more sensitive to the background noise level.

Data Exchange

Pick exchange was initiated between the Northern and Southern California Management Centers in 2001-2002. Although the CISON has developed software to exchange the reduced amplitude timeseries, this aspect of data exchange has been delayed while certain problems in the codes that generate the time series are addressed.

The CISON partners completed the final stage of a system to exchange peak ground motion data this year. Using a common format, the CISON partners are exchanging observations with one another following an event or a trigger. This step increases the robustness of generating products such as ShakeMap, since all CISON partners are now exchanging data directly with one another. It also

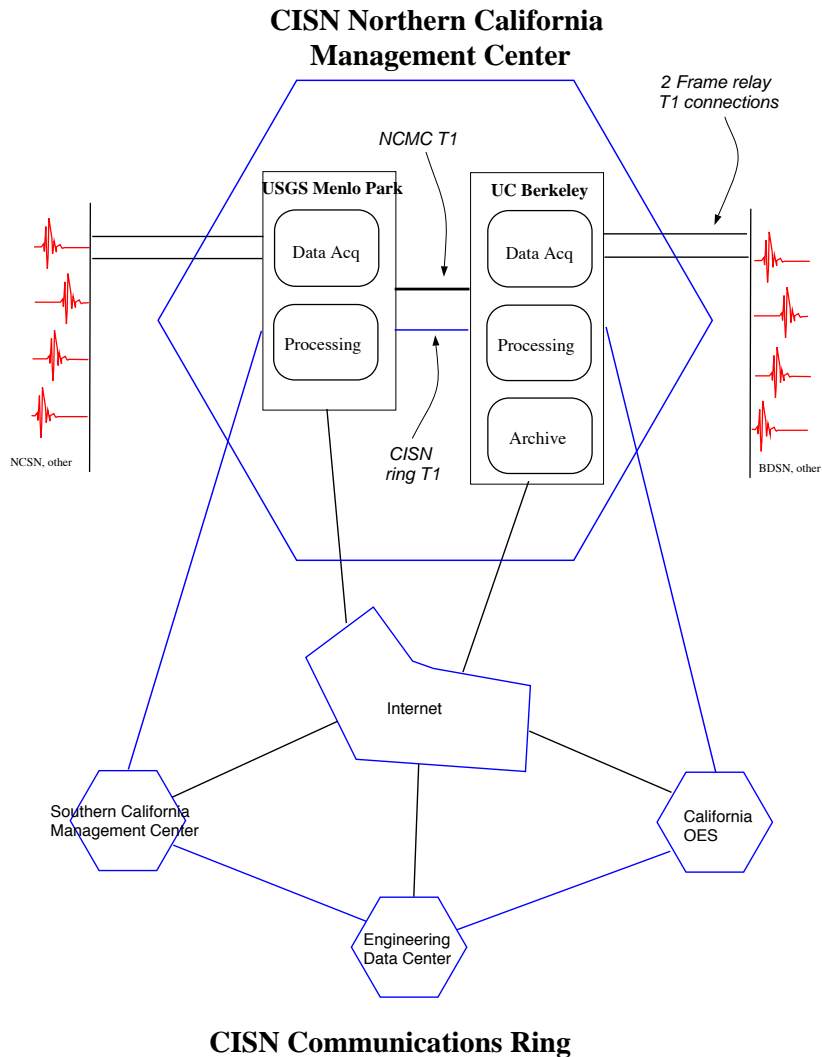


Figure 2.3: Schematic diagram illustrating the connectivity between the real-time processing systems at the USGS Menlo Park and UC Berkeley, forming the northern California Management Center, and with other elements of the CISN.

improves the quality of ShakeMaps on the boundary between northern and southern California, such as the San Simeon earthquake, by allowing all data to be combined in a single map. Finally, it is a necessary step toward the goal of generating statewide ShakeMaps.

Software Calibration

The CISN partners are working together on the problem of software calibration, particularly as it pertains to automated earthquake processing. Currently, the software implemented in the Northern and Southern Cali-

fornia Management Centers is very different. Eventually, there may be standardization of software across the management centers, but in the short term, the focus is on calibrating the software to produce the same answers, given the same input data.

In 2002-2003, effort was focused on phase pickers (*pick-ew*), the association algorithm (*binder*), the location algorithm (*hypoinverse*), and magnitude estimation (various). In the last year, magnitude estimation continued to be a significant area of focus, as well as ShakeMap configuration, metadata exchange, and

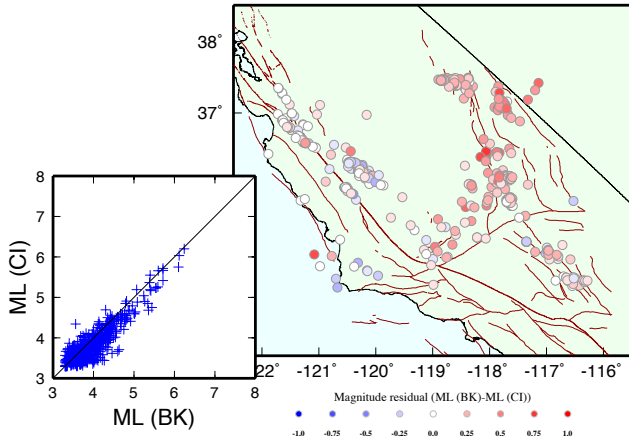


Figure 2.4: Comparison of the estimates of M_L reported by Caltech and Berkeley for 480 earthquakes of M3.5 and higher from 1981-2003. Focusing on an area that spans the boundary between the networks, we observe a systematic bias between the estimates, with a strong apparent geographic signal.

database standardization.

At this point, the issues of a statewide detection and location system are largely addressed. Configuration files have been standardized and a statewide system has been running in Menlo Park for nearly a year. It performed well during the December 2003 San Simeon sequence.

In contrast, the calibration of magnitude has proven to be a more difficult problem, particularly local magnitude, M_L . Last year, we reported initial results from two separate inversions of Wood Anderson amplitudes from the BDSN to estimate local magnitude adjustments. Bob Uhrhammer of the BSL and Jascha Polet of Caltech compared their independent results as a first step to determine a common set of adjustments. Jascha's method estimates the adjustments and attenuation relationship simultaneously, while Bob's uses a differential approach while fixing the attenuation relationship. The good agreement between the estimates of the adjustments provided confidence in the first step of the process.

However, efforts to combine BDSN and TriNet data in a single inversion have been challenging (Gee *et al.*, 2003; 2004b). After much probing, it appears as if there is a bias between the northern and southern California magnitude estimates (Figure 2.4), as illustrated by the three lines of evidence. First, a comparison of nearly 500 earthquakes over a 20 year period in central California recorded by both networks shows a bias of 0.14 magnitude units, with NC magnitudes higher than SC magnitudes.

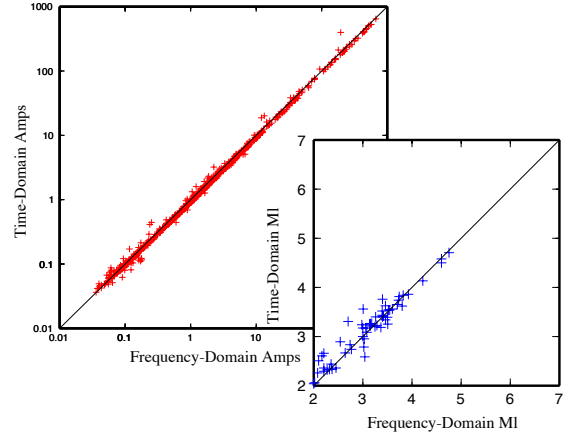


Figure 2.5: Left: Comparison of time domain and frequency domain estimates of Wood Anderson synthetic amplitudes. In general, there is good agreement, although the frequency domain amplitudes are consistently larger than the time domain amplitudes. Right: Comparison between M_L estimates based on the two different amplitude types.

tudes. Second, efforts to invert Wood Anderson amplitudes using a differential approach, a constraint that the BKS and PAS adjustments sum to zero, and fixing the attenuation relationship to one determined by Kanamori (1993), indicates a bias of 0.14. Finally, an independent inversion of a different dataset (absolute approach, a different set of station constraints, and simultaneous inversion for attenuation) suggests a bias of 0.20.

Efforts to understand this issue were hampered by the lack of a good statewide dataset. We now have a good set of 86 events, but some effort remains to clean up the data set and remove observations of multiple channels at the same site for a given earthquake (that is, observations from the BH, HH, and HL channels for a single station) as this multiplicity results in overweighting of some stations. Potential sources of the magnitude discrepancy are drift in station adjustments, differences in the attenuation functions, and other path effects.

In parallel, the BSL has been working on other issues related to magnitude. We have installed a version of the TriNet software that processes waveforms to produce resampled timeseries of amplitudes as well as codes to compute magnitudes and peak ground motions from these timeseries. The system has been running since late 2003. In general, the amplitudes computed by the time-domain approach agree very well with the frequency domain approach that has been the core of the REDI system since 1994. However, the frequency domain amplitudes are consistently higher than the time domain amplitudes (Figure 2.5). The slight difference (the mean amplitude

ratio is 1.05 from 781 observations) may be due to differences in using the full versus simplified instrument responses.

Magnitudes from the time-domain approach agree well with the frequency-domain method, although there is some scatter at lower magnitudes. This is due to differences in the window selection, use of signal to noise ratios to select stations, and differences in the attenuation relations.

Another issue facing the magnitude Working Group is the difference in the station distribution. In southern California, the density of broadband stations permits the computation of M_L for every earthquake. In northern California, the more sparse station distribution does not allow the reliable estimate of M_L below magnitude 3. As a result, the Working Group is looking into the necessary steps to implement M_d on a statewide basis.

A final component of the magnitude efforts is the designation of a magnitude reporting hierarchy. There is general agreement at the low end and at the high end, but the working group is still reviewing issues related to transition points from one magnitude type to another. More details about the magnitude calibration effort are documented in Chapter 9.

In addition to the efforts in standardizing earthquake locations and magnitudes, a CISON working group has been addressing issues related to ShakeMaps. At present, ShakeMaps are currently generated on 5 systems within the CISON. 2 systems in Pasadena generate "SoCal" Shakemaps; 2 systems in the Bay area generate "No-Cal" Shakemaps; and 1 system in Sacramento generates ShakeMaps for all of California. The Sacramento system uses QDDS to provide the authoritative event information for northern and southern California.

Over last 6 months, the Working Group has addressed a number of issues in the standardization of ShakeMap. Initially focusing on the look and feel of the maps (topography, geology, faults, road, lake outlines, cities, and fonts), the Working Group has just started to review a comprehensive compilation of the differences in configuration among the 3 implementations. The remaining differences between the centers range from the small (URL used in the "addon" message) to the significant (use of regressions, linear versus log amplitude weighting). This effort will move the CISON forward toward having fully standardized ShakeMaps.

The lack of stations in the near source region of the 2003 San Simeon earthquake raised a number of issues related to ShakeMap and how to measure the quality of the product as well as quantify the uncertainty. Over the past 6 months, a subset of the Working Group has been working on this issue, based on the work of *Hok and Wald (2003)*. One of the first projects has been to make a map to illustrate current CISON capabilities, based on the existing station distribution. The next step is to look

at calculating uncertainty for some example earthquakes and comparing the uncertainty estimates with different realizations of the ShakeMap produced by using various subsets of the data. Once the method to quantify the uncertainty is validated, then we can use this information to determine a grade.

Location Codes

The CISON adopted a standard for the use of "location" codes (part of the Standard for the Exchange of Earthquake Data (SEED) nomenclature to describe a time-series based on network-station-channel-location) in the late fall of 2003. Over the past few months, USGS and UC Berkeley developers have been working to modify the Earthworm software to support the use of location codes. This effort is nearly complete and the centers are working on a plan to begin migration to the modified codes.

Metadata Exchange

The CISON is also working on issues related to metadata exchange. This is an important component of CISON activities, as correct metadata are required to insure valid interpretation of data. A Standards Working Group has developed and initiated testing of a model for database replication of metadata, and is currently reviewing how much of the schema to exchange and how to address metadata from partners such as CGS, who do not currently maintain their metadata in a database.

Last year, the Metadata Working Group compiled a list of metadata necessary for data processing and developed a model for exchanging metadata. In this model, each CISON member is responsible for the metadata of their stations and other stations that enter into CISON processing through them. For example, Menlo Park is responsible for the NSMP, Tremor, and PG&E stations and Caltech is responsible for the Anza data. The Working Group believes that metadata exchange should proceed on a timely basis, not just when data are generated, and is testing an approach using database replication.

For database exchange, the Working Group proposed that each group or organization have a working or interim database as a staging area (a private sandbox) and a master database. The interim database would contain snapshots of the master tables (that the group/organization is responsible for) and the changes would be pushed manually to the master database by snapshot replication. Changes would be propagated among the master databases by multi-master replication.

To start this off, the Working Group agreed to test replication with a limited number of tables, focusing initially on tables relevant to the real-time system (but not sufficient for archiving). In order to test this solution, the NCMC and SCMC needed to resolve some inconsistencies in the database implementations. This included both differences in the physical schema as well as differences

in use of the schema. The Working Group initiated a pilot test in early 2004, using the tables SimpleResponse and StaMapping and a test database at the NCMC and SCMC. The initial results were successful and the effort has expanded to other tables. As of June 2004, 11 tables are being replicated between the test databases. The next step for the Working Group is to validate the use of the metadata in the real-time system. When this is done, the database replication can be migrated to the primary databases.

In parallel, the Working Group has developed a plan for importing metadata from CGS. Their metadata is not currently stored in a database and is maintained in simple files. Their policy is to distribute the metadata as part of a waveform package and the V0 format was developed to allow for that. The Working Group developed the concept of a "dataless" V0 format (analogous to the dataless SEED files) which will be used to distribute the metadata. In the current plan, CGS will initially prepare and distribute dataless V0 files providing the current metadata for ShakeMap quality stations (i.e., with channels meeting CISM Reference Station or better standards) in the CGS network. These current-information metadata files for the stations will be distributed (probably using a mechanism like sendfile/getfile) and will also be placed at the CGS FTP site. As agreed, the comment field in the V0 header will be used to define the valid time period for the metadata. Each dataless V0 file will contain the 3 channels of the reference sensor at the site. The Working Group plan includes the ability to handle corrections, as well as updates as stations are serviced.

In order to make use of the dataless V0 file, tools have been developed to parse the file and write an XML file containing the information (an expansion of capabilities of the v02ms program). The NCMC has taken advantage of previously existing tools to create a system where the XML is converted into a spreadsheet format and then imported into the database. This plan will be further tested as CGS generates more dataless V0 files and the database is populated.

As part of this process, the issue of mapping the sensor orientation into the SEED channel nomenclature has come up. The v02ms program now uses the same algorithm for generating channel names as used by CGS.

3.8 Earthquake Information Distribution

In response to a request from the PMG, USGS and OES management established an *Ad Hoc* panel in May 2003 to develop specifications for an earthquake information system and to review existing systems as well as systems under development. Lind Gee of the BSL and David Oppenheimer of the USGS were asked to co-chair this panel and to provide a written report within 90 days. The panel met on July 9-10th at the BSL and the re-

port was published on September 16 (*Ad Hoc Panel on Earthquake Information Distribution*, 2003). The panel reviewed the three major existing or planned distribution systems (QDDS, QuakeWatch, and ShakeCast) and noted that none of the systems addressed all the current needs for earthquake information distribution. In particular, firewalls are a growing problem for systems relying on socket-based connections. The panel recommended that a new system be developed, and outlined preliminary specifications for such a system.

Following the publication of the report, OES asked to BSL to write a proposal for the development of the Earthquake Information Distribution System or EIDS. OES approved the proposal and forwarded it to FEMA for review. FEMA agreed to provide \$100,000 toward the development of the system out of the 2002 Emergency Management Program Grant to the State of California.

The award from FEMA was combined with the OES funding of the CISM and the contract was received by UC Berkeley on May 13th. In parallel, Lind Gee and David Oppenheimer worked with the members of the *Ad Hoc* panel to develop detailed specifications – appropriate for a Request For Proposal or RFP – based on the September 2003 report. The specifications were completed in late June and submitted to UC Berkeley Purchasing on July 6, 2004. Unfortunately, the late award of the funding combined with the difficulties of issuing an RFP are complicating efforts to award the funding in a timely fashion. The FEMA contract will terminate on September 30th, 2004.

[Update: In mid-August, the BSL decided to proceed with a sole source award to Instrumental Software Technologies, Inc (ISTI). Paul Friberg of ISTI was one of two vendors who made presentations to the AdHoc Panel in July of 2003 regarding an earthquake information distribution system. On September 28, the BSL was notified that an extension from FEMA has been awarded. Development is now under way.]

3.9 Outreach

There has been significant progress at www.cisn.org in FY03/04. A year ago, the CISM shared the Web server at the Northern California Earthquake Data Center. With the purchase of new, dedicated Web computers, the CISM Web site is now supported by two servers located at Berkeley and Caltech. The Web servers are set up so that the load can be distributed between them, providing improved access during times of high demand.

With the increased robustness provided by the new servers, the CISM has begun to provide access to certain earthquake products directly from www.cisn.org. For example, ShakeMaps are now served directly from the CISM Web site, in addition to being available from several USGS Web servers and the CGS.

In early December, the CISM began offering a sign-

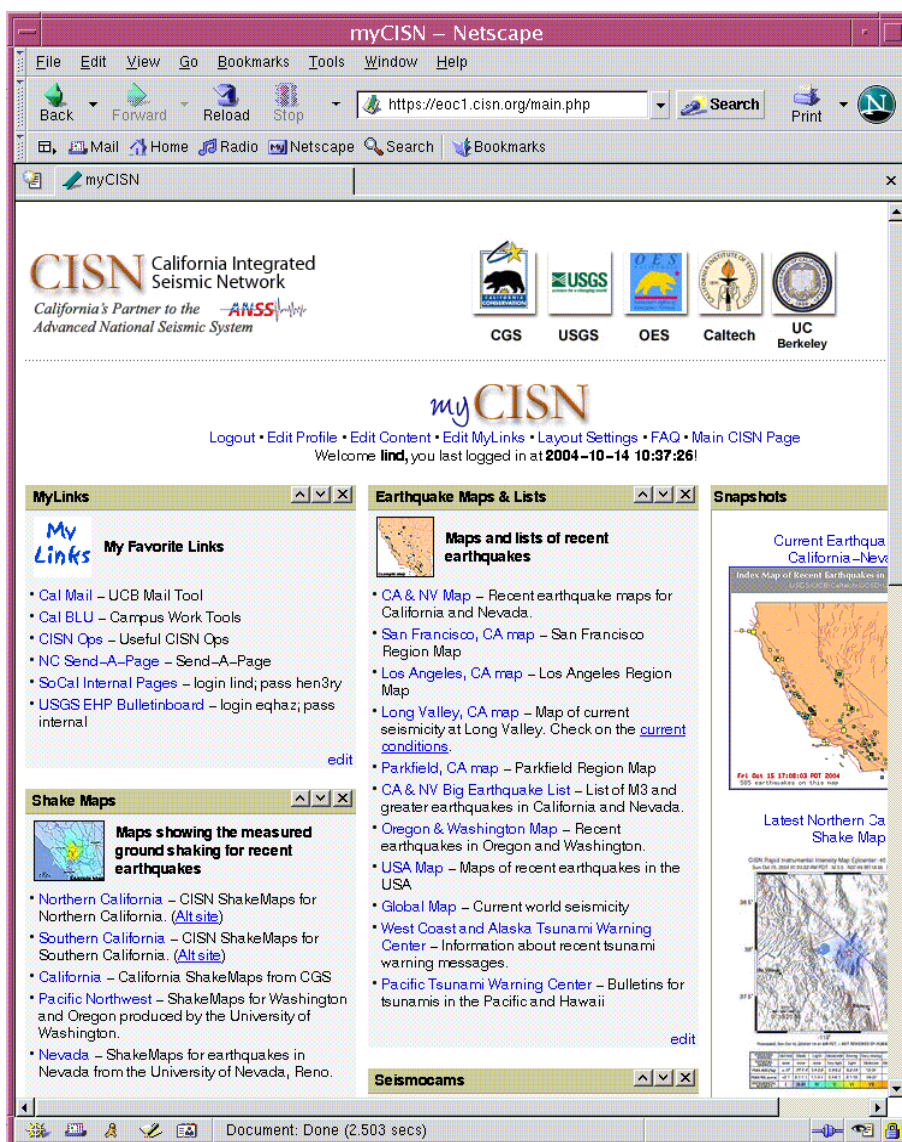


Figure 2.6: Screenshot of the myCISN Web site, as personalized for Lind Gee. The interface allows users to select and organize the earthquake information they want to see. New modifications under development also allow users to create a section of personalized links.

up for earthquake notifications by email. Although both northern and southern California have offered individual sign-ups in the past, the new service provides uniform notification messages for earthquakes of M3.5 and higher in California. In addition, users can sign up to be notified when ShakeMaps are generated.

Design and content of www.cisn.org continues to evolve. The Web site is an important tool for CISN outreach as well as for communication and documentation among the CISN partners.

Also in FY03/04, the CISN established a Web site dedicated for emergency managers. Following a suggestion from the Advisory Committee, we have designed a Web

site to provide personalized access to earthquake information. Known as "myCISN", the Web site is available at eoc.cisn.org (Figure 2.6). Access to the Web site is limited to registered users in order to provide highly reliable access.

At present, "myCISN" is a single Web server located at UC Berkeley. However, modifications to the database are underway to allow for multiple servers in the future. A second computer was purchased with FY03/04 funds and will either be installed in Sacramento or in southern California.

4. Acknowledgements

CISN activities at the BSL are supported by funding from the Governor's Office of Emergency Services.

Barbara Romanowicz and Lind Gee are members of the CISN Steering Committee. Lind Gee is a member of the CISN Program Management Committee and she leads the CISN project at the BSL. Doug Neuhauser is chair of the CISN Standards Committee, which includes Lind Gee and Pete Lombard as members.

Because of the breadth of the CISN project, many BSL staff have been involved including: John Friday, Lind Gee, Wade Johnson, Bill Karavas, Pete Lombard, Doug Neuhauser, Charley Paffenbarger, Dave Rapkin, and Stephane Zuzlewski. Lind Gee contributed to this chapter. Additional information about the CISN is available through reports from the Program Management Committee (*Hauksson et al.*, 2003).

5. References

Ad Hoc Panel on Earthquake Information Distribution (L. Gee and D. Oppenheimer, chairs), Requirements for an Earthquake Information Distribution System, http://www.cisn.org/ahpeid/ahpeid_final.pdf, 2003.

Gee, L., D. Dreger, G. Wurman, Y. Gung, B. Uhrhammer, and B. Romanowicz, A Decade of Regional Moment Tensor Analysis at UC Berkeley, *EOS Trans. AGU*, 84(46), Fall Meet. Suppl., Abstract S52C-0148, 2003.

Gee, L., D. Oppenheimer, T. Shakal, D. Given, and E. Hauksson, Performance of the CISN during the 2003 San Simeon Earthquake, http://www.cisn.org/docs/CISN_SanSimeon.pdf, 2004a.

Gee, L., J. Polet, R. Uhrhammer, and K. Hutton, Earthquake Magnitudes in California, *Seism. Res. Lett.*, 75(2), 272, 2004b.

Hauksson, E., L. Gee, D. Given, D. Oppenheimer, and T. Shakal, Report to the CISN Advisory and Steering Committees, #5, <http://www.cisn.org/oes/2003.05.30.pdf>, 2003.

Hok, S., and D. J. Wald, Spatial Variability of Peak Strong Ground Motions: Implications for ShakeMap Interpolations, *EOS. Trans. AGU*, 84(46), F1121, 2003.

Kanamori, H., J. Mori, E. Hauksson, T. Heaton, L. Hutton, and L. Jones, Determination of earthquake energy release and M_L using TERRASCOPE, *Bull. Seis. Soc. Am.*, 83, 330-346, 1993.

Chapter 3

Berkeley Digital Seismic Network

1. Introduction

The Berkeley Digital Seismic Network (BDSN) is a regional network of very broadband and strong motion seismic stations spanning northern California and linked to UC Berkeley through continuous telemetry (Figure 3.1 and Table 3.1). This network is designed to monitor regional seismic activity at the magnitude 3+ level as well as to provide high quality data for research projects in regional and global broadband seismology.

The network upgrade and expansion initiated in 1991 has continued, and it has grown from the original 3 broadband stations installed in 1986-87 (BKS, SAO, MHC) to 27 stations in 2004, including the ocean-bottom seismometer in Monterey Bay. One new station was added in the past year (GASB).

We take particular pride in high quality installations, which often involve lengthy searches for appropriate sites away from sources of low-frequency noise, as well as continuous improvements in installation procedures and careful monitoring of noise conditions at existing stations.

Future expansion of our network is contingent on the availability of funding and coordination with other institutions for the development of a denser state-of-the-art strong motion/broadband seismic network and joint earthquake notification system in this seismically hazardous region.

2. BDSN Overview

Twenty-five of the BDSN sites are equipped with 3 component broadband seismometers and strong-motion accelerometers, and a 24-bit digital data acquisition system or data logger. Two additional sites (RFSB and SCCB) consist of a strong-motion accelerometer and a 24-bit digital data logger. Data from all BDSN stations are transmitted to UC Berkeley using continuous telemetry. In order to insure against data loss during utility disruptions, each site has a 3-day supply of battery power and is accessible via a dialup phone line. The combination of high-dynamic range sensors and digital data log-

gers ensures that the BDSN has the capability to record the full range of earthquake motion for source and structure studies. Table 3.2 lists the instrumentation at each site.

Most BDSN stations have Streckeisen three-component broadband sensors (*Wielandt and Streckeisen, 1982; Wielandt and Steim, 1986*). Guralp CMG-3T downhole broadband sensors contributed by LLNL are deployed in post-hole installations at BRIB and FARB. The strong-motion instruments are Kinemetrics FBA-23 or FBA-EST with ± 2 g dynamic range. The recording systems at all sites are either Q730, Q680, Q980 or Q4120 Quanterra data loggers, with 3, 6, 8, or 9 channel systems. The Quanterra data loggers employ FIR filters to extract data streams at a variety of sampling rates. In general, the BDSN stations record continuous data at .01, 0.1, 1.0, 20.0 or 40.0, and 80 or 100 samples per second, although some sites send triggered data at the highest sampling rate using the Murdock, Hutt, and Halbert event detection algorithm (*Murdock and Hutt, 1983*) (Table 3.3). In addition to the 6-channels of seismic data, signals from thermometers and barometers are recorded at nearly every site (Figure 3.2).

In parallel with the upgrade of the broadband network, a grant from the CalREN Foundation (California Research and Education Network) in 1994 enabled the BSL to convert data telemetry from analog leased lines to digital frame-relay connections. The frame-relay network uses digital phone circuits that can support 56 Kbit/s to 1.5 Mbit/s throughput. Since frame-relay is a packet-switched network, a site may use a single physical circuit to communicate with multiple remote sites through the use of "permanent virtual circuits". Frame Relay Access Devices (FRADs), which replace modems in a frame-relay network, can simultaneously support multiple interfaces such as RS-232 async ports, synchronous V.35 ports, and ethernet connections. In practical terms, the upgrade to frame relay communication provides faster data telemetry between the remote sites and the BSL, remote console control of the data loggers, additional services such as FTP and telnet to the data loggers, data transmission to multiple sites, and the ability to com-

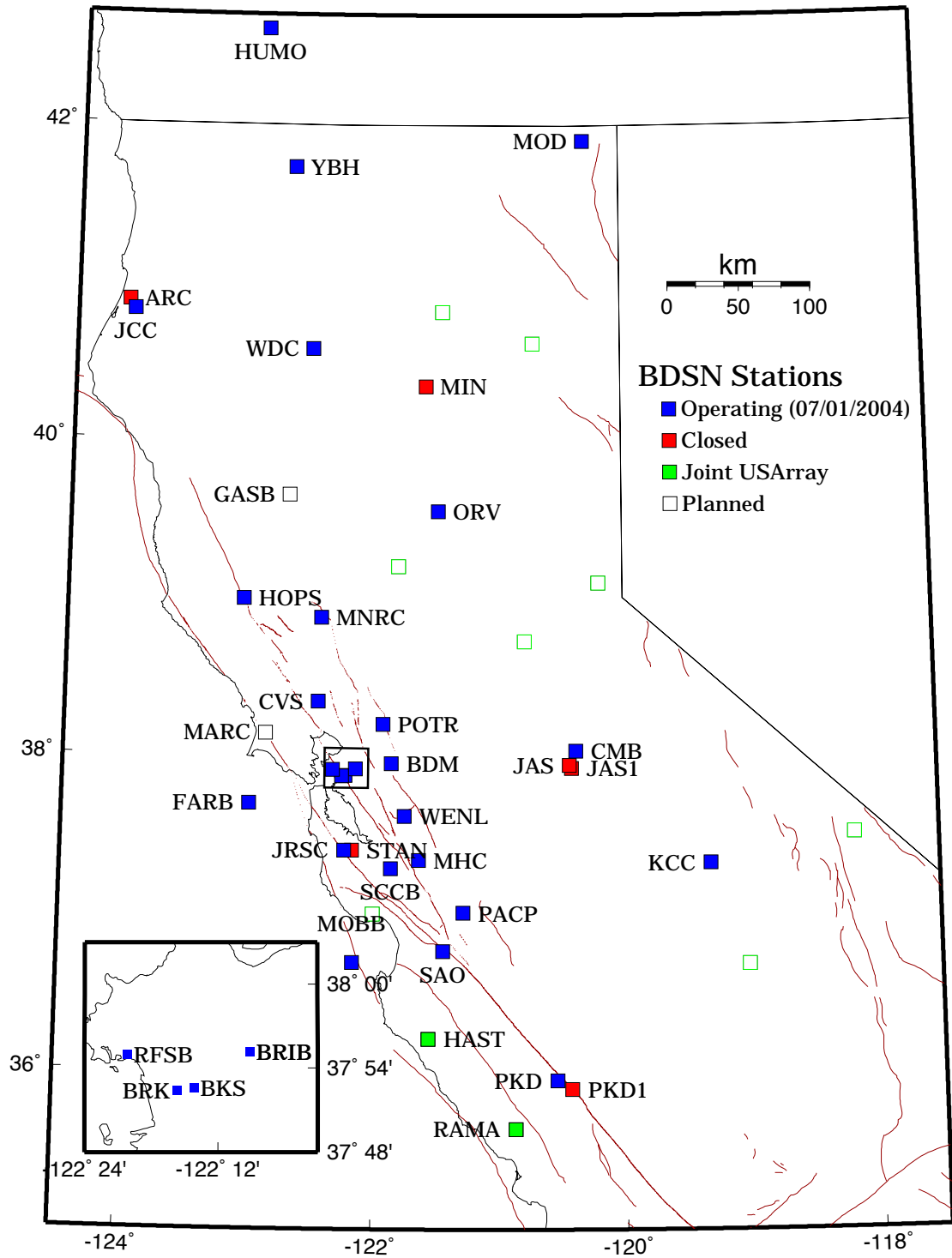


Figure 3.1: Map illustrating the distribution of operational (filled squares), planned (open squares), and closed (grey squares) BDSN stations in northern and central California. The open squares (except for the one labelled GASB) indicate sites developed in collaboration with USArray.

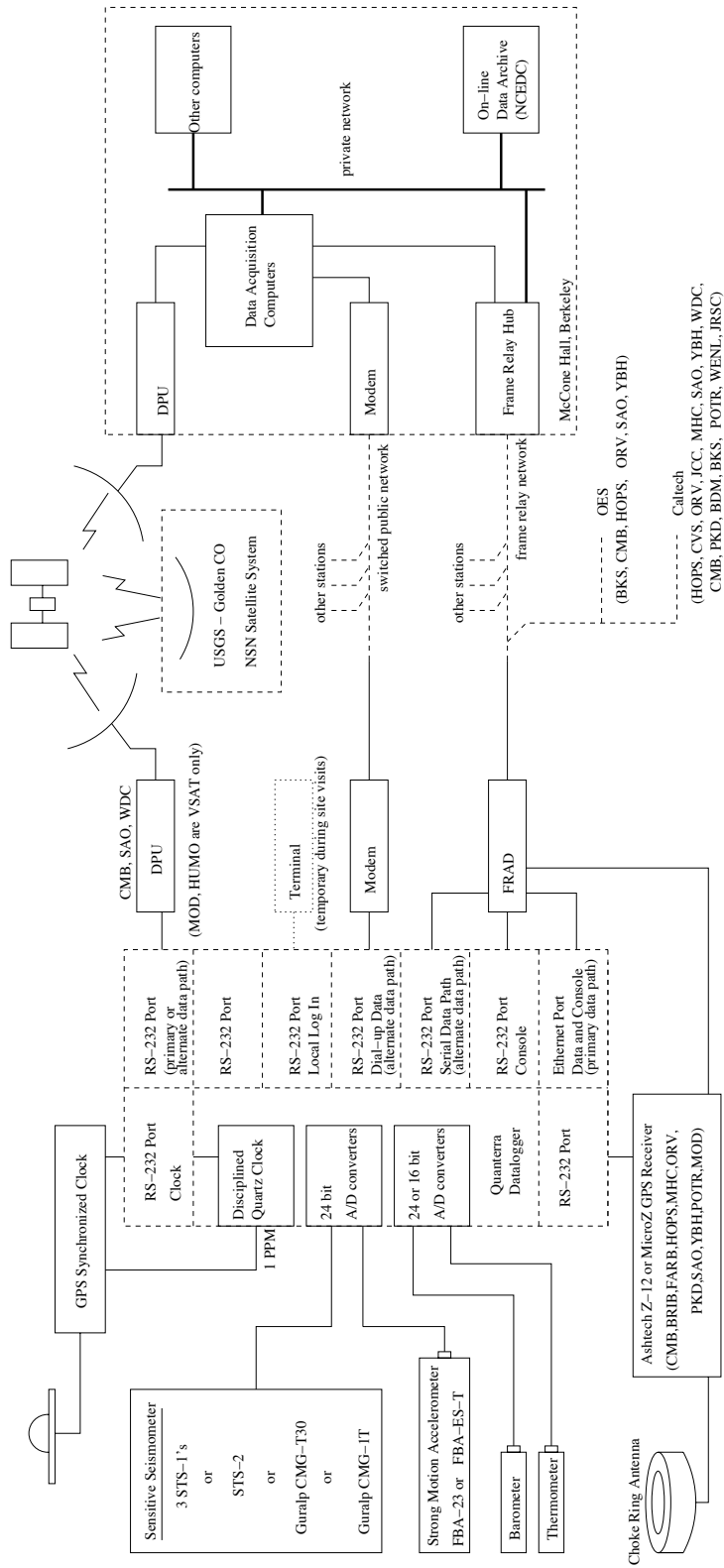


Figure 3.2: Schematic diagram showing the flow of data from the sensors through the data loggers to the central acquisition facilities of the BSL.

municate and transmit data from multiple instruments such as GPS receivers and/or multiple data loggers at a single site. Today, 23 of the BDSN sites use frame-relay telemetry for all or part of their communications system.

As described in Chapter 8, data from the BDSN are acquired centrally at the BSL. These data are used for rapid earthquake reporting as well as for routine earthquake analysis (Chapters 2 and 9). As part of routine quality control (Chapter 8), power spectral density analyses are performed weekly and Figure 3.3 shows a summary of the results for 2003-2004. The occurrence of a significant teleseism also provides the opportunity to review station health and calibration. Figure 3.4 displays BDSN waveforms for a M_w 6.8 deep focus earthquake in the Primor'ye, Russia region on July 27, 2003.

BDSN data are archived at the Northern California Earthquake Data Center. This is described in detail in Chapter 10.

Sensor	Channel	Rate (sps)	Mode	FIR
Broadband	UH?	0.01	C	Ac
Broadband	VH?	0.1	C	Ac
Broadband	LH?	1	C	Ac
Broadband	BH?	20/40	C	Ac
Broadband	HH?	80/100	C	Ac/Ca
SM	LL?	1	C	Ac
SM	BL?	20/40	C	Ac
SM	HL?	80/100	C	Ac/Ca
Thermometer	LKS	1	C	Ac
Barometer	LDS	1	C	Ac

Table 3.3: Typical data streams acquired at BDSN stations, with channel name, sampling rate, sampling mode, and the FIR filter type. SM indicates strong-motion; C continuous; T triggered; Ac acausal; Ca causal. The LL and BL strong-motion channels are not transmitted over the continuous telemetry but are available on the Quanterra disk system if needed. The HH channels are recorded at two different rates, depending on the datalogger type. Q4120s provide 100 sps and causal filtering; Q680/980s provide 80 sps and acausal filtering. The BH channels were changed from 20 to 40 sps this year as described below.

2.1 Electromagnetic Observatories

In 1995, the BSL installed two well-characterized electric and magnetic field measuring systems at two sites along the San Andreas Fault which are part of the Berkeley Digital Seismic Network in collaboration with Dr. Frank Morrison. Since then, magnetotelluric (MT) data have been continuously recorded at 40 Hz and 1 Hz and archived at the NCEDC (Table 3.4). At least one set of orthogonal electric dipoles measures the vector horizon-

Sensor	Channel	Rate (sps)	Mode	FIR
Magnetic	VT?	0.1	C	Ac
Magnetic	LT?	1	C	Ac
Magnetic	BT?	40	C	Ac
Electric	VQ?	0.1	C	Ac
Electric	LQ?	1	C	Ac
Electric	BQ?	40	C	Ac

Table 3.4: Typical MT data streams acquired at SAO and PKD, with channel name, sampling rate, sampling mode, and FIR filter type. C indicates continuous; T triggered; Ac acausal.

tal electric field, E, and three orthogonal magnetic sensors measure the vector magnetic field, B. These reference sites, now referred to as electromagnetic (EM) observatories, are co-located with seismographic sites so that the field data share the same time base, data acquisition, telemetry and archiving system as the seismometer outputs.

The MT observatories are located at Parkfield (PKD1, PKD) 300 km south of the San Francisco Bay Area and Hollister (SAO), halfway between San Francisco and Parkfield (Figure 3.1). In 1995, initial sites were established at PKD1 and SAO, separated by a distance of 150 km, and equipped with three induction coils and two 100 m electric dipoles. PKD1 was established as a temporary seismic site, and when a permanent site (PKD) was found, a third MT observatory was installed in 1999 with three induction coils, two 100 m electric dipoles, and two 200 m electric dipoles. PKD and PKD1 ran in parallel for one month in 1999, and then the MT observatory at PKD1 was closed.

Data at the MT sites are fed to Quanterra data loggers, shared with the collocated BDSN stations, synchronized in time by GPS and sent to the BSL via dedicated communication links.

3. 2003-2004 Activities

3.1 USArray

As mentioned in Chapter 2, the BSL concluded an agreement with IRIS during 2003-2004 to contribute 19 stations of the BDSN to USArray while the experiment is deployed in California. This includes 17 existing stations: CMB, CVS, FARB, HOPS, HUMO, JCC, JRSC, KCC, MNRC, MOD, ORV, PACP, PKD, POTR, WDC, WENL, and YBH as well as two sites currently under construction: GASB and MARC.

The 19 BDSN sites provide USArray with a running start in northern California. In June of 2004, the BSL set up the software necessary to exchange data with USArray and made modifications to the dataloggers to change the

Code	Net	Latitude	Longitude	Elev (m)	Over (m)	Date	Location
BDM	BK	37.9540	-121.8655	219.8	34.7	1998/11 -	Black Diamond Mines, Antioch
BKS	BK	37.8762	-122.2356	243.9	25.6	1988/01 -	Byerly Vault, Berkeley
BRIB	BK	37.9189	-122.1518	219.7	2.5	1995/06 -	Briones Reservation, Orinda
BRK	BK	37.8735	-122.2610	49.4	2.7	1994/03 -	Haviland Hall, Berkeley
CMB	BK	38.0346	-120.3865	697.0	2	1986/10 -	Columbia College, Columbia
CVS	BK	38.3453	-122.4584	295.1	23.2	1997/10 -	Carmenet Vineyard, Sonoma
FARB	BK	37.6978	-123.0011	-18.5	0	1997/03 -	Farallon Island
GASB	BK	39.65	-122.72	TBD	TBD	2004/06 -	Alder Springs
HOPS	BK	38.9935	-123.0723	299.1	3	1994/10 -	Hopland Field Stat., Hopland
HUMO	BK	42.6071	-122.9567	554.9	50	2002/06 -	Hull Mountain, Oregon
JCC	BK	40.8175	-124.0296	27.2	0	2001/04 -	Jacoby Creek
JRSC	BK	37.4037	-122.2387	70.5	0	1994/07 -	Jasper Ridge, Stanford
KCC	BK	37.3236	-119.3187	888.1	87.3	1995/11 -	Kaiser Creek
MHC	BK	37.3416	-121.6426	1250.4	0	1987/10 -	Lick Obs., Mt. Hamilton
MNRC	BK	38.8787	-122.4428	704.8	3	2003/06 -	McLaughlin Mine, Lower Lake
MOBB	BK	36.6907	-122.1660	-1036.5	1	2002/04 -	Monterey Bay
MOD	BK	41.9025	-120.3029	1554.5	5	1999/10 -	Modoc Plateau
ORV	BK	39.5545	-121.5004	334.7	0	1992/07 -	Oroville
PACP	BK	37.0080	-121.2870	844	0	2003/06 -	Pacheco Peak
PKD	BK	35.9452	-120.5416	583.0	3	1996/08 -	Bear Valley Ranch, Parkfield
POTR	BK	38.2026	-121.9353	20.0	6.5	1998/02 -	Potrero Hill, Fairfield
RFSB	BK	37.9161	-122.3361	-26.7	0	2001/02 -	RFS, Richmond
SAO	BK	36.7640	-121.4472	317.2	3	1988/01 -	San Andreas Obs., Hollister
SCCB	BK	37.2874	-121.8642	98	0	2000/04 -	SCC Comm., Santa Clara
WDC	BK	40.5799	-122.5411	268.3	75	1992/07 -	Whiskeytown
WENL	BK	37.6221	-121.7570	138.9	30.3	1997/06 -	Wente Vineyards, Livermore
YBH	BK	41.7320	-122.7104	1059.7	60.4	1993/07 -	Yreka Blue Horn Mine, Yreka

Table 3.1: Currently operating stations of the Berkeley Digital Seismic Network. Each BDSN station is listed with its station code, network id, location, operational dates, and site description. The latitude and longitude (in degrees) are given in the WGS84 reference frame and the elevation (in meters) is relative to the WGS84 reference ellipsoid. The elevation is either the elevation of the pier (for stations sited on the surface or in mining drifts) or the elevation of the well head (for stations sited in boreholes). The overburden is given in meters. The date indicates either the upgrade or installation time.

BH sampling rate from 20 Hz to 40 Hz. This is discussed more extensively in Chapter 8.

In addition, the BSL is collaborating with USArray to identify other sites that may be suitable to become BDSN stations. During the past year, BSL staff have been working to identify 8 potential sites for USArray/BDSN instrumentation, many at UC reserves and field stations (shown in Figure 3.1). One of these sites is the Hastings Reserve.

The BSL identified the Hastings Biological Field Station as a potential site of interest over five years ago, but did not have the funding to proceed. Hastings is a biological field station of the University of California, located in the Carmel Valley. The occurrence of the 12/22/2003 San Simeon earthquake, 70 km to the SW, provided additional motivation for establishing this station.

Bob Uhrhammer visited Hastings in April 2004 and met with Mark Stromberg, the reserve director. They

identified two potential sites for broadband instrumentation. Bob Busby, the USArray field manager, made the final selection and the station was installed in July 2004 by a USArray field team.

In the coming year, BSL staff will be working to permit other sites of interest in northern and central California.

3.2 Station Maintenance

Given the remoteness of the off-campus stations, BDSN data acquisition equipment and systems have been designed, configured, and installed for both cost effectiveness and reliability. As a result, the need for regular station visits has been reduced. Most station visits are necessitated by some catastrophic failure. The 2003-2004 fiscal year was no exception, with the additional complication of a reduction in staff.

Code	Broadband	Strong-motion	Data logger	T/B	GPS	Other	Telemetry	Dial-up
BDM	STS-2	FBA-23	Q4120	X			FR	
BKS	STS-1	FBA-23	Q980	X		Baseplates	FR	X
BRIB	CMG-3T	FBA-23	Q980		X	Vol. Strain	FR	X
BRK	STS-2	FBA-23	Q680				POTS	
CMB	STS-1	FBA-23	Q980	X	X	Baseplates	FR/NSN	X
CVS	STS-2	FBA-23	Q4120	X			FR	
FARB	CMG-3T	FBA-23	Q4120	X	X		R-FR/R	
GASB	STS-2	FBA-ES-T	Q4120	X			TBD	
HOPS	STS-1	FBA-23	Q980	X	X	Baseplates	FR	X
HUMO	STS-2	FBA-ES-T	Q4120	X			NSN	X
JCC	STS-2	FBA-23	Q980	X			FR	X
JRSC	STS-2	FBA-23	Q680				FR	X
KCC	STS-1	FBA-23	Q980	X		Baseplates	R-Mi-FR	X
MHC	STS-1	FBA-23	Q980	X	X		FR	X
MNRC	STS-2	FBA-ES-T	Q4120	X			None	X
MOBB	CMG-1T		GEOsense			Current meter, DPG	None	
MOD	STS-1	FBA-ES-T	Q980	X	X	Baseplates	NSN	X
ORV	STS-1	FBA-23	Q980	X	X	Baseplates	FR	X
PACP	STS-2	FBA-ES-T	Q4120	X			Mi/FR	
PKD	STS-2	FBA-23	Q980	X	X	EM	R-FR	X
POTR	STS-2	FBA-ES-T	Q4120	X	X		FR	X
RFSB		FBA-ES-T	Q730				FR	
SAO	STS-1	FBA-23	Q980	X	X	Baseplates, EM	FR/NSN	X
SCCB		FBA-ES-T	Q730		X		FR	
WDC	STS-2	FBA-23	Q980	X			FR/NSN	X
WENL	STS-2	FBA-23	Q4120	X			FR	
YBH	STS-1 & STS-2	FBA-23	Q980	X	X	Baseplates	FR	X

Table 3.2: Instrumentation of the BDSN as of 06/30/2003. Every BDSN station consists of collocated broadband and strong-motion sensors, with the exception of PKD1, RFSB and SCCB which are strong-motion only, with a 24-bit Quanterra data logger and GPS timing. Additional columns indicate the installation of a thermometer/barometer package (T/B), collocated GPS receiver as part of the BARD network (GPS), and additional equipment (Other) such as warpless baseplates or electromagnetic sensors (EM). The obs station MOBB also has a current meter and differential pressure gauge (DPG). The main and alternate telemetry paths are summarized for each station. FR - frame relay circuit, R - radio, Mi - microwave, POTS - plain old telephone line, NSN - USGS NSN satellite link, None - no telemetry at this time. An entry like R-Mi-FR indicates multiple telemetry links, in this case, radio to microwave to frame relay.

NSN VSAT modifications

The BSL cooperates with the US NSN on the following sites in northern California: SAO, CMB, WDC, MOD, and HUMO. At each of these sites, the NSN has provided a VSAT to support a communications link. The MOD and HUMO sites are sufficiently remote that the VSAT is the only communications link available.

In 2003, the US NSN began to replace the older VSAT systems and, in February 2004, the USGS turned off the original satellite system. Prior to the end of February, BSL staff traveled to HUMO and MOD to work with USGS contractors on the installation of the new VSAT system. Fortunately, these two installations were completed just before the older system was turned off, avoid-

ing the loss of communications.

Unfortunately, we have not completed the VSAT modifications at the three remaining sites. Hopefully this task will be completed during FY04/05, as the VSATs provide an important secondary communication link at these stations. At this time, data from the non-upgraded stations is provided to NEIC via the BSL data acquisition.

In May, the USGS contractors installed an NSN VSAT at McCone Hall. The replacement of the older VSAT restored the capability of the BSL to receive data directly from the satellite system, rather than over the Internet.

Problems with accelerometers

The San Simeon earthquake highlighted problems with the FBA-23s and Episensors at several BDSN sites. JRSC (FBA-23), MHC (FBA-23), WENL (FBA-23), and RFSB (Episensor) showed problems with the San Simeon recording (primarily poor response to ground motions). Thus far, we have replaced the sensors at WENL and the JRSC sensor has been sent for repair.

PKD telemetry

At the time the station PKD was installed in 1996, continuous telemetry from the site was achieved by interconnection of a digital spread spectrum radio (900 MHz) with the frame-relay circuit at Carr Hill. Radios in this spectrum have the advantage of not requiring federal licensing or permits. The BSL installation in 1996 was the first use of such equipment in Parkfield. At least two other investigating groups in Parkfield subsequently installed similar radios, ultimately causing interference and a reduction in data bandwidth. In December of 2003, BSL and USGS engineers went to Parkfield to coordinate frequencies, align antennas, and replace and move radio equipment in order to minimize future interference. Over two days, the telemetry path from the PKD vault to the Carr hill site was redirected to a repeater site operated by UCSD. RF signal levels were tested and confirmed. In January of 2004 however, the signal levels on the new path had faded as much as 20 db, apparently due to the increased water absorption by vegetation within the direct line of site. During a January trip by BSL engineers, antennas were once again this time redirecting the data path directly to Carr Hill. Unfortunately, that solution was short lived as the signal level fell again faded more than 10 db in the following two weeks. During a third trip, BSL engineers installed a solar powered radio repeater. This solar powered radio repeater has continued to operate satisfactorily through the dry summer months. A replacement for this repeater is planned at a location which will further improve the radio signal level pending permission from the local landowner.

Other maintenance

At KCC, we replaced all the batteries, removing over 1600 lbs of worn out batteries.

The ownership of the POTR site has changed and we are in the process of negotiating with the new owner.

A landslide at WDC resulted in flooding in the tunnel and water entering the dome. As part of bringing the station back online, the dome was opened (for the first time in over 7 years) and the sensors were replaced.

An optoisolator and a DC-DC converter were installed at YBH to reduce the noise.

3.3 New Installations

In the past year, two installations were completed and one new site was started. The installations at PACP and MNRC were completed and a new site at Alder Springs was started. A fourth site, Marconi, is in the process of being permitted and installation will start soon.

Pacheco Peak

The Pacheco Peak site was installed in June 2003. In the initial installation, the seismometers were temporarily placed on the floor in the communications building. During 2003-2004, a pier and vault were constructed. The seismometers were relocated to the vault in September, 2003.

McLaughlin Mine

With the conclusion of mining operations, the McLaughlin Mine in Lake and Yolo counties will be managed as a UC Reserve by UC Davis. The site is on property owned and formerly operated by Homestake Mining Company as a surface gold mine. The site is located approximately 20 kilometers east of the town of Lower Lake, California in an area of Franciscan sandstone with volcanic precipitates forming the gold deposit.

Last year, a steel and concrete vault from a shipping container similar to those found at stations JCC, PKD, and HOPS was constructed. Power and telephone lines were trenched approximately 300 meters to the site. Because of the remoteness of the site, digital telephone data circuits are not available. During 2003-2004, BSL engineers permitted, designed, prefabricated and installed a two-hop wireless radio bridge to a State of California radio and microwave facility on Mt Saint Helena twenty-five kilometers away. From the Mt Saint Helena site, data are relayed to the California Department of Forestry and Fire Protection (CDF) command center in the Napa Valley, where a connection to the frame-relay network is made. A dial up connection is also available for data downloading or communicating with the McLaughlin Mine site.

Alder Springs

The Alder Springs site located approximately 35 kilometers west of the central valley town of Willows. Local geology is mostly serpentine and Franciscan. Previously, a short period observatory has been operated at the Alder Springs site by the California Department of Water Resources.

In June 2004, construction began on a steel and concrete seismographic vault similar to those at JCC, PKD, HOPS, and MNRC. On site excavation was contracted. Inmates from the CDF Valley View Conservation Camp provided labor for the concrete pour and back filling of the excavation. BSL engineers built the forms and framing for the concrete, as well as all electrical wiring at the

site. The site is permit was provided by the US Forest Service, Mendocino National Forest.

Continuous telemetry is planned for the site. Again, the remote nature of the site will necessitate a combination of radios and digital circuits. Our initial investigations and efforts to relay the data via the same Mt Saint Helena radio connection as the McLaughlin Mine site proved impossible. We expect to achieve continuous telemetry in the second quarter of 2004-05. This site has been named GASB by the BSL.

Marconi

We permitted a site at the Marconi Conference Center, near Marshall, CA. The conference center is operated by the State of California. This site will be installed in collaboration with the USGS and will form part of the ANSS backbone network. Installation will take place in the fall of 2004.

3.4 MOBB: An Ocean Floor Broadband Station

The Monterey Ocean Bottom Broadband observatory (MOBB) is a collaborative project between the Monterey Bay Aquarium Research Institute (MBARI) and the BSL. Supported by funds from the Packard Foundation to MBARI, NSF/OCE funds and UC Berkeley funds to BSL, its goal has been to install and operate a permanent seafloor broadband station as a first step towards extending the on-shore broadband seismic network in northern California, to the seaside of the North-America/Pacific plate boundary, providing better azimuthal coverage for regional earthquake and structure studies. It also serves the important goal of evaluating background noise in near-shore buried ocean floor seismic systems, such as may be installed as part of temporary deployments of "leap-frogging" arrays (e.g. Ocean Mantle Dynamics Workshop, September 2002). In this context, evaluating the possibility of a posteriori noise deconvolution using auxiliary data (e.g. current meter, differential pressure gauge) as well as comparison with land based recordings (see section 7. in Chapter 12). BSL staff put significant effort in the development of procedures to minimize instrumental noise caused by air circulation inside the seismometer package casing (see 2001-2002 and 2002-2003 BSL Annual Reports). These procedures were later applied to the preparation of 3 similar packages destined for installation on the Juan de Fuca plate in the framework of University of Washington's Keck project.

This project follows the 1997 MOISE experiment, in which a three component broadband system was deployed for a period of 3 months, 40 km off shore in Monterey Bay, with the help of MBARI's "Point Lobos" ship and ROV "Ventana" (Figure 3.5). MOISE was a cooperative program sponsored by MBARI, UC Berkeley and the INSU, Paris, France (*Stakes et al.*, 1998; *Romanowicz*

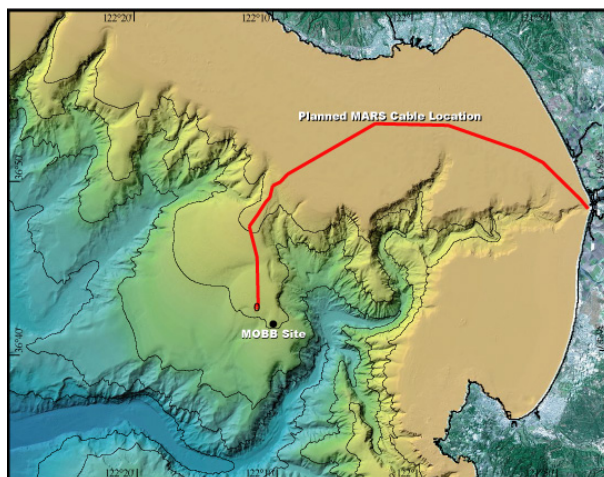


Figure 3.5: Location of the MOBB station in Monterey Bay, California, against seafloor and land topography. The projected path of the MARS cable is indicated by the solid line.

et al., 1999; *Stutzmann et al.*, 2001). During the MOISE experiment, valuable experience was gained on the technological aspects of such deployments, which contributed to the success of the present MOBB installation.

The successful MOBB deployment took place April 9-11, 2002 and the station is currently recording data autonomously (e.g. *Romanowicz et al.*, 2003). Eleven "dives" involving the MBARI ship "Point Lobos" and ROV "Ventana" have so far taken place to exchange data loggers and battery packages. In February 2004, the N/S component seismometer failed. It was temporarily replaced, from 05/19/04 to 07/09/04 by one of the Keck seismometer packages which was conveniently available at that time. The original seismometer was sent back to Guralp Inc. for repair and successfully reinstalled on 07/09/04. Unfortunately, we are continuing to experience problems with the data from the Differential Pressure Gauge (DPG, *Cox et al.*, 1984), which are crucial for the development and implementation of a posteriori noise deconvolution procedures to help counteract the large contribution of infragravity noise in the period range 20-200 sec (Figure 3.6).

With input from BSL staff, MBARI engineers are currently working on hardware and software developments needed to connect the MOBB sensors to the MARS (Monterey Accelerated Research System; <http://www.mbari.org/mars/>) cable, which is scheduled to be deployed in Fall 2005 (Figure 3.5). This will provide access to real-time, continuous seismic data from MOBB to be merged with the rest of the northern California real-time seismic system.

4. Acknowledgements

Under Barbara Romanowicz's general supervision, Lind Gee and Doug Neuhauser oversee the BDSN data acquisition operations and Bill Karavas is head of the engineering team. John Friday, Dave Rapkin, and Bob Uhrhammer contribute to the operation of the BDSN. Sierra Boyd has been responsible for the operation of the EM observatories. Bill Karavas, Bob Uhrhammer, and Lind Gee contributed to the preparation of this chapter.

The California Governor's Office of Emergency Services provided funding toward the development of sites MNRC, PACP, and GASB as part of the CISON.

MOBB is a collaboration between the BSL and MBARI, involving Barbara Romanowicz, Bob Uhrhammer, and Doug Neuhauser from the BSL and Debra Stakes and Paul McGill from MBARI. The MBARI team also includes Steve Etchemendy (Director of Marine Operations), Jon Erickson, John Ferreira, Tony Ramirez and Craig Dawe. The MOBB effort at the BSL is supported by funds from NSF/OCE and UC Berkeley. The MOBB seismometer package was funded by NSF/OCE grant #9911392.

5. References

Cox, C., T. Deaton and S. Webb, A deep-sea differential pressure gauge, *J. Atm. Ocean. Tech.*, 1, 237-245, 1984.

Murdock, J., and C. Hutt, A new event detector designed for the Seismic Research Observatories, *USGS Open-File-Report 83-0785*, 39 pp., 1983.

Peterson, J. R., Observations and modeling of seismic background noise, *U. S. Geological Survey Open File Report*, 93-322, 94 pp., 1993.

Romanowicz, B., D. Stakes, J. P. Montagner, P. Tarits, R. Uhrhammer, M. Begnaud, E. Stutzmann, M. Pasyanos, J.F. Karczewski, S. Etchemendy, MOISE: A pilot experiment towards long term sea-floor geophysical observatories, *Earth Planets Space*, 50, 927-937, 1999.

Romanowicz, B., D. Stakes, R. Uhrhammer, P. McGill, D. Neuhauser, T. Ramirez and D. Dolenc, The MOBB experiment: a prototype permanent off-shore ocean bottom broadband station, *EOS Trans. AGU*, Aug 28 issue, 2003.

Stakes, D., B. Romanowicz, J.P. Montagner, P. Tarits, J.F. Karczewski, S. Etchemendy, D. Neuhauser, P. McGill, J-C. Koenig, J.Savary, M. Begnaud and M. Pasyanos, MOISE: Monterey Bay Ocean Bottom International Seismic Experiment, *EOS Trans. AGU*, 79, 301-309, 1998.

Stutzmann, E., J.P. Montagner et al., MOISE: a prototype multiparameter ocean-bottom station, *Bull. Seism. Soc. Am.*, 81, 885-902, 2001.

Wielandt, E., and J. Steim, A digital very broad band seismograph, *Ann. Geophys.*, 4, 227-232, 1986.

Wielandt, E., and G. Streckeisen, The leaf spring seismometer: design and performance, *Bull. Seis. Soc. Am.*, 72, 2349-2367, 1982.

BDSN PSD Low Noise Synopsis (2003–2004)

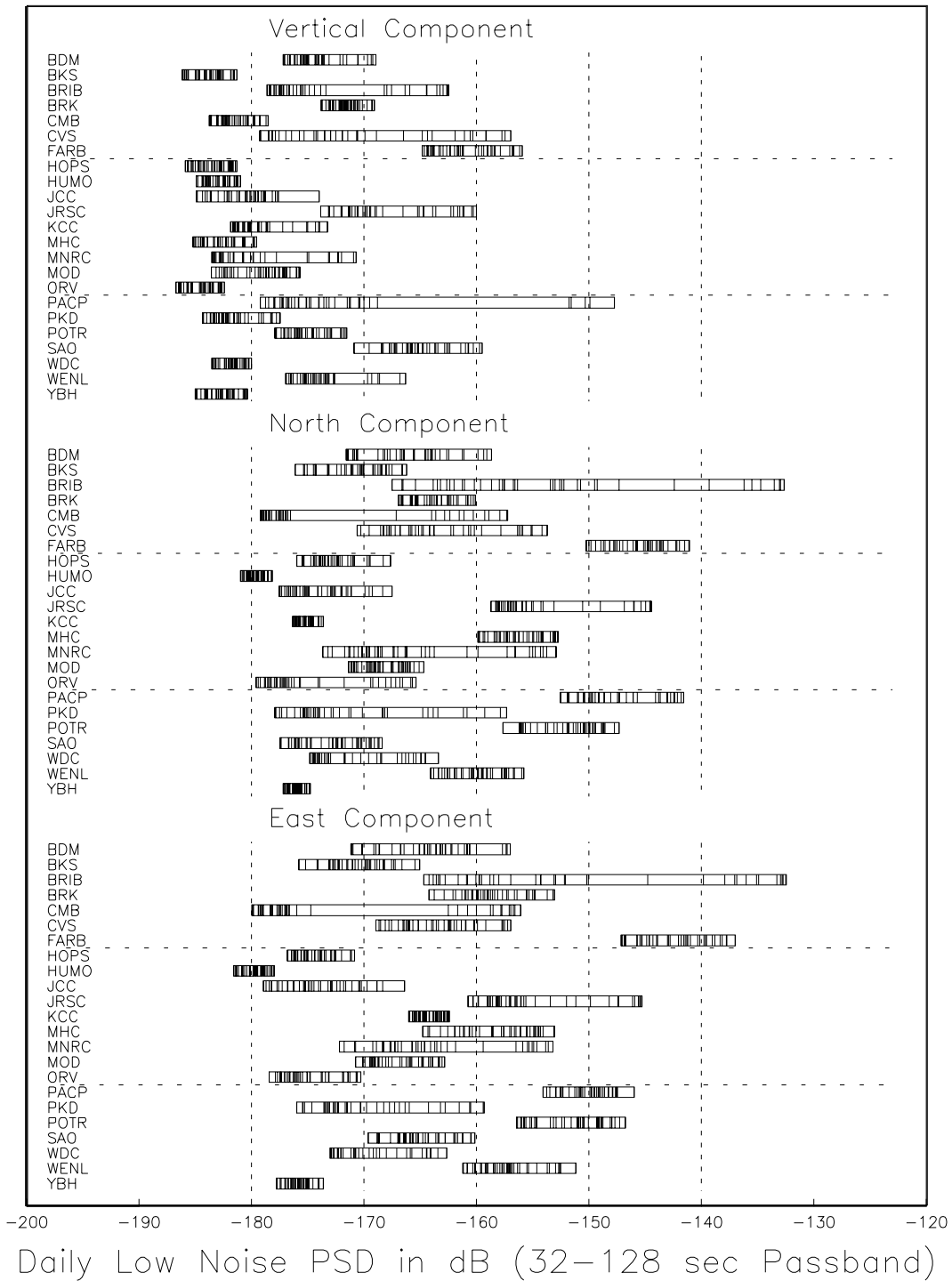


Figure 3.3: PSD noise analysis for BDSN stations, by channel, in the period range from 32-128 sec from 7/1/2003-6/30/2004. BRIB (situation in a shallow vault that is prone to tilting) and FARB (located on the Farallon Islands) stand out as sites with high noise levels. HUMO (located in an abandoned mine) stands out as an exceptionally quiet site.

2003.208.06:25 Mw 6.8, h=470km, BK.BHZ Waveforms

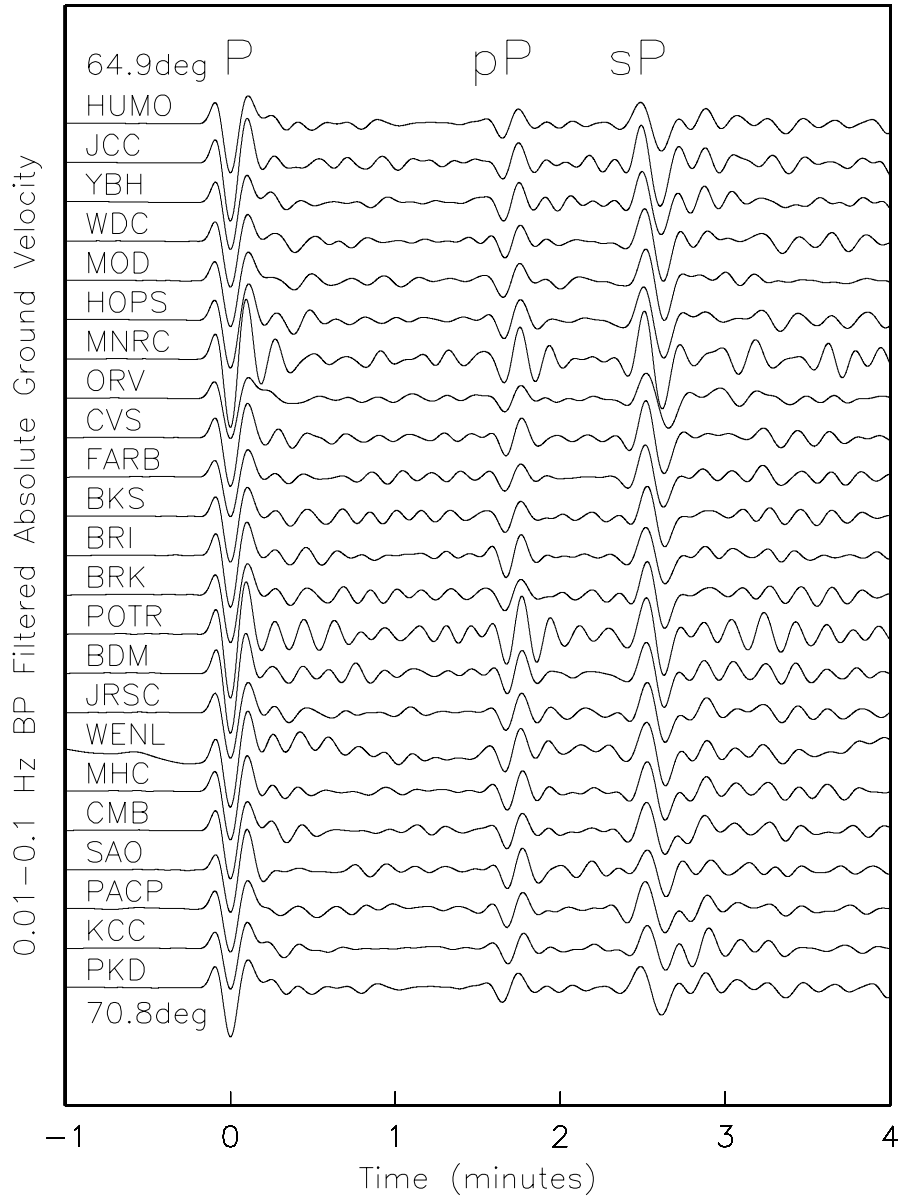


Figure 3.4: BDSN broadband vertical-component waveforms for a M_w 6.8 deep focus earthquake (470 km) which occurred in the Primor'ye, Russia region on July 27, 2003. This earthquake was felt in Hokkaido and Honshu, Japan. The waveforms were deconvolved to absolute ground velocity, 0.01-0.1 Hz band pass filtered, and plotted in order of increasing distance from HUMO at 64.9 degrees to PKD at 70.8 degrees. Shown are the P, pP, and sP body wave phases. Note that the body waves are highly similar across the BK network and that most noticeable differences are in the coda detail and the absolute amplitudes. This provides confirmation that the station transfer function and polarities are correct. The stations MNRC and POTR especially stand out in that their amplitudes are significantly larger than is observed at the other BDSN stations, owing primarily to their siting in the proximity of thick alluvial deposits which amplify the ground motions.

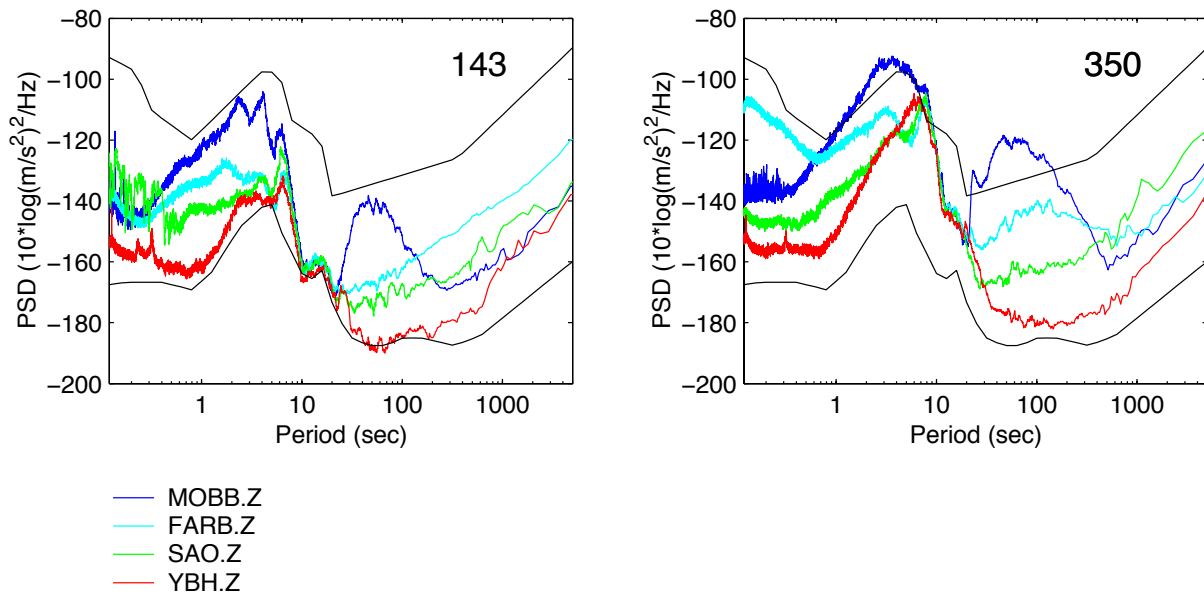


Figure 3.6: Comparison of noise recorded at MOBB and 3 other stations of the BDSN network, on two days in 2002 when no significant earthquake signals were recorded: a "quiet day" (143, left), and a "stormy" day (350, right), as assessed by the mean wave height recordings at a nearby NOAA buoy, located in Monterey Bay. Spectra were calculated using 4 hours of data. The USGS high- and low-noise models for land stations are shown in black (*Peterson, 1993*). Increased noise levels for periods between 20 and 300 sec, are observed at MOBB on both quiet and stormy days, as well as at the island station FARB on the stormy day. The noise level at MOBB between 10 and 20 sec is comparable to the land station YBH, one of the quietest stations of the BDSN. Note how the height and also the width of the infragravity noise band increases on stormy days.

Chapter 4

Northern Hayward Fault Network

1. Introduction

Complementary to the regional broadband network, a deployment of borehole-installed, wide-dynamic range seismographic stations is being established along the Hayward Fault and throughout the San Francisco Bay toll bridges network. This network is a cooperative development of the BSL and the USGS, with support from USGS, Caltrans, EPRI, the University of California Campus/Laboratory Collaboration (CLC) program, LLNL, and LBNL (Figure 4.1 and Table 4.1). Efforts at ongoing development of the network have also recently been enhanced by through coordinated efforts with the Mini-PBO project (Chapter 7, which is partially funded by NSF and by the member institutions of that project).

The purpose of the network is threefold: 1) to lower substantially the threshold of microearthquake detection, 2) to increase the recorded bandwidth for events along the Hayward fault, and 3) to obtain bedrock ground motion signals at the bridges from small earthquakes for investigating bridge responses to stronger ground motions. A lower detection threshold increases the resolution of the fault-zone seismic structure; allows seismologists to monitor the spatial and temporal evolution of seismicity at magnitudes down to $M \sim -1.0$, where earthquake rates are many times higher than those captured by surface sites; allows researchers to look for pathologies in seismicity patterns that may be indicative of the nucleation of large damaging earthquakes; and allows scientists to investigate fault and earthquake scaling, physics and processes in the San Francisco Bay Area. This new data collection will also contribute to improved working models for the Hayward fault. The bedrock ground motion recordings are also being used to provide input for estimating the likely responses of the bridges to large, potentially damaging earthquakes. Combined with the improved Hayward fault models, source-specific response calculations can be made, as well.

The Hayward Fault Network (HFN) consists of two parts. The Northern Hayward Fault Network (NHFN) is operated by the BSL and currently consists of 25 stations, including those located on Bay Area bridges and at

borehole sites of the Mini-PBO (MPBO) project. This network is considered part of the BDSN and uses the network code BK. The Southern Hayward Fault Network (SHFN) is operated by the USGS and currently consists of 5 stations. This network is considered part of the NCSN and uses the network code NC. This chapter is primarily focused on the NHFN and activities associated with the BSL operations.

2. NHFN Overview

The five MPBO sites have 3-component borehole geophone packages. All the remaining HFN sites have six-component borehole sensor packages. The packages were designed and fabricated at LBNL's Geophysical Measurement Facility by Don Lippert and Ray Solbau, with the exception of site SFAB. For the HFN sites, three channels of acceleration are provided by Wilcoxon 731A piezoelectric accelerometers and three channels of velocity are provided by Oyo HS-1 4.5 Hz geophones. Velocity measurements for the MPBO sites are provided by Mark Products L-22 2 Hz geophones (Table 4.2). The 0.1-400 Hz Wilcoxon accelerometers have lower self-noise than the geophones above about 25-30 Hz, and remain on scale and linear to 0.5 g. In tests performed in the Byerly vault at UC Berkeley, the Wilcoxon is considerably quieter than the FBA-23 at all periods, and is almost as quiet as the STS-2 between 1 and 50 Hz.

Sensors are generally installed at depths of about 100 m, but several sites have sensors emplaced at depths of over 200 m and the Dumbarton bridge sites have sensors at multiple depths (Table 4.1). During initial stages of the project, the NHFN sensors provided signals to on-site Quanterra Q730 and RefTek 72A-07 data loggers.

Today, twelve of the NHFN sites currently have Quanterra data loggers with continuous telemetry to the BSL. Similar to BDSN sites, these stations are capable of on-site recording and local storage of all data for more than one day and have batteries to provide backup power. Signals from these stations are digitized at a variety of data rates up to 500 Hz at 24-bit resolution (Table 4.3). In contrast to the BDSN implementation, the NHFN data

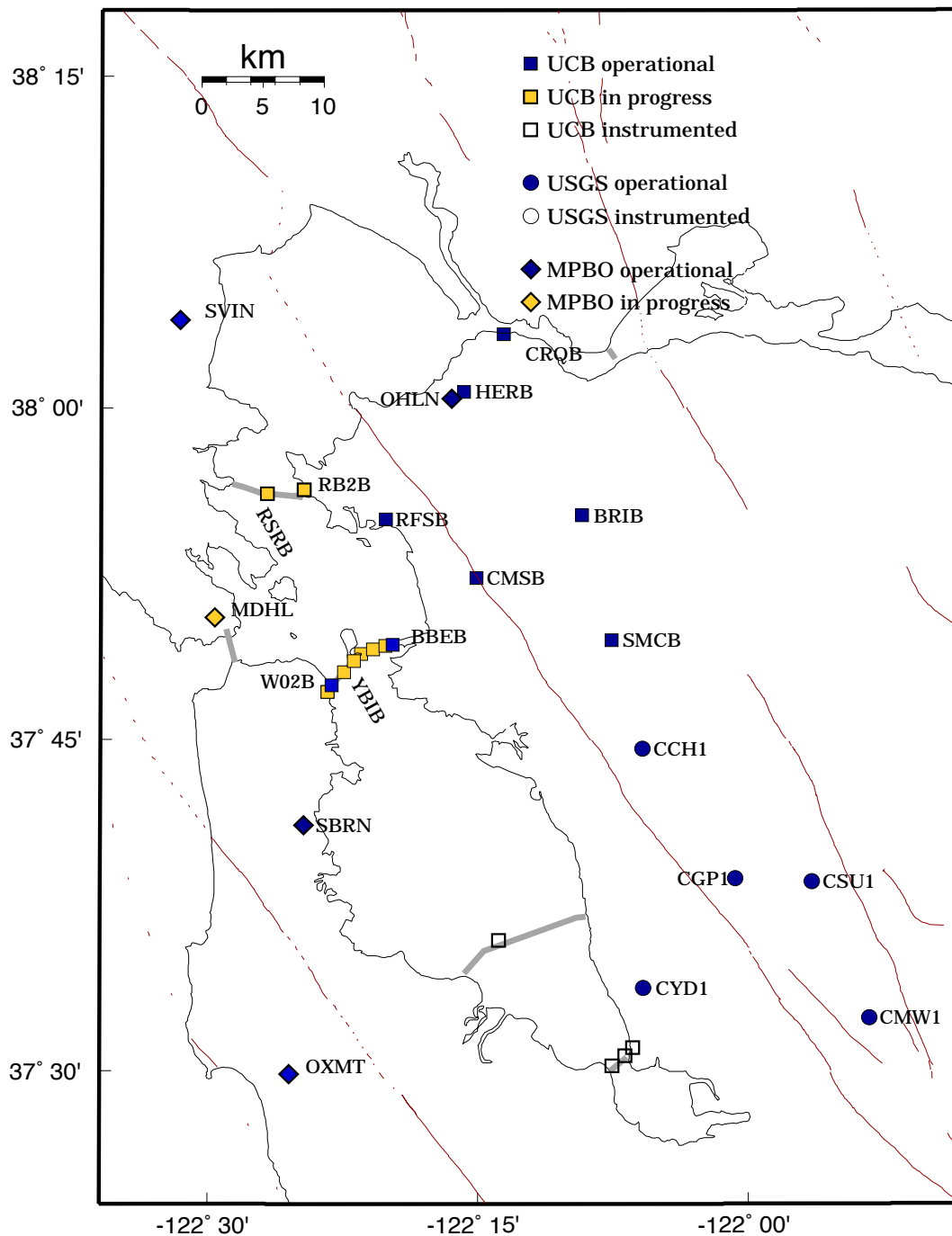


Figure 4.1: Map showing the locations of the HFN stations operated by the BSL (NHFN - squares) and the USGS (SHFN - circles) and Mini-PBO stations (diamonds) in the San Francisco Bay Area. Operational sites are filled, while sites in progress are grey. Other instrumented boreholes are indicated as open symbols.

loggers employ casual FIR filters at high data rates and acausal FIR filters at lower data rates. Because of limitations in telemetry bandwidth and disk storage, 8 of these sites transmit triggered data at 500 sps, using the Murdock, Hutt, and Halbert (MHH) event detection algorithm (*Murdock and Hutt, 1983*), and continuous data at reduced rates (100, 20 and 1 sps) to the BSL, while the four MPBO sites transmit continuous data at 100 sps (one MPBO site does not have telemetry yet).

The remaining 12 sites of the NHFN have in the past recorded data using RefTek data loggers. These sites do not have continuous telemetry for acquisition and required visits from BSL staff for data recovery. Collection of data from these sites has been discontinued, but efforts are underway to upgrade them with Quanterra Q4120 data loggers and continuous telemetry.

Signals from the 5 SHFN stations are digitized by Nanometrics data loggers at 100 sps and transmit continuous data to Menlo Park by radio. These digital data streams are processed by the Earthworm system with the NCSN data and waveforms are saved when the Earthworm detects an event.

Experience has shown that the MHH detector does not provide uniform triggering across the NHFN on the smallest events of interest. In order to insure the recovery of 500 sps data for these earthquakes, a central-site controller has recently been implemented at the BSL using the 500 sps vertical component geophone data for event detection. Originally the 100 sps vertical component geophone data was used for event detection but the bandwidth proved to be inadequate for detection of the smaller events where most of the seismic wave energy was at frequencies above 40 Hz. Triggers from this controller are being used to recover the 500 sps data from the NHFN data loggers.

Data from the NHFN and SHFN are archived at the NCEDC. At this time, the tools are not in place to archive the Hayward fault data together. The NHFN data are archived with the BDSN data, while the SHFN are archived with the NCSN data (Chapter 10). However, the new central-site controller will provide the capability to both include SHFN data in the event detection and extract SHFN waveforms for these events in the future.

As originally planned, the Hayward Fault Network was to consist of 24 to 30 stations, 12-15 each north and south of San Leandro, managed respectively by UCB and USGS. This is not happening quickly, although west of the fault, Caltrans has provided sites along the Bay bridges. This important contribution to the Hayward Fault Network has doubled the number of sites with instrumentation. At times, Caltrans provides holes of opportunity away from the bridges (e.g., HERB), so we have plans for additional stations that will bring the network geometry to a more effective state for imaging and real-time monitoring of the fault.

Sensor	Channel	Rate (sps)	Mode	FIR
Accelerometer	CL?	500.0	T	Ca
Accelerometer	HL?	100.0	C	Ca
Accelerometer	BL?	20.0	C	Ac
Accelerometer	LL?	1.0	C	Ac
Geophone	DP?	500.0	T	Ca
Geophone	EP?	100.0	C	Ca
Geophone	BP?	20.0	C	Ac
Geophone	LP?	1.0	C	Ac

Table 4.3: Typical data streams acquired at each NHFN site, with channel name, sampling rate, sampling mode and FIR filter type. C indicates continuous; T triggered; Ca causal; and Ac acausal. The 100 sps channels (EP & HL) are only archived when the 500 sps channels are not available.

As a check on the calibration and an example of the capabilities of a borehole installed network, we compare the bandpass filtered (0.4-4 Hz) ground velocity data recorded at NHFN and MPBO stations for a M 7.3 deep focus teleseism that occurred in the vicinity of the Fiji Islands at a depth of 582 km. in Figure 4.2.

3. 2003-2004 Activities

In addition to routine maintenance, operations and data collection; activities of the NHFN project over the past year have also included numerous efforts at network expansion, quality assurance, performance enhancement and catalog development.

3.1 Station Maintenance

Shown in Figure 4.3 are power spectral density (PSD) distributions of background noise for a sample of 8 NHFN land and bridge site stations. In general, background noise levels of the borehole HFN stations is more variable and generally higher than that of the Parkfield HRSN borehole stations (Figure 5.2). This is due in large part to the significantly greater level of cultural noise in the Bay Area, and to the fact that noise reduction efforts on the much more recently installed NHFN stations are still underway. For example the two noisiest stations (i.e. BBEB and W02) are located on the Bay Bridge which is currently undergoing earthquake retrofit and east span reconstruction. These stations have also only recently come back on-line with upgraded infrastructure and instrumentation, so the full complement of noise reduction modifications have not yet been completed.

On average the MPBO NHFN sites are more consistent and quieter (Figure 7.4). This is due in large part to the greater depth of the MPBO sensors, the locations of MPBO stations in regions of generally less industrial and other cultural noise sources, and possibly to the absence

Code	Net	Latitude	Longitude	Elev (m)	Over (m)	Date	Location
CRQB	BK	38.05578	-122.22487	-25.0	38.4	1996/07 - current	CB
HERB	BK	38.01250	-122.26222	-25.0	217.9	2000/05 - current	Hercules
BRIB	BK	37.91886	-122.15179	219.7	108.8	1995/07 - current	BR, Orinda
RFSB	BK	37.91608	-122.33610	-27.3	91.4	1996/01 - current	RFS, Richmond
CMSB	BK	37.87195	-122.25168	94.7	167.6	1994/12 - current	CMS, Berkeley
SMCB	BK	37.83881	-122.11159	180.9	3.4	1997/12 - current	SMC, Moraga
SVIN	BK	38.03325	-122.52638		158.7	2003/08 - current	MPBO, St. Vincent's school
OHLN	BK	38.00742	-122.27371		196.7	2001/07 - current	MPBO, Ohlone Park
MDHL	BK	37.84227	-122.49374		160.6	in progress	MPBO, Marin Headlands
SBRN	BK	37.68562	-122.41127		157.5	2001/08 - current	MPBO, San Bruno Mtn.
OXMT	BK	37.498	-122.425		194.2	2003/12 - current	MPBO, Ox Mtn.
BBEB	BK	37.82167	-122.32867		150.0	2002/05 - current	BB, Pier E23
E17B	BK	37.82086	-122.33534		160.0	1995/08 - current *	BB, Pier E17
E07B	BK	37.81847	-122.34688		134.0	1996/02 - current *	BB, Pier E7
YBIB	BK	37.81420	-122.35923	-27.0	61.0	1997/12 - current *	BB, Pier E2
YBAB	BK	37.80940	-122.36450		3.0	1998/06 - current *	BB, YB Anchorage
W05B	BK	37.80100	-122.37370		36.3	1997/10 - current *	BB, Pier W5
W02B	BK	37.79120	-122.38525		57.6	2003/06 - current	BB, Pier W2
SFAB	BK	37.78610	-122.3893		0.0	1998/06 - current *	BB, SF Anchorage
RSRB	BK	37.93575	-122.44648	-48.0	109.0	1997/06 - current *	RSRB, Pier 34
RB2B	BK	37.93	-122.41		133.8	2003/07 - current *	RSRB, Pier 58
SM1B	BK	37.59403	-122.23242		298.0	not recorded	SMB, Pier 343
DB3B	BK	37.51295	-122.10857		1.5	1994/09 - 1994/11	DB, Pier 44
					62.5	1994/09 - 1994/09	
					157.9	1994/07 - current *	
DB2B	BK	37.50687	-122.11566			1994/07 - current *	DB, Pier 27
					189.2	1992/07 - 1992/11	
DB1B	BK	37.49947	-122.12755		0.0	1994/07 - 1994/09	DB, Pier 1
					1.5	1994/09 - 1994/09	
					71.6	1994/09 - 1994/09	
					228.0	1993/08 - current *	
CCH1	NC	37.7432	-122.0967	226		1995/05 - current	Chabot
CGP1	NC	37.6454	-122.0114	340		1995/03 - current	Garin Park
CSU1	NC	37.6430	-121.9402	499		1995/10 - current	Sunol
CYD1	NC	37.5629	-122.0967	-23		2002/09 - current	Coyote
CMW1	NC	37.5403	-121.8876	343		1995/06 - current	Mill Creek

Table 4.1: Stations of the Hayward Fault Network. Each HFN station is listed with its station code, network id, location, operational dates, and site description. The latitude and longitude (in degrees) are given in the WGS84 reference frame. The elevation of the well head (in meters) is relative to the WGS84 reference ellipsoid. The overburden is given in meters. The start dates indicate either the upgrade or installation time. The abbreviations are: BB - Bay Bridge; BR - Briones Reserve; CMS - Cal Memorial Stadium; CB - Carquinez Bridge; DB - Dumbarton Bridge; MPBO - mini-Plate Boundary Observatory RFS - Richmond Field Station; RSRB - Richmond-San Rafael Bridge; SF - San Francisco; SMB - San Mateo Bridge; SMC - St. Mary's College; and, YB - Yerba Buena. The * for stations indicates that the stations are not currently recording data. RSRB is shut down while Caltrans is retrofitting the Richmond-San Rafael bridge (as of April 19, 2001) and YBIB has been off-line since August 24, 2000 when power cables to the site were shut down. Other off-line stations are in the process of being upgraded as funding for equipment becomes available. The table also includes 2 MPBO stations which became operational in the last 2 years, and 3 MPBO borehole sensors that have recently been installed.

of powered sensors (i.e. accelerometers) in their borehole sensor packages.

One of the most pervasive problems at NHFN sta-

tions equipped with the Q4120 data loggers is power line noise (60 Hz and its harmonics at 120, 180, and 240 Hz). This noise reduces the sensitivity of the MHH detectors.

Site	Geophone	Accelerometer	Z	H1	h2	Data logger	Notes	Telem.
CRQB	Oyo HS-1	Wilcoxon 731A	-90	251	341	Q4120		FR
HERB	Oyo HS-1	Wilcoxon 731A	-90	TBD	TBD	Q4120		FR
BRIB	Oyo HS-1	Wilcoxon 731A	-90	79	349	Q4120	Acc. failed, Dilat.	FR
RFSB	Oyo HS-1	Wilcoxon 731A	-90	256	346	Q4120		FR
CMSB	Oyo HS-1	Wilcoxon 731A	-90	19	109	Q4120		FR
SMCB	Oyo HS-1	Wilcoxon 731A	-90	76	166	Q4120	Posthole	FR
SVIN	Mark L-22		-90	298	28	Q4120	Tensor.	FR/Rad.
OHLN	Mark L-22		-90	313*	43*	Q4120	Tensor.	FR
MDHL	Mark L-22		-90	TBD	TBD	None at present	Tensor.	
SBRN	Mark L-22		-90	347	77	Q4120	Tensor.	FR
OXMT	Mark L-22		-90	163	253	Q4120	Tensor.	FR
BBEB	Oyo HS-1	Wilcoxon 731A	-90	TBD	TBD	Q4120	Acc. failed	Radio
E17B	Oyo HS-1	Wilcoxon 731A	-90	TBD	TBD	None at present		
E07B	Oyo HS-1	Wilcoxon 731A	-90	TBD	TBD	None at present		
YBIB	Oyo HS-1	Wilcoxon 731A	-90	257	347	None at present	Z geop. failed	FR/Rad.
YBAB	Oyo HS-1	Wilcoxon 731A	-90	TBD	TBD	None at present		
W05B	Oyo HS-1	Wilcoxon 731A	-90	TBD	TBD	None at present		
W02B	Oyo HS-1	Wilcoxon 731A	-90	TBD	TBD	Q4120		Radio
SFAB	None	LLNL S-6000	TBD	TBD	TBD	None at present	Posthole	
RSRB	Oyo HS-1	Wilcoxon 731A	-90	50	140	None at present	2 acc. failed	FR
RB2B	Oyo HS-1	Wilcoxon 731A	-90	TBD	TBD	None at present	1 acc. failed	
SM1B	Oyo HS-1	Wilcoxon 731A	-90	TBD	TBD	None at present		
DB3B	Oyo HS-1	Wilcoxon 731A	-90	TBD	TBD	None at present	Acc. failed	
DB2B	Oyo HS-1	Wilcoxon 731A	-90	TBD	TBD	None at present		
DB1B	Oyo HS-1	Wilcoxon 731A	-90	TBD	TBD	None at present	Acc. failed	
CCH1	Oyo HS-1	Wilcoxon 731A	-90	TBD	TBD	Nanometrics HRD24	Dilat.	Radio
CGP1	Oyo HS-1	Wilcoxon 731A	-90	TBD	TBD	Nanometrics HRD24	Dilat.	Radio
CSU1	Oyo HS-1	Wilcoxon 731A	-90	TBD	TBD	Nanometrics HRD24	Dilat.	Radio
CYD1	Oyo HS-1	Wilcoxon 731A	-90	TBD	TBD	Nanometrics HRD24	Dilat.	Radio
CMW1	Oyo HS-1	Wilcoxon 731A	-90	TBD	TBD	Nanometrics HRD24	Dilat.	Radio

Table 4.2: Instrumentation of the HFN as of 06/30/2004. Every HFN downhole package consists of co-located geophones and accelerometers, with the exception of MPBO sites. 6 HFN sites also have dilatometers (Dilat.) and the 5 MPBO sites have tensor strainmeters (Tensor.) 12 NHFN sites have Quanterra data loggers with continuous telemetry to the BSL. The remaining sites are being upgraded to Quanterra data loggers. The 5 SHFN sites have Nanometrics data loggers with radio telemetry to the USGS. The orientation of the sensors (vertical - Z, horizontals - H1 and H2) are indicated where known or identified as "to be determined" (TBD). The azimuths of the horizontal component geophones have a 180 degree ambiguity owing to the dead vertical component geophone.

Whenever a NHFN station is visited, the engineer at the site and a seismologist at the BSL work together to expedite the testing process, especially when attempting to identify and correct ground-loop faults which generally induce significant 60, 120, 180, and 240 Hz seismic signal contamination due to stray power line signal pickup, generally inductively coupled and aggravated by the presence of ground loops.

Below is a synopsis of maintenance efforts performed over the past year for several NHFN stations that gives some idea of the ongoing maintenance and performance enhancing measures that we are continuing to implement.

Geophone Calibrations

Comparisons of the inferred ground accelerations generated by local earthquakes, from co-sited HFN geophone and accelerometer pairs, shows that the waveforms generally are quite coherent in frequency and phase response but that their inferred ground accelerations differ significantly. At times the amplitudes differ by up to a factor of 2 while the times of the peak amplitudes are identical. This implies that the free period and damping of the geophones are well characterized and also that the generator constant is not accurate (assuming that the corresponding ground accelerations inferred from the accelerometers are accurate).

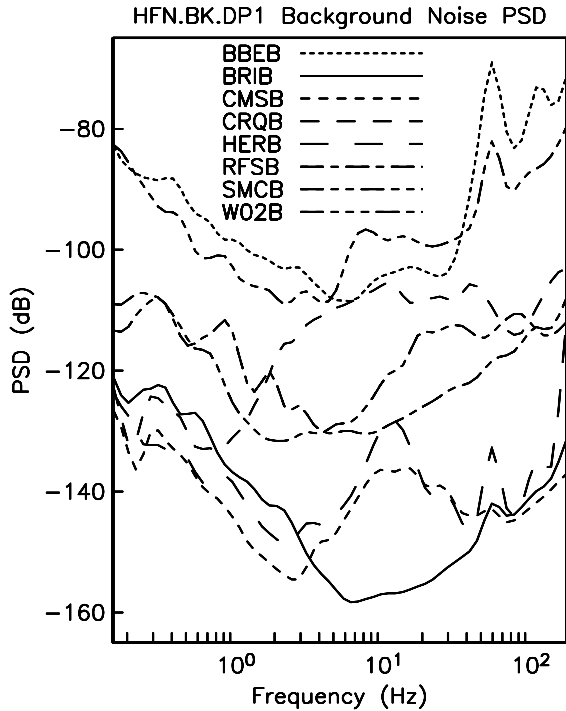


Figure 4.3: Plot showing the HFN.BK.DP1 background noise, PSD, for 8 of the NHFN stations. Plotted are the background low-noise PSD estimates. Ten minutes of .BK.DP1 data starting at 2003.225.0900 (2 AM PDT) were used in the analysis. Note that there is considerable variation in the general level and structure of the individual station background noise PSD estimates. Some of the stations show peaks at 60 Hz and its harmonics while others have a high average background level. The two bridge sites, BBEB and W02B are the noisiest while land site BRIB in Briones Regional Park (well away from the heavy cultural noise of the more populated region of the Bay Area) is the quietest. Two stations, CMSB and HERB show a peak in the 20-30 Hz range. The peak at CMSB is probably due to excitation of modes in the open bore hole and the peak at HERB is due to excitation of the local structure by the adjacent railway line and highways 4 and 80. The three stations in the middle of the group (RFSB, SMCB and CRQB) are responding to the local cultural noise. There are numerous ongoing experiments at the Richmond Field Station which are affecting the noise level at RFSB, CRQB is sited near a sewage treatment plant and the Carquinez bridge, and SMCB is currently only installed at post hole depth (3.5 m) on the St. Mary's campus.

Generally speaking, the accelerometers, being an active device, are more accurate and also more stable than the geophones so it is reasonable to assume that the most likely reason for the difference is that the assumed genera-

tor constants for the geophones are not accurate. *Rodgers et al.* (1995) describe a way to absolutely calibrate the geophones in situ and to determine their generator constant, free period and fraction of critical damping. The only external parameter that is required is the value of the geophones inertial mass.

We have built a calibration test box which allows us to routinely perform the testing described by *Rodgers et al.* whenever site visits are made. The box drives the signal coil with a known current step and rapidly switches the signal coil between the current source and the data logger input. From this information, expected and actual sensor response characteristics can be compared and corrections applied. Also, changes in the sensor response over time can be evaluated so that adjustments can be made and pathologies arising in the sensors due to age can be identified. Once a geophone is absolutely calibrated, we can also check the response of the corresponding accelerometer.

We are now performing the initial calibration tests and response adjustments for all NHFN stations as sites are visited for routine maintenance. We also plan a scheduled re-tests of all sites to monitor for sensor response changes through time.

NHFN Station Maintenance Synopsis

The NHFN station hardware has proven to be quite reliable and half of the currently operating stations (BRIB, CMSB, CRQB and SMCB) did not require a site visit during the past year. The following stations were visited to perform various maintenance and/or repair operations.

BBEB: Prepped BBEB hardware for installation of station at pier E7. Data will be telemetered from pier E7 to BBEB via FreeWave 900 MHz radio and forwarded by the Q4120 to the BSL via 2.4 GHz radio along with the BBEB data. Ran Wilan radio tests on simultaneous links to BBEB and W02B.

HERB: Revamped the FRAD power supply and installed a twist-lock plug on the input power cable.

RFSB: Upgraded Q4120 data logger with installation of Q730PWR board and new software. Set battery charge voltage to 13.6 Vdc. Upgraded Q730 with software version is MS001122AL.bo, and config version is mscfg011004.lzh. Changed Q730 datalogger configuration of the B?? channels from 20 Hz to 40 Hz in support of USArray.

W02B: Installed grounding clamp and changed wiring to reduce 60 Hz noise on velocity channel. Extended DC cables of AC adapters for the FRAD and Cylink radio so that they will reside in the battery box instead of the electronics box. Replaced blown fuse on battery positive cable with a 7.5A. Realigned and securely clamped antenna at McCone roof end of the W02B telemetry link to stop it from moving in high winds. Changed the AC

power adapter on the McCone master Cylink radio. Encountered problems with GPS clock not locking and subsequently fixed problem using Quanterra supplied procedure to reset the GPS clock.

3.2 New Installations

San Francisco-Oakland Bay Bridge

The infrastructure at seven stations along the San Francisco-Oakland Bay Bridge (SFAB, W02B, W05B, YBAB, E07B, E17B, and BBEB) was upgraded with the installation of weatherproof boxes, power, and telemetry in anticipation of installing Q4120 data loggers and telemetering the data back to Berkeley. BBEB was brought on-line in May of 2002, and W02B in June of 2003.

Land Sites

Agreements with Caltrans and St. Mary's college have been made to replace the post hole installation at St. Mary's college (SMCB) with a deep borehole installation. The hole is to be drilled by Caltrans as a hole of opportunity when the schedule of a Caltrans drilling crew has an opening. The site has been reviewed by UCB, Caltrans and St. Mary's college personnel, and we are now in the drilling queue. Depending on the geology at borehole depth, this site may either become a MPBO site (w/o accelerometers) or a standard land site installation including both geophones and accelerometers.

Caltrans has also provided funding for instrumentation of several other land sites which we will install as future Caltrans drill time becomes available. Currently we are considering sites for these additional holes-of-opportunity at Pt. Pinole, on Wildcat Mtn. in the north Bay. We are in the process of obtaining permission from the East Bay Regional Park District (EBRPD) to site a HFN station at the Point Isabel Regional Shoreline.

Mini-PBO

The stations of the Mini-PBO project (Chapter 7) are equipped with borehole seismometers. As these stations have become operational, they augment HFN coverage (Figure 4.1). In the last year, SVIN and SBRN have added coverage to the north bay and east side of the south bay, respectively.

3.3 Data Analysis and Results

Combined Catalog

We are building a HF-specific data archive from the existing waveform data that have been collected by the heterogeneous set of recording systems in operation along the Hayward fault (i.e. the NHFN, SHFN, NCSN, and BDSN continuous and triggered waveforms). Recently

we have taken the NHFN triggers collected during operations between 1995.248 and 1998.365 (recorded on portable RefTek recorders) and origin times from the Northern California catalog for this time period and undertaken a massive association of event and trigger times. The purpose of the effort is to compile a relatively uniform catalog of seismic data to low magnitudes and extending back in time to the beginning of reliable HFN data collection. The process has reduced nearly a million individual time segments to 316 real events along the Hayward fault during the period—an increase in the number of events of a factor of about 2.5 to 3 over the Northern California catalog alone in the same area.

Event Detection

As noted in the Introduction, one of the purposes of the HFN is to lower the threshold of microearthquake detection. Towards this goal, we have been developing new algorithms: a pattern recognition approach to identify small events; a phase onset time detector with sub-sample timing resolution, and; a phase coherency method for single component identification of highly similar events.

Pattern Recognition: In order to improve the detection and analysis of small events (down to $M_L \sim -1.0$) some specialized algorithms are being developed. The Murdock-Hutt detection algorithms used by MultiSHEAR, which basically flags an event whenever the short-term average exceeds a longer-term average by some threshold ratio, is neither appropriate for nor capable of detecting the smallest seismic events. One solution is to use a pattern recognition approach to identify small events associated with the occurrence of an event which was flagged by the REDI system. Tests have indicated that the pattern recognition detection threshold is $M_L \sim -1.0$ for events occurring within ~ 10 km of a NHFN station. The basic idea is to use a quarter second of the initial P-wave waveform, say, as a master pattern to search for similar patterns that occur within \pm one day, say, of the master event. Experimentally, up to six small CMSB recorded events, at the $M_L \sim -1.0$ threshold and occurring within \pm one day of a master pattern, have been identified.

The pattern recognition method is CPU intensive, however, and it will require a dedicated computer to handle the pattern recognition tasks. To expedite the auto-correlation processing of the master pattern, an integer arithmetic cross-correlation algorithm has been developed which speeds up the requisite processing by an order of magnitude.

Phase Onset Time Detection: The phase onset time detector makes use of the concept that the complex spectral phase data, over the bandwidth of interest (i.e., where the SNR is sufficiently high), will sum to a minimum at the onset of an impulsive P-wave. The algorithm searches for the minimum phase time via phase shifting in

the complex frequency domain over the bandwidth where the SNR is above 30 dB, say, to identify the onset time of the seismic phase. The algorithm requires that the recorded waveforms be deconvolved to absolute ground displacement. This implicitly requires that any acausality in the anti-aliasing filtration chain, such as the FIR filters used in the BDSN Quanterra data loggers, be removed. The algorithm typically resolves P-wave onset times to one-fiftieth of the sample interval or better.

Phase Coherency: A spectral phase coherency algorithm was developed to facilitate high resolution quantification of the similarities and differences between highly similar Hayward fault events which occur months to years apart. The resolution of the complex spectral phase coherency methodology is an order of magnitude better than the cross correlation method which is commonly used to identify highly similar events with resolution of order a few meters. This method, originally developed using NHFN borehole data, is now being applied as well to data from another borehole network (the HRSN) to provide more rapid and objective identification of the large fraction (approx. 40%) of characteristically repeating microearthquakes that occur at Parkfield, CA.

Orinda Sequence

On October 19 and 20, 2003, two earthquakes with M_L 3.5 and 3.4 occurred ENE of Orinda, CA. Fortunately, their hypocenters were located almost directly below the northern HFN borehole station at Briones (BRIB). While the automatic system report depths of approximately 10 km for these two events, the S-P times at BRIB indicates that they must be located at depths of less than 5 km. More than 4000 fore- and aftershocks were recorded, during the first week of the sequence, with magnitudes down to -2. At the beginning of December, 2003 the aftershocks were continuing at a rate of six per day with a M_d 2.9 occurring on January 1, 2004.

This sequence, which has events spanning six orders of magnitude, is ideal for testing the pattern recognition, phase onset time detection and phase coherence algorithms discussed above.

4. Acknowledgements

Thomas V. McEvelly, who passed away in February 2002, was instrumental in developing the Hayward Fault Network, and without his dedication and hard work the creation and continued operation of the NHFN would not have been possible.

Under Bob Nadeau's, Bob Uhrhammer's and Doug Dreger's general supervision, Rich Clymer, Wade Johnson, Doug Neuhauser, Bill Karavas, John Friday, and Dave Rapkin all contribute to the operation of the NHFN. Bob Nadeau, Bob Uhrhammer and Lind Gee contributed to the preparation of this chapter.

Partial support for the NHFN is provided by the USGS through the NEHRP external grant program. Expansion of the NHFN has been made possible through generous funding from Caltrans, with the assistance of Pat Hipley. Larry Hutchings of LLNL has been an important collaborator on the project.

5. References

Rogers, P.W., A.J. Martin, M.C. Robertson, M.M. Hsu, and D.B. Harris, Signal-Coil Calibration of Electromagnetic Seismometers, *Bull. Seism. Soc. Am.*, 85(3), 845-850, 1995.

Murdock, J., and C. Hutt, A new event detector designed for the Seismic Research Observatories, *USGS Open-File-Report 83-0785*, 39 pp., 1983.

2004/07/25 14:35 UT Mw 7.3 P-wave

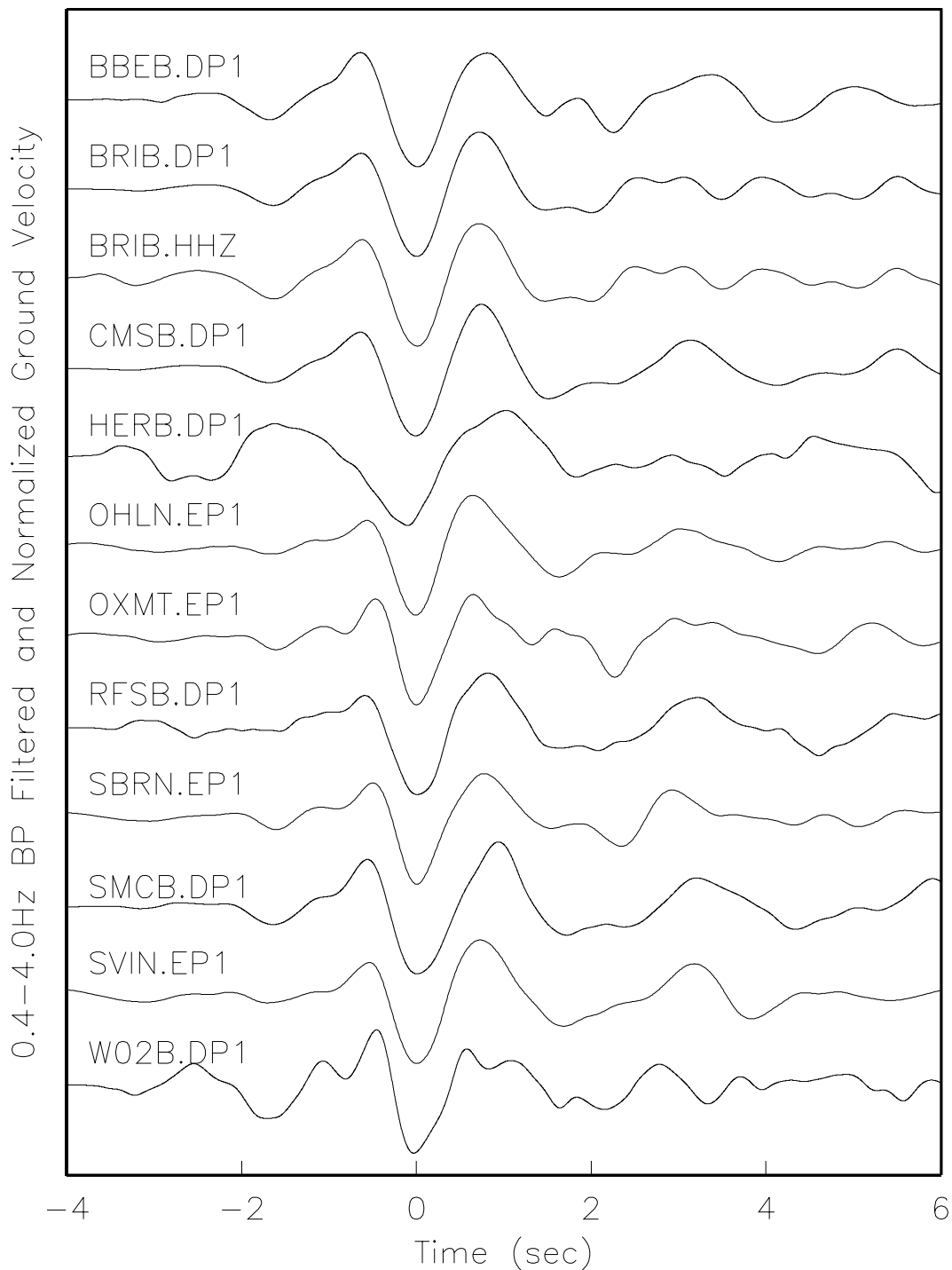


Figure 4.2: Plot of the P-wave waveforms, recorded by the NHFN/MPBO borehole stations, for a major deep focus Fiji Islands earthquake (2004/07/25,14:35 UT; 582 km deep; M_w 7.3; 8514 km S55W of Berkeley). The waveform data were deconvolved to ground velocity, 0.4-4.0 Hz band pass filtered to enhance the P-wave signal and normalized prior to plotting. For comparison, the traces were time shifted to align the P-wave on the dominant trough (at 0 seconds) except at HERB and W02B where the time shift was estimated from the apparent slowness of the P-wave. The waveforms are highly similar at all stations except HERB where the geophone response is problematic and W02B where there the trace was inverted for plotting. For reference, the BRIB.HHZ (surface) broadband recorded waveform (third trace) is also shown.

Chapter 5

Parkfield Borehole Network

1. Introduction

The operation of the High Resolution Seismic Network (HRSN) at Parkfield, California began in 1987, as part of the U.S. Geological Survey initiative known as the Parkfield Prediction Experiment (PPE) (*Bakun and Lindh, 1985*).

Figure 5.1 shows the location of the network, its relationship to the San Andreas fault, sites of significance from previous and ongoing research using the HRSN, double-difference relocated earthquake locations from 1987-1998.5, routine locations of seismicity since August 2002, and the epicenter of the 1966 M6 earthquake that motivated the PPE. The HRSN records exceptionally high-quality data, owing to its 13 closely spaced three-component borehole sensors (generally emplaced in the extremely low attenuation and background noise environment at 200 to 300 m depth (Table 5.1)), its high-frequency wide bandwidth recordings (0-100 Hz), and its low magnitude detection threshold (below magnitude -1.0).

Several aspects of the Parkfield region make it ideal for the study of small earthquakes and their relationship to tectonic processes. These include the fact that the network spans the expected nucleation region of a repeating magnitude 6 event and a significant portion of the transition from locked to creeping behavior on the San Andreas fault, the availability of three-dimensional P and S velocity models (*Michelini and McEvilly, 1991*), the existing long-term HRSN seismicity catalogue that is complete to very low magnitudes and that includes at least half of the M6 seismic cycle, a well-defined and simple fault segment, and a homogeneous mode of seismic energy release as indicated by the earthquake source mechanisms (over 90% right-lateral strike-slip).

In a series of journal articles and Ph.D. theses, we have presented the cumulative, often unexpected, results of U.C. Berkeley's HRSN research efforts (see: http://www.seismo.berkeley.edu/seismo/faq/parkfield_bib.html). They trace the evolution of a new and exciting picture of the San Andreas fault zone responding to its plate-boundary loading, and they are forcing new thinking on the dynamic processes and condi-

tions within the fault zone at the sites of recurring small earthquakes.

More recently, the Parkfield area has become an area of focus of the Earthscope Project (<http://www.earthscope.org>) through the San Andreas Fault Observatory at Depth (SAFOD) experiment (<http://www.icdp-online.de/sites/sanandreas/news/news1.html>). SAFOD is a comprehensive project to drill into the hypocentral zone of repeating $M \sim 2$ earthquakes on the San Andreas Fault at a depth of about 3 km. The goals of SAFOD are to establish a multi-stage geophysical observatory in close proximity to these repeating earthquakes, to carry out a comprehensive suite of downhole measurements in order to study the physical and chemical conditions under which earthquakes occur and to exhume rock and fluid samples for extensive laboratory studies (*Hickman et al., 2004*).

2. HRSN Overview

2.1 1986 - 1998

Installation of the HRSN deep (200-300m) borehole sensors initiated in 1986 and recording of triggered 500 sps earthquake data began in early 1987. The HRSN sensors are 3-component geophones in a mutually orthogonal gimbaled package. This ensures that the sensor corresponding to channel DP1 is aligned vertically and that the others are aligned horizontally. In November 1987, the Varian well vertical array was installed and the first VSP survey was conducted, revealing clear S-wave anisotropy in the fault zone (*Daley and McEvilly, 1990*). During 1988, the original 10 station network was completed which included a deep (572 m) sensor from the Varian well string. Data from network stations was telemetered into a central detection/recording system operating in triggered mode. Also in 1988 the Varian string system was slaved, for about two years, to the Vibroseis control signals, allowing simultaneous recording of vibrator signals on both systems. For several years beginning in 1991, low-gain event recorders (from PASSCAL) were installed at several of the sites to extend the dynamic range from about M_L 1.5 to M_L about 4.5.

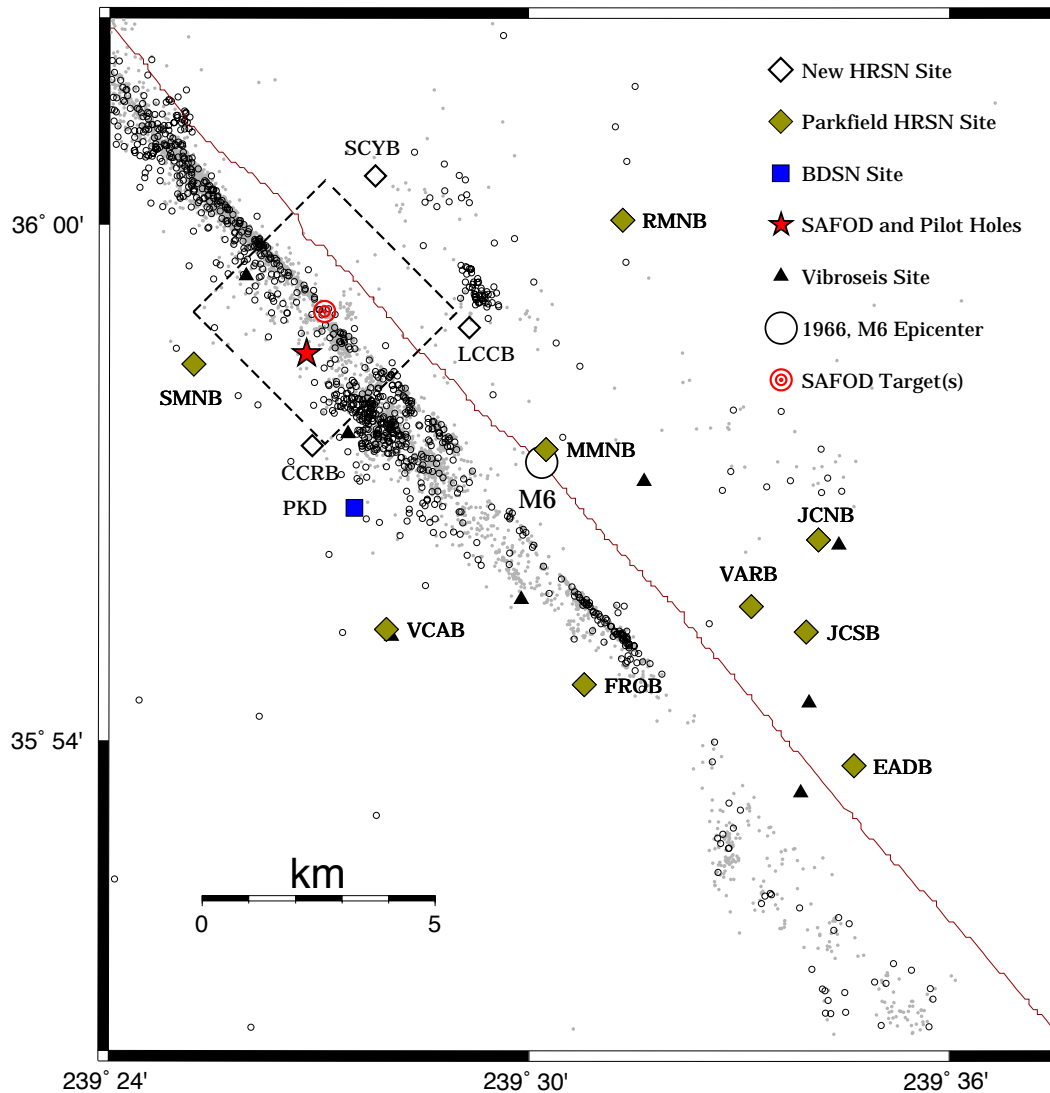


Figure 5.1: Map showing the San Andreas Fault trace, the location of the original 10 Parkfield HRSN stations (filled diamonds) and the 3 new sites (open diamonds) installed to enhance coverage around the SAFOD facility. Station GHIB (Gold Hill, not shown) is located on the San Andreas Fault about 8 km to the Southeast of station EADB. The location of the BDSN broadband station PKD is also shown (filled square). The location of the SAFOD pilot hole and main drill site are shown by the filled star. Location of the 2 alternative M2 repeating earthquake targets (70 meters apart) are shown as concentric circles. Because of the SAFOD experiment, the 4 km by 4 km dashed box surrounding the SAFOD zone is a region of particular interest to BSL researchers. The epicenter of the 1966 M6 Parkfield main shock is located at the large open circle. Routine locations of earthquakes recorded by the expanded and upgraded 13 station HRSN are shown as open black circles. Locations of events recorded by the earlier vintage 10 station HRSN, relocated using an advanced 3-D double-differencing algorithm applied to a cubic splines interpolated 3-D velocity model (*Michelini and McEvilly, 1991*), are shown as gray points. The locations of the 8 source points for the Vibroseis wave propagation monitoring experiment (*Karageorgi et al., 1992, 1997*) are represented by small black triangles.

The data acquisition system operated quite reliably until late 1996, when periods of unacceptably high down time developed. During this period, as many as 7 of the remote, solar-powered telemetered stations were occasionally down simultaneously due to marginal solar generation capacity, old batteries, and recording system outages of a week or more were not uncommon. In July 1998, the original data acquisition system failed permanently. This system was a modified VSP recorder acquired from LBNL, based on a 1980- vintage LSI-11 cpu and a 5 MByte removable Bernoulli system disk with a 9-track tape drive, configured to record both triggered microearthquake and Vibroseis data (Vibroseis discontinued in 1994, *Karageorgi et al.*, 1997). The system was remote and completely autonomous, and data tapes were mailed about once a month to Berkeley for processing and analysis. The old system also had a one-sample timing uncertainty and a record length limitation because the tape write system recovery after event detection was longer than the length of the record, leaving the system off-line after record termination and until write recovery was completed.

2.2 1998 - 1999

In December 1998, the original HRSN acquisition system was replaced by 10 stand-alone PASSCAL RefTek systems with continuous recording. To process these data, development of a major data handling procedure will be required, in order to identify the microearthquakes down to $M = -1$, since continuous telemetry to the Berkeley Seismological Laboratory (BSL) and application of a central site detection scheme was not an option at that time.

In July 1999, the network was reduced to four RefTeks at critical sites that would ensure continuity in monitoring at low magnitudes and the archive of characteristic events for studying the evolution of their recurrence intervals. Properties of the 10 original sites are summarized in Table 5.2.

2.3 Upgrade and SAFOD Expansion

Thanks to emergency funding from the USGS NEHRP, we replaced the original 10-station system with a modern 24-bit acquisition system (Quanterra 730 4-channel digitizers, advanced software using flash disk technology, spread-spectrum telemetry, Sun Ultra 10/440 central processor at the in-field collection point, with 56K frame-relay connectivity to Berkeley) in 2001. The new system is now online and recording data continuously at a central site located on California Department of Forestry (CDF) fire station property in Parkfield.

We have also added three new borehole stations, with NSF support, at the NW end of the network as part of the SAFOD project to improve resolution of the structure,

Sensor	Channel	Rate (sps)	Mode	FIR
Geophone	DP?	250.0	T and C	Ca
Geophone	BP?	20.0	C	Ac

Table 5.3: Data streams currently being acquired at each HRSN site. Sensor type, channel name, sampling rate, sampling mode, and type of FIR filter are given. C indicates continuous; T triggered; Ac acausal; Ca causal. "??" indicates orthogonal vertical and 2 horizontal components.

kinematics and monitoring capabilities in the SAFOD drill-path and target zones. Figure 5.1 illustrates the location of the drill site, the new borehole sites, and locations of earthquakes recorded by the initial and upgraded/expanded HRSN.

The three new SAFOD stations have a similar configuration as the original upgraded 10 station network and include an additional channel for electrical signals. Station descriptions and instrument properties are summarized in Tables 5.1 and 5.2. All HRSN Q730 data loggers employ FIR filters to extract data at 250 and 20 Hz (Table 5.3).

The remoteness of the drill site and new stations required an installation of an intermediate data collection point at Gastro Peak, with a microwave link to the CDF facility. The HRSN stations use SLIP to transmit TCP and UDP data packets over bidirectional spread-spectrum radio links between the on-site data acquisition systems and the central recording system at the CDF. Six of the sites transmit directly to a router at the central recording site. The other seven sites transmit to a router at Gastro Peak, where the data are aggregated and transmitted to the central site over a 4 MBit/second digital 5.4 GHz microwave link. All HRSN data are recorded to disk at the CDF site.

The upgraded and expanded system is compatible with the data flow and archiving common to all the elements of the BDSN/NHFN and the NCEDC, and is providing remote access and control of the system. It is also providing data with better timing accuracy and longer records, which are to eventually flow seamlessly into NCEDC. The new system also solves the problems of timing resolution, dynamic range, and missed detections, in addition to providing the added advantage of conventional data flow (the old system recorded SEG Y format).

Because of limitations in bandwidth, a modified version of the REDI system (Chapter 9) is used to detect events in the HRSN data, extract waveform triggers, and transmit the waveform segments to the BSL. However, the December 22, 2003 San Simeon earthquake and its aftershocks sent the HRSN into nearly continuous triggering. As a result, BSL staff disabled the transmission of triggered data.

Site	Net	Latitude	Longitude	Surf. (m)	Depth (m)	Date	Location
EADB	BP	35.89525	-120.42286	466	245	01/1988 -	Eade Ranch
FROB	BP	35.91078	-120.48722	509	284	01/1988 -	Froelich Ranch
GHIB	BP	35.83236	-120.34774	400	63	01/1988 -	Gold Hill
JCNB	BP	35.93911	-120.43083	527	224	01/1988 -	Joaquin Canyon North
JCSB	BP	35.92120	-120.43408	455	155	01/1988 -	Joaquin Canyon South
MMNB	BP	35.95654	-120.49586	698	221	01/1988 -	Middle Mountain
RMNB	BP	36.00086	-120.47772	1165	73	01/1988 -	Gastro Peak
SMNB	BP	35.97292	-120.58009	699	282	01/1988 -	Stockdale Mountain
VARB	BP	35.92614	-120.44707	478	572	01/1988 - 08/19/2003	Varian Well
VARB	BP	35.92614	-120.44707	478	298	08/25/2003 -	Varian Well
VCAB	BP	35.92177	-120.53424	758	200	01/1988 -	Vineyard Canyon
CCRB	BP	35.95718	-120.55158	595	251	05/2001 -	Cholame Creek
LCCB	BP	35.98005	-120.51424	640	252	08/2001 -	Little Cholame Creek
SCYB	BP	36.00938	-120.53660	945	252	08/2001 -	Stone Canyon

Table 5.1: Stations of the Parkfield HRSN. Each HRSN station is listed with its station code, network id, location, date of initial operation, and site description. The latitude and longitude (in degrees) are given in the WGS84 reference frame, the surface elevation (in meters) is relative to mean sea level, and the depth to the sensor (in meters) below the surface. Coordinates and station names for the 3 new SAFOD sites are given at the bottom.

Site	Sensor	Z	H1	H2	RefTek 24	RefTek 72-06	Quanterra 730
EADB	Mark Products L22	-90	170	260	01/1988 - 12/1998	12/1998 - 07/1999	03/2001 -
FROB	Mark Products L22	-90	338	248	01/1988 - 12/1998	12/1998 - 07/1999	03/2001 -
GHIB	Mark Products L22	90	failed	unk	01/1988 - 12/1998	12/1998 - 07/1999	03/2001 -
JCNB	Mark Products L22	-90	0	270	01/1988 - 12/1998	12/1998 - 06/2001	03/2001 -
JCSB	Geospace HS1	90	300	210	01/1988 - 12/1998	12/1998 - 07/1999	03/2001 -
MMNB	Mark Products L22	-90	175	265	01/1988 - 12/1998	12/1998 - 06/2001	03/2001 -
RMNB	Mark Products L22	-90	310	40	01/1988 - 12/1998	12/1998 - 07/1999	03/2001 -
SMNB	Mark Products L22	-90	120	210	01/1988 - 12/1998	12/1998 - 06/2001	03/2001 -
VARB	Litton 1023	90	15	285	01/1988 - 12/1998	12/1998 - 07/1999	03/2001 -
VCAB	Mark Products L22	-90	200	290	01/1988 - 12/1998	12/1998 - 06/2001	03/2001 -
CCRB	Mark Products L22	-90	N45W	N45E	-	-	05/2001 -
LCCB	Mark Products L22	-90	N45W	N45E	-	-	08/2001 -
SCYB	Mark Products L22	-90	N45W	N45E	-	-	08/2001 -

Table 5.2: Instrumentation of the Parkfield HRSN. Most HRSN sites have L22 sensors and were originally digitized with a RefTek 24 system. After the failure of the WESCOMP recording system, PASSCAL RefTek recorders were installed. In July of 1999, 6 of the PASSCAL systems were returned to IRIS and 4 were left at critical sites. The upgraded network uses a Quanterra 730 4-channel system. For the three new stations (bottom) horizontal orientations are approximate (N45W and N45E) and will be determined more accurately as available field time permits.

At present, all continuous 20 sps data streams and 7 vertical component channels at 250 sps are telemetered to the BSL and archived on the NCEDC in near-real-time. All continuous 250 sps data are migrated periodically from HRSN computer in Parkfield to DLT tape. These tapes are then mailed periodically to the BSL and then are processed for archiving at the NCEDC.

A feature of the new system that has been particularly useful both for routine maintenance and for pathology identification has been the internet connectivity of the central site processing computer and the station data loggers with the computer network at BSL. Through this connection, select data channels and on-site warning messages from the central site processor are sent directly to BSL for evaluation by project personnel. If, upon these evaluations, more detailed information on the HRSN's performance is required, additional information can also be remotely accessed from the central site processing computer at Parkfield. Analysis of this remotely acquired information has been extremely useful for trouble shooting by allowing field personnel to schedule and plan the details of maintenance visits to Parkfield. The connectivity also allows certain data acquisition parameters to be modified remotely when needed, and commands can be sent to the central site computer and data loggers to modify or restart processes when necessary.

The network connectivity also allows remote monitoring of the background noise levels being recorded by the HRSN stations. For example shown in Figure 5.2 are power spectral density plots of background noise for vertical components of the 7 HRSN stations that are most critical for monitoring seismicity in the region containing SAFOD. The PSD analysis gives a rapid assessment of the HRSN seismometer responses across their wide bandwidth. By routinely generating these plots with data telemetered from Parkfield, changes in the seismometer responses, often indicating problems with the acquisition system, can be easily identified, and corrective measures can then be planned and executed on a relatively short time-frame.

3. 2003-2004 Activities

Over the past year, activities associated with the operation of the HRSN primarily involved five components: 1) routine operations and maintenance of the network, 2) enhancement of the network's performance for detection and recording of very low amplitude seismic signals, 3) repair of the severed 48 pair cable at the VARB site, 4) collaborative integration and analysis of HRSN and SAFOD's temporary deployments for refining the structure and target location estimates in the SAFOD drill path, 5) data processing and analysis of the pre-San Simeon, and post-San Simeon data.

3.1 Operations and Maintenance

In addition to the routine maintenance tasks required to keep the HRSN in operation, various refinements and adjustments to the networks infrastructure and operational parameters have been needed this year to enhance the HRSN's performance and to correct for pathologies that continue to manifest themselves in the recently upgraded and expanded system.

Smaller scale maintenance issues addressed this year include cleaning and replacement of corroded electrical connections, grounding adjustments, cleaning of solar panels, re-seating, resoldering and replacement of faulty pre-amp circuit cards, and the testing and replacement of failing batteries. Larger efforts included the implementation of periodic emergency generator tests, replacement of the central site air conditioning unit, a major insulation, painting and power enhancement effort at our Gastro Peak repeater site to address problems with outages and low power during cold weather, and a switch to an alternative sensor on the VARB station deep string due to the failure of one of the 1877' deep sensor components.

3.2 Enhancing HRSN Performance

Over the past year significant efforts were made to identify and reduce noise problems arising from the new and expanded data acquisition system. Detection, monitoring, and high-resolution recording of earthquakes down to the smallest possible magnitudes with the highest possible signal-to-noise (especially in the region of the proposed SAFOD drilling) is a major objective of the HRSN data collection effort. Consequently, elimination of all sources of unnaturally occurring system noise is a primary goal. The minimization of data loss due to station outages and data-dropouts is also critical to this objective.

The HRSN data acquisition involves integration of a number of distinct components at each station (i.e., sensor, pre-amp, solar panels, solar regulator, batteries, Freewave radio, antenna, lightning arresters, and associated cabling, connectors and grounds) and radio telemetry apparatus between the seismic stations, telemetry relay stations, and the central processing site on the CDF site in Parkfield.

This complex integration of station and communication components combined with a variety of associated concerns (e.g., ground loops, cable resistances, radio feedback into recording equipment at stations, radio interference between stations, marginal line of site paths, cloud cover and solar power, the integration of older (pre-upgrade) hardware components with new components, old component deterioration and failures, and malfunctioning and unexpected performance characteristics of newer components) all make identification of specific causes of network generated (i.e. artificial) noise difficult to identify.

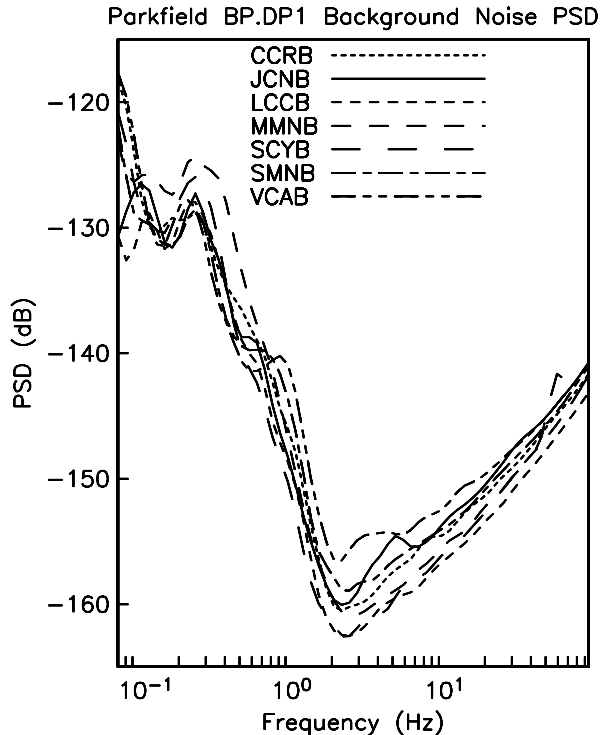


Figure 5.2: Background noise PSD plot for the seven continuously telemetered BP.DP1 data streams from Parkfield. The data are 20 minute samples starting at 2003.225.0900 (2 AM PDT). The plots show the background noise PSD as a function of frequency for the highest available sampling rate (250 sps) vertical component data which are continuously telemetered to Berkeley. Note the relatively low PSD levels and the overall consistency for all the HRSN stations. By comparison, the PSD curves among the borehole Northern Hayward Fault Network land and bridge stations are much more variable and show a generally higher background noise level (Figure 4.3). On the other hand, PSD curves for the MPBO stations of the NHFN are much more consistent with the HRSN PSD's (Figure 7.4). The differences among the various station PSD's can, in large part, be explained by the relative cultural noise levels at the various stations, by the depth of the borehole sensors, and by whether the boreholes remain open holes (noisier) or have been filled with cement. The 2 Hz minimum in the PSD plots for the HRSN sensor results from the 2 Hz sensors used at these sites. Below 2 Hz, noise levels rise rapidly and the peak at 3 sec (.3 Hz) is characteristic of teleseismic noise observed throughout California. In the 2 to 5 Hz range, VCAB and JCNB have historically shown higher background noise which is believed to result from excitation modes in the local structure. A small 60 Hz blip can be seen in the SCYB curve due to its close proximity to a power-line.

Exhaustive and iterative testing of HRSN performance has identified two primary causes for observed artificial noise remaining in the system (i.e. solar regulator spiking and pre-amp self-noise generation). Over the past year we have designed and have implemented fixes for these problems.

Solar Regulators

Regularly occurring spikes occurring during the daylight hours were observed in the continuous data streams and found to be due to the solar regulators. We have tested a variety of solar regulator designs and have identified the Prostar 30 as having the optimal cost-benefit. We have purchased and installed several of these devices at several of the HRSN sites with the ultimate goal of installing the Prostar's at all the HRSN stations as time and funding permit.

Pre-amplifier Noise

We found that a significant source of artificial noise was coming from the station pre-amplifiers. In the upgraded system, pre-amps from the older network were used. During integration of the older pre-amps with the increased dynamic range capabilities of the 24-bit Quanterra system, gain settings of the pre-amps were reduced from $\times 10,000$ to $\times 80$ in order to match signal sensitivity of the new system with the older one. While these lower pre-amp gain levels are still within the operational design of the pre-amps, they are no longer in their optimal range and a significant contribution of preamp's self-generated noise is present in the recorded seismograms. Initially, this was not expected to be a significant problem. However, we have subsequently found that even the small increase in pre-amp noise that results from the pre-amp gain reduction significantly impacts the sensitivity of the network for detecting and recording the smallest locatable events.

Figure 5.3 shows the pre-amp noise reduction effect observed on background noise signals at three vertical components of the HRSN when gains are raised from $\times 80$ to $\times 1,000$. Considerable signal hash is seen at gain levels of $\times 80$ (top waveform in each station pair), and significantly reduced when gains are increased to $\times 1,000$ (lower waveforms). Since we are also interested in recording large earthquakes on-scale, simply increasing gain levels on all stations is not the preferred solution, since doing so causes the recording system to saturate at much lower magnitudes. Instead we are attempting to redesign the pre amps using modern components to reduce the noise levels at the lower gain levels. However our attempts at redesign have not yet yielded satisfactory results.

Since a primary objective of the HRSN is to monitor the evolving patterns of the numerous small earthquakes that occur at very low magnitudes, and since this objective also complements the scientific objectives

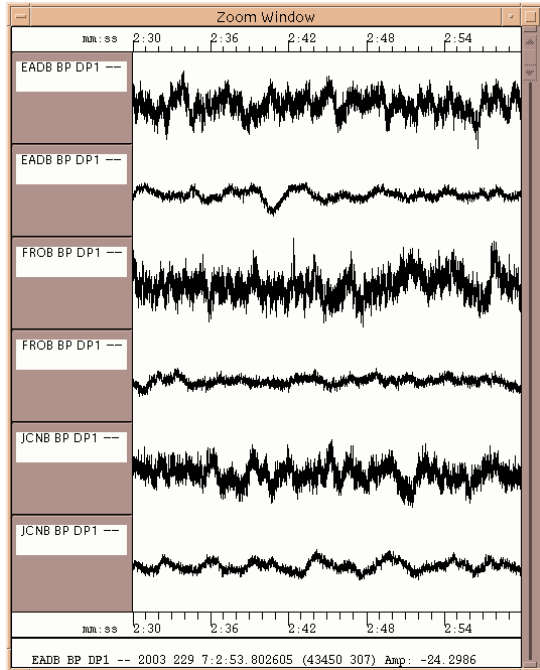


Figure 5.3: Preamp noise reduction test. Shown are 30 seconds of vertical background signal recorded at stations EADB, FROB and JCNB on day 229 of 2003 at 0700 UTC (top of station pairs, recorded at x80 gain and scaled up by 1000/80 for comparison to the x1000 preamp gain levels) and 0700 UTC on day 233 (bottom of station pairs, recorded at x1000 preamp gain). Note the substantial reduction in background noise, due primarily to the lower preamp generated noise at higher preamp gain.

of the recently funded SAFOD experiment, the pre-amp noise problem was a priority maintenance item. We have opted, therefore, to raise the gain levels for the near-term on all the station pre-amps from x80 to x1,000. By early October of 2003, these gain changes were implemented at all 13 HRSN stations. Plans are to continue investigating pre-amp redesigns until a suitable alternative is found at which time we will install the new pre-amps and lower the pre-amp gain back to x80—allowing both the increased detection of small events and the on-scale recording of events up to about magnitude 4 to 4.5.

3.3 Repairs at VARB

In August 2003, we observed problems with the recording of data at VARB, located at the Varian well site. After contacting the USGS field technician at Parkfield we learned that the sensor cable to the seismic string down the Varian well had been severed as part of a cleanup ef-

fort at the site. This activity not only cut the connection to the 1877' deep sensor, but also severed connection to the full seismic string of functional seismometers and accelerometers that existed down the deep VARB borehole.

During joint planning of the cleanup effort, we made it clear that it was important to retain connectivity to the seismic sensors at VARB, and the importance of this fact was acknowledged by the USGS personnel managing the effort. Subsequent plans for the cleanup specified coordination of the effort with field personnel from UC Berkeley. Unfortunately, BSL staff were not notified of the cleanup date, nor the specifics of the cleanup plan (which apparently included severing the deep strings cable at the well head and of course we would have loudly objected to).

Because VARB has the deepest HRSN borehole sensor and is centrally located within the network, it is a critical site for the HRSN. In addition at that time, we were in the process of preparing VARB and all the HRSN stations to make high-gain recordings of the controlled source shots from the SAFOD related 50 km line experiment to aid in characterizing the velocity and Fault Zone Guided Wave propagation structure in the region around SAFOD. Needless to say, the loss of VARB severely hampered these efforts. The situation was further complicated by the details of how the Varian well cable disconnect was made.

It was important for a number of scientific reasons to reconnect our VARB acquisition system to a sensor of known depth. However, there are 48 pairs of wires in the severed seismic string cable, and unfortunately, the mapping of these wires to their corresponding sensors was not documented when the cable was severed. In addition because the cable was severed at the well head, some 100' of trenching and cable was needed to reconnect the sensor and recording installation.

The estimated cost for the additional man-hours, parts, travel and lodging needed to do the necessary repairs at VARB was several thousand dollars. With emergency funding from NEHRP and assistance from the USGS field technician at Parkfield, we put VARB back on-line and made the high-gain HRSN adjustments in time for the 50 km line experiment shots.

3.4 SAFOD Collaboration

An intensive and ongoing effort by the SAFOD target event location working group is underway with its goals being: 1) the characterization of the detailed velocity and seismicity structure in the crustal volume containing the SAFOD main hole and 2) to determine the most accurate estimates of the absolute locations of SAFOD's target events. As part of this effort, a series of coincident active and passive source seismic experiments was performed during Oct. - Nov. of 2003. The HRSN data played a key role in this effort by providing complementary seismic

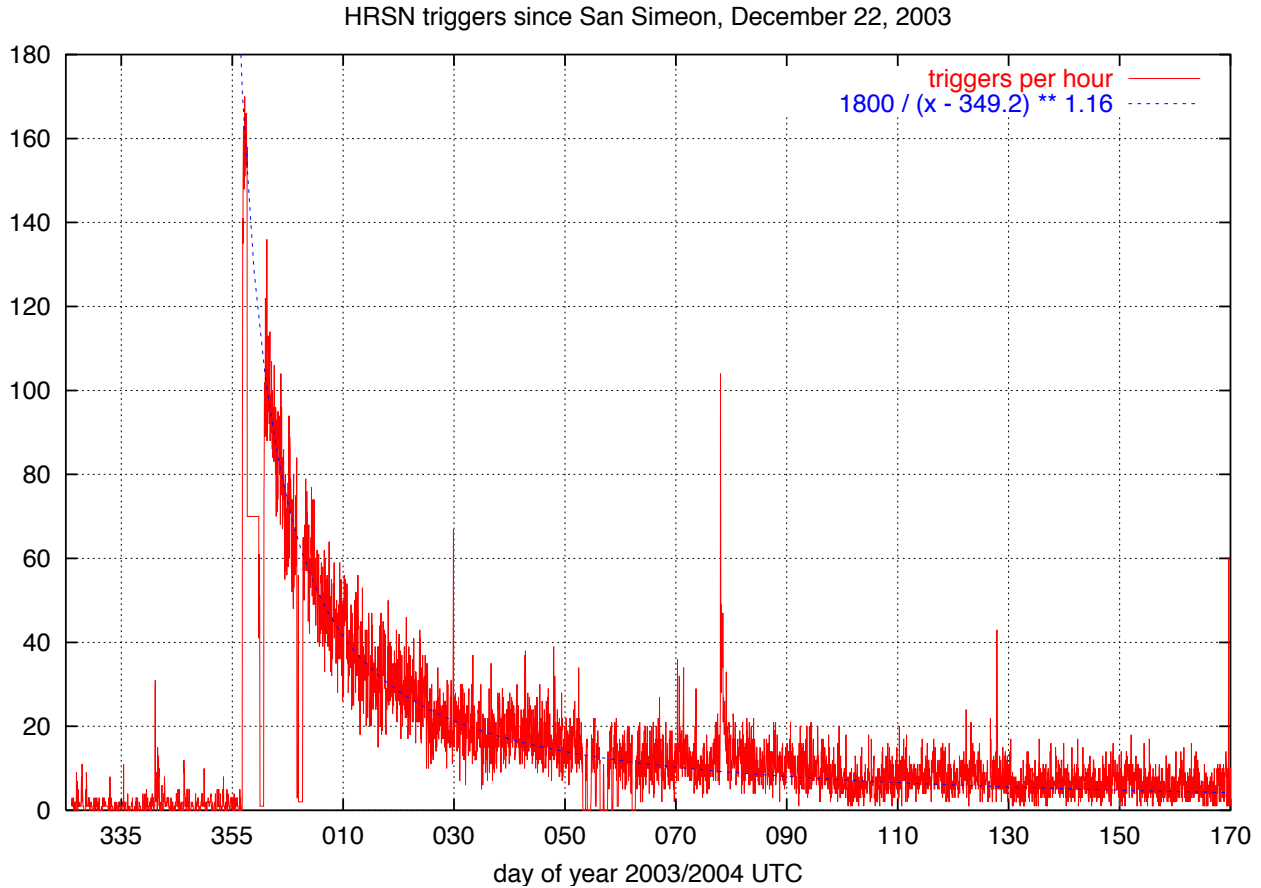


Figure 5.4: Shown are the number of triggers per hour for a period between 1 month prior to and 6 months following the San Simeon earthquake, and an "eyeball" fit of the decay curve (dashed curve). The cumulative number of HRSN triggers in the first 5 months following San Simeon exceeds 70,000 and trigger levels continued to be over 200 triggers per day through June of 2004. Extrapolation of the decay curve fit indicates that daily trigger levels will not return to near pre-San Simeon levels until well into 2005 (assuming no other large earthquakes in the area occur).

waveform data from the active sources and by providing a backbone of earthquake detection, waveform, and location data from the numerous microearthquakes that occurred within the SAFOD local zone during the Oct. 15 through Nov. 11 experimental period (256 events within 5 km of the SAFOD target(s)).

In a special section of Geophysical Research Letters from May of 2004, several papers make significant use of the HRSN data for characterizing the SAFOD area and illustrate the role that the HRSN data have played in the SAFOD effort over the past year (e.g., *Oye et al.*, 2004; *Roecker et al.*, 2004; *Thurber et al.*, 2004; *Nadeau et al.*, 2004).

3.5 Data Analysis and Results

Monitoring the evolution of microseismicity, particularly in the SAFOD drilling and target zone, is a primary objective of the HRSN project. In addition, the contin-

ued analysis of the HRSN data for determining detailed seismic structure, for the study of similar and characteristic microearthquake systematics, for estimation of deep fault slip rate evolution, and for various studies of fault zone and earthquake physics is also of great interest to seismologists. Before advanced studies of the Parkfield microseismicity can take place, however, initial processing, analysis and routine cataloging of the earthquake data must be done. An integral part of this process is quality control of the processed data, including a final check of the routine catalog results. The numerous aftershocks from the M6.5 San Simeon earthquake (Figure 5.4) have seriously complicated the tasks of initial processing, analysis and location of the routine event catalog. And, a significant revision of the "traditional" processing scheme we have used since 1987 will be required to deal with the post-San Simeon data. We have requested funding for this effort in a proposal to EarthScope, and if

granted our intent is to more fully develop, test and implement the new procedures for processing of these data.

Most of our efforts during the 2000-2002 were spent on implementing the emergency upgrade and SAFOD expansion of the HRSN, and routine processing of the data collected during that period was deferred until after upgrade and installation efforts were completed. In 2003 we began in earnest the task of routine processing of the ongoing data that was being collected. Our initial focus was on refining and developing our processing procedures to make the task more efficient and to ensure quality control of the processed catalogs. We also began working back in time to fill in the gap that developed during the deferment period. Because routine processing of the post-San Simeon data is effectively impossible at this time, because of the overwhelming number of aftershocks, we have suspended our efforts at processing the ongoing data and focused our efforts at filling in the complete gap of unprocessed data (i.e., back to March of 2001). Outlined below in the "Pre-San Simeon Processing" subsection are the procedures and issues related to this effort. In the subsequent subsection we illustrate and discuss briefly the issues that need to be addressed in order to process the post-San Simeon event data.

Pre-San Simeon Processing

Initial Processing. Continuous data streams on all 38 HRSN components are recorded at 20 and 250 sps on disk on the local HRSN computer at the CDF facility. The 20 sps data are transmitted continuously to the Berkeley Seismological Laboratory (BSL) over a frame-relay link and then archived at the NCEDC. In addition, the vertical component channels for the 7 stations critical to resolving seismicity in the SAFOD area are also being transmitted continuously to the BSL at 250 sps over the frame relay-circuit for purposes of quality control and fine tuning the triggering algorithm for the detection of the smallest possible events around SAFOD. These telemetered 250 sps data are archived on disk for only about 1 week at the BSL and are then deleted. When the local HRSN computer disk space is full, the continuous 250 sps data on the HRSN local computer are migrated onto DLT tape, and the tapes sent to Berkeley for long-term storage and for data upload to the NCEDC archive in some cases.

Shortly after being recorded to disk on the central site HRSN computer, event triggers for the individual station data are determined and a multi-station trigger association routine then processes the station triggers and identifies potential earthquakes. For each potential earthquake that is detected, a unique event identification number (compatible with the NCEDC classification scheme) is assigned. Prior to San Simeon earthquake of December 22, 2003, 30 second waveform segments were then collected for all stations and components and saved to

local disk as an event gather, and event gathers were then periodically telemetered to BSL and included directly into the NCEDC earthquake database (dbms) for analysis and processing.

An ongoing effort has been the development of a new earthquake detection scheme, with the goal of routinely detecting SAFOD area events to magnitudes below -1.0. A first cut version of the new scheme has been implemented and is currently detecting real earthquakes at an increased rate—nearly 3 times the number of earthquakes detected before the upgrade. In order to facilitate the processing and archiving of the increased number of potential earthquakes (~ 350 per month), the BSL has recently developed a Graphical User Interface (GUI). The GUI is integrated with the NCEDC dbms and allows review of the waveforms from every potential event. Initial analysis of the data using the GUI involves review of the waveforms and classification of the event as an earthquake or non-earthquake. The GUI also allows the analyst to log potential network problems that become apparent from the seismograms. The HRSN analyst then classifies the earthquakes as either a local, distant-local, regional, or teleseismic event and then systematically hand picks the P- and S-phases for the local and distant local events (for the period Sept. 2002 - Aug. 2003 the number of picked events was ~ 2000).

Picking of the numerous microearthquake events is no mean task. On average about 7 P-phases and 4 S-phases are picked for each event, putting the total number of annual phase picks for the HRSN data on the order of to 22,000. We have experimented with algorithms that make initial auto-picks of the phase arrivals, but have so far found picking by hand to be significantly more accurate and has the added advantage of allowing the analyst to assess the state of health of each station-component. In all our tests, autopicks have also invariably resulted in some missed events and catalog locations that are significantly more scattered and with higher residuals than locations done with purely hand-picked data.

A peculiarity of processing very small earthquake data, is that multiple events commonly occur within a few seconds of one another. The close timing of these events does not allow the local triggering algorithm to recover from one event before another occurs. As a result, the central site processor often does not trigger uniquely for each event. In such cases only one, 30 sec waveform gather and one earthquake identifier will be created for all the events. These multiple earthquake records (MER) account for only 3 to 5% of the total seismicity recorded by the HRSN. However, there are times when this rate rises to over 10%. In order to assign each event in an MER a unique event identifier for the NCEDC dbms and to make picking and automated processing of these events more manageable an additional feature of the GUI was developed that allows the analyst to "clone" MER into

separate gathers for each event.

Quality Control. Once false triggers have been removed and picks for the local and distant local events have been completed, quality control on the picks is made to ensure that all picks have phase and weights assigned, that extraneous characters have been removed from the pick files, that double station-phase picks have not inadvertently been made, and that no repicks of the same event had been accidentally made during any cloning that was performed. Initial locations are then performed and phase residuals analyzed in order to determine whether severe pick outliers must be removed or adjusted. Unstable location solutions based on events with few picks are also assessed to see if the addition of marginal phases will improve the stability of the location determination. After any required pick adjustments have been made, the events are then relocated, and combined with error information to allow ranking of the confidence of location quality.

These procedures have all been put in place and tested for the new HRSN configuration. Currently we have located 13 months of local earthquakes recorded by the new HRSN (over 2200 events) and are moving backwards in time to pick and locate the earlier data collected since March of 2001. We currently have enough data and are confident enough with the procedures to begin organizing the locations for formal inclusion into the NCEDC dbms and dissemination to the community. These efforts are now underway. We are also in the early stages of establishing a scalar seismic moment catalog for the new HRSN events that is also to be included in the NCEDC dbms.

Catalog Assessment. We continue to examine the earthquake data in search of possible earthquake precursors. This includes quality control and evaluation of the routine earthquake catalog locations and analyses of the spatial and temporal distribution of the microseismicity in relation to the occurrence of larger earthquakes in the area and heightened alert levels declared as part of the Parkfield Prediction Experiment. The new data and event detection scheme allows complete event detection down to \sim magnitude 0.0. As a result, the rate of earthquake detection by the HRSN exceeds that of the NCSN by about a factor of 5 in the 30 km stretch of the SAF centered at the location of the 1966 M6 Parkfield event (Figure 5.1). The additional rate of HRSN event detection significantly increases both the spatial and temporal resolution of the changing seismicity patterns and provide unique additional information on the earthquake pathology at very low magnitudes.

Post-San Simeon Data

Because of its mandate to detect and record very low magnitude events in the Parkfield area, the HRSN is extremely sensitive to changes in very low amplitude seis-

mic signals. As a consequence, in addition to detecting very small local earthquakes at Parkfield, the HRSN also detects numerous regional events. Since the beginning of the network's data collection in 1987, the local and regional events were discriminated based on analyst assessment of S-P times, and only local events with S-P times less than \sim 2.5 sec at the first arriving station were picked and located as part of the HRSN routine catalog.

Following the occurrence of the M6.5 San Simeon earthquake on December 22, of 2003, the long-standing data handling procedure outlined in the previous section was no longer viable due to the enormous rate of San Simeon aftershock detections (Figures 5.5 and 5.6). In the first 5 months following the mainshock, over 70,000 event detections were made by the HRSN system (compared to a yearly average detection rate of 6000 prior to San Simeon), and spot checks of the continuous 20 sps data revealed that the overwhelming majority of these detections resulted from seismic signals generated by San Simeon's aftershocks.

Data from the California Integrated Seismic Network (CISN) show that there were \sim 1,150 San Simeon aftershocks with magnitudes $>$ 1.8 occurring in the week following the mainshock. During this same period, the number of event detections from the HRSN was \sim 10,500 (compared to an average weekly for the year prior to San Simeon of 115 detections/per week). This suggests that the HRSN is detecting San Simeon aftershocks well below magnitude 1, despite the network's \sim 50 km distance from the mainshock (Figures 5.5 and 5.6).

The dramatic increase in event detections vastly exceeded the HRSN's capacity to process both the continuous and triggered event waveform data. To prevent the loss of seismic waveform coverage, processing of the triggered waveform data has been suspended to allow archiving of the 250 sps continuous data to tape to continue uninterrupted. Cataloging of the event detection times from the modified REDI real-time system algorithm is also continuing, and the 250 sps waveform data is currently being periodically uploaded from the DLT tapes onto the NCEDC for access to the research community. Research funding has also been requested from NSF-EarthScope to develop and apply new techniques to process these continuous data with the aim of identifying the Parkfield local events from among the San Simeon aftershocks and of compiling waveform and location catalogs for the local earthquakes.

4. Acknowledgements

Thomas V. McEvelly, who passed away in February 2002, was the PI on the HRSN project for many years. Without his dedication the creation and of the HRSN would not have been possible. Under Bob Nadeau's and Doug Dreger's general supervision, Rich Clymer, Bob

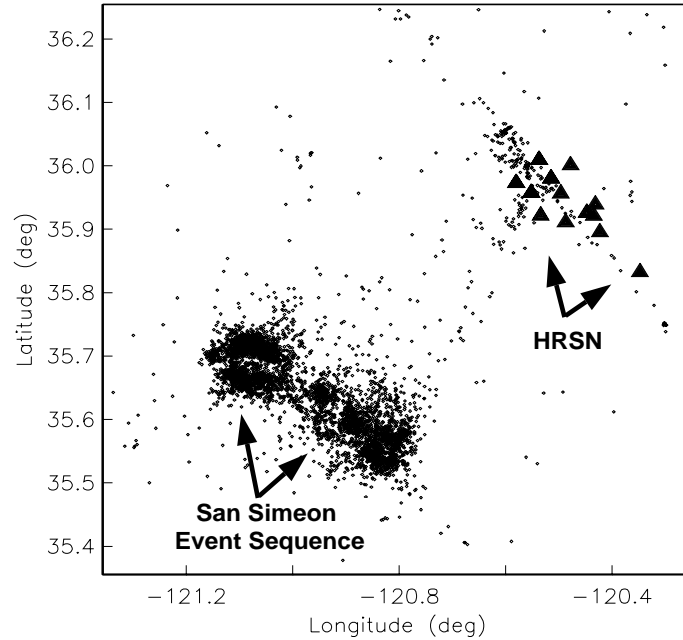


Figure 5.5: Earthquake locations of 5847 events in the San Simeon and Parkfield areas of California occurring between December 1, 2003 and April 1, 2004, inclusive (small black circles). Locations are from the Northern California Seismic Network catalog. Black triangles are the stations of the borehole High Resolution Seismic Network (HRSN). The M6.5 San Simeon event of December 22, 2003 and its aftershocks occurred in a region approximately 40 to 50 km southwest of the HRSN. Prior to the mainshock, seismicity in this region was predominantly quiescent.

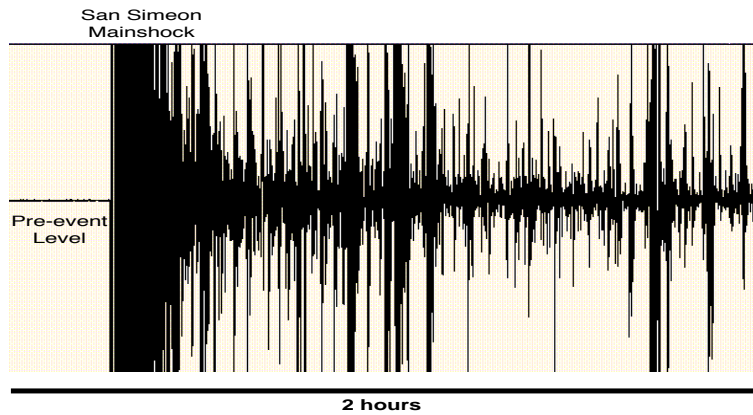


Figure 5.6: Unfiltered seismogram of the San Simeon mainshock and immediate aftershocks. Shown is a two hour snapshot of continuous 250 sps data recorded by the vertical component of the borehole HRSN station SMNB (located ~ 50 km to the northeast of the mainshock). Approximately 15 minutes of background pre-event recording is shown before the mainshock. Following the mainshock seismic signal levels are elevated well above the background level almost continuously and signals from multiple aftershocks (and possibly Parkfield local events) generally overlap. The very low background noise recordings of the borehole HRSN stations and the network's high detection sensitivity (designed for detecting very low magnitude Parkfield local events) causes the network to trigger on 10's of thousands of distant and small San Simeon aftershocks (many below magnitude 1), this despite the HRSN's distance of ~ 50 km from the sequence.

Uhrhammer, Doug Neuhauser, Don Lippert, Bill Karavas, John Friday, and Pete Lombard all contribute to the operation of the HRSN. Bob Nadeau prepared this chapter. During this reporting period, operation, maintenance, and data processing for the HRSN project was supported by the USGS, through grants: 03HQGR0065 and 04HQGR0085. NSF also provided support during the 2000-2003 period for the SAFOD expansion of the HRSN through grant EAR-9814605.

5. References

Bakun, W. H., and A. G. Lindh, The Parkfield, California, prediction experiment, *Earthq. Predict. Res.*, *3*, 285-304, 1985.

Daley, T.M. and T.V. McEvelly, Shear wave anisotropy in the Parkfield Varian Well VSP, *Bull. Seism. Soc. Am.*, *80*, 857-869, 1990.

Hickman, S., M.D. Zoback and W. Ellsworth, Introduction to special section: Preparing for the San Andreas Fault Observatory at Depth, *Geophys. Res. Lett.*, *31*, L12S01, doi:10.1029/2004GL020688, 2004.

Karageorgi, E., R. Clymer and T.V. McEvelly, Seismological studies at Parkfield. II. Search for temporal variations in wave propagation using Vibroseis, *Bull. Seism. Soc. Am.*, *82*, 1388-1415, 1992.

Karageorgi, E., R. Clymer and T.V. McEvelly, Seismological studies at Parkfield. IV: Variations in controlled-source waveform parameters and their correlation with seismic activity, 1987-1994, *Bull. Seismol. Soc. Am.*, *87*, 39-49, 1997.

Michelini, A. and T.V. McEvelly, Seismological studies at Parkfield: I. Simultaneous inversion for velocity structure and hypocenters using B-splines parameterization, *Bull. Seismol. Soc. Am.*, *81*, 524-552, 1991.

Nadeau, R.M., A. Michelini, R.A. Uhrhammer, D. Dolenc, and T.V. McEvelly, Detailed kinematics, structure and recurrence of micro-seismicity in the SAFOD target region, *Geophys. Res. Lett.*, *31*, L12S08, doi:10.1029/2003GL019409, 2004.

Oye, V., J.A. Chavarría and P.E. Malin, Determining SAFOD area microearthquake locations solely with Pilot Hole seismic array data, *Geophys. Res. Lett.*, *31*, L12S10, doi:10.1029/2003GL019403, 2004.

Roecker, S., C. Thurber and D. McPhee, Joint inversion of gravity and arrival time data from Parkfield: New constraints on structure and hypocenter locations near the SAFOD drillsite, *Geophys. Res. Lett.*, *31*, L12S04, doi:10.1029/2003GL019396, 2004.

Thurber, C., S. Roecker, H. Zhang, S. Baher and W. Ellsworth, Fine-scale structure of the San Andreas fault zone and location of the SAFOD target earthquakes, *Geophys. Res. Lett.*, *31*, L12S02, doi:10.1029/2003GL019398, 2004.

Chapter 6

Bay Area Regional Deformation Network

1. Introduction

The Bay Area Regional Deformation (BARD) network of continuously operating Global Positioning System (GPS) receivers monitors crustal deformation in the San Francisco Bay area (“Bay Area”) and northern California (Murray *et al.*, 1998). It is a cooperative effort of the BSL, the USGS, and several other academic, commercial, and governmental institutions. Started by the USGS in 1991 with 2 stations spanning the Hayward fault (King *et al.*, 1995), BARD now includes 80 permanent stations (Figure 6.1). The principal goals of the BARD network are: 1) to determine the distribution of deformation in northern California across the wide Pacific–North America plate boundary from the Sierras to the Farallon Islands; 2) to estimate three-dimensional interseismic strain accumulation along the San Andreas fault (SAF) system in the Bay Area to assess seismic hazards; 3) to monitor hazardous faults and volcanoes for emergency response management; and 4) to provide infrastructure for geodetic data management and processing in northern California in support of related efforts within the surveying and other interested communities.

BARD currently includes 80 continuously operating stations in the Bay Area and northern California (Tables 6.1 and 6.2), including 14 near Parkfield along the central San Andreas fault, and 17 near the Long Valley caldera near Mammoth. The BSL maintains 23 stations (including 2 with equipment provided by Lawrence Livermore National Laboratory (LLNL) and UC Santa Cruz). Other stations are maintained by the USGS (Menlo Park and Cascade Volcano Observatory), LLNL, Stanford University, UC Davis, UC Santa Cruz, Hat Creek Radio Observatory, U. Wisconsin, Haselbach Surveying Instruments, East Bay Municipal Utilities District, the City of Modesto, the National Geodetic Survey, Thales, Inc., and the Jet Propulsion Laboratory. Many of these stations are part of larger networks devoted to real-time navigation, orbit determination, and crustal deformation.

Between 1993 and 2001, the BSL acquired 29 Ashtech Z-12 and Micro-Z receivers from a variety of funding sources, including from federal (NSF and USGS), state

(CLC), and private (EPRI) agencies. The network enhances continuous strain measurements in the Bay Area and includes several profiles between the Farallon Islands and the Sierra Nevada in order to better characterize the larger scale deformation field in northern California (Figure 6.1). Five sites have been equipped as part of the NSF-funded Mini-PBO project to establish collocated GPS, and borehole strainmeter and seismometer observatories in the Bay Area (see Chapter 7).

The number of continuous GPS stations in northern California will dramatically increase over the next 5 years, with over 250 new site installations planned as part of the Plate Boundary Observatory (PBO) component of the NSF-funded Earthscope project. UNAVCO and researchers from BARD and the other regional networks, such as SCIGN, BARGEN, and PANGA, have submitted a proposal to NSF to fold operation and maintenance of portions of the existing networks into the PBO array at the end of the 5 years. Due to incompatible management plans for real-time telemetry and site maintenance procedures between the BSL and UNAVCO, only two BSL-maintained stations (SUTB and MUSB), out of a total of 25 BARD stations, are proposed to become PBO stations. The other BSL stations are either collocated with seismic instrumentation or are located near the San Andreas fault where real-time processing of the GPS data for earthquake notification is a high priority. We are working closely with UNAVCO to facilitate the transition of the 25 stations and are acting in an advisory role on siting issues for the planned new installations.

Today, raw and RINEX data files from the BSL stations and the other stations run by BARD collaborators are archived at the BSL/USGS Northern California Earthquake Data Center data archive maintained at the BSL (Romanowicz *et al.*, 1994). The data are checked to verify their integrity, quality, completeness, and conformance to the RINEX standard, and are then made accessible, usually within 2 hours of collection, to all BARD participants and other members of the GPS community through Internet, both by anonymous FTP and by the World Wide Web (<http://quake.geo.berkeley.edu/bard/>).

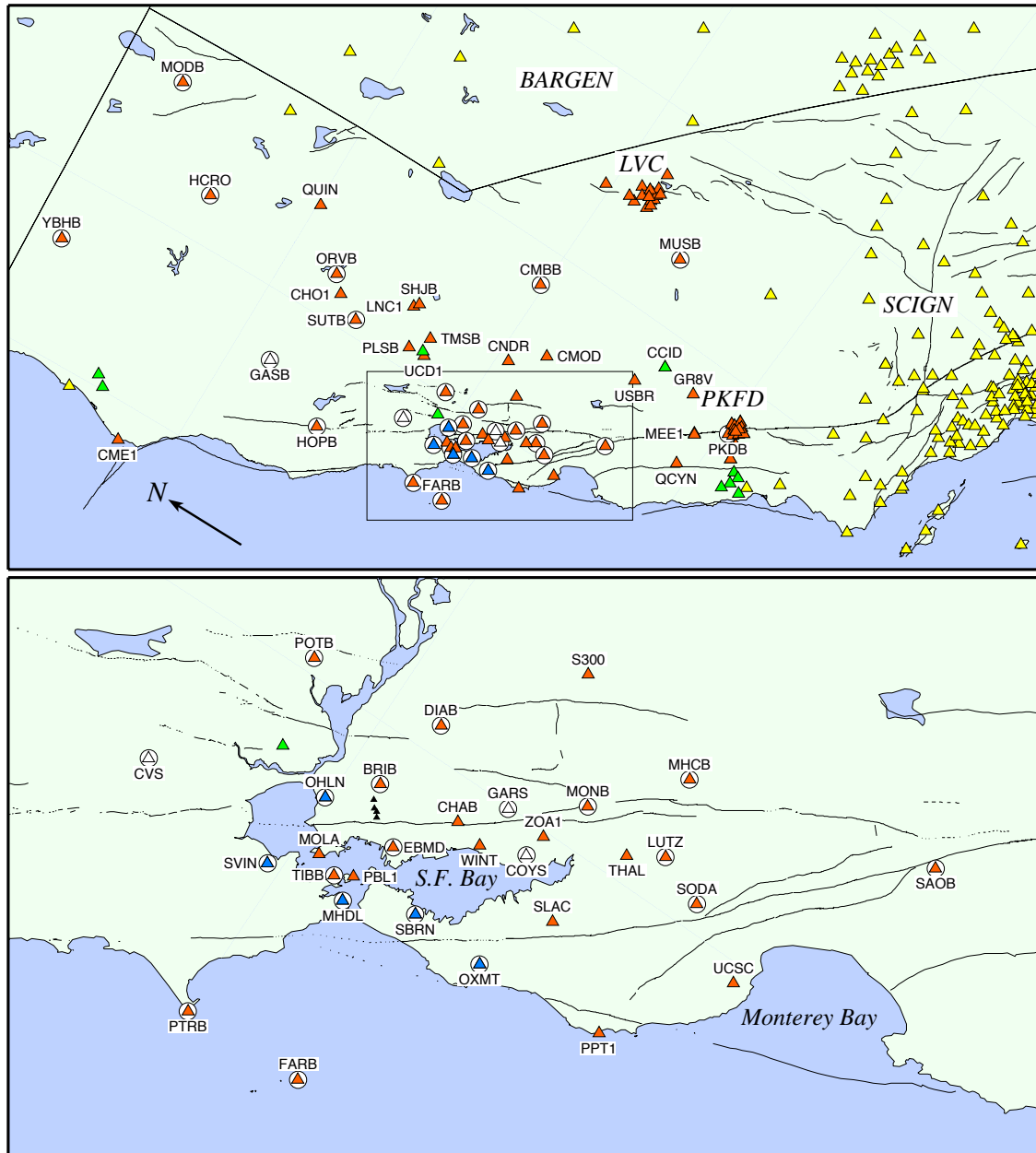


Figure 6.1: Operational (red) and planned (blue) BARD stations in northern California (top) and in the San Francisco Bay area (bottom). In the oblique Mercator projection expected Pacific–North America relative plate motion is parallel to the horizontal. Circled stations use continuous real-time telemetry. The 18-station Long Valley Caldera (LVC) network and 15-station Parkfield (PKFD) networks are also part of BARD. The small black triangles near BRIB are the experimental L1 stations. Mini-PBO stations are OHLN and SBRN (existing), and MHDL, OXMT, and SVIN (planned), all located along the northern Hayward and San Andreas fault. We plan to install 3 other stations at CVS, GARS, and COYS. The 2 Central Valley sites (USBR and CCID) are being installed in cooperation with the CSRC. Other nearby networks (open triangles) include: Basin and Range (BARGEN), and Southern California Integrated GPS Network (SCIGN).

Code	Latitude	Longitude	Start	Receiver	Maint.	Telem.	Location
BRIB	37.91940	-122.15255	1993.58	A-Z12	BSL	FR	Briones Reservation, Orinda
CMBB	38.03418	-120.38604	1993.92	A-Z12	BSL	FR	Columbia College, Columbia
DIAB	37.87858	-121.91563	1998.33	A-Z12	BSL	FR	Mt. Diablo
FARB	37.69721	-123.00076	1994.00	A-Z12	BSL	R-FR/R	Farallon Island
HOPB	38.99518	-123.07472	1995.58	A-Z12	BSL	FR	Hopland Field Station, Hopland
LUTZ	37.28685	-121.86522	1996.33	A-Z12	BSL	FR	SCC Comm., Santa Clara
MHCB	37.34153	-121.64258	1996.33	A-Z12	BSL	FR	Lick Obs., Mt. Hamilton
MODB	41.90233	-120.30283	1999.83	A-Z12	BSL	NSN	Modoc Plateau
MOLA	37.94657	-122.41992	1993.75-2002.22	T-SSE	BSL		Pt. Molate, Richmond
MONB	37.49892	-121.87131	1998.50	A-Z12	BSL	FR	Monument Peak, Milpitas
MUSB	37.16994	-119.30935	1997.83	A-Z12	BSL	R-Mi-FR	Musick Mt.
OHLN	38.00742	-122.27371	2001.83	A-uZ	BSL	FR	Ohlone Park, Hercules
ORVB	39.55463	-121.50029	1996.83	A-Z12	BSL	FR	Oroville
OXMT	37.49936	-122.42432	2004.12	A-uZ	BSL	FR	Ox Mt., Half Moon Bay
PKDB	35.94524	-120.54155	1996.67	A-Z12	BSL	FR	Bear Valley Ranch, Parkfield
POTB	38.20258	-121.95560	1998.92	A-Z12	BSL	FR	Potrero Hill, Fairfield
PTRB	37.99640	-123.01490	1998.58	A-Z12	BSL	R-FR	Point Reyes Lighthouse
SAOB	36.76530	-121.44718	1997.58	A-Z12	BSL	FR	San Andreas Obs., Hollister
SBRN	37.68622	-122.41044	2003.18	A-uZ	BSL	FR	San Bruno Mt., Brisbane
SODB	37.16640	-121.92552	1996.33	A-Z12	BSL	R-FR	Soda Springs, Los Gatos
SUTB	39.20584	-121.82060	1997.33	A-Z12	BSL	R-FR	Sutter Buttes
SVIN	38.03318	-122.52632	2003.89	A-uZ	BSL	R-FR	St. Vincents, San Rafael
TIBB	37.89087	-122.44760	1994.42	A-Z12	BSL	R	Tiburon
YBHB	41.73166	-122.71073	1996.75	A-Z12	BSL	FR	Yreka Blue Horn Mine, Yreka
CAND	35.93935	-120.43370	1999.33	A-Z12	USGS	R-FR	Cann, Parkfield
CARH	35.88838	-120.43082	2001.58	A-Z12	USGS	R-FR	Carr Hill 2, Parkfield
CARR	35.88835	-120.43084	1989.00-2003.31	A-Z12	JPL		Carr Hill, Parkfield
CRBT	35.79161	-120.75075	2001.67	A-Z12	USGS	R-FR	Camp Roberts, Parkfield
HOGS	35.86671	-120.47949	2001.50	A-Z12	USGS	R-FR	Hogs, Parkfield
HUNT	35.88081	-120.40238	2001.58	A-Z12	USGS	R-FR	Hunt, Parkfield
LAND	35.89979	-120.47328	1999.33	A-Z12	USGS	R-FR	Lang, Parkfield
LOWS	35.82871	-120.59428	2001.58	A-Z12	USGS	R-FR	Lowes, Parkfield
MASW	35.83260	-120.44306	2001.58	A-Z12	USGS	R-FR	Mason West, Parkfield
MIDA	35.92191	-120.45883	1999.75	A-Z12	USGS	R-FR	Mida, Parkfield
MNMC	35.96947	-120.43405	2001.58	A-Z12	USGS	R-FR	Mine Mt., Parkfield
POMM	35.91991	-120.47843	1999.75	A-Z12	USGS	R-FR	Pomm, Parkfield
RNCH	35.89999	-120.52482	2001.58	A-Z12	USGS	R-FR	Ranchita, Parkfield
TBLP	35.91741	-120.36034	2001.67	A-Z12	USGS	R-FR	Table, Parkfield

Table 6.1: Currently operating stations of the BARD GPS network maintained by the BSL and by the BSL/USGS/SCIGN in the Parkfield region. Receivers: A = Ashtech, T = Trimble. See Table 3.2 for telemetry codes and for BSL sites collocated with seismic stations. Data from other agencies retrieved or pushed by FTP or from the Web.

Many of the BARD sites are classified as CORS stations by the NGS, and are used as reference stations by the surveying community. We coordinate efforts with surveying community at meetings of the Northern California GPS Users Group and the California Spatial Reference Center, and are currently developing plans to use the existing infrastructure at the NCEDC to provide a hub for a high-frequency real-time surveying network in the Bay Area. Data and ancillary information about BARD

stations are also made compatible with standards set by the International GPS Service (IGS), which administers the global tracking network used to estimate precise orbits and has been instrumental in coordinating the efforts of other regional tracking networks. The NCEDC also retrieves data from other GPS archives, such as at SIO, JPL, and NGS, in order to provide a complete archive of all high-precision continuous GPS measurements collected in northern California.

Code	Latitude	Longitude	Start	Receiver	Maint.	Location
CHAB	37.72412	-122.11931	1992.00	A-Z12	USGS	Chabot, San Leandro
WINT	37.65264	-122.14056	1992.00	A-Z12	USGS	Winton, Hayward
EBMD	37.81501	-122.28380	1999.18	T-SSi	EBMUD	EBMUD, Oakland
QUIN	39.97455	-120.94443	1992.68	Rogue	JPL	Quincy
S300	37.66642	-121.55815	1998.48	T-SSi	LLNL	Site 300, Livermore
HCRO	40.81563	-121.46915	2003.50	T-SSi	HCRO	Hat Creek Radio Obs.
CHO1	39.43264	-121.66496	1999.50	A-Z12	NGS	Chico
CME1	40.44177	-124.39633	1995.74	A-Z12	NGS	Cape Mendocino
CMOD	37.64130	-121.99997	2000.76	T-SSi	City	Modesto
CNDR	37.89641	-121.27849	1999.27	A-Z12	NGS	Condor, Stockton
PBL1	37.85306	-122.41944	1995.50-2004.19	A-Z12	NGS	Point Blunt, Angel Island
PPT1	37.18167	-122.39333	1996.00	A-Z12	NGS	Pigeon Point
SLAC	37.41652	-122.20426	2002.34	Leica	SLAC	Stanford Linear Accel. Center
SUAA	37.42691	-122.17328	1994.30	A-Z12	SU	Stanford University
THAL	37.35149	-121.93549	2003.00	A-uZ	Thales	Thales, Inc., Santa Clara
UCD1	38.53624	-121.75123	1996.38	T-SSi	UCD	UC Davis
UCSC	36.99279	-122.05219	2000.31	T-SSi	UCSC	UC Santa Cruz
ZOA1	37.54305	-122.01594	2002.50	Novatel	FAA	Fremont
GR8V	36.39901	-120.41577	2003.04	T-5700	UWisc	San Andreas Creeping Segment
MEE1	36.18690	-120.75860	2003.02	T-5700	UWisc	San Andreas Creeping Segment
MEE2	36.18052	-120.76684	2003.03	T-5700	UWisc	San Andreas Creeping Segment
QCYN	36.16116	-121.13748	2003.05	T-5700	UWisc	San Andreas Creeping Segment
USBR	36.84257	-120.43567	2004.30	T-SSi	CVWD	Central Valley
CCID	36.73901	-120.35657	2004.30	T-NetRS	CVWD	Mendota, Central Valley (P304)
LNC1	38.84651	-121.35023	2003.51	A-Z12	NGS	Lincoln
PLSB	38.68530	-121.76150	2004.14	Leica	Haselbach	Woodland
SHJB	38.81418	-121.29606	2003.22	Leica	Haselbach	Rocklin
TMSB	38.57078	-121.54922	2003.22	Leica	Haselbach	West Sacramento
BALD	37.78330	-118.90130	1999.67	A-ZFX	CVO	Bald Mt., LVC
CA99	37.64460	-118.89670	1999.67	A-ZFX	CVO	Casa 1999, LVC
CASA	37.64464	-118.89666	1993.00	Rogue	JPL	Casa Diablo, LVC
DDMN	37.74430	-118.98120	1999.67	A-ZFX	CVO	Deadman Creek, LVC
DECH	38.05150	-119.09060	2001.58	A-ZFX	CVO	Dechambeau Ranch, LVC
HOTK	37.65860	-118.82130	2001.67	A-Z12	CVO	Hot Creek, LVC
JNPR	37.77170	-119.08470	1997.81	A-Z12	USGS	Juniper, LVC
KNOL	37.65912	-118.97917	1998.58	A-ZFX	CVO	Knolls, LVC
KRAC	37.71330	-118.88050	2001.67	A-Z12	CVO	Krakatoa-USGS, LVC
KRAK	37.71313	-118.88114	1994.73-2004.04	Rogue	JPL	Krakatoa, LVC
LINC	37.63719	-119.01729	1998.67	A-Z12	CVO	Lincoln, LVC
MINS	37.65376	-119.06090	1995.92	A-Z12	USGS	Minaret Summit, LVC
MWTP	37.64052	-118.94473	1998.58	A-ZFX	CVO	Mammoth Water Treat Plant, LVC
PMTN	37.83130	-119.05690	1999.67	A-Z12	CVO	Panorama Mt., LVC
RDOM	37.67707	-118.89794	1998.58	A-ZFX	CVO	Resurgent Dome, LVC
SAWC	37.68990	-118.95310	2000.65	A-ZFX	CVO	Saw, LVC
TILC	37.61890	-118.86280	2000.65	A-Z12	CVO	Tilla, LVC
WATC	37.66440	-118.65390	2001.67	A-Z12	CVO	Waterson, LVC

Table 6.2: Currently operating stations of the BARD GPS network maintained by other agencies and by the USGS Cascade Volcano Observatory (CVO) in the Long Valley caldera region. Other agencies include: EBMUD = East Bay Mun. Util. Dist., UCD = UC Davis, SU = Stanford Univ., UCSC = UC Santa Cruz, UWisc = U. of Wisconsin, City = City of Modesto (see also Table 1.1). Data from other agencies retrieved or pushed by FTP or from the Web.

2. 2003-2004 Activities

The typical configuration of a BSL continuous GPS station installation has been described in detail in previous annual reports. We here provide a brief description and highlight some of the recent changes. During July 2003–June 2004, we performed maintenance on existing BARD stations, installed 2 new stations, and prepared for a new station installation in the Marin Headlands.

2.1 BARD Stations

Each BSL BARD station uses a low-multipath choking antenna, most of which are mounted to a reinforced concrete pillar approximately 0.5–1.0 meter above local ground level. The reinforcing steel bars of the pillar are drilled and cemented into rock outcrop to improve long-term monument stability. A low-loss antenna cable is used to minimize signal degradation on the longer cable setups that normally would require signal amplification. Low-voltage cutoff devices are installed to improve receiver performance following power outages. Most use Ashtech Z-12 receivers that are programmed to record data once every 30 seconds and observe up to 12 satellites simultaneously at elevations down to the horizon. The antennas are equipped with SCIGN antenna adapters and hemispherical domes, designed to provide security and protection from weather and other natural phenomena, and to minimize differential radio propagation delays. The BSL acquired 7 Ashtech MicroZ-CGRS (uZ) receivers with NSF funding for the Mini-PBO project. These receivers, designed for continuous station applications, use less power (5.6 W) than the Z-12 receivers due to the lack of an interactive screen, provide better remote receiver control, and can support serial telemetry in both native raw format and the receiver independent BINEX format.

Data from most BSL-maintained stations are collected at 30-second intervals and transmitted continuously over serial connections (Table 6.1). Station TIBB uses a direct radio link to Berkeley, and MODB uses VSAT satellite telemetry. Most stations use frame relay technology, either alone or in combination with radio telemetry. Fourteen GPS stations are collocated with broadband seismometers and Quanterra data loggers (Table 3.2). With the support of IRIS we developed software that converts continuous GPS data to MiniSEED opaque blockettes that are stored and retrieved from the Quanterra data loggers (*Perin et al.*, 1998), providing more robust data recovery from onsite disks following telemetry outages.

Data from DIAB, MONB, POTB, and TIBB in the Bay Area, the 4 Mini-PBO stations, and 13 stations in the Parkfield regional (all but PKDB), are now being collected at 1-second intervals. Collecting at such high-frequency (for GPS) allows dynamic displacements due to large earthquakes to be better measured, such as was

demonstrated by several studies following the 2002 Denali fault earthquake. However, this 30-fold increase in data pose telemetry bandwidth limitations. Data from the Parkfield stations are collected on an on-site computer, written to removable disk once per month, and sent to SOPAC for long-term archiving (decimated 30-sec data is acquired daily via the BSL frame relay circuit). In the Bay Area, we have converted stations that have sufficient bandwidth and are currently assessing bandwidth issues at other stations. We are planning to convert to 1-second sampling where possible during the next year.

The BSL also acquired several Wi-Lan VIP 110-24 VINES Ethernet bridge radios. These 2.4 GHz spread spectrum radios use a tree structure to create a distributed Ethernet backbone with speeds up to 11 Mbps. Each system uses a directional antenna to talk to its “parent” in the tree, and an omni-directional antenna to talk to its children, if multiple, or a directional antenna if it has only 1 child. These radios offer several advantages over the Freewave radios used at other sites, including TCP/IP Ethernet control, higher bandwidth, and greater flexibility for setting up networks. We installed a set of Wi-Lan radios at the SVIN Mini-PBO station to transmit data from the site to the frame relay circuit, and are assisting EBMUD in converting their continuous station to real-time telemetry using Wi-Lan radios.

2.2 Station Maintenance

In September 2003, data telemetry from Sutter Buttes (SUTB) was interrupted. SUTB uses a Freewave radio to telemeter data to Oroville (ORVB) where it is aggregated with the ORVB GPS and seismic data on the Quanterra dataloggers and then telemetered to BSL in real time. Two problems were found. The Freewave radio at ORVB was replaced due to a bad serial port. Also, the circuit breaker on the GPS receiver at SUTB had been tripped. After resetting the breaker, data acquisition and telemetry were restarted. It is possible that a lightning storm was responsible for both problems, although workers at the communication facility on Sutter Buttes said they had been having problems with turkey vultures flying into the power lines and shorting out the power system.

In February 2003, telemetry flow of GPS data stopped at MUSB. Access to the site was initially limited by the winter snowpack, and then by the need to coordinate the visit with Southern California Edison engineers. During a visit to the site in August 2003 continuity tests revealed that the hardline antenna cable had apparently failed. This 70 m cable apparently was damaged by repeated water freezing in the PVC conduit that houses it. We replaced the hardline antenna cable, improved the drainage of the conduit, and restarted data acquisition in October 2003.

In February 2004, the site installation at Diablo (DIAB) was refurbished, including replacement of dead

batteries and cooling fans, and removal of animal waste and nesting material that was degrading the performance of the cooling system.

2.3 New Installations

Throughout the year, we continued installations for the NSF-funded Mini-PBO project to establish collocated GPS, and borehole strainmeter and seismometer observatories in the Bay Area. In November 2003, we installed the GPS instrumentation at the Mini-PBO station at St. Vincents School for Boys (SVIN). In February 2004, we installed the GPS instrumentation at the Mini-PBO station at Ox Mountain (OXMT). Both of these sites employed the borehole antenna mount we designed to provide a stable, compact GPS monument. In the coming year we plan to complete the Mini-PBO GPS installations after PG&E has installed AC power at the Marin Headlands (MHDL) site. See Chapter 7 for more details about the Mini-PBO station installations.

Additional continuous GPS stations were installed in northern California by collaborating agencies during the last year, including 4 stations (GR8V, MEE1, MEE2, QCYN) by the University of Wisconsin to study the creeping section of the San Andreas fault between San Juan Bautista and Parkfield, 3 stations (PLSB, SHJB, TMSB) by Haselbach Instruments in the Central Valley for surveying applications, one station (LNC1) in the Central Valley by the US Coast Guard for navigation applications (replacing PBL1, which was decommissioned), and SLAC by the Stanford Linear Accelerator surveying group, which effectively replaces the nearby SUAA site that had been used for navigation research. Due to lack of funding, JPL discontinued the operation of KRAK on the resurgent dome in the Long Valley caldera. However, continued monitoring of this geophysically interesting location is provided by the nearby station KRAC operated by CVO.

3. Data Analysis and Results

We use the GAMIT/GLOBK software developed at MIT and SIO to process data from the BARD and other nearby continuous GPS networks. Recent improvements to GAMIT/GLOBK include better accounting of ocean-tide effects, estimating gradients in atmospheric variations, and applying elevation-dependent weighting to the data observables. We process data from more than 70 stations within hours of the completion of the day using rapid or predicted orbits. We have also reprocessed older data from the present to 1991 using improved orbits. Data from 5 primary IGS fiducial sites located in North America and Hawaii are included in the solutions to help define a global reference frame. For long-term velocity estimates, we combine these solutions with global

and regional solutions provided by SOPAC to better define a stable North America reference frame. We are currently porting our processing system to a Linux-based cluster that will significantly decrease the time required to analyze the data and allow us to process the much larger number of stations anticipated by the installation of the PBO network.

The estimated relative baseline determinations typically have 2–4 mm long-term scatter in the horizontal components and the 10–20 mm scatter in the vertical. Average velocities for the longest running BARD stations during 1993–2004 are shown in Figure 6.2, with 95% confidence regions assuming only white noise. The velocities are relative to stable North America, as defined by the IGS and CORS fiducial stations. In a study using only the continuous GPS stations in northern California and Nevada (*Murray and Segall, 2001*), we found that most of the Sierra Nevada sites (CMBB, QUIN, and ORVB), as well as SUTB in the Central Valley, show little relative motion, indicating that the northern Sierra Nevada–Central Valley is tectonically stable. The motion of these sites relative to North America differs from the inferred motion of the western Basin and Range Province, suggesting 3 mm/yr right-lateral shear across the Walker Lane–Mt. Shasta seismicity trend. Deformation along the coast in central California is dominated by the active SAF system, which accommodates about 35 mm/yr of right-lateral shear. The Farallon Island site (FARB) off the coast of San Francisco is moving at nearly the rate predicted by the NUVEL-1A Pacific–North America Euler pole. Two-dimensional modeling of the observed fault-parallel strain accumulation predicts deep slip rates for the San Andreas, Hayward, and Calaveras/Concord faults in good agreement with estimated geologic rates.

We are completing a more comprehensive study that combines survey-mode and continuous GPS solutions into a self-consistent velocity field in the San Francisco Bay area (*D’Alessio et al., 2004*). This Bay Area Velocity Unification (BĀVŪ) study, which employs more sophisticated three-dimensional block modeling methods that allow for complex fault geometries and enable along-strike variations to be estimated, is described in more detail in the research section (12.8.).

We are assessing the BARD time series for transient deformation signals (short-term deviations from the long-term average velocities). Stations within stable continental regions typically move at constant velocities, but near plate boundaries, earthquake cycle deformation associated with strain accumulation and release on faults causes transient behavior both from coseismic static displacements and from postseismic deformation as the crust re-equilibrates to the stress changes induced by the earthquake.

Transient signals have been observed from numerous earthquakes worldwide, but in northern California,

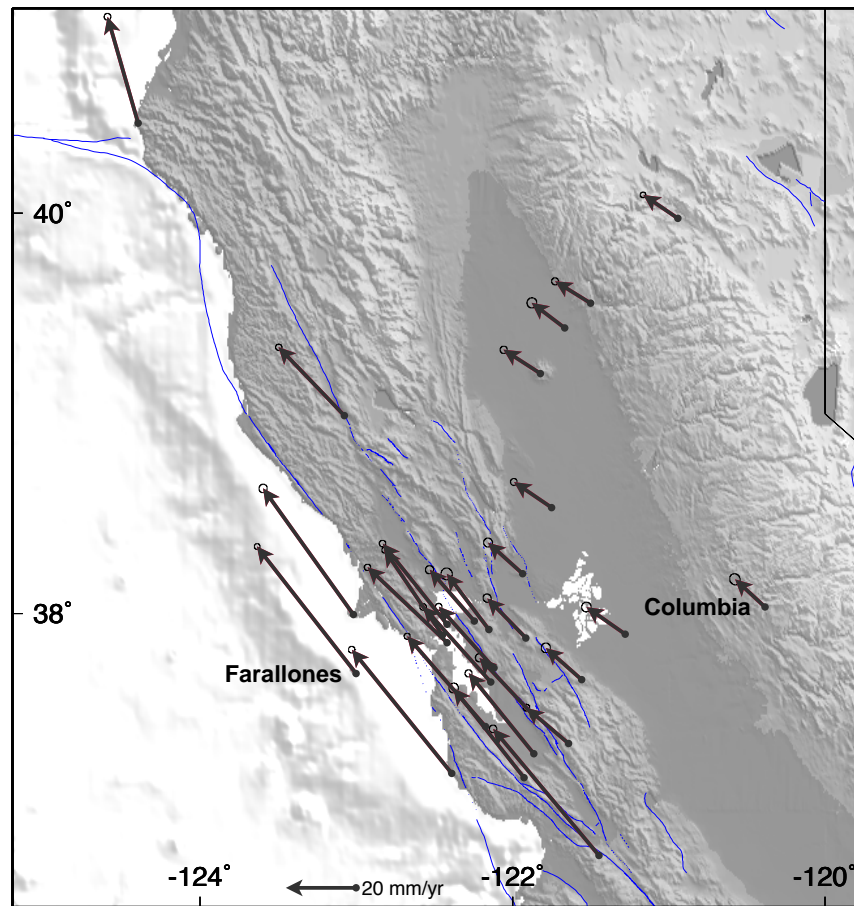


Figure 6.2: Velocities relative to stable North America for the BARD stations derived from 1993–2004 data. Ellipses show 95% confidence regions, assuming white noise only. The 35 mm/yr motion between Columbia and the Farallones is primarily due to shear across the San Andreas fault system.

the August 1998 $M=5.1$ San Juan Bautista earthquake (Uhrhammer *et al.*, 1999) was the only event to have produced a detectable earthquake displacement signal (of 4 mm at the SAOB station) prior to 2003. This changed on 22 December 2003 when the M_w 6.5 San Simeon earthquake significantly displaced all the BARD stations along the creeping and Parkfield sections of the San Andreas fault. Most of these stations are located 50 km from the epicenter and were displaced southwest by about 15 mm. The closest continuous station, CRBT, about 25–30 km from the epicentral region, was displaced southwest by 68 mm and shows a modest postseismic transient in the first month following the earthquake (Figure 6.3). Preliminary results from our investigations of finite-fault rupture models for the San Simeon earthquake from inversions of seismic and geodetic data, including more coseismic dis-

placements from survey-mode observations (Rolandone *et al.*, 2004; Murray *et al.*, 2004), are presented in the research section (12.3.).

Transient deformation has also been observed using GPS from aseismic processes that can occur over hours to days, such as episodic slow earthquakes. These events, often associated with earthquake tremors, have been detected in both Japan and the northern Cascadia subduction zone, and recent studies suggest that they may also be occurring along the southern Cascadia subduction zone in northern California. In the research section (12.16.), we report on our preliminary study of deformation and tremor observations in the southern Cascadia subduction zone to better constrain and characterize this possible episodic behavior.

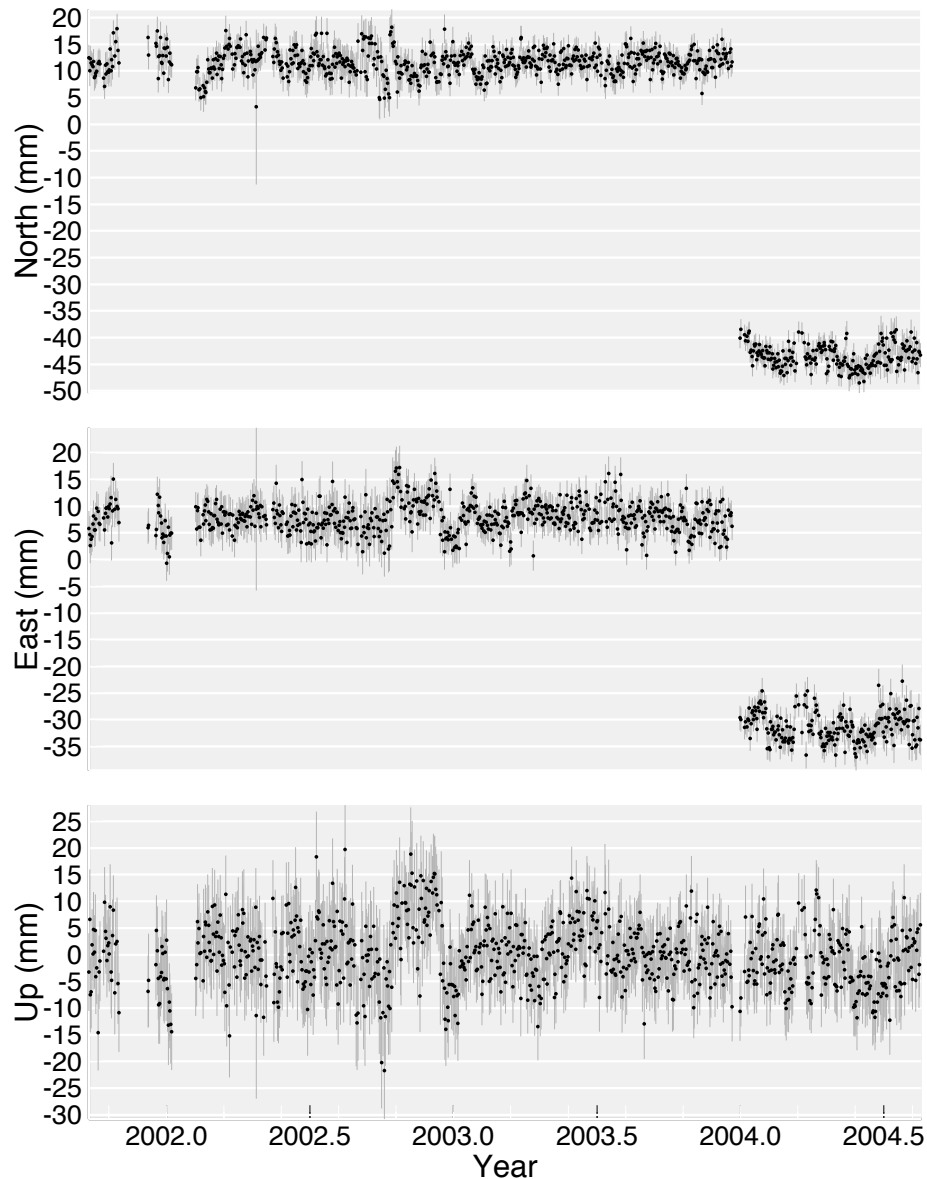


Figure 6.3: Daily position timeseries for CRBT, the continuous GPS station located closest to the epicenter of the 22 December 2003 San Simeon earthquake. The coseismic displacement is about 68 mm to the southwest. A modest amount of postseismic deformation occurs in the month following the event.

4. Real-Time Processing

We are developing real-time analysis techniques that will enable rapid determinations (within minutes) of deformation following major earthquakes to complement seismological information. We use GAMIT/GLOBK processing techniques to estimate independent hourly solutions at the several cm-level horizontal precision and during the past year established an extension of the REDI system where estimates of postseismic positions are attempted when 10 minutes of data become available fol-

lowing an earthquake (*Murray et al., 2002*).

We currently process 1-hour data batches available within 20 minutes of measurement from more than 20 continuously telemetered BSL and other stations providing hourly data. The hourly solutions have higher scatter than the 24-hour solutions (3–10 mm in the horizontal and 10–30 mm in the vertical), but our simulations suggest that displacements 3–5 times these levels should be reliably detected, and that the current network should be able to resolve the finite dimensions and slip magni-

tude of a M7 earthquake on the Hayward fault. Due to the poor ability of GAMIT to resolve ambiguities from short data spans, estimates of coseismic displacements within minutes of an event have high (decimeter-level) uncertainty. We are testing a relatively new component of GAMIT that uses Kalman filtering techniques and improved ambiguity resolution methods to provide higher-precision kinematic positions. This method works well for networks with small interstation distances (e.g., near the 1999 Hector Mine earthquake), which aids ambiguity resolution, but has less success on more widely spaced networks, such as the continuous GPS stations in the vicinity of the 2002 Denali earthquake.

These rapid processing techniques can also be applied to estimating higher frequency 1-Hz GPS displacements, which have been used to detect surface from large earthquakes and can potentially add valuable information about the seismic source. We are also developing methods to rapidly estimate finite-source models from coseismic GPS displacements and to use these models to predict strong-ground motions and improve ShakeMap depictions of these motions as rapidly as possible after an earthquake. The first step of this project has been the development of a new methodology to improve prediction of strong ground motion from a simple uniform-slip geodetic model of the source. This methodology is based on a simple assumption that the large slip should take longer to terminate. We use well known scaling relations between stress drop and slip velocity to develop a spatio-temporal slip model. We have tested this model on the 1992 Northridge earthquake and found that the predicted ground motions agree well with observed motions and with other models derived from combinations of seismic and geodetic data (Rhie *et al.*, 2004).

5. Acknowledgements

Mark Murray oversees the BARD program. André Basset, Wade Johnson, Rich Clymer, Cedric de La Beaujardiere, Bill Karavas, John Friday, Dave Rapkin, and Doug Neuhauser contributed to the operation of the BARD network.

6. References

Bürgmann, R., D. Schmidt, R.M. Nadeau, M. d’Alessio, E. Fielding, D. Manaker, T. V. McEvelly, and M. H. Murray, Earthquake potential along the northern Hayward fault, California, *Science*, 289, 1178–1182, 2000.

D’Alessio, M. A., I. A. Johanson, R. Bürgmann, D. A. Schmidt, and M. H. Murray, Slicing up the San Francisco Bay Area: Block kinematics from GPS-derived surface velocities, *J. Geophys. Res.*, in prep., 2004.

King, N. E., J. L. Svarc, E. B. Fogleman, W. K. Gross,

K. W. Clark, G. D. Hamilton, C. H. Stiffler, and J. M. Sutton, Continuous GPS observations across the Hayward fault, California, 1991-1994, *J. Geophys. Res.*, 100, 20,271–20,283, 1995.

Murray, M. H., and P. Segall, Continuous GPS measurement of Pacific–North America plate boundary deformation in northern California and Nevada, *Geophys. Res. Lett.*, 28, 4315–4318, 2001.

Murray, M. H., R. Bürgmann, W. H. Prescott, B. Romanowicz, S. Schwartz, P. Segall, and E. Silver, The Bay Area Regional Deformation (BARD) permanent GPS network in northern California, *EOS Trans. AGU*, 79(45), Fall Meeting Suppl., F206, 1998.

Murray, M., Neuhauser D., Gee, L., Dreger, D., Basset, A., and Romanowicz, B., Combining real-time seismic and geodetic data to improve rapid earthquake information, *EOS. Trans. AGU*, 83(47), G52A-0957, 2002.

Murray, M.H., D.C. Agnew, R. Bürgmann, K. Hurst, R.W. King, F. Rolandone, J. Svarc, GPS Deformation measurements of the 2003 San Simeon earthquake, *Seism. Res. Lett.*, 75, 295, 2004.

Perin, B. J., C. M. Meertens, D. S. Neuhauser, D. R. Baxter, M. H. Murray, and R. Butler, Institutional collaborations for joint seismic and GPS measurements, *Seismol. Res. Lett.*, 69, 159, 1998.

Rhie, J., D. Dreger, and M. H. Murray, A prediction of strong ground motions from geodetic data for PGV ShakeMaps, *Geophys. Res. Lett.*, in prep., 2004.

Rolandone, F., I. Johanson, and R. Bürgmann, Geodetic observations of the M6.5 San Simeon earthquake with focus on the response of the creeping segment of the San Andreas fault, *Seism. Res. Lett.*, 75, 293, 2004.

Romanowicz, B., B. Bogaert, D. Neuhauser, and D. Oppenheimer, Accessing northern California earthquake data via Internet, *EOS Trans. AGU*, 75, 257–260, 1994.

Uhrhammer, R., L. S. Gee, M. Murray, D. Dreger, and B. Romanowicz, The M_w 5.1 San Juan Bautista, California earthquake of 12 August 1998, *Seismol. Res. Lett.*, 70, 10–18, 1999.

Chapter 7

Plate Boundary Deformation Project

1. Introduction

The Integrated Instrumentation Program for Broadband Observations of Plate Boundary Deformation, commonly referred to as “Mini-PBO”, is a joint project of the BSL, the Department of Terrestrial Magnetism at Carnegie Institution of Washington (CIW), the IGPP at UC San Diego (UCSD), and the U.S. Geological Survey (USGS) at Menlo Park, Calif. It augments existing infrastructure in central California to form an integrated pilot system of instrumentation for the study of plate boundary deformation, with special emphasis on its relation to earthquakes. This project is partially funded through the EAR NSF/IF program with matching funds from the participating institutions and the Southern California Integrated Geodetic Network (SCIGN).

Because the time scales for plate boundary deformation range over at least 8 orders of magnitude, from seconds to decades, no single technique is adequate. We have initiated an integrated approach that makes use of three complementary and mature geodetic technologies: continuous GPS, borehole tensor strainmeters, and interferometric synthetic aperture radar (InSAR), to characterize broadband surface deformation. Also, ultrasensitive borehole seismometers monitor microearthquake activity related to subsurface deformation.

The project has three components: 1) the installation of broadband deformation stations in the San Francisco Bay area; 2) the installation of GPS stations in the Parkfield region; and 3) support for skeletal operations of a 5-m X-band SAR downlink facility in San Diego to collect and archive radar data, and develop an online SAR database for WInSAR users. The BSL has participated in the first two of these components. Additional details about the Parkfield GPS stations, installed in 2001 to link the BARD network in central and northern California to the SCIGN network in southern California and currently operating in real-time streaming mode with instantaneous position analysis, are provided in the BARD chapter of this report. The remainder of this chapter describes San Francisco Bay area broadband deformation station component of this project.

The broadband deformation stations augment existing instrumentation along the Hayward and San Andreas faults in the San Francisco Bay area (Figure 7.1). During July 2001 to August 2002, five boreholes were drilled and equipped with tensor strainmeters and 3-component L22 (velocity) seismometers (Table 7.1). These were the first deployments of a new type of strainmeter developed by CIW that use 3 sensing volumes placed in an annulus with 120-degree angular separation (Figure 7.2, which allows the 3-component horizontal strain tensor to be determined. All of the stations include pore pressure sensors and 2-component tiltmeters. Four of the stations now are equipped with GPS receivers recording at 1 sample per second and Quanterra recording systems that provide 100-Hz seismic and strainmeter data. The GPS antennas at these stations are mounted at the top of the borehole casings to achieve stable compact monuments. These stations complement existing Bay Area stations of the BARD continuous network, the BDSN and HFN seismic networks, and borehole dilatometers along the southern Hayward fault and in the San Juan Bautista region.

2. Mini-PBO Station Configuration

The general configuration of borehole instrument installation at each Mini-PBO station is shown in Figure 7.3. A 6.625” steel casing was cemented into a 10.75” hole to 500-650’ depth to prevent the upper, most unconsolidated materials from collapsing into the hole. Below this depth a 6” uncased hole was drilled to the target region for the strainmeter and seismometer packages. Coring, in order to identify the region with the most competent rock for the strainmeter, was attempted with only moderate success at a few of the holes and was not attempted at St. Vincents. We found that video logs provided a reasonable substitute. The target region of each hole was filled with a non-shrink grout into which the strainmeter was lowered, allowing the grout to completely fill the inner cavity of the strainmeter within the annulus formed by the sensing volumes to ensure good coupling to the

entirely enclose the package. The pipe above this depth was left open for later installation of the pore pressure sensor. To allow water to circulate into the pipe from the surrounding rock for the pore pressure measurements, the steel casing was perforated, a sand/gravel pack was emplaced, and a PVC screen was used at this depth. At each hole, the casing was then cemented inside to about 200', and outside to about 20' depth. A 12" PVC conductor casing was cemented on the outside from the surface to 20' to stabilize the hole for drilling and to provide an environmental health seal for shallow groundwater flow. The annulus between the 12" conductor casing and the 6.625" steel casing was cemented to about 10' depth and above was left decoupled from the upper surface to help minimize monument instability for the GPS antenna mounted on top of the steel casing.

The BSL developed a GPS mount for the top of the borehole casings to create a stable, compact monument. This design will be used at the more than 140 PBO strainmeter stations to be installed over the next 5 years. The antennas, using standard SCIGN adapters and domes for protection, are attached to the top of the 6-inch metal casing, which will be mechanically isolated from the upper few meters of the ground. The casing below this level is cemented fully to the surrounding rock. The GPS mount design consists of two 11-inch diameter stainless steel flanges. The lower slip- and- weld type flange is welded onto the top of the 6 5/ 8"- inch borehole casing providing a level surface for the second flange. The upper blind-type flange, to which the 1 1/ 4" stainless steel pipe used to connect to the SCIGN DC3 adaptor is attached, is bolted to the lower flange using four 3/ 4" by 3" stainless steel bolts. Two half- inch stainless steel dowels are press fit with high location precision (radius 7.500" +/- 0.001") into the lower flange. Two matching holes are machined into the upper flange with a high location precision (radius 7.500" +/- 0.001") and hole diameter precision (0.005"). One of the dowels is offset to insure unique directional alignment. During the period July 2003–June 2004, the BSL completed the installation of GPS systems using the borehole mount at St. Vincents School for Boys (SVIN) near San Rafael and at the Ox Mt site (OXMT) near Half Moon Bay.

Two-component tiltmeters were installed at all the stations by the USGS in 2003. Data from these sensors are recorded at 10-minute intervals and telemetered using the GOES system. Pore pressure sensors are also installed at all the stations and data are recorded at 1 Hz on the Quanterra dataloggers, except at Marin Headlands, where 10-minute interval data are also recorded on the Zeno datalogger.

The 1-Hz GPS, and 100-Hz strainmeter and seismometer data is acquired on Quanterra data loggers and continuously telemetered by frame relay to the BSL. Low frequency (600 second) data (including strainmeters, for re-

dundancy) is telemetered using the GOES system to the USGS. All data is available to the community through the Northern California Earthquake Data Center (NCEDC) in SEED format, using procedures developed by the BSL and USGS to archive similar data from 139 sites of the USGS ultra-low-frequency (UL) geophysical network, including data from strainmeters, tiltmeters, creep meters, magnetometers, and water well levels.

The BSL is supervising GPS, power, frame relay telemetry, and Quanterra 4120 datalogger installation and maintenance at all the broadband deformation stations. Power, telemetry, and dataloggers are currently installed at all stations except MHDL, where we are waiting for PG&E to install the power drop. Telemetry at SVIN was established in June 2003 using Wi-LAN radios, a new type of radio that the BSL is currently beginning to adopt. These radios act as Ethernet bridges, providing superior access to console control on the Quanterras. The radios can also provide a spanning tree network structure for a regional wireless network, which allows greater flexibility for future network installations. We will use Wi-LAN radios at MHDL as well to provide a link between the borehole site and the frame-relay network interface circuit, which is located about 0.5 miles from the site.

The BSL and USGS are addressing minor problems at the stations. Highly correlated low-amplitude noise is contaminating the seismic and strain channels at several of the stations, mostly due to electrical ground loop issues. The USGS and CIW are also investigating anomalies in the strainmeter channels, including unusual steps in several of the instruments related to resetting of the secondary valves that serve as an overflow buffer in the event of a large strain signal. These investigations have included tests of several variations of the strainmeter electronics boxes, which may have components that are poorly isolated. grounded. These tests, still ongoing, also introduce grounding loop problems that contaminate the high-frequency strain channels. In January 2004, the vertical component of the geophone at OHLN began to develop problems, which were most evident during seismic events. Testing indicated that the spring may have not functioned properly and that the sensor had lodged against a stop. The geophone returned to normal operation after it was pulsed with a high amplitude (.5V 4Hz) sine wave, which presumably dislodged the sensor.

3. Broadband Deformation Data

We are in the initial stages of assessing the data quality of the broadband deformation instrumentation. The borehole seismic packages provide good signal to noise characteristics compared to the NHFN stations due to their relatively deep installation. The systems have the best signal to noise near their 2-Hz characteristic frequency, but typical microseismic noise around 0.1 Hz is

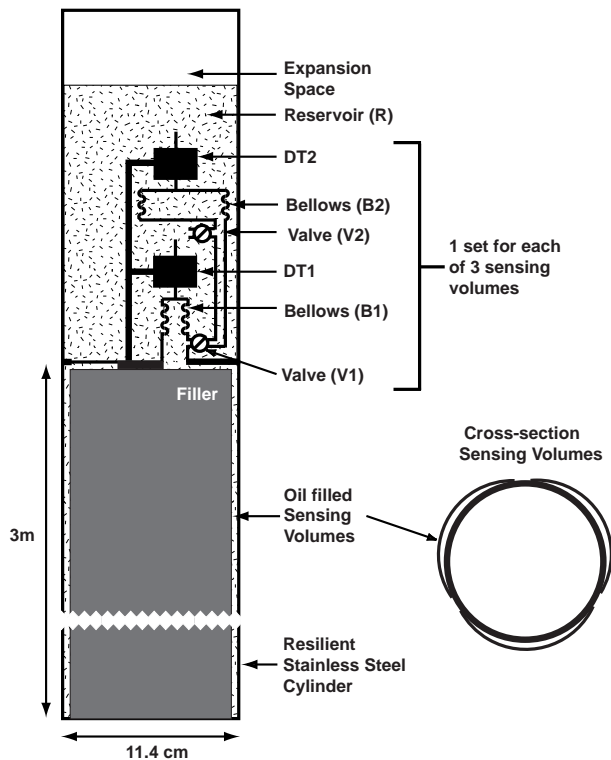


Figure 7.2: Tensor strainmeter diagram. These instruments are a modification of hydraulic sensing dilatometer design to achieve a volume strain sensitivity of 10^{*-12} with constant frequency response from 0 to more than 10 Hz and a dynamic range of about 130 dB. The design incorporates a second bellows- DT- valve sub- system which provides extended dynamic range, complete preservation of baseline during required instrumental resets, and redundant sensing electronics. Figure courtesy A. Linde (USGS).

not evident (Figure 7.4). It is possible that the micro-seismic noise could be resolved if the systems included a pre-amplifier. We are planning to test this at OXMT and MHDL when the power and telemetry issues at those sites are resolved. These stations currently sample at 100-Hz, so they miss some of the seismic energy at high frequencies that are observed on the 500-Hz Parkfield borehole stations.

Analysis of GPS observations show that the short-term daily repeatabilities in the horizontal components are about 0.5-1 mm, and annual signals with about 1 mm amplitude. These values are similar to those obtained with more typical monuments, such as concrete piers or braced monuments, but it is too early to assess the long-term stability of the borehole casing monument, which might also be affected by annual thermal expansion effects on the casing.

The newly designed tensor strainmeters appear to

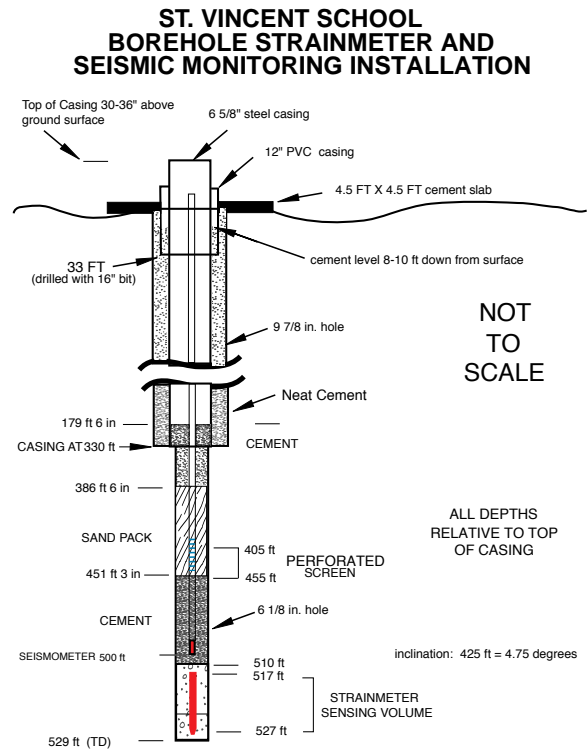


Figure 7.3: The Mini-PBO borehole configuration at St. Vincents, showing the emplacement of the strainmeter and seismometer instruments downhole. The GPS receiver is mounted on the top. Figure courtesy B. Mueller (USGS).

faithfully record strain signals over a broad frequency range, except at the longest periods where the strains show a long-term exponential signal. This large signal is most likely due to cement hardening effects and re-equilibration of stresses in the surrounding rock in response to the sudden appearance of the borehole. These effects can last for many years and are the principal reason that borehole strainmeters cannot reliably measure strain at periods greater than a few months.

At periods around 1 day, tidally induced strains are the dominant strain signal. Since the response of the strainmeter volumes is difficult to estimate independently, theoretically predicted Earth tides are typically used to calibrate the strainmeters. Figure 7.5 shows the approximate microstrain of the OHLN strainmeter over a several month period interval, and some of the steps required to clean the data, including removing the tides and atmospheric pressure effects. The remaining signal is highly correlated with rainfall, indicating the extent that hydrologic events can affect strain. The proximity of the strainmeters to the San Francisco Bay complicates the determinations of theoretical tides due to ocean and bay loading effects. Figure 7.6 gives results from a tidal

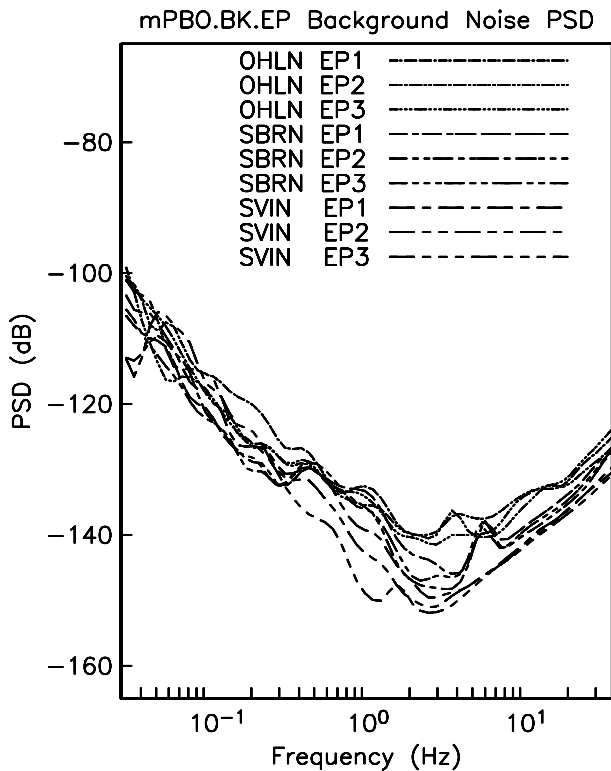


Figure 7.4: Background noise measured by the borehole seismic packages at OHLN, SBRN, and SVIN. Component 1 is vertical. The systems have the best signal to noise ratio near their 2-Hz characteristic frequency. Typical microseismic noise around 0.1 Hz is not evident.

analysis provided by D. Agnew (UCSD) that shows good agreement in amplitude and phase of the two principal tidal components used for strainmeter calibrations (M2 and O1) at most of the stations, but a negative M2 tide at Ohlone, which is physically implausible.

At higher frequencies, strains due to seismic events are also evident. Figure 7.7 shows borehole strain measurements with clear seismic phases at OHLN for a 2003 Carlsberg Ridge earthquake. The dilatational component is bandpass filtered to show 100-300 second period Raleigh waves. Also shown are synthetic straingrams computed from a summation of the fundamental normal mode branch assuming a 1D Earth model (PREM), showing reasonably good agreement in amplitude. We are developing methods to use seismic surface waves to estimate the amplitude calibrations of the strainmeters to help resolve some of the problems observed with the tidal comparisons. The synthetic surface-wave and tidal-period amplitude calibrations currently agree to within 40%, which we expect will be significantly improved by using better Earth models and more sophisticated analysis techniques, such as phase-matched filtering.

We are also examining the strain data for other types of

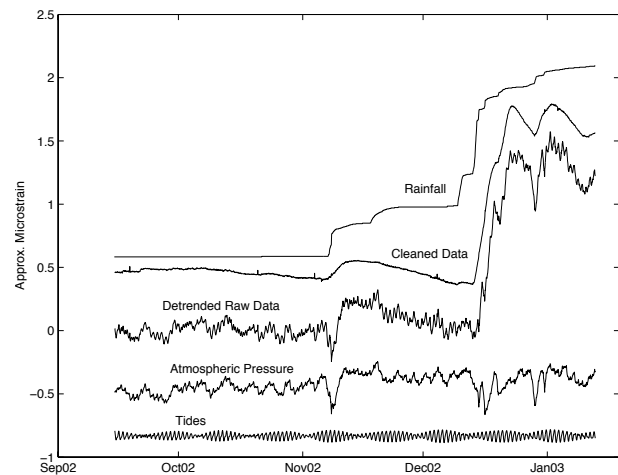


Figure 7.5: Four-month subset of OHLN data, detrended to flatten the first 50 days (middle trace), separated using BAYTAP-G (Tamura et al., 1991) into tidal, atmospheric pressure, and "cleaned" data components (with arbitrary vertical offsets). The atmospheric pressure time series measured at the site was also used for this decomposition. Approximate microstrain values are based on peak-to-peak tidal amplitude. The remaining large strain signals in the cleaned data are highly correlated with rainfall measured at an instrument located about 5 km from the site (40 cm total cumulative rainfall during this interval), and therefore are probably not geophysically interesting.

transient behavior, such as episodic creep or slow earthquake displacements. These multiparameter stations are providing a prototype for more than 140 planned borehole strainmeter, seismometer, and GPS stations in Cascadia and along the San Andreas fault as part of the Plate Boundary Observatory.

4. Acknowledgements

This project is sponsored by the National Science Foundation EAR/IF program with matching funds from the participating institutions and the Southern California Earthquake Center (SCEC) (PI Romanowicz).

Under Mark Murray's supervision, André Basset, Bill Karavas, John Friday, Dave Rapkin, Doug Neuhauser, Tom McEvelly, Wade Johnson, and Rich Clymer have contributed to the development of the BSL component of the Mini-PBO project. Several USGS colleagues, especially Malcolm Johnston, Bob Mueller, and Doug Myren, played critical roles in the drilling and instrument installation phases.

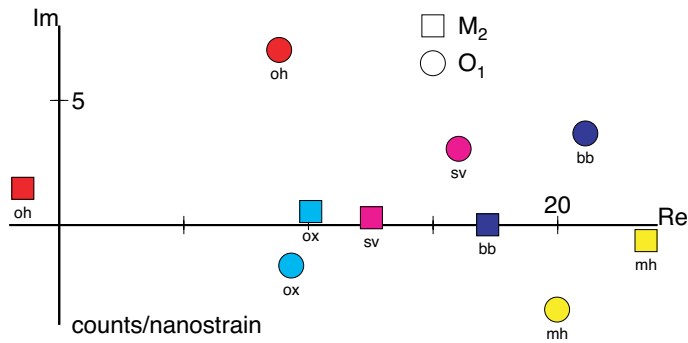


Figure 7.6: Tidal analysis performed by D. Agnew on areal strain from the Mini-PBO stations, showing agreement within about 20% in both amplitude and phase between the O1 and M2 tides, except at Ohlone (oh), whose negative M2 tide is physically implausible.

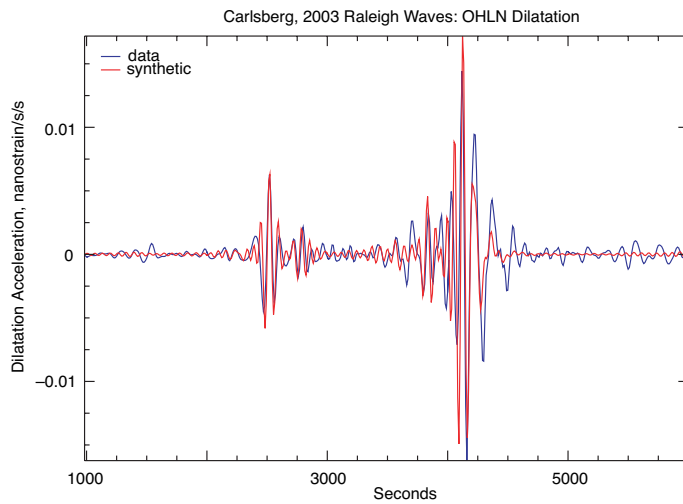


Figure 7.7: Comparison between data (blue) and synthetic (red) straingrams at the OHLN strainmeter for the 2003 Carlsberg Ridge earthquake. The dilatational component is bandpass filtered to show 100-300 second period Raleigh waves. The synthetics are computed from a summation of spheroidal modes assuming a 1D Earth model (PREM). Surface-wave and tidal-period amplitude calibrations agree to within 40%, which we expect will be significantly improved by using better Earth models and more sophisticated analysis techniques, such as phase-matched filtering.

Chapter 8

Data Acquisition and Quality Control

1. Introduction

Stations from nearly all networks operated by the BSL transmit data continuously to the BSL facilities on the UC Berkeley campus for analysis and archive. In this chapter, we describe activities and facilities which cross-cut the individual networks described in Chapters 3 - 7, including the facilities in McCone Hall, procedures for data acquisition and quality control, sensor testing capabilities and procedures, and a collaborative experiment in early warning.

While some of these activities are continuous from year to year, we have identified changes or activities which are specific to 2003-2004.

2. McCone Hall Facilities

The routine data acquisition, processing, and archiving activities of the BSL are carried out in McCone Hall. The BSL facilities in McCone are designed to provide air conditioning, 100-bit switched network, and reliable power with UPS and generator.

Because of the mission-critical nature of the automated earthquake processing, most computer systems operated by the BSL run on circuits with both UPS and generator power. Air conditioning is provided through both "building air" and two additional AC units.

2.1 Power

Over the years, the BSL has experienced problems with the McCone generator system, including a failure in 1999 due to a combination of a weakened power system and a leak in the water pump. In the 2001-2002 Annual Report, we described the failure of the McCone and Byerly generators in the March 7, 2002 campus-wide power outage.

While the failure of the generator at Byerly Vault was traced to PPCS human error (the generator had been left in a mode where it would not automatically start when power was lost), the failure of the McCone generator was due to poor maintenance. Similar to the situation in

1999, it failed due to problems in the power system combined with a leak in the water pump.

In the fall of 2002, BSL staff met with Eric Haemer, Sara Shirazi, and several others from PPCS to discuss maintenance and routine load testing of the McCone generator. As a result, the McCone generator is scheduled for quarterly load tests and bi-monthly run tests.

2.2 Air Conditioning

In parallel with power problems, the BSL has faced cooling problems in room 237 in the past year. As with power, the growth of the computing systems in the past year has led to an increased heat load. This came to a crisis during the fall of 2002, with peak temperatures in the computer room exceeded 85° when the AC unit failed. After consideration of several options, the BSL decided to add an additional AC unit to room 237. The new unit (which is not supported by UPS/generator power) has helped keep systems running, although the BSL held a summit with PPCS staff in February 2004 to review ongoing cooling problems. As a result, PPCC worked with the contractor to install a larger impeller on the chilled water circulation pump. This has increased the cooling capacity of our dry cooler on the roof. In addition, PPCS has been coming by more regularly to inspect the filters on the unit.

2.3 New Facilities

The BSL is actively working with the campus to relocate the critical operations of data acquisition, processing, archiving, and distribution to a more robust facility. With assistance from the Office of the Vice Chancellor for Research, the BSL has been granted space in 2195 Hearst, a recently completed building on the Oxford Tract. 2195 Hearst was designed to current codes and has been given special attention for post-earthquake operations. The BSL is gearing up to relocate their critical computers in the fall of 2004.

BDSN and REDI Telemetry and Data Flow

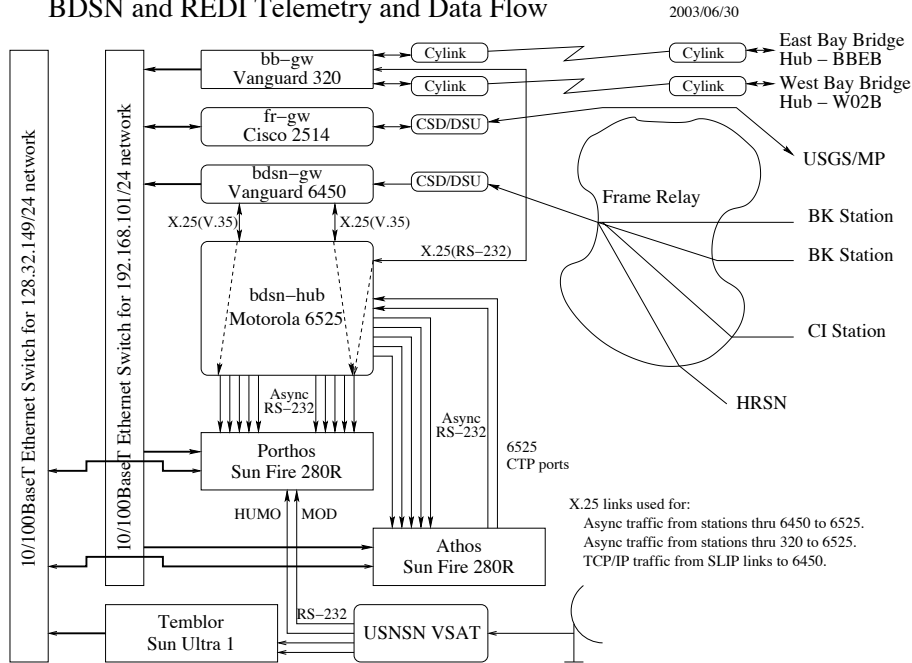


Figure 8.1: Data flow from the BDSN, NHFN, MPBO, HRSN, and BARD network into the BSL central processing facility.

3. Data Acquisition

Central-site data acquisition for the BDSN/NHFN/MPBO is performed by two computer systems located at the BSL (Figure 8.1). These acquisition systems are also used for the Parkfield-Hollister electromagnetic array and for the BARD network. A third system is used primarily as data exchange system with the USNSN and receives a feed from CMB, HUMO, MOD, SAO, and WDC from the the NSN VSAT. This system also transmits data to the USNSN from HOPS, CMB, SAO, WDC, and YBH. Data acquisition for the HRSN follows a more complicated path, as described in Chapter 5.

3.1 Comserv

The BSL uses the `comserv` program for central data acquisition, which was developed by Quanterra. The `comserv` program receives data from a remote Quanterra data logger, and redistributes the data to one or more `comserv` client programs. The `comserv` clients used by REDI include `dataLog`, which writes the data to disk files for archival purposes, `cdafill`, which writes the data to the shared memory region for REDI analysis, and other programs such as the seismic alarm process, the DAC480 system, and the feed for the Memento Mori Web page (Figure 8.2).

The two computers that perform data acquisition also serve as REDI processing systems. In order to facilitate

REDI processing, each system maintains a shared memory region that contains the most recent 30 minutes of data for each channel used by the REDI analysis system. All REDI analysis routines first attempt to use data in the shared memory region, and will only revert to retrieving data from disk files if the requested data is unavailable in the shared memory region.

Most stations transmit data to only one or the other of the two REDI systems. The `comserv` client program `cs2m` receives data from a `comserv` and multicasts the data over a private ethernet. The program `mcast`, a modified version of Quanterra's `comserv` program, receives the multicast data from `cs2m`, and provides a `comserv`-like interface to local `comserv` clients. This allows each REDI system to have a `comserv` server for every station.

We have extended the multicasting approach to handle data received from other networks such as the NCSN and UNR. These data are received by Earthworm data exchange programs, and are then converted to MiniSEED and multicast in the same manner as the BSL data. We use `mserv` on both REDI computers to receive the multicast data, and handle it in an identical fashion to the BSL MiniSEED data.

3.2 BH Sampling Rate

The BSL converted most - but not quite all - of the BDSN BH data streams from 20 samples per second to 40 samples per second at the beginning of the

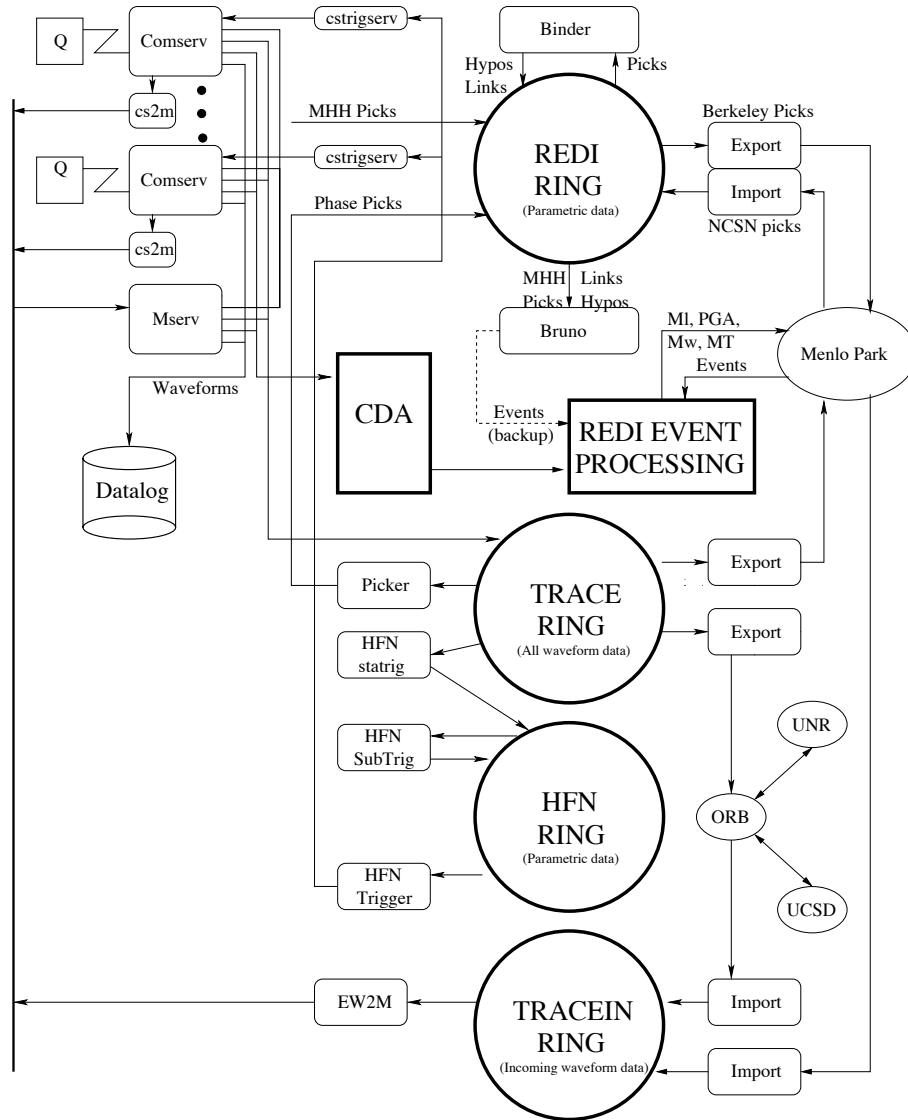


Figure 8.2: Dataflow in the REDI processing environment, showing waveform data coming in from the Quanterra data loggers (Q) into `comserv`. From `comserv`, data are logged to disk (via `datalog`), distributed to other computers (`mserv`), fed into the CDA for REDI processing, and spooled into a trace ring for export.

GMT day on June 15, 2004 (day 167). This change affects: BDM, BKS, BRIB (broadband sensor only), CMB, CVS, FARB, HOPS, HUMO, JCC, JRSC, MHC, MNRC, MOD, ORV, PACP, PKD, POTR, RFSB (surface strong-motion only), SAO, SCCB, WDC, and YBH. Stations BRK, KCC, and WENL were converted at the beginning of day 168.

This change in sampling rate was made in order to be consistent with the USArray specifications. At this time, we do not intend to change the sampling rate of the BP channels associated with the BSL borehole networks - the NHFN, MPBO, and HRSN.

4. Seismic Noise Analysis

BSL seismic data are routinely monitored for state-of-health. An automated analysis is computed weekly to characterize the seismic noise level recorded by each broadband seismometer. The estimation of the Power Spectral Density (PSD) of the ground motion recorded at a seismic station provides an objective measure of background seismic noise characteristics over a wide range of frequencies. When used routinely, the PSD algorithm also provides an objective measure of seasonal and secular variation in the noise characteristics and aids in the

early diagnoses of instrumental problems. A PSD estimation algorithm was developed in the early 1990's at the BSL for characterizing the background seismic noise and as a tool for quality control. As presently implemented, the algorithm sends the results via email to the engineering and some research staff members and generates a bargraph output which compares all the BDSN broadband stations by components. A summary of the results for 2003-2004 is displayed in Figure 3.3. Other PSD plots for the NHFN, HRSN, and MPBO are shown in Figures 4.3, 5.2, and 7.4 respectively.

Three years ago, we expanded our use of the weekly PSD results to monitor trends in the noise level at each station. In addition to the weekly bar graph, additional figures showing the analysis for the current year are produced. These cumulative PSD plots are generated for each station and show the noise level in 5 frequency bands for the broadband channels. These cumulative plots make it easier to spot certain problems, such as failure of a sensor. In addition to the station-based plots, a summary plot for each channel is produced, comparing all stations. These figures are presented as part of a noise analysis of the BDSN on the WWW at <http://www.seismo.berkeley.edu/seismo/bdsn/psd/>.

The PSD algorithm has been documented in previous annual reports.

5. Sensor Testing Facility

The BSL has set up an instrumentation test facility in the Byerly Seismographic Vault in order to systematically determine and to compare the characteristics of up to eight sensors at a time. The test equipment consists of an eight-channel Quanterra Q4120 high-resolution data logger and a custom interconnect panel that provides isolated power and preamplification when required to facilitate the connection and routing of signals from the sensors to the data logger with shielded signal lines. Upon acquisition of the 100 samples-per-second (sps) data from the instruments under test, PSD analysis and spectral phase coherency analysis are used to characterize and compare the performance of each sensor. Tilt tests and seismic signals with a sufficient signal level above the background seismic noise are also used to verify the absolute calibration of the sensors. A simple vertical shake table is used to access the linearity of a seismic sensor.

The sensor testing facility of the BSL is described in detail in the 2001-2002 Annual Report.

Instruments tested during the past year include three Keck OBS broadband seismometers, three STS-2 broadband seismometers, CITRIS accelerometers and a tilt-meter.

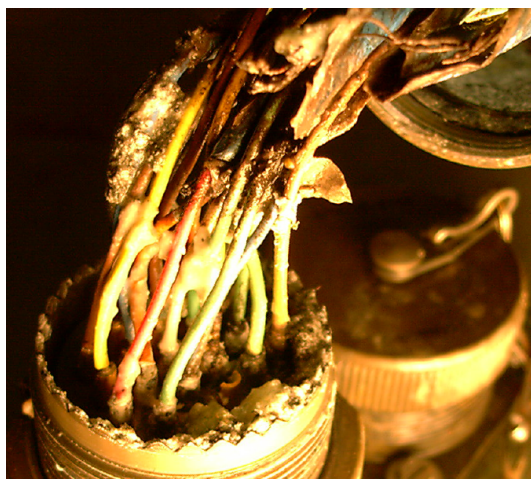


Figure 8.3: Closeup photo of the back of the signal/power cable connector on the STS-2 control box, installed at WDC, showing the corrosion of the wires. The subsequent leakage between the cables generated coherent long period noise.



Figure 8.4: Photo of STS-2 sensors #50205 (right) and #20022 (left) after they were installed and leveled on the seismic pier in the BKS vault. After this photo was taken, the sensors were covered with a couple layers of R-13 fiberglass batt insulation to minimize temperature variations and improve their low frequency performance.

5.1 STS-2s

On August 26th, 2003, the malfunctioning STS-2 broadband sensor (#39335), which was removed from WDC, was installed for testing. The symptom was that there is coherent long period noise on all three broadband channels and the external signal/power connector was visibly corroded (owing to water standing in the dome in which it was installed at WDC) (see Figure 8.3).

The conductors in the signal/power cable were reterminated and the sensor was taken to BKS for noise testing. During the installation in the sensor testing facility, it was discovered that the bubble level on the base plate of the sensor, which is critical for leveling the seismometers, had no bubble. The fluid had leaked out of the bubble level so that it could not be used to level the instrument. On September 8th, after installing a new bubble level on its base plate, STS-2 #39335 was installed and successfully leveled for testing. The subsequent background noise PSD tests showed that the STS-2 was operating within its nominal specifications.

During the month of February 2004, a pair of STS-2 broadband seismometers (#20022 and #50205) were installed in the BKS vault (see Figure 8.4) to characterize their performance prior to installation at remote BDSN seismic stations. STS-2 #20022 is a "low power" unit, for which the factory supplied only nominal calibration information, which was originally installed at HUMO in June 2002. It was removed from service at HUMO in November 2002 because it was determined to be the source of the excessively high noise level observed on the broadband channels. As is our routine policy, it was tested after it was repaired. STS-2 #50205 is a new sensor for which the factory supplied detailed calibration information (with 5 complex zeros and 11 complex poles) for each of the three orthogonal triaxial sensors in the unit. The resulting tests showed that both sensors were operating within their nominal specifications. STS-2 #50205 was subsequently installed at FARB on August 21, 2004 and STS-2 #20022 awaits installation at a new BDSN station.

5.2 CITRIS Accelerometer

During the month of November, several calibration and noise tests were performed on prototype CITRIS accelerometers developed by a team working with Steven Glaser in Civil Engineering. The calibration testing was done in the BSL machine shop in Room 298 McCone Hall during the first two weeks on November. The absolute calibration for each accelerometer was determined by tilting the sensor through an accurately measured angle (see Figures 8.5 and 8.6) and measuring its response. The data were transmitted to a laptop computer via a spread spectrum transceiver and the data logging was done on the laptop with custom software written by graduate students working on the project. After the accelerometers were calibrated, the quiet background noise PSD test was done in the BKS Vault and the results are shown in Figure 8.7.

5.3 Keck OBS

The Keck OBS testing reported on last year continued through July 2004 with the application of insulation to inhibit convection induced noise.

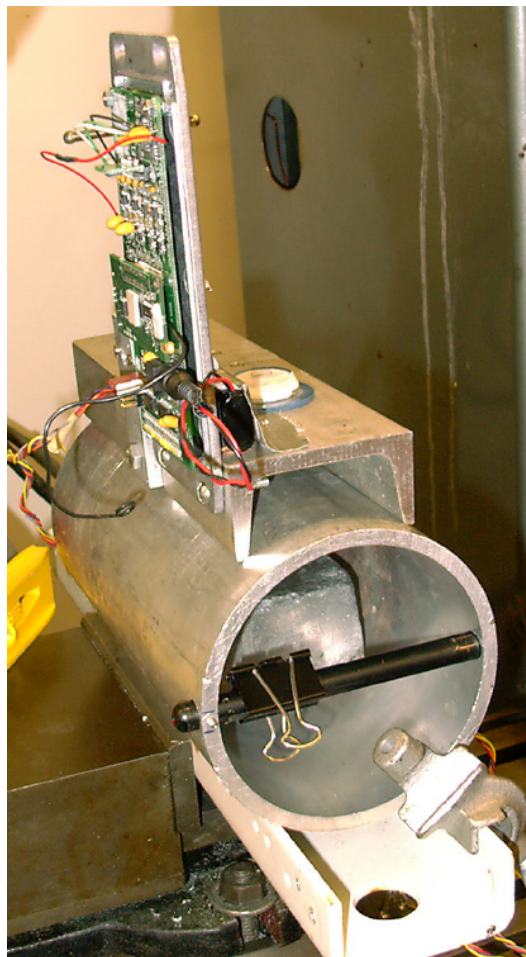


Figure 8.5: Closeup photo of the custom test apparatus assembled to rotate the CITRIS accelerometer through a range of accurately measurable angles up to ± 30 degrees. The accelerometer is an integral component on the circuit board (top) and the large pipe (bottom center) is rotated on the channel to tilt the accelerometer. A laser pointer (black tube mounted on pipe diagonal) is used to infer the rotation angle from the position of the projected laser beam (see Figure 8.6).

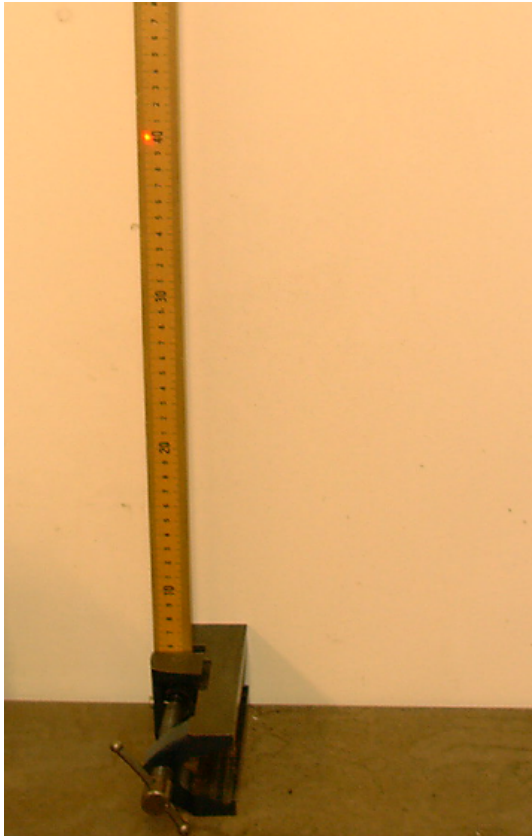


Figure 8.6: Photo of the laser beam projected on a meter stick located 300 cm from the center of the rotation axis of the pipe in Figure 8.5. The position of the beam can be determined to an accuracy of 0.5 mm which is equivalent to measuring the tilt angle to an accuracy of 0.6 minutes of arc.

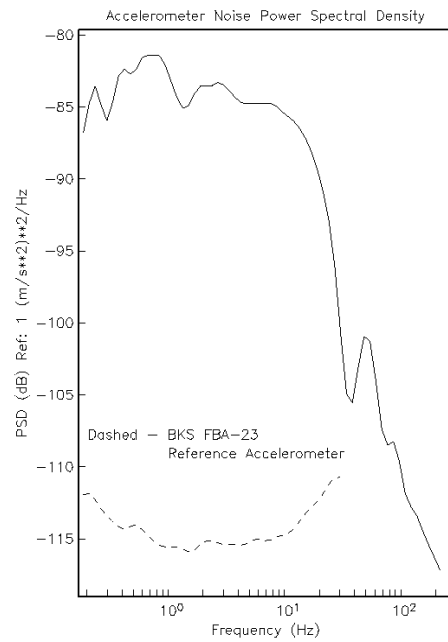


Figure 8.7: Plot of the background noise PSD for one of the CITRIS horizontal accelerometers under test. The background noise PSD estimate from the co-sited BKS Kinematics FBA-23 strong motion accelerometer (dashed line) is provided for reference. The low frequency noise PSD floor of the CITRIS accelerometer averages ~ 83 dB.

Between March and June another round of testing of the Keck OBS sensor began. Sensor #T1046 (see Figure 8.8) was tested to characterize its performance prior to installation on the sea floor at the MOBB site in Monterey Bay. Fiberglass batt insulation (see Figure 8.9) was tied around the titanium pressure sphere to improve the thermal stability of the sensor. During the testing in early April, we found the horizontal components to be excessively noisy. Upon investigation, we found that one of the washers was sited on what appeared to be a CaCl deposit which was powdery and loose and the pier had some small loose debris on its surface. Also, the thick cable which is attached at the top of the pressure vessel is a source of tilt related noise. We swept off the seismic pier and re-installed OBS on three ceramic washers, suspended the cable from the overhead airduct girders, and reinstalled the fiberglass batt insulation. The horizontal component noise was reduced significantly.



Figure 8.8: Photo of cast titanium pressure sphere housing Keck OBS #T1046. The disc shaped base is standing on three ceramic washers for stability on the seismic pier. The orange signal cable exiting at the top of the sphere is draped overhead to minimize the generation of noise at the cable responds to temperature changes.

5.4 Other Tests

During June, Pinnacle Technologies tested a prototype nanoradian resolution tiltmeter in the BKS vault. They supplied the sensor and recording system and they also did all the analysis. We provided only the quiet vault environment in which they could test their sensor.



Figure 8.9: Photo of fiberglass batt insulation surrounding the pressure sphere.

6. Acknowledgements

Doug Neuhauser, Bob Uhrhammer, Lind Gee, Pete Lombard, and Rick McKenzie are involved in the data acquisition and quality control of BDSN/NHFN/MBPO data.

Development of the sensor test facility and analysis system was a collaborative effort of Bob Uhrhammer, Tom McEvelly, John Friday, and Bill Karavas. IRIS and DTRA provided, in part, funding and/or incentive to set up and operate the facility and we thank them for their support.

Bob Uhrhammer led the testing and problem solving effort of the Keck sensors, with help from John Friday, Doug Neuhauser, and Bill Karavas.

Bob Uhrhammer, Lind Gee, and Doug Neuhauser contributed to the preparation of this chapter.

7. References

Scherbaum, Frank. Of Poles and Zeros: Fundamentals in Digital Seismology, Volume 15 of Modern Approaches in Geophysics, G. Nolet, Managing Editor, Kluwer Academic Press, Dordrecht, xi + 257 pp., 1996.

Tapley, W. C. and J. E. Tull, SAC - Seismic Analysis Code: Users Manual, *Lawrence Livermore National Laboratory*, Revision 4, 388 pp., March 20, 1992.

Chapter 9

Northern California Earthquake Monitoring

1. Introduction

Routine analysis of the data produced by BSL networks begins as the waveforms are acquired by computers at UC Berkeley, and ranges from automatic processing for earthquake response to analyst review for earthquake catalogs and quality control.

Over the last 10 years, the BSL has invested in the development of the hardware and software necessary for an automated earthquake notification system (*Gee et al.*, 1996; 2003a). The Rapid Earthquake Data Integration (REDI) project is a research program at the BSL for the rapid determination of earthquake parameters with three major objectives: to provide near real-time locations and magnitudes of northern and central California earthquakes; to provide estimates of the rupture characteristics and the distribution of ground shaking following significant earthquakes, and to develop better tools for the rapid assessment of damage and estimation of loss. A long-term goal of the project is the development of a system to warn of imminent ground shaking in the seconds after an earthquake has initiated but before strong motions begin at sites that may be damaged.

In 1996, the BSL and USGS began collaboration on a joint notification system for northern and central California earthquakes. The current system merges the programs in Menlo Park and Berkeley into a single earthquake notification system, combining data from the NCSN and the BDSN.

Today, the BSL and USGS system forms the Northern California Management Center (NCMC) of the California Integrated Seismic Network (Chapter 2).

2. Northern California Management Center

The details of the Northern California processing system and the REDI project have been described in past annual reports. In this section, we will describe how the Northern California Management Center fits within the

CISN system, detail recent developments, and discuss plans for the future development.

Figure 2.3 in Chapter 2 illustrates the NCMC as part of the the CISN communications ring. The NCMC is a distributed center, with elements in Berkeley and Menlo Park. The 35 mile separation between these two centers is in sharp contrast to the Southern California Management Center, where the USGS Pasadena is located across the street from the Caltech Seismological Laboratory. As described in Chapter 2, the CISN partners are connected by a dedicated T1 communications link, with the capability of falling back to the Internet. In addition to the CISN ring, the BSL and the USGS Menlo Park have a second dedicated communication link to provide bandwidth for shipping waveform data and other information between their processing systems.

Figure 9.1 provides more detail on the current system at the NCMC. At present, two Earthworm-Earlybird systems in Menlo Park feed two "standard" REDI processing systems at UC Berkeley. One of these systems is the production or paging system; the other is set up as a hot backup. The second system is frequently used to test new software developments before migrating them to the production environment. The Earthworm-Earlybird-REDI systems perform the standard detection, location, estimation of M_d , M_L , and M_w , as well as processing of ground motion data. The computation of ShakeMaps is also performed on two systems, one in Menlo Park and one in Berkeley, as described below. An additional system performs finite-fault processing and the computation of higher level ShakeMaps.

The dense network and Earthworm-Earlybird processing environment of the NCSN provides rapid and accurate earthquake locations, low magnitude detection thresholds, and first-motion mechanisms for smaller quakes. The high dynamic range data loggers, digital telemetry, and broadband and strong-motion sensors of the BDSN and REDI analysis software provide reliable magnitude determination, moment tensor estimation, peak ground motions, and source rupture charac-

Northern California Management Center Current Implementation

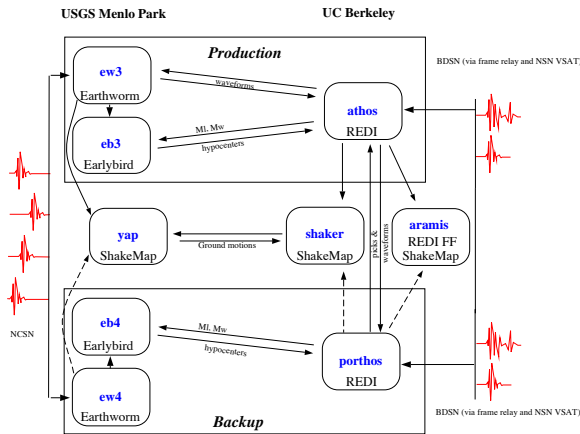


Figure 9.1: Detailed view of the current Northern California processing system, showing the two Earthworm-Earlybird-REDI systems, the two ShakeMap systems, and the finite-fault system.

teristics. Robust preliminary hypocenters are available about 25 seconds after the origin time, while preliminary coda magnitudes follow within 2-4 minutes. Estimates of local magnitude are generally available 30-120 seconds later, and other parameters, such as the peak ground acceleration and moment magnitude, follow within 1-4 minutes (Figure 9.2).

Earthquake information from the joint notification system is distributed by pager/cellphone, e-mail, and the WWW. The first two mechanisms "push" the information to recipients, while the current Web interface requires interested parties to actively seek the information. Consequently, paging and, to a lesser extent, e-mail are the preferred methods for emergency response notification. The *recenteqs* site has enjoyed enormous popularity since its introduction and provides a valuable resource for information whose bandwidth exceeds the limits of wireless systems and for access to information which is useful not only in the seconds immediately after an earthquake, but in the following hours and days as well.

3. 2003-2004 Activities

Most of the effort in the last year has gone toward designing the Northern California Seismic System.

3.1 System Development

As part of ongoing efforts to improve the monitoring systems in northern California, the BSL and the USGS Menlo Park have started to develop the next generation

of the northern California joint notification system or the Northern California Seismic System (NCSS).

Figure 9.1 illustrates the current organization of the two systems. As described above, an Earthworm/Earlybird component is tied to a REDI component and the pair form a single "joint notification system". Although this approach has functioned reasonably well over the last eight years, there are a number of potential problems associated with the separation of critical system elements by ~35 miles of San Francisco Bay.

Recognizing this, we intend to redesign the Northern California operations so that a single independent system operates at the USGS and at UC Berkeley. In FY01/02, our discussions proceeded to the stage of establishing specifications and determining the details required for design. However, in the last year, most of the development effort focused on CISN activities and specific plans for the "next generation" Northern California system were put on hold. This enforced wait provided the opportunity for some ideas to mature and the current plans for the NCMC are somewhat different from those envisioned in 2001.

The current design draws strongly on the experience in Southern California for the development of TriNet (Figure 9.3), with some modifications to allow for local differences (such as very different forms of data acquisition and variability in network distribution). In addition, the BSL and the USGS want to minimize use of proprietary software in the system. The TriNet software uses three forms of proprietary software: Talerian Smart Sockets (TSS) for inter-module communication via a "publish and subscribe" method; RogueWave software for database communication, and Oracle as the database management system. As part of the development of the Northern California Earthquake Data Center, the USGS and BSL have worked extensively with Oracle databases and extending this to the real-time system is not viewed as a major issue. However, we did take the opportunity to review options for replacing Smart Sockets and RogueWave with Southern California, resulting in joint agreement on replacement packages and shared development effort.

In the last two years, BSL staff, particularly Pete Lombard, have become extremely familiar with portions of the TriNet software. We have begun to adapt the software for Northern California, making adjustments and modifications along the way. For example, Pete Lombard has adapted the TriNet magnitude module to northern California, where it is running on a test system. Pete made a number of suggestions on how to improve the performance of the magnitude module and has worked closely with Caltech and the USGS/Pasadena on modifications. One of the recent discoveries with the magnitude module was related to differences in time references as implemented in the database schema.

More recently, the BSL and the USGS Menlo Park

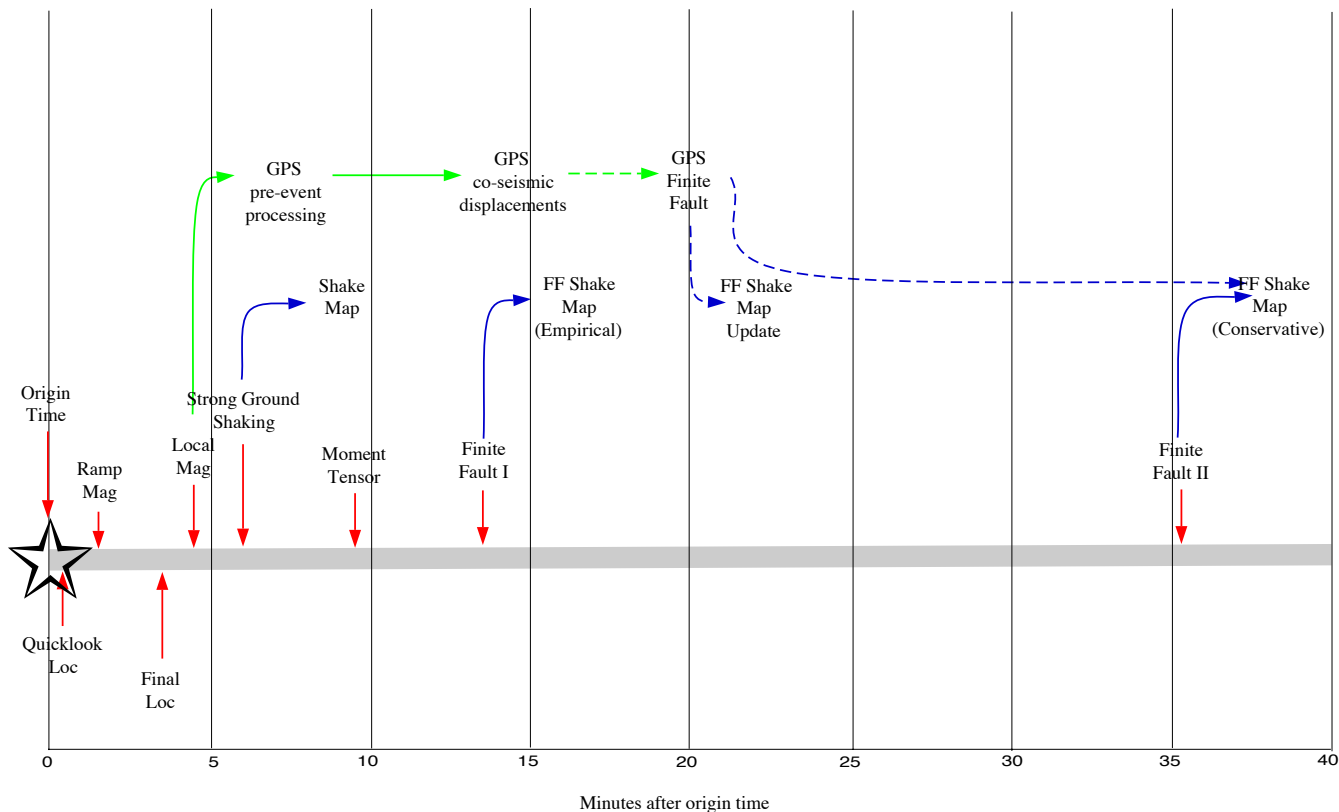


Figure 9.2: Illustration of the current (solid lines) and planned/proposed (dotted lines) development of real-time processing in northern California. The Finite Fault I and II are fully implemented within the REDI system at UC Berkeley and are integrated with ShakeMap. The resulting maps are still being evaluated and are not currently available to the public.

undertook the effort to develop and test a design to exchange "reduced amplitude timeseries". One of the important innovations of the TriNet software development was the concept of continuous processing (*Kanamori et al., 1999*), where waveform data are processed to produce Wood Anderson synthetic amplitudes and peak ground motions constantly. A program called `rad` produces a reduced timeseries, sampled every 5 secs, and stores it in a memory area called an "Amplitude Data Area" or ADA. Other modules can access the ADA to retrieve amplitudes to calculate magnitude and ShakeMaps as needed. In the the past year, the BSL and the USGS Menlo Park have collaborated to establish the tools for the ADA-based exchange. As part of the software development in northern California, several modules have been developed:

The first, `ada2ring`, reads from an ADA, creates an EW message, and plops it into a ring where it can be picked up and transferred between computers using the

standard EW import/export. The second, `ring2ada`, will take the EW amplitude message and put it into the ADA. More recently, some development in northern California now allows multiple `rads` to work on the same time base and feed a single ADA (solving the problem of multiple `rads` working on the same channels).

This system is currently being tested in northern California, with ADAs in Menlo Park and Berkeley feeding an ADA in Berkeley that is being used to test the magnitude codes.

Additional capability needed in the future includes the capability to filter channels in the ADA (so that NoCal does not send CI timeseries back to SoCal, for example), and the ability to handle location codes (currently in the NC version but not in the SC version).

More information on the Northern California software development efforts is available at <http://www.cisn.org/ncmc/>.

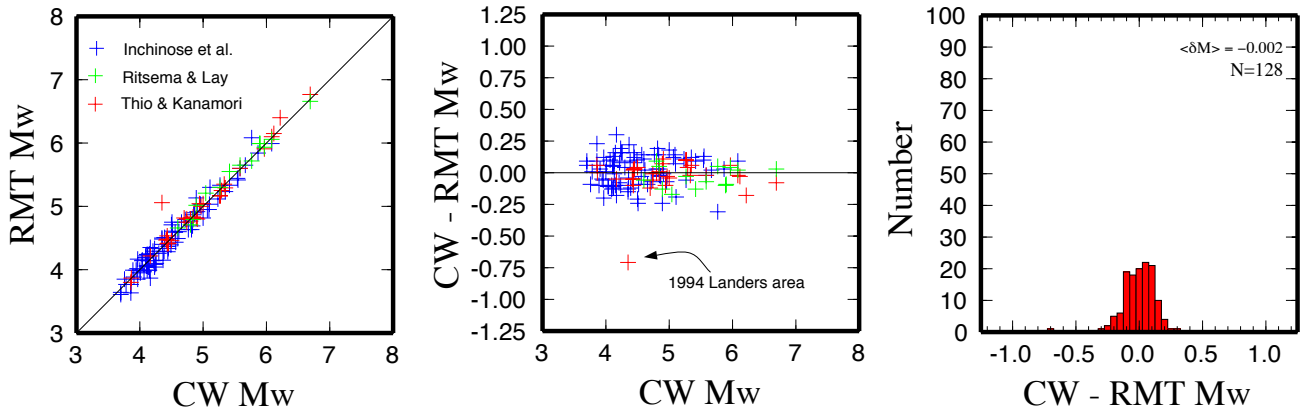


Figure 9.4: Left: Comparison of the estimates of M_w from the complete waveform (CW) method (*Dreger and Romanowicz, 1994*) with other regional moment tensor (RMT) methods (*Thio and Kanamori, 1995*; *Ritsema and Lay, 1995*; *Inchinose et al., 2003*). Middle: Difference between the estimates of M_w , plotted against M_w . Right: Histogram of the magnitude differences.

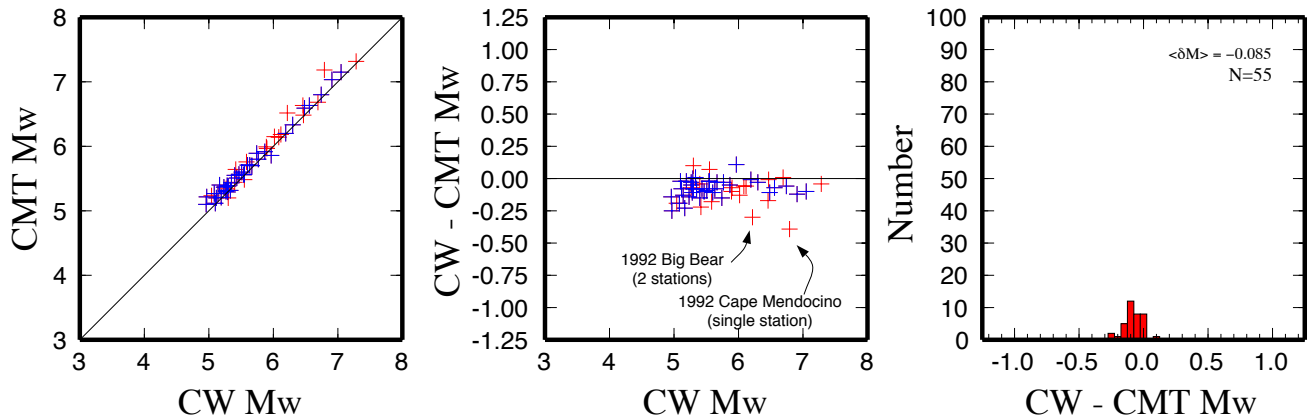


Figure 9.5: Left: Comparison of the estimates of M_w from the CW method with the Harvard CMT method (*Dziewonski and Woodhouse, 1981*). Middle: Difference between the estimates of M_w , plotted against M_w . Right: Histogram of the magnitude differences, showing the very tight distribution.

Comparison between the CW method and other regional moment tensor studies in northern California and the western United States show excellent agreement in the estimate of seismic moment and M_w (Figure 9.4). Over 128 events, the average difference in M_w is 0.002 magnitude units.

There is also very good agreement between the regional complete waveform method and global methods such as the Harvard Centroid Moment Tensor (CMT) (*Dziewonski and Woodhouse, 1981*). Figure 9.5 shows the excellent agreement between the CW and CMT solutions, with an

apparent bias: the CMT estimates of M_w are on average 0.09 higher than the CW estimates. There is a slight suggestion that the residual is increasing at the lower magnitude range, which may be attributed to the global methods reaching the end of their resolution for small earthquakes.

Comparison of the CW estimates of M_w with other regional methods and the CMT solutions indicate the robustness of the procedures and the continuity between the regional and global estimates. The difference between the CW and CMT estimates of M_w shows more scatter

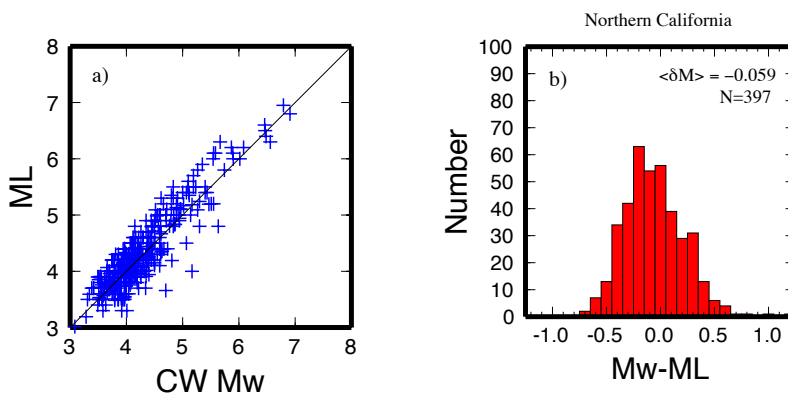
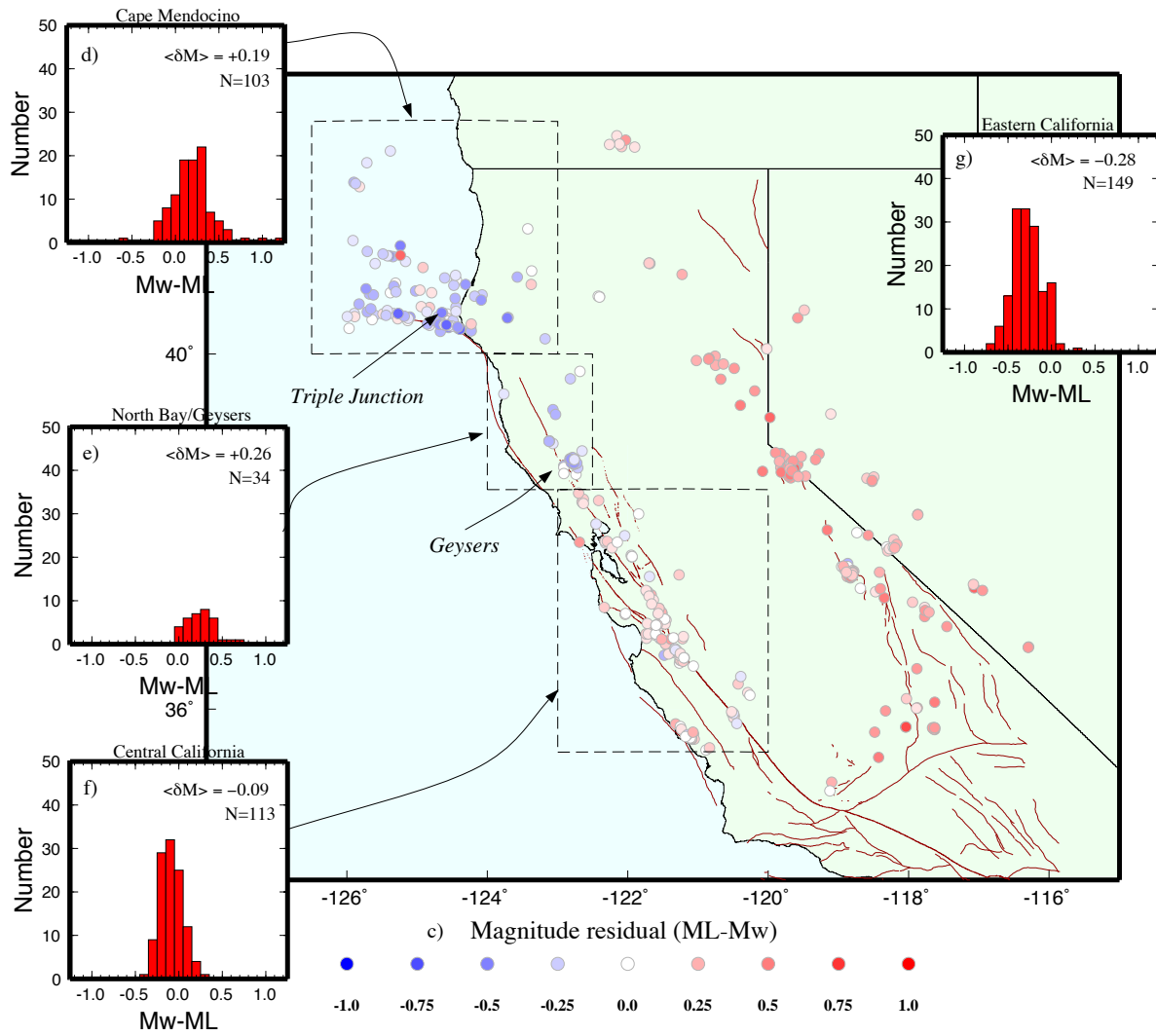


Figure 9.6: Comparison between M_w and M_L for earthquakes in northern California. a) & b) Plots of the M_L versus M_w for all events. The magnitude difference shows a broad spread, with an average of 0.06. c) Map showing the distribution of the magnitude residual, illustrating the strong geographic signal of the Cape Mendocino, Geysers, and eastern California regions. d)-h) Plots showing the distribution of the magnitude residual for different areas.

for events in the early 1990s (red crosses in Figure 9.5), reflecting the limited distribution of regional broadband stations at that time. However, the bias is consistent over time. We do not observe a correlation with this difference and the difference in depth, and are currently investigating the influence of different velocity models.

In comparing regional estimates of M_w to M_L in northern California, we observe an interesting pattern. Overall, the average magnitude difference is quite small (-0.06). However, there is a strong geographic signal in the data. In Figure 9.6, earthquakes with $M_L > M_w$ are drawn in red; events with $M_w > M_L$ are drawn in blue. In general, M_L is consistently larger than M_w with the exception of two regions - the North Bay/Geysers and the Cape Mendocino/Gorda plate areas. In the North Bay Geysers area, the mean difference between M_w and M_L is 0.26 and in Cape Mendocino, the mean difference is 0.19 (although there are 9 events with a difference greater than 0.5). In both areas, there is evidence that this is due to source processes.

At this point in time, we believe that the variation in the magnitude residuals is due to path effects (particularly for events on the east side of the Sierra).

4. Routine Earthquake Analysis

In fiscal year 2003-2004, over 12,500 earthquakes were detected by the automatic systems in northern California. This compares with over 8,300 events last year. The 50% increase in the number of events can be attributed to the 2003 San Simeon earthquake. Of those 12,500+ events, over 560 had preliminary magnitudes greater than 3. 46 events had M_L greater than 4. The largest event recorded by the system was the M_w 6.5 San Simeon earthquake, which is discussed below.

During the last year, the BSL modified its routine analysis procedures, both in response to the increase in seismicity and to a change in personnel.

In the past, BSL analysts routinely located and determined the magnitude of earthquakes in northern California and adjacent regions. As a general rule, events were analyzed if their magnitude is greater than 2.8 in the Central Coast ranges, greater than 3.0 in all of northern California, or greater than 3.8 in the bordering regions. Traditionally, these events were located using hand-picked arrival times from the BDSN stations in conjunction with P-arrival times from the NCSN using the program *strelp*. Over the past several years, the BSL has made a transition in the daily analysis to take advantage of the automatic processing system. As part of this transition, events which have been processed by the automatic system are not generally relocated, although phase arrivals are still hand-picked and the synthetic Wood-Anderson readings are checked.

In the past year, we migrated to a system where the

analyst imports and exports data from the database for review. A graphical user interface allows the analyst to select events for review, export picks and amplitudes, modify and update those readings, and import new readings as well as new hypocenters and magnitudes. While this new system is an improvement in many ways (in particular, it has allowed us to stop depending on an older PC database), there are several components that are difficult to work with since *Seistool* is not designed to work in a database environment. This system is an interim solution while the development of the new northern California system is underway.

During this transition, the M6.5 San Simeon earthquake occurred. The significant increase in seismicity associated with its vigorous aftershock sequence, combined with a reduction in staff, presented significant challenges for the earthquake analysis at the BSL (see, for example, Chapter 5). Recognizing that the BSL efforts to locate local earthquakes duplicates efforts of the USGS, the BSL changed their policy for local and regional reading. As of March 2004, BSL staff are no longer reading BDSN records for local and regional earthquakes. Instead, the BSL analysis effort is being redirected to help with the HRSN readings.

The BSL continues to focus on the unique contributions that can be made from the broadband network. From July 2003 through June 2004, BSL analysts reviewed nearly 179 earthquakes in northern California and adjoining areas of magnitude 3.5 and higher. Reviewed moment tensor solutions were obtained for 65 events (through 6/30/2004). Figure 9.7 and Table 9.1 display the earthquakes located in the BSL catalog and the moment tensor solutions.

4.1 San Simeon Earthquake

The December 22, 2003 M6.5 San Simeon earthquake is the largest event in California since the 1999 M7.1 Hector Mine earthquake and resulted in 2 deaths and over 50 injuries (Figure 9.8). Preliminary reports suggest that the most severe damage was to unreinforced masonry structures that had not yet been retrofitted (e.g., EERI, 2004). Significant damage to water tanks has also been reported and a number of wineries suffered significant loss of wine barrels and their contents. In the following description, we draw upon the San Simeon report of the CISN (*Gee et al.*, 2004a).

The automated procedures of earthquake location and magnitude determination worked well (Tables 9.2 and 9.3). A preliminary location was available within 30 seconds, and a final location with a saturated duration magnitude (M_d) of 5.6 was released approximately 4 minutes after the event occurred. An updated and more reliable local magnitude (M_L) of 6.4 was released 30 seconds later, and the final moment magnitude (M_w) of 6.5 was released 6.5 minutes after the earthquake origin time.

Location	Date	UTC Time	Lat.	Lon.	MT Depth	M_l	M_w	Mo	Str.	Dip	Rake
Petrolia	07/04/03	20:52:57.30	40.318	-124.584	21	3.7	4.3	3.69e22	189	88	14
Healdsburg	07/30/03	04:50:06.00	38.679	-122.910	8	4.0	4.0	1.08e22	311	86	176
Geysers	08/03/03	12:00:53.00	38.796	-122.767	5	3.8	4.2	2.18e22	345	64	-153
Ferndale	08/15/03	09:15:13.00	40.984	-125.596	8	5.0	5.1	5.75e23	42	73	-19
Punta Gorda	08/26/03	02:29:55.80	40.451	-124.648	24	3.9	4.4	4.48e22	124	83	170
Orinda	09/05/03	01:39:54.00	37.846	-122.222	14	4.1	4.0	1.15e22	141	76	-177
Petrolia	09/10/03	21:19:24.00	40.493	-125.657	11	3.9	4.2	2.08e22	360	87	-34
Tres Pinos	09/25/03	14:33:45.70	36.820	-121.354	8	3.5	3.5	2.15e21	137	89	176
Geysers	10/03/03	16:56:34.00	38.839	-122.810	5	3.9	4.3	2.73e22	27	51	-95
Eureka	10/09/03	06:11:33.00	41.073	-125.238	8	4.3	4.5	6.70e22	47	49	-5
Lafayette	10/19/03	15:32:52.00	37.907	-122.150	5	3.5	3.5	2.12e21	245	77	-6
Morgan Hill	11/06/03	22:04:13.00	37.209	-121.661	8	3.9	3.8	4.98e21	134	55	89
Nevada	11/15/03	20:11:59.00	38.222	-117.873	8	4.5	4.1	1.60e22	181	81	-160
Nevada	11/15/03	21:19:36.00	38.219	-117.870	8	4.5	4.2	2.21e22	183	81	-168
San Simeon	12/22/03	19:15:56.00	35.706	-121.102	8	6.4	6.5	5.93e25	290	58	78
San Simeon	12/22/03	21:31:36.00	35.713	-121.069	5	4.3	4.2	2.03e22	103	65	64
Templeton	12/22/03	23:52:36.00	35.529	-120.890	5	4.1	4.1	1.58e22	92	50	71
San Simeon	12/23/03	02:06:55.00	35.689	-121.113	8	4.2	4.1	1.64e22	315	59	113
San Simeon	12/23/03	02:56:49.00	35.709	-121.072	8	4.1	3.9	7.98e21	352	63	160
Paso Robles	12/23/03	03:46:00.00	35.699	-121.116	14	4.3	4.3	3.07e22	162	90	-162
San Simeon	12/23/03	05:30:19.00	35.667	-121.110	5	4.2	4.1	1.61e22	116	54	91
Cambria	12/23/03	18:17:11.00	35.654	-121.054	5	4.9	4.7	1.30e23	293	60	98
San Simeon	12/25/03	05:20:13.00	35.706	-121.102	5	4.2	3.9	7.03e21	282	51	79
San Simeon	12/25/03	05:21:59.00	35.652	-121.094	5	4.2	4.0	1.05e22	293	58	91
San Simeon	12/25/03	06:34:49.00	35.657	-121.091	5	4.1	3.9	9.05e21	295	50	73
San Simeon	12/25/03	09:45:55.00	35.666	-121.091	5	4.1	3.9	7.31e21	308	49	99
Templeton	12/25/03	11:50:01.00	35.553	-120.839	8	4.4	4.5	5.30e22	313	58	131
San Simeon	12/27/03	21:29:39.00	35.668	-121.109	5	4.0	4.0	1.00e22	331	42	46
San Simeon	01/02/04	10:44:51.00	35.705	-121.153	5	3.9	4.1	1.69e22	322	49	105
San Simeon	01/02/04	10:47:39.00	35.682	-121.180	5	4.2	4.2	2.38e22	327	56	112
San Martin	01/31/04	02:11:23.00	37.099	-121.568	8	3.7	3.7	3.46e21	136	87	133
Bakersfield	02/14/04	12:43:11.00	35.052	-119.125	5	4.6	4.6	8.50e22	50	60	49
Geysers	02/18/04	20:37:46.00	38.834	-122.765	5	4.4	4.5	5.46e22	14	50	-100
San Juan Bautista	03/16/04	06:38:32.00	36.806	-121.521	5	4.6	4.3	3.01e22	42	82	13
San Simeon	03/17/04	23:53:07.00	35.735	-121.075	5	4.8	4.5	5.50e22	298	49	88
San Simeon	06/05/04	02:46:51.00	35.548	-121.298	5	3.6	3.6	2.63e21	322	81	170
San Simeon	06/06/04	08:40:52.00	35.552	-121.284	8	3.8	3.8	6.13e21	238	90	-1
Mendocino	06/17/04	18:43:55.00	40.754	-125.076	5	3.7	3.8	5.64e21	149	79	-165
Offshore Baja Calif.	06/15/04	22:28:49.00	32.383	-117.847	5	5.3	5.0	3.14e23	231	74	-18
Lakeview,OR	06/27/04	07:00:13.00	42.208	-120.318	5	5.0	4.1	1.64e22	168	67	-105
Lakeview,OR	06/30/04	12:21:50.00	42.175	-120.295	5	5.0	4.7	1.09e23	165	61	-114

Table 9.1: Moment tensor solutions for significant events from July 1, 2003 to June 31, 2004 using a complete waveform fitting inversion. Epicentral information from the UC Berkeley/USGS Northern California Earthquake Data Center. Moment is in dyne-cm and depth is in km.

The automatically determined first motion mechanism and moment tensor solution each showed a reverse mechanism, in excellent agreement with the reviewed mechanisms.

One of the most challenging aspects of this event was the lack of ShakeMap-quality stations in the vicinity of the earthquake, particularly stations with communications capability. The closest such station to the epicenter with continuous telemetry was the UC Berkeley station PKD, in Parkfield, CA, at a distance of 56 km. The California Geological Survey (CGS) operates three stations in the area - Cambria at 13 km, San Antonio Dam at 22 km, and Templeton at 38 km from the epicenter. How-

ever, since these stations did not have telemetry, their data were not available until hours after the earthquake. Caltech/USGS Pasadena operate stations to the south of the event, but their nearest station was 60 km from the epicenter.

The first automatic ShakeMap was posted 8 minutes after the event, based on the M_L of 6.4 and with 29 stations contributing. The first update occurred 6 minutes later based on the revised M_w of 6.5 and the addition of 45 stations (mostly distant). Throughout December 22nd and 23rd, the ShakeMap was updated multiple times with additional data (including the observations from the CGS stations at Templeton and Cambria) and as more infor-

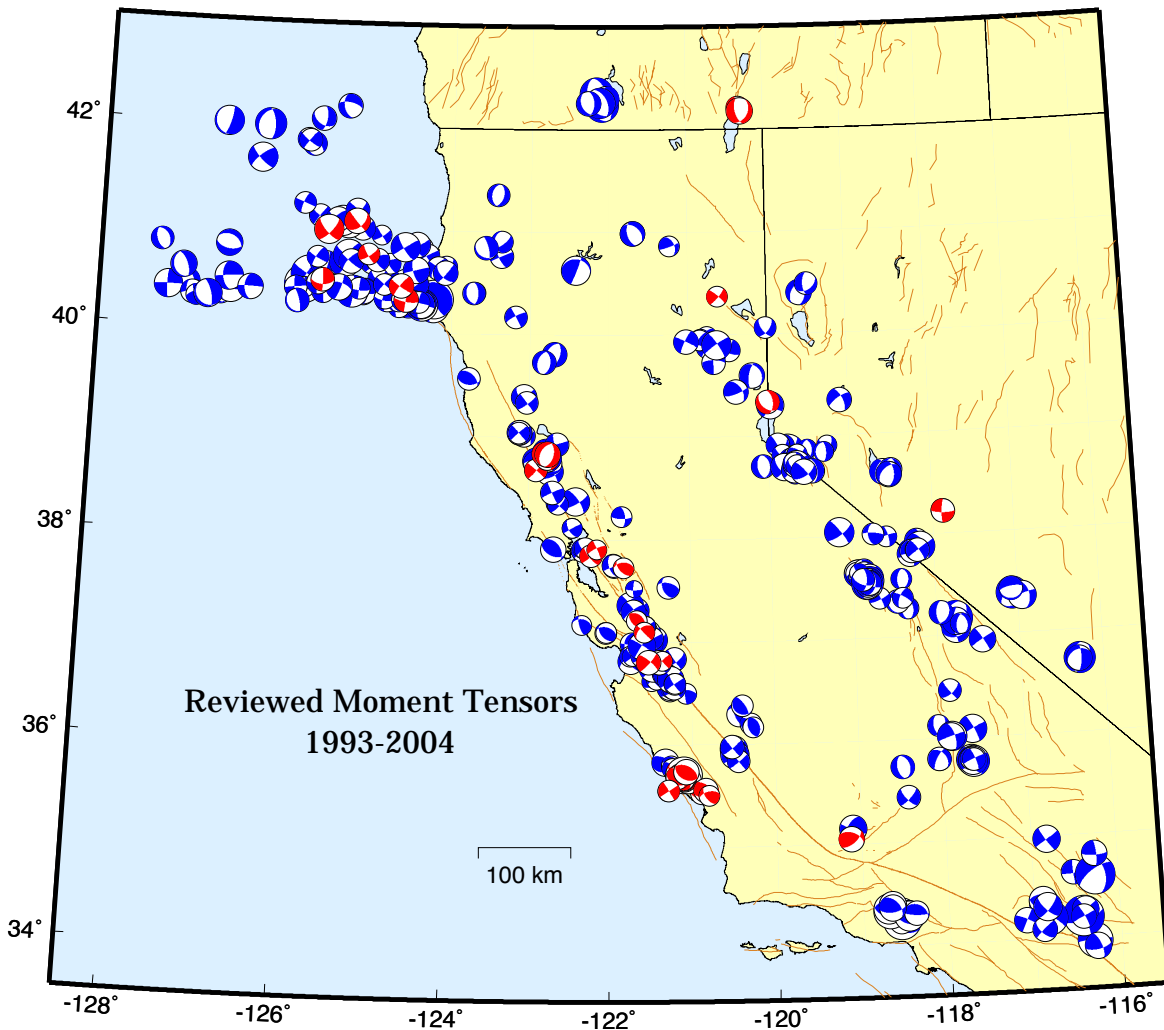


Figure 9.7: Map comparing the reviewed moment tensor solutions determined by the BSL in the last 11 years (blue) and those from the last fiscal year (red).

mation about the earthquake rupture (fault orientation and length) became available.

The San Simeon event provided an important proving ground for the finite fault processing (see section 12.2.) for more details. The automatic codes performed correctly, although a configuration mistake caused the inversion to use the lower quality of the two moment tensor solutions obtained. As a result, the finite-fault system did not obtain optimal results. The computations proved to be relatively fast in this implementation, with the line source inversion completed approximately eight minutes after the event occurred and the resulting predicted ground motions available six minutes later. The 2-D inversion and the predicted ground motions were com-

pleted 30 minutes after the earthquake.

Although the automated system had a configuration error, the processed data were available for rapid review by the seismic analyst. Using available strong motion and broadband displacement waveforms, both line-source and planar-source analyses indicated that this event ruptured nearly horizontally to the SE from the epicenter, essentially in the null-axis direction of the NE dipping reverse mechanism. Because of this nearly horizontal, along dip rupture, it was not possible to uniquely determine the causative fault plane, although there was a slight preference for the NE dipping plane which is consistent with the aftershock distribution. The southeast rupture produced directivity-amplified ground motions toward the SE that

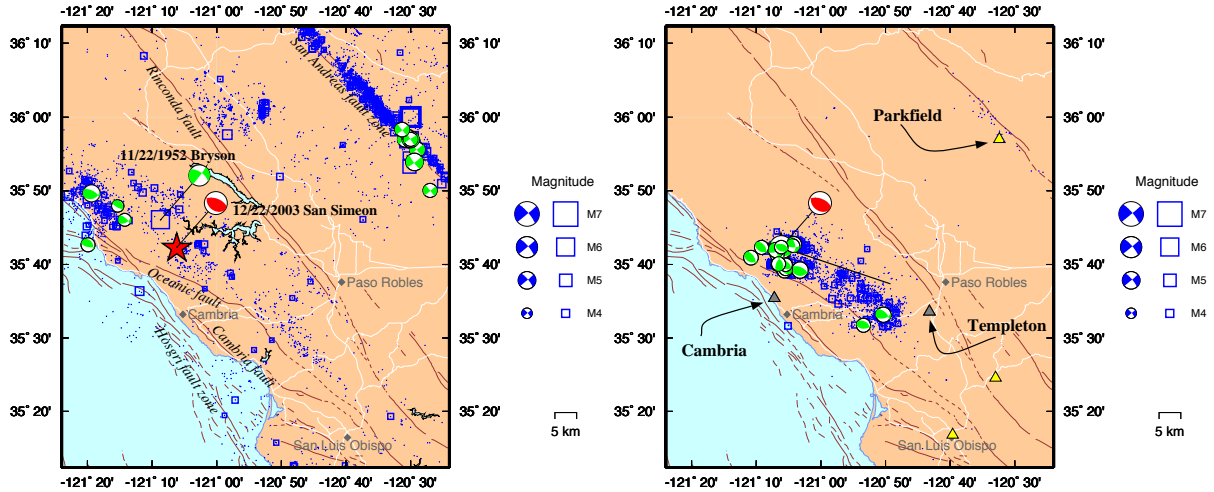


Figure 9.8: Left: Map showing the seismicity from 1966-2003 in the region of the San Simeon earthquake. Earthquakes with magnitude less than 3 are plotted as points; events with magnitude greater than 3 are plotted as squares. Moment tensors solutions over the last 10 years are plotted in green. The location and mechanism of the M6.5 event are shown in red. Also shown is the location and first-motion mechanisms of the 1952 Bryson earthquake (Dehlinger and Bolt, 1987). Right: Earthquakes and moment tensors in the region of the San Simeon earthquake since the 12/22/03 mainshock. The aftershock region extends from the mainshock to the southeast. The solid line indicates the extent of the line source determined on the 22nd for improving the ShakeMap. Triangles indicate the location of stations used in the ShakeMap - yellow indicates near real time stations; grey indicates stations without communications that were not available in near real time. Stations mentioned in the text - Cambria, Templeton, and Parkfield - are labelled.

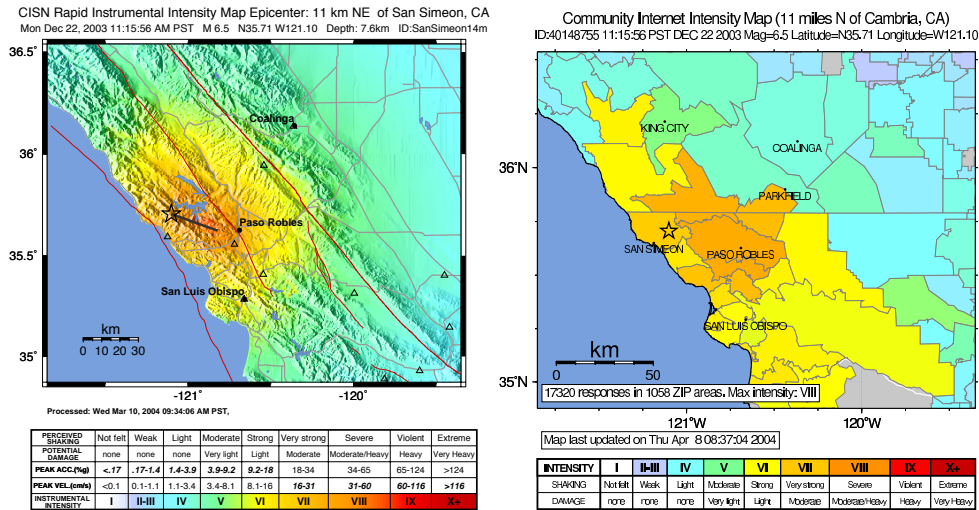


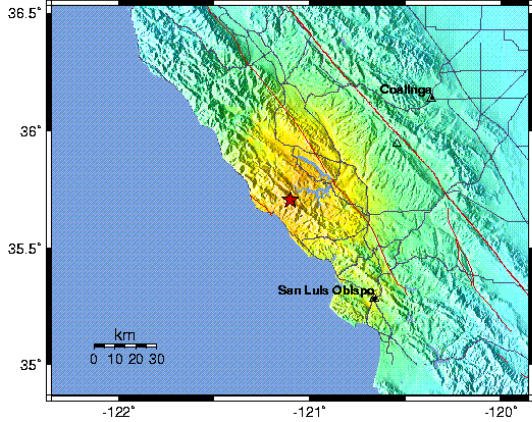
Figure 9.9: Left: Map of instrumental intensity for the M6.5 San Simeon earthquake, after correction for the fault distance calculation. Right: Close-up of the Community Internet Intensity Map for the San Simeon earthquake.

is consistent with felt reports and the damage in Paso Robles. The preliminary results from the reviewed finite source analysis were included in the ShakeMap system approximately 4 hours after the earthquake.

Only a few ShakeMaps have made use of finite source

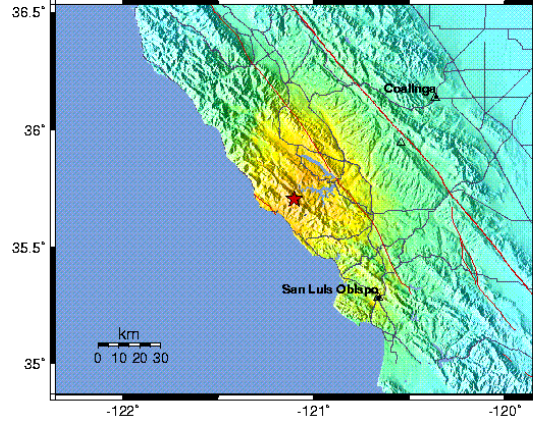
information in the past - the 1999 Hector Mine and 2001 Denali earthquakes are examples. As noted earlier, the use of finite source information is not automatically included in the ShakeMaps available to the public. Because this component of the system has been seldom exercised,

CISN Rapid Instrumental Intensity Map Epicenter: 11 km NE of San Simeon, CA
 Mon Dec 22, 2003 11:15:56 AM PST M 6.4 N35.71 W121.10 Depth: 7.6km ID:SanSimeon1



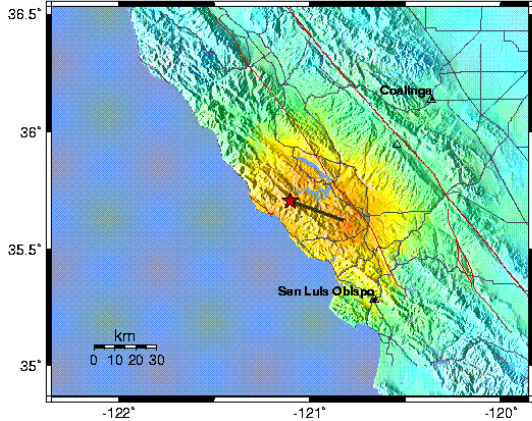
A: 12/22 11:24 AM First ShakeMap with ML 6.4.

CISN Rapid Instrumental Intensity Map Epicenter: 11 km NE of San Simeon, CA
 Mon Dec 22, 2003 11:15:56 AM PST M 6.5 N35.71 W121.10 Depth: 7.6km ID:SanSimeon2



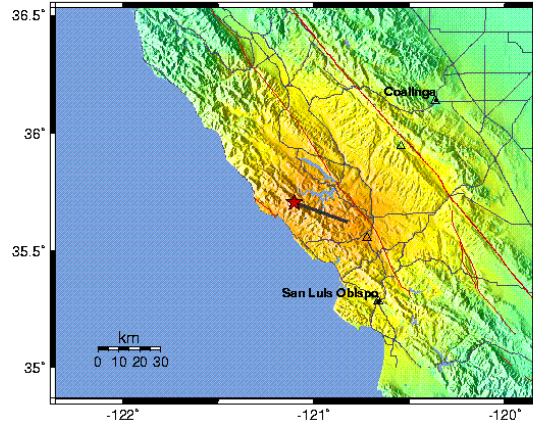
B: 12/22 11:38 Update with additional stations and Mw 6.5

CISN Rapid Instrumental Intensity Map Epicenter: 11 km NE of San Simeon, CA
 Mon Dec 22, 2003 11:15:56 AM PST M 6.5 N35.71 W121.10 Depth: 7.6km ID:SanSimeon7m



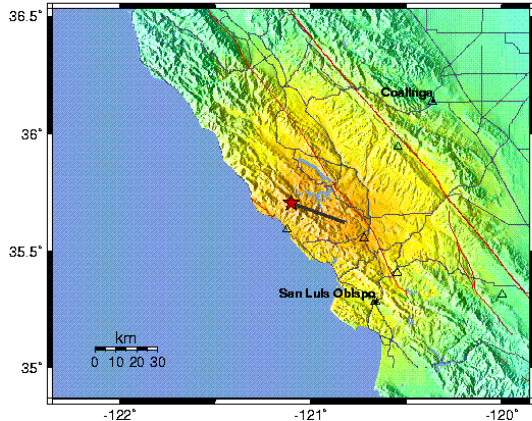
C: 12/22 15:33 Update with addition of finite fault description.

CISN Rapid Instrumental Intensity Map Epicenter: 11 km NE of San Simeon, CA
 Mon Dec 22, 2003 11:15:56 AM PST M 6.5 N35.71 W121.10 Depth: 7.6km ID:SanSimeon8m



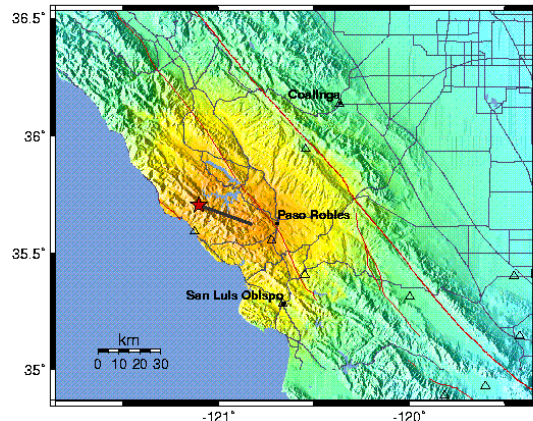
D: 12/22 18:34 Update with data from the Templeton station.

CISN Rapid Instrumental Intensity Map Epicenter: 11 km NE of San Simeon, CA
 Mon Dec 22, 2003 11:15:56 AM PST M 6.5 N35.71 W121.10 Depth: 7.6km ID:SanSimeon12m



E: 12/23 16:28 Update with data from the Cambria station.

CISN Rapid Instrumental Intensity Map Epicenter: 11 km NE of San Simeon, CA
 Mon Dec 22, 2003 11:15:56 AM PST M 6.5 N35.71 W121.10 Depth: 7.6km ID:40148735



F: ShakeMap as of 1/5/2004.

Figure 9.10: The temporal evolution of ShakeMaps for the San Simeon earthquake, as illustrated through the intensity maps. All times are local.

the San Simeon earthquake uncovered a problem in the code used to compute distances to a rupture segment. As a result, the ShakeMaps in Figure 9.10c-f underestimate ground motions near the middle of the fault trace. Figure 9.9 displays the revised intensity map, which shows a broader area of intensity VIII than observed in Figure 9.10f.

The lack of nearby ShakeMap-quality stations resulted in maps with an overwhelming reliance on theoretically predicted ground motions. Figure 9.10 illustrates the evolution of the intensity map with time. In Figure 9.10a and b, the source is modeled as a point source and the maps show areas of significant ground motions south and north of the epicenter. Four hours after the earthquake, information about the fault rupture was added (c), based on the inversion results of *Dreger et al.* (2004). The addition of the finite fault information (in this case, limited to the linear extent and orientation of the fault) focused the higher ground motions to the southeast and showed more damaging shaking in the vicinity of Paso Robles. However the most significant change in the ShakeMap came with the addition of data from the Templeton station, seven hours after the earthquake (d). The high shaking observed at Templeton (47% g), raised all the intensity levels significantly. Maps (e) and (f) show the intensity level after the addition of the Cambria data and the map as of January 5, 2004.

As seen in Figure 9.10c, the addition of information about the fault length and orientation was an important addition to the ShakeMap, particularly given the sparseness of instrumentation. This methodology provides an important tool in areas with limited station distribution to improve ShakeMaps.

4.2 Other Events of Interest

Other significant events in fiscal year 2003-2004 include a small swarm in the Livermore area (largest magnitude M3.5) in January 2004, a M4.4 near the Geysers on February 18th, an M4.3 near San Juan Bautista on March 16th, an M4.2 near King's Beach (Lake Tahoe) on June 3rd, and a sequence in southeastern Oregon which began on June 23rd and continues as of this writing.

4.3 Teleseisms

In addition to the routine analysis of local and regional earthquakes, the BSL also processes teleseismic earthquakes. Taking advantage of the ANSS catalog, analysts review teleseisms of magnitude 5.8 and higher. All events of magnitude 6 and higher are read on the quietest BDSN station, while events of magnitude 6.5 and higher are read on the quietest station and BKS. Earthquakes of magnitude 7 and higher are read on all BDSN stations. The phase and amplitude data are provided to the NEIC, along with the locations and magnitudes, as

contributions to the global catalogs, such as that of the ISC.

5. Acknowledgements

Lind Gee leads the development of the REDI system and directs the routine analysis. Peter Lombard and Doug Neuhauser contribute to the development of software. Rick McKenzie, Doug Dreger, Dennise Templeton, Peggy Hellweg, and David Dolenc contribute to the routine analysis. Lind Gee, Doug Neuhauser, and Dennise Templeton contributed to the writing of this chapter.

Partial support for the develop of the REDI system is provided by the USGS.

6. References

- Dehlinger, P., and B. Bolt, Earthquakes and associated tectonics in a part of coastal central California, *Bull. Seis. Soc. Am.*, *77*, 2056-2073, 1987.
- Dreger, D., Lombard, O., Boatwright, J., Wald D., and L. Gee, Finite source models of the December 22, 2003 San Simeon earthquake and applications to ShakeMap (abstract), *Seismol. Res. Lett.*, *75*, 293, 2004.
- Dreger, D., and B. Romanowicz, Source characteristics of events in the San Francisco Bay region, *USGS Open File Report 94-176*, 301-309, 1994.
- Dziewonski, A.M., T.-A. Chou and J.H. Woodhouse, Determination of earthquake source parameters from waveform data for studies of global and regional seismicity, *J. Geophys. Res.*, *86*, 2825-2852, 1981.
- Earthquake Engineering Research Institute, Preliminary observations on the December 22, 2003, San Simeon earthquake, http://www.eeri.org/lfe/usa_san_simeon.html, 2004.
- Gee, L., D. Oppenheimer, T. Shakal, D. Given, and E. Hauksson, Performance of the CISN during the 2003 San Simeon Earthquake, http://www.cisn.org/docs/CISN_SanSimeon.pdf, 2004a.
- Gee, L., J. Polet, R. Uhrhammer, and K. Hutton, Earthquake Magnitudes in California, *Seism. Res. Lett.*, *75(2)*, 272, 2004b.
- Gee, L., D. Neuhauser, D. Dreger, M. Pasyanos, R. Uhrhammer, and B. Romanowicz, The Rapid Earthquake Data Integration Project, *Handbook of Earthquake and Engineering Seismology*, IASPEI, 1261-1273, 2003a.
- Gee, L., D. Dreger, G. Wurman, Y. Gung, B. Uhrhammer, and B. Romanowicz, A Decade of Regional Moment Tensor Analysis at UC Berkeley, *Eos Trans. AGU*, *84(46)*, Fall Meet. Suppl., Abstract S52C-0148, 2003b.
- Gee, L., D. Neuhauser, D. Dreger, M. Pasyanos, B. Romanowicz, and R. Uhrhammer, The Rapid Earthquake Data Integration System, *Bull. Seis. Soc. Am.*, *86*, 936-945, 1996.

CISN Timing		
Earthquake Information	UTC Time	Elapsed time (HH:MM:SS)
Origin Time (OT)	12/22 19:15:56	00:00:00
Quick Look hypocenter	12/22 19:16:20	00:00:24
Final hypocenter & M_d	12/22 19:20:25	00:04:29
Local Magnitude	12/22 19:20:58	00:05:02
First Motion mechanism	12/22 19:21:36	00:05:40
Moment Tensor mechanism & M_w	12/22 19:22:40	00:06:44
1st ShakeMap completed (M_L 6.4)	12/22 19:24:13	00:08:17
Analyst review/1st aftershock probability	12/22 19:32:00	00:16:04
2nd ShakeMap completed (M_w 6.5)	12/22 19:38:28	00:22:32
Analyst review of moment tensor	12/22 20:16:49	01:00:53
1st Internet Quick Report at cism-edc.org	12/22 20:30:--	01:14:--
Analyst review of line source	12/22 21:54:--	02:38:--
ShakeMap update with line source	12/22 23:33:--	04:17:--
ShakeMap update with Templeton data	12/23 02:34:--	07:18:--
Earthquake Report at cism.org	12/23 17:34:--	22:18:--
Updated aftershock probability	12/23 22:54:--	27:38:--
ShakeMap update with Cambria data	12/24 00:28:--	29:12:--
Preliminary science report at cism.org	12/24 23:44:--	52:28:--

Table 9.2: Timing of earthquake information for the San Simeon earthquake.

Parameters of the Dec 22, 2003 San Simeon Earthquake		
	Automatic	Reviewed
Origin Time (UTC)	19:15:56.24	19:15:56.20
Location (latitude longitude)	35.7058 -121.1013	35.7043 -121.1032
Depth (km)	7.59	7.34
M_d	5.62	5.35
M_L	6.43	6.44
M_w	6.50	6.50
FM Mechanism (strike/dip/rake)	297/56/97 105/35/80	305/60/71 160/35/120
MT Mechanism (strike/dip/rake)	294/59/83 128/32/102	290/58/78 131/34/108
MT Depth (km)	8.0	8.0

Table 9.3: Comparison of parameters as determined by the automatic earthquake processing system with those obtained after analyst review. Note that the value of M_d is lower than the M_L or M_w as the duration magnitude estimate generally saturates around M4.0-4.5. FM - first motion; MT - moment tensor.

Hardebeck, J., Boatwright, J., Dreger, D., Goel, R., Graizer, V., Hudnut, K., Ji, C., Jones, L., Langbein, J., Lin, J., Roeloffs, E., Simpson, R., Stark, K., Stein, R., and J. Tinsley, Preliminary report on the 22 December 2003 M6.5 San Simeon, California, earthquake, *Seismol. Res. Lett.*, *75*, 155-172, 2004.

Ichinose, G., J. Anderson, K. Smith, and Y. Zeng, Source parameters of eastern California and western Nevada earthquakes from regional moment tensor solutions, *Bull. Seis. Soc. Am.*, *93*, 61-84, 2003.

Ritsema, J., and T. Lay, Long-period regional waveform moment tensor inversion for earthquakes in the western United States, *J. Geophys. Res.*, *100*, 9853-9864,

1995.

Romanowicz, B., D. Dreger, M. Pasyanos, and R. Uhrhammer, Monitoring of strain release in central and northern California using broadband data, *Geophys. Res. Lett.*, *20*, 1643-1646, 1993.

Pasyanos, M., D. Dreger, and B. Romanowicz, Toward real-time estimation of regional moment tensors, *Bull. Seis. Soc. Am.*, *86*, 1255-1269, 1996.

Thio, H. K., and H. Kanamori, Moment-tensor inversions for local earthquakes using surface waves recorded at TERRAScope, *Bull. Seis. Soc. Am.*, *85*, 1021-1038, 1995.

Chapter 10

Northern California Earthquake Data Center

1. Introduction

The Northern California Earthquake Data Center, a joint project of the Berkeley Seismological Laboratory (BSL) and the U.S. Geological Survey at Menlo Park, serves as an online archive for various types of digital data relating to earthquakes in central and northern California. The NCEDC is located at the Berkeley Seismological Laboratory, and has been accessible to users via the Internet since mid-1992.

The primary goal of the NCEDC is to provide a stable and permanent archival and distribution center of digital geophysical data for networks in northern and central California. These data include seismic waveforms, electromagnetic data, GPS data, strain, creep, and earthquake parameters. The principal networks contributing seismic data to the data center are the Berkeley Digital Seismic Network (BDSN) operated by the Seismological Laboratory, the Northern California Seismic Network (NCSN) operated by the USGS, and the Bay Area Regional Deformation (BARD) GPS network. The collection of NCSN digital waveforms dates from 1984 to the present, the BDSN digital waveforms date from 1987 to the present, and the BARD GPS data date from 1993 to the present. The BDSN includes stations that form the specialized Northern Hayward Fault Network (NHFN) and the MiniPBO (MPBO) borehole seismic and strain stations in the SF Bay Region.

2. NCEDC Overview

The NCEDC is located within the computing facilities at the Berkeley Seismological Laboratory in McCone Hall. The BSL facility provides the NCEDC with air conditioning, 100 bit switched network, and reliable power from a UPS with generator backup.

The currently installed NCEDC facilities consist of a Sun 280R host computer with a 15-slot AIT tape library which holds 25 GBytes per tape, two SCSI/ATA RAID systems with a total capacity of 4.6 TBytes, and the

SAM-FS hierarchical storage management (HSM) software. A dual processor Sun Ultra 60 provides Web services and research account access to the NCEDC, and a Sun Ultra 450 computer is used for quality control procedures.

In order to increase capacity and reliability, the NCEDC has ordered a Sun L100 tape library with a capacity of 100 LTO-2 tapes, two LTO-2 tape drives, an additional 7 TBytes of RAID, and a fiber-channel switch to support a local SAN. With this additional hardware, we plan to implement a full online copy of the NCEDC data at an alternate location.

The hardware and software system can be configured to automatically create multiple copies of each data file. The NCEDC uses this feature to create an online copy of each data file on online RAID, and another copy on AIT tape which is stored offline. All waveform and GPS data are currently stored on magnetic disk, with backup copies on tape media.

The NCEDC acquired a single processor unlimited user Oracle database license from other funding sources to provide public access to the NCEDC earthquake catalog and waveform inventory, and has ordered a single processor computer on which to run this database.

3. 2003-2004 Activities

By its nature, data archiving is an ongoing activity. In 2003-2004, the NCEDC continued to expand its data holdings and enhance access to the data. Projects and activities of particular note include:

- Population of the hardware information and SEED instrument responses for all NCSN operated stations into the NCEDC database.
- Conversion of all NCSN waveforms from 1984 through 2003 from CUSP format to standard MiniSEED format using standard SEED channel names.

- Association of NCSN event waveforms with the NCSN eventids in the NCEDC database to support data retrieval by eventid.
- Enhanced *BREQ_FAST* and *NetDC* data retrieval interfaces to provide access to NCSN waveform data in SEED format.
- Continued development of IRIS *FISSURES DHI* services as a data distribution method for data from the NCEDC.
- Continued development of *STP* at the NCEDC.
- Development of XML tools for import/export and maintenance of hardware tracking data in the NCEDC database.
- Archiving data from 15 shared SCSN (network CI) stations in southern California in support of the statewide earthquake system developed for the California Integrated Seismic Network (CISN), which represents one of the ANSS monitoring regions.
- Began archiving process for SAFOD Pilot Hole data.
- Began archiving process for LBL Gesers waveform data.
- Purchase of new hardware to support data migration and expansion of the NCEDC.

These activities and projects are described in detail below.

4. Data Collections

The bulk of the data at the NCEDC consists of waveform and GPS data from northern California. Figure 10.1 shows the relative proportion of each data set at the NCEDC. The total size of the datasets archived at the NCEDC is shown in Table 10.1. Figure 10.2 shows the geographic distribution of data archived by the NCEDC.

4.1 BDSN/NHFN/MPBO Seismic Data

The archival of current BDSN (Chapter 3), NHFN (Chapter 4), and Mini-PBO (Chapter 7) (all stations using the network code BK) seismic data is an ongoing task. These data are telemetered from more than 30 seismic data loggers in real-time to the BSL, where they are written to disk files. Each day, an extraction process creates a daily archive by retrieving all continuous and event-triggered data for the previous day. The daily archive is run through quality control procedures to correct any timing errors, triggered data is reselected based

on the REDI, NCSN, and BSL earthquake catalogs, and the resulting daily collection of data is archived at the NCEDC.

All of the data acquired from the BDSN/NHFN/MPBO Quanterra data loggers are archived at the NCEDC. The NCEDC has made an effort to archive older digital data, and the 16-bit BDSN digital broadband data from 1987-1991 have been converted to MiniSEED and are now online. In late June 2002, the NCEDC initiated a project to convert the remaining 16-bit BDSN data (MHC, SAO, and PKD1) from late 1991 through mid-1992 to MiniSEED. An undergraduate student was hired to read the old tapes and to work on the conversion. All remaining 20 Hz 16 bit BDSN data has been converted to MiniSEED, and we are working on the decimation procedures to create the 1 Hz data channels. Data acquired by portable 24-bit RefTek recorders before the installation of Quanterra data loggers at NHFN sites has not yet been converted to MiniSEED and archived.

4.2 NCSN/SHFN Seismic Data

NCSN and SHFN waveform data are sent to the NCEDC via the Internet. The NCSN event waveform files are automatically transferred from the USGS Menlo Park to the NCEDC as part of the routine analysis procedure by the USGS, and are automatically verified and archived by the NCEDC.

The NCEDC maintains a list of teleseismic events recorded by the NCSN, which is updated automatically whenever a new NCSN event file is received at the NCEDC, since these events do not appear in the NCSN catalog.

The NCSN operates a total of 11 continuously telemetered digital broadband stations in northwest California and southwest Oregon in support of the USGS/NOAA Consolidated Reporting of EarthquakeS and Tsunamis (CREST) system, two digital broadband stations in the Mammoth region, and one digital broadband station in the Parkfield region. The NCEDC established procedures to create an archive of continuous data from these stations, in addition to the event waveform files. These data initially included channels at 50 and 100 Hz, but now are all 100 Hz sampling and are archived continuously. At the USGS's request, the 3 component 500 Hz data from the Mammoth Deep Hole are now continuously archived.

4.3 Parkfield High Resolution Seismic Network Data

Event seismograms from the Parkfield High Resolution Seismic Network (HRSN) from 1987 through June 1998 are available in their raw SEG Y format via NCEDC research accounts. A number of events have faulty timing

Volume of Data archived at the NCEDC

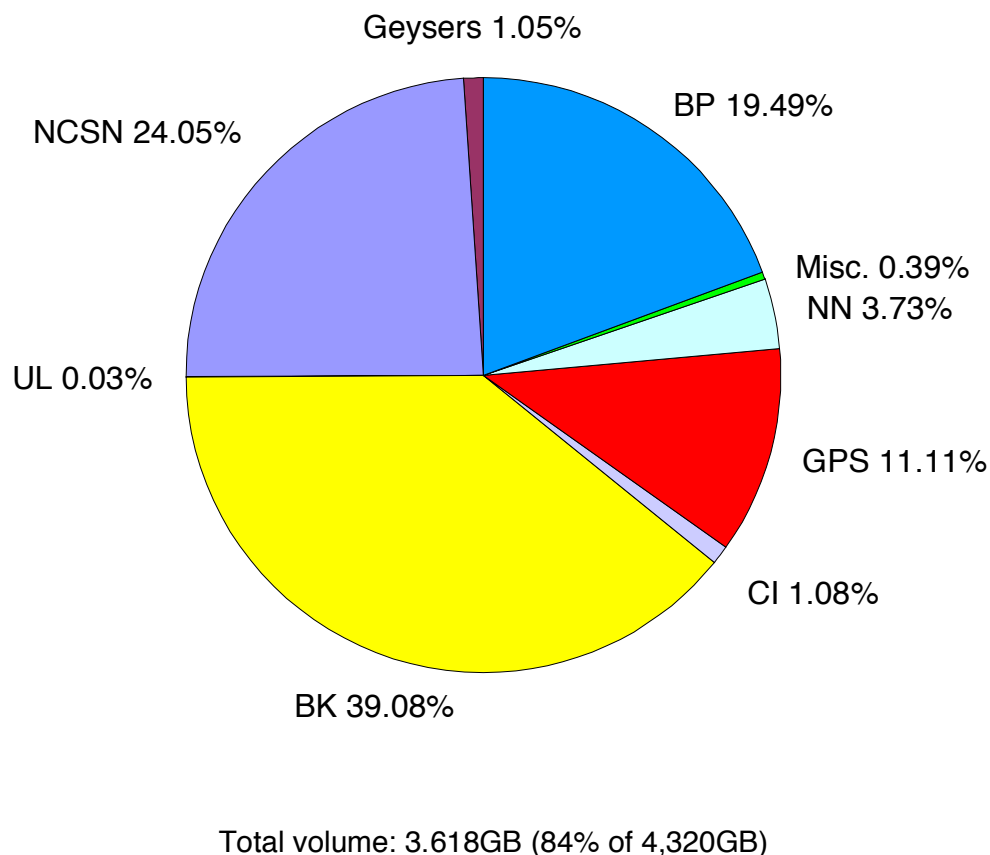


Figure 10.1: Chart showing the relative proportion of each data set at the NCEDC.

Data Type	GBytes
BDSN/NHFN/MPBO (broadband, electric and magnetic field, strain) waveforms	1,414
NCSN seismograms	870
Parkfield HRSN seismograms	705
BARD GPS (RINEX and raw data)	402
UNR Nevada seismograms	135
SCSN seismograms	39
Calpine/Unocal Geysers region seismograms	38
USGS Low frequency geophysical waveforms	1
Misc data	14
Total size of archived data	3,618

Table 10.1: Volume of Data Archived at the NCEDC by network

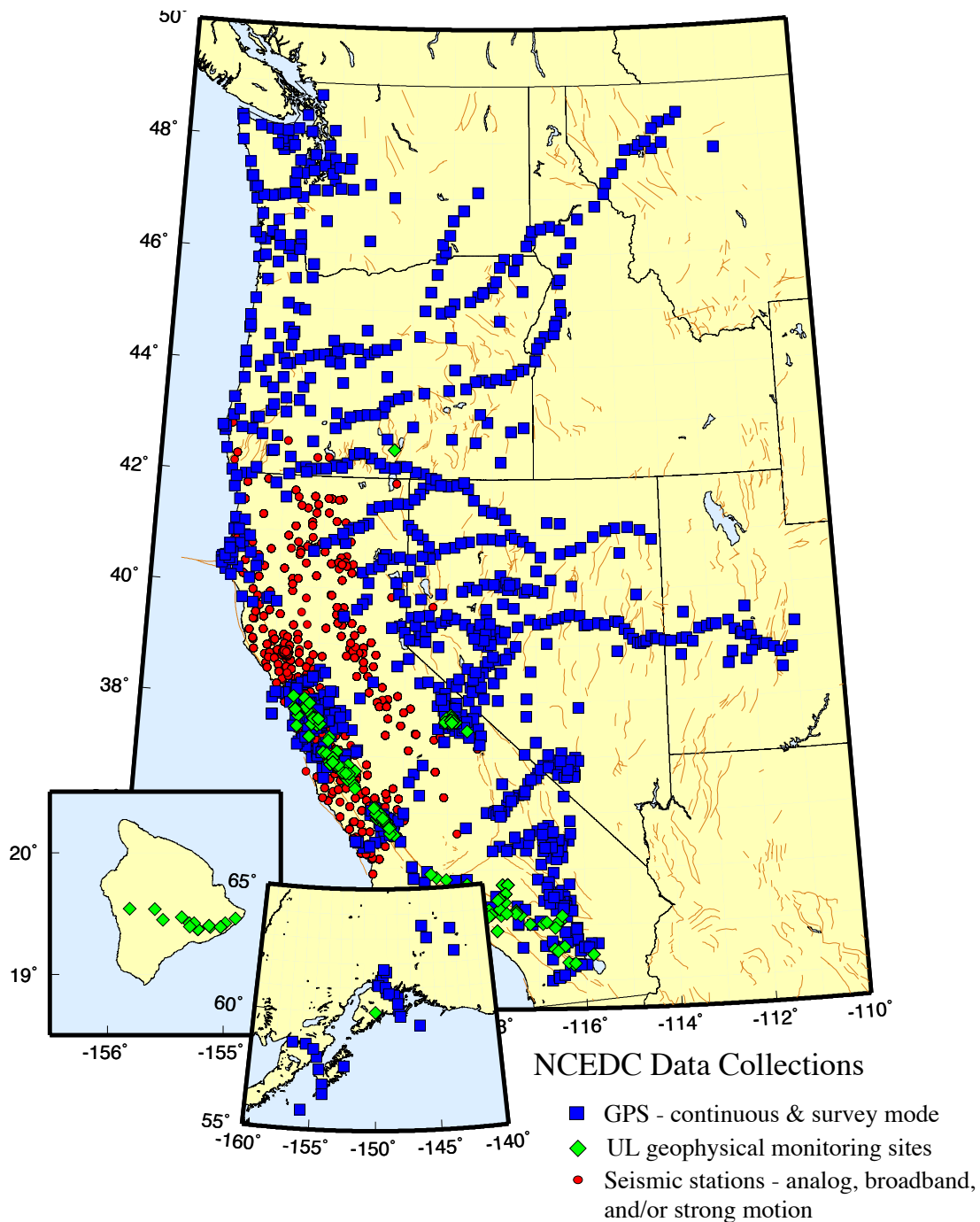


Figure 10.2: Map showing the location of stations whose data are archived at the NCEDC. Circles are seismic sites; squares are GPS sites, and diamonds are the locations of USGS Low-frequency experiments.

due to the lack or failure of a precision timesource for the network. Due to funding limitations, there is currently no ongoing work to correct the timing problems in the older events or to create MiniSEED volumes for these events. However, a preliminary catalog for a significant number of these events has been constructed, and the

catalog is available via the web at the NCEDC.

As described in Chapter 5, the original HRSN acquisition system died in late 1998, and an interim system of portable RefTek recorders were installed at some of the sites. Data from this interim system are not currently available online.

BK Data Availability

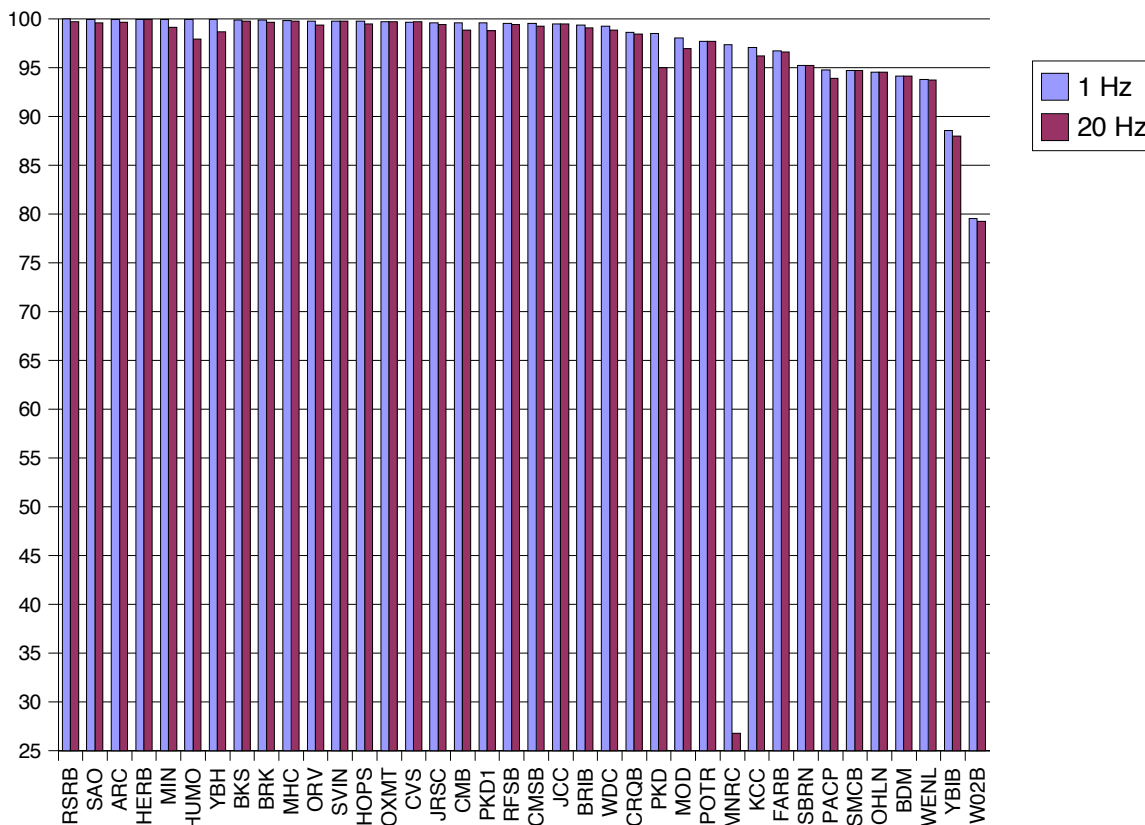


Figure 10.3: Chart showing the availability of BDSN/NHFN/MPBO (BK network) data at the NCEDC for the 1 Hz and 20 Hz channels from 01/01/1996 - 06/30/2004. The data availability from these networks is better than 95% at nearly all stations. Notable exceptions are MNRC (operated for the first year with only dialup telemetry before the installation of continuous telemetry), YBIB (lost AC power before decommissioning the site), and W02B (experienced significant radio problems). In general, a difference between the 1 and 20 Hz data is indicative of one or more significant telemetry problems. Following a major telemetry outage, BSL staff will recover 1 Hz continuous data but only event data for the 20 Hz channels.

In 2000 and 2001, 3 new borehole sites were installed, and the network was upgraded to operate with Quanterra Q730 data loggers and digital telemetry. The upgraded acquisition system detects events using the HRSN stations and extracts waveforms from both the HRSN and the PASO stations. The event waveform files are automatically transferred to the NCEDC, where they are made available to the research community via anonymous ftp until they are reviewed and permanently archived. In 2000-2003 the PASO array, a temporary IRIS PASS-CAL broadband network with real-time telemetry, was installed in the Parkfield area and its recording system was housed at the HRSN recording site in Parkfield. Dur-

ing this time, the HRSN collected event data from both the HRSN and PASO array and provided this integrated data set to researchers in near-real-time.

The HRSN 20 Hz (BP) and state-of-health channels are being archived continuously at the NCEDC. As an interim measure, the NCEDC also archived the continuous 250 Hz (DP) data channels through late 2002 in order to help researchers retrieve events that were not detected during the network upgrade.

The increased seismic activity related to the magnitude 6.5 earthquake in nearby San Simeon on December 22, 2003 drastically increased the number of triggers by the HRSN network. From December 2003 through August

2004, the HRSN had over 70,000 triggers. The 56Kb frame relay connection from Parkfield to UC Berkeley, which was installed to transmit continuous 20 Hz data, selected 250 Hz channels, and event triggered 250 Hz waveforms from the network, was saturated from the increased activity. The HRSN stopped telemetering the event-triggered waveforms, and the NCEDC started to archive continuous 20 and 250 Hz data from the entire network from tapes created at the HRSN operations center in Parkfield in order to preserve this unique dataset. The NCEDC plans to continue archiving both the continuous 250 Hz and 20 Hz data streams for the foreseeable future.

4.4 SAFOD

In July 2002, scientists from Duke University successfully installed a three component 32 level downhole-seismic array in the pilot hole at the EarthScope SAFOD site in collaboration with Steve Hickman (USGS), Mark Zoback (Stanford University) and the Oyo Geospace Engineering Resources International (GERI) Corporation. High frequency event recordings from this array has been provide by Duke University for archiving at the NCEDC. We are currently converting the original SEG-2 format data files to MiniSEED, and developing the SEED instrument responses for this data set.

4.5 UNR Broadband Data

The University of Reno in Nevada (UNR) operates several broadband stations in western Nevada and eastern California that are important for northern California earthquake processing and analysis. Starting in August 2000, the NCEDC has been receiving and archiving continuous broadband data from four UNR stations. The data are transmitted in real-time from UNR to UC Berkeley, where they are made available for real-time earthquake processing and for archiving. Initially, some of the stations were sampled at 20 Hz, but all stations are now sampled and archived continuously at 100 Hz.

The NCEDC installed Simple Wave Server (SWS) software at UNR, which provides an interface to UNR's recent collection of waveforms. The SWS is used by the NCEDC to retrieve waveforms from UNR that were missing at the NCEDC due to real-time telemetry outages between UNR and UC Berkeley.

4.6 Electro-Magnetic Data

The NCEDC continues to archive and process electric and magnetic field data acquired from data loggers at two sites (SAO and PKD). At PKD and SAO, 3 components of magnetic field and 2 or 4 components of electric field are digitized and telemetered in real-time along with seismic data to the Berkeley Seismological Laboratory, where they are processed and archived at the NCEDC in

a similar fashion to the seismic data. The system generates continuous data channels at 40 Hz, 1 Hz, and .1 Hz for each component of data. All of these data are archived and remain available online at the NCEDC. Using programs developed by Dr. Martin Fullerkrug at the Stanford University STAR Laboratory (now at the Institute for Meteorology and Geophysics at the University of Frankfurt), the NCEDC is computing and archiving magnetic activity and Schumann resonance analysis using the 40 Hz data from this dataset. The magnetic activity and Schumann resonance data can be accessed from the Web.

In addition to the electro-magnetic data from PKD and SAO, the NCEDC archives data from a low-frequency, long-baseline electric field project operated by Dr. Steve Park of UC Riverside at site PKD2. This experiment (which is separate from the original equipment at PKD1 described in Chapter 3), uses an 8-channel Quanterra data logger to record the data, which are transmitted to the BSL using the same circuit as the BDSN seismic data. These data are acquired and archived in an identical manner to the other electric field data at the NCEDC.

4.7 GPS Data

The NCEDC continues to expand its archive of GPS data through the BARD (Bay Area Regional Deformation) network of continuously monitored GPS receivers in northern California (Chapter 6). The NCEDC GPS archive now includes 67 continuous sites in northern California. There are approximately 50 core BARD sites owned and operated by UC Berkeley, USGS (Menlo Park and Cascade Volcano Observatory), LLNL, UC Davis, UC Santa Cruz, Trimble Navigation, and Stanford. Data are also archived from sites operated by other agencies including East Bay Municipal Utilities District, the City of Modesto, the National Geodetic Survey, and the Jet Propulsion Laboratory.

The NCEDC continues to archive non-continuous survey GPS data. The initial dataset archived is the survey GPS data collected by the USGS Menlo Park for northern California and other locations. The NCEDC is the principal archive for this dataset. Significant quality control efforts were implemented by the NCEDC to ensure that the raw data, scanned site log sheets, and RINEX data are archived for each survey. All of the USGS MP GPS data has been transferred to the NCEDC and virtually all of the data from 1992 to the present has been archived and is available for distribution.

4.8 Geysers Seismic Data

The Calpine Corporation currently operates a micro-seismic monitoring network in the Geysers region of northern California. Prior to 1999 this network was operated by Unocal. Through various agreements, both Unocal and Calpine have released triggered event wave-

form data from 1989 through 2000 along with preliminary event catalogs for the same time period for archiving and distribution through the NCEDC. This dataset represents over 296,000 events that were recorded by Calpine/Unocal Geysers network, and are available via research accounts at the NCEDC.

The Lawrence Berkeley Laboratory (LBL), with funding from the California Energy Commission, operates a 22 station network in the Geysers region with an emphasis on monitoring seismicity related to well water injection. The earthquake locations and waveforms from this network are sent to the NCEDC, and the locations are forwarded to the NCSN so that they can be merged into the NCSN earthquake catalog. The LBL Geysers waveforms will be available at the NCEDC once the events have been merged into the NCSN catalog.

4.9 USGS Low Frequency Data

Over the last 26 years, the USGS at Menlo Park, in collaboration with other principal investigators, has collected an extensive low-frequency geophysical data set that contains over 1300 channels of tilt, tensor strain, dilatational strain, creep, magnetic field, water level, and auxiliary channels such as temperature, pore pressure, rain and snow accumulation, and wind speed. In collaboration with the USGS, we assembled the requisite information for the hardware representation of the stations and the instrument responses for many channels of this diverse dataset, and developed the required programs to populate and update the hardware database and generate the instrument responses. We developed the programs and procedures to automate the process of importing the raw waveform data and convert it to MiniSEED format.

We have currently archived timeseries data from 887 data channels from 167 sites, and have instrument response information for 542 channels at 139 sites. The waveform archive is updated on a daily basis with data from 350 currently operating data channels. We will augment the raw data archive as additional instrument response information is assembled by the USGS for the channels, and will work with the USGS to clearly define the attributes of the "processed" data channels.

4.10 SCSN/Statewide Seismic Data

In 2004, the NCEDC started to archive broadband and strong motion data from 15 SCSN (network CI) stations that are telemetered to the Northern California Management Center (NCMC) of the California Integrated Seismic Network (CISN). These data are used in the prototype real-time state-wide earthquake processing system and also provide increased coverage for northern California events. Since the data are telemetered directly from the stations in real-time to both the SCSN and to the NCMC, the NCEDC archives the NCMC's copy of the

data to ensure that at least one copy of the data will be preserved.

4.11 Northern California Seismicity Project

The objective of the Northern California Seismicity Project (NCSP), which commenced in fiscal year 2001, is to transcribe the pre-1984 data for $M_L \geq 2.8$ earthquakes which have occurred in Northern and Central California (NCC) outside of the San Francisco Bay region (SFBR), from the original reading/analysis sheets of the Berkeley Seismological Archives, into a computer readable format. This work complements the ongoing Historical Earthquake Relocation Project (HERP) of the Berkeley Seismological Laboratory, which concentrates solely on the San Francisco Bay Region.

The long-term goal of this project is to characterize the spatial and temporal evolution of northern California seismicity during the initial part of the earthquake cycle as the region emerges from the stress shadow of the great 1906 San Francisco earthquake. The problem is that the existing BSL seismicity catalog for the SFBR, which spans most of the past century (1910-present), is inherently inhomogeneous because the location and magnitude determination methodologies have changed, as seismic instrumentation and computational capabilities have improved over time. As a result, NCC seismicity since 1906 is poorly understood.

Creation of a NCC seismicity catalog that is homogeneous, that spans as many years as possible, and that includes formal estimates of the parameters and their uncertainty is a fundamental prerequisite for probabilistic studies of the NCC seismicity. The existence of the invaluable BSL seismological archive containing the original seismograms as well as the original reading/analysis sheets, coupled with the recently acquired BSL capability to scan and digitize historical seismograms at high resolution, allows the application of modern analytical algorithms towards the problem of determining the source parameters of historical SFBR earthquakes.

The funding level for this project has not allowed us to transcribe all of the pre-1984 reading/analysis sheets from the Berkeley Seismological Archive. However, limiting our work to earthquakes of $M_L \geq 3.0$ provides a significant contribution to the uniformity of the NCC seismicity catalog. Although some funding was provided this year, we were unable to hire staff to work on this project and will complete it in 2004.

4.12 Earthquake Catalogs

Northern California

Currently both the USGS and BSL construct and maintain earthquake catalogs for northern and central

California. The "official" UC Berkeley earthquake catalog begins in 1910, and the USGS "official" catalog begins in 1966. Both of these catalogs are archived and available through the NCEDC, but the existence of 2 catalogs has caused confusion among both researchers and the public. The BSL and the USGS have spent considerable effort over the past years to define procedures for merging the data from the two catalogs into a single northern and central California earthquake catalog in order to present a unified view of northern California seismicity. The differences in time period, variations in data availability, and mismatches in regions of coverage all complicate the task.

Worldwide

The NCEDC, in conjunction with the Council of the National Seismic System (CNSS), produced and distributed a world-wide composite catalog of earthquakes based on the catalogs of the national and various U.S. regional networks for several years. Each network updates their earthquake catalog on a daily basis at the NCEDC, and the NCEDC constructs a composite world-wide earthquake catalog by combining the data, removing duplicate entries that may occur from multiple networks recording an event, and giving priority to the data from each network's *authoritative region*. The catalog, which includes data from 14 regional and national networks, is searchable using a Web interface at the NCEDC. The catalog is also freely available to anyone via ftp over the Internet.

With the demise of the CNSS and the development of the Advanced National Seismic System (ANSS), the NCEDC was asked to update its Web pages to present the composite catalog as a product of the ANSS. This conversion was completed in the fall of 2002.

5. Data Quality Control

The NCEDC developed a GUI-based state-driven system *CalQC* to facilitate the quality control processing that is applied to the continuously archived data sets at the NCEDC.

The quality control procedures for these datasets include the following tasks:

- data extraction of a full day of data,
- quickcheck program to summarize the quality and stability of the stations' clocks,
- determine if there is missing data for any data channel,
- retrieve missing data from the stations and incorporate it into the day's data,

- optional creation of multi-day timeseries plots for state-of-health data channels,
- optional timing corrections for data,
- optional extraction of event-based waveforms from continuous data channels,
- optional repacking of MiniSEED data,
- creating waveform inventory entries in the NCEDC database,
- publishing the data for remote access on the NCEDC.

CalQC uses previously developed programs to perform each function, but it provides a graphical point-and-click interface to automate these procedures, and to provide the analyst with a record of when each process was started, whether it executed correctly, and whether the analyst has indicated that a step has been completed. *CalQC* is used to process all data from the BDSN network, and all continuous data from the NCSN, UNR, SCSN, and HRSN networks that are archived by the NCEDC.

6. User Interface Development

6.1 SeismiQuery

During 2000 and 2001, the NCEDC developed a generalized database query system to support the development of portable database query applications among data centers with different internal database schemas. The initial goal was to modify the IRIS *SeismiQuery* web interface program to make installation easier at the NCEDC and other data centers, as well as to introduce a new query language that would be schema independent.

In order to support *SeismiQuery* and other future database query applications, we defined a set of Generic Data Views (GDV) for the database that encompass the basic objects we expect most data centers to support. We introduced a new language we call MSQL (Meta SeismiQuery Language), which is based on generic SQL, and uses the GDV's for its core schema. MSQL queries are converted to Data Center specific SQL queries by the parsing program MSQL2SQL. This parser stores the MSQL parsing tree in a data structure, and API's were implemented to browse and modify elements in the parsing tree. These API's are the only datacenter or database specific source codes. We finally modified the *SeismiQuery* web interface to uniformly generate MSQL requests and to process these requests in a consistent fashion.

We have installed *SeismiQuery* at the NCEDC, where it provides a common interface for querying attributes

and available data for SEED format data, and have provided both IRIS and the SCEC Data Center with our modified version of *SeismiQuery*. We envision using this approach to support other database query programs in the future.

6.2 NetDC

In a collaborative project with the IRIS DMC and other worldwide datacenters, the NCEDC helped develop and implement *NetDC*, a protocol which will provide a seamless user interface to multiple datacenters for geophysical network and station inventory, instrument responses, and data retrieval requests. The *NetDC* builds upon the foundation and concepts of the IRIS *BREQ_FAST* data request system. The *NetDC* system was put into production in January 2000, and is currently operational at three datacenters worldwide – the NCEDC, IRIS DMC, and Geoscope. The *NetDC* system receives user requests via email, automatically routes the appropriate portion of the requests to the appropriate datacenter, optionally aggregates the responses from the various datacenters, and delivers the data (or ftp pointers to the data) to the users via email.

6.3 STP

In 2002, the NCEDC wrote a collaborative proposal with the SCEDC to the Southern California Earthquake Center, with the goal of unifying data access between the two data centers. As part of this project, the NCEDC and SCEDC are working to support a common set of 3 tools for accessing waveform and parametric data: *SeismiQuery*, *NetDC*, and *STP*.

The *Seismogram Transfer Program* or *STP* is a simple client-server program, developed at the SCEDC. Access to *STP* is either through a simple direct interface that is available for Sun or Linux platforms, or through a GUI Web interface. With the direct interface, the data are placed directly on a user's computer in several possible formats, with the byte-swap conversion performed automatically. With the Web interface, the selected and converted data are retrieved with a single ftp command. The *STP* interface also allows rapid access to parametric data such as hypocenters and phases.

The NCEDC has continued work on *STP*, working with the SCEDC on extensions and needed additions. We added support for the full SEED channel name (Station, Network, Channel, and Location), and are now able to return event-associated waveforms from the NCSN waveform archive.

6.4 EVT_FAST

In order to provide Web access to the NCSN waveform before the SEED conversion and instrument response for the NCSN has been completed, the NCEDC implemented

EVT_FAST, an interim email-based waveform request system similar to the *BREQ_FAST* email request system. Users can email *EVT_FAST* requests to the NCEDC and request NCSN waveform data based on the NCSN event id. The NCSN waveform data is converted to either SAC ASCII, SAC binary, or AH format, and placed in the anonymous ftp directory so that users can retrieve the data. The *EVT_FAST* waveforms are currently named with the USGS's native NCSN channel names. We have just begun the work to provide *EVT_FAST* waveform data in SEED format with SEED channel names.

6.5 FISSURES

The *FISSURES* project developed from an initiative by IRIS to improve earth scientists' efficiency by developing a unified environment that can provide interactive or programatic access to waveform data and the corresponding metadata for instrument response, as well as station and channel inventory information. *FISSURES* was developed using CORBA (Common Object Request Broker Architecture) as the architecture to implement a system-independent method for the exchange of this binary data. The IRIS DMC developed a series of services, referred to as the *Data Handling Interface (DHI)*, using the *FISSURES* architecture to provide waveform and metadata from the IRIS DMC.

The NCEDC has implemented the *FISSURES Data Handling Interface (DHI)* services at the NCEDC, which involves interfacing the DHI servers with the NCEDC database schema. We started with the source code for the IRIS DMC's DHI servers, which reduced significantly the implementation's time. We now have the waveform and event *FISSURES* services running in demonstration mode at the NCEDC. These services interact with the NCEDC database and data storage system, and can deliver NCEDC event and channel metadata as well as waveforms using the *FISSURES* interfaces. We have installed the *FISSURES DHI* servers, and worked with the IRIS DMC in 2003-2004 to register with the *FISSURES* naming services which are run at both the IRIS DMC and the NCEDC.

6.6 GSAC

Since 1997, the NCEDC has collaborated with UNAVCO and other members of the GPS community on the development of the *GPS Seamless Archive Centers (GSAC)* project. This project allows a user to access the most current version of GPS data and metadata from distributed archive locations. The NCEDC is participating at several levels in the *GSAC* project: as a primary provider of data collected from core BARD stations and USGS MP surveys, and as a wholesale collection point for other data collected in northern California. We helped to define database schema and file formats for the

GSAC project, and have produced complete and incremental monumentation and data holdings files describing the data sets that are produced by the BARD project or archived at the NCEDC so that other members of the *GSAC* community can provide up-to-date information about our holdings. Currently, the NCEDC is the primary provider for over 120,000 data files from over 1400 continuous and survey-mode monuments. The data holdings records for these data have been incorporated into the *GSAC* retailer system, which became publicly available in late 2002.

7. Database Development

Most of the parametric data archived at the NCEDC, such as earthquake catalogs, phase and amplitude readings, waveform inventory, and instrument responses, have been stored in flat text files. Flat files are easily stored and viewed, but are not efficiently searched. Over the last year, in collaboration with the Southern California Earthquake Data Center (SCEDC) and the California Integrated Seismic Network (CISN), the NCEDC has continued development of database schemas to store the parametric data from the joint earthquake catalog, station history, complete instrument response for all data channels, and waveform inventory.

The parametric schema supports tables and associations for the joint earthquake catalog. It allows for multiple hypocenters per event, multiple magnitudes per hypocenter, and association of phases and amplitudes with multiple versions of hypocenters and magnitudes respectively. The instrument response schema represents full multi-stage instrument responses (including filter coefficients) for the broadband data loggers. The hardware tracking schema will represent the interconnection of instruments, amplifiers, filters, and data loggers over time. This schema will be used to store the joint northern California earthquake catalog and the ANSS composite catalog.

The entire description of the BDSN/NHFN/MPBO, HRSN, and USGS Low Frequency Geophysical networks and data archive has been entered into the hardware tracking, SEED instrument response, and waveform tables. Using programs developed to perform queries of waveform inventory and instrument responses, the NCEDC can now generate full SEED volumes for these networks based on information from the database and the waveforms on the mass storage system.

During 2002-2003, the NCEDC and NCSN jointly developed a system consisting of an extensive spreadsheet containing per-channel information that describes the hardware of each NCSN data channel and provides each channel with a SEED-compliant channel name. This spreadsheet, combined with a limited number of files that describe the central-site analog digitizer, FIR decimation

filters, and general characteristics of digital acquisition systems, allow the NCSN to assemble its station history in a format that the NCEDC can use to populate the hardware tracking and instrument response database tables for the NCSN.

During 2003-2004, the NCEDC and NCSN finalized the CUSP-to-SEED channel mapping for the NCSN waveforms, and entered all of the hardware tracking and response information into the NCEDC database for the sites operated by the NCSN, and can now generate complete SEED responses for all of those data channels. There is, however, additional work that needs to be done in conjunction with contributing networks such as CA DWR, UNR, and SCSN to provide responses for shared stations.

The second part of this project is the conversion of the NCSN waveforms from their native CUSP format into MiniSEED, the standard NCEDC waveform format. Multiple problems needed to be addressed, such as ambiguous or erroneously labeled CUSP data channel, sensors that were recorded on multiple data channels, and ensuring that each distinct data channel is mapped to a distinct SEED channel name. The NCEDC developed programs to use the time-dependent NCSN instrument response spreadsheet and NCSN-supplied channel name transformation rules to determine the SEED channel naming, and to provide feedback to the NCSN on channel naming problems. In 2004, the NCEDC converted all of the NCSN waveform data from the period 1984 through 2003 from CUSP format into MiniSEED format. We entered the waveform descriptors into the NCEDC database, and provided association information between the NCSN event ids and the corresponding waveform data. We are currently developing procedures to convert new NCSN waveforms into MiniSEED format and archive them as they are received by the NCEDC, and to convert the remaining 2004 CUSP waveforms.

The NCEDC has developed XML import and export procedures to provide better maintenance of the hardware tracking information and resulting instrument responses for stations in our database. When changes are made to either existing hardware or to station configurations, we export the current view in XML format, use a GUI-based XML editor to easily update the information, and import the changes back into the database. When adding new stations or hardware, we can easily use information from existing hardware or stations as templates for the new information. This allows us to treat the database as the authoritative source of information, and to use off-the-shelf tools such as the XML editor and XML differencing programs as part of our database maintenance procedures.

We distributed all of our programs and procedures for populating the hardware tracking and instrument response tables to the SCEDC in order to help them pop-

ulate their database.

During 2002-2003, the BSL had been processing events detected by the HRSN (BP) network. The waveform data and event parameters (picks and hypocenters) are stored in separate HRSN database tables, and will be merged with events from the NCSN when the NCSN catalog is migrated to the database. However, human event processing stopped after the San Simeon earthquake due to the rapid increase in seismicity related to that event.

Additional details on the joint catalog effort and database schema development may be found at <http://quake.geo.berkeley.edu/db>

8. Data Distribution

The NCEDC continues to use the World Wide Web as a principal interface for users to request, search, and receive data from the NCEDC. The NCEDC has implemented a number of useful and original mechanisms of data search and retrieval using the World Wide Web, which are available to anyone on the Internet. All of the documentation about the NCEDC, including the research users' guide, is available via the Web. Users can perform catalog searches and retrieve hypocentral information and phase readings from the various earthquake catalogs at the NCEDC via easy-to-use forms on the Web. In addition, users can peruse the index of available broadband data at the NCEDC, and can request and retrieve broadband data in standard SEED format via the Web. Access to all datasets is available via research accounts at the NCEDC. The NCEDC's Web address is <http://quake.geo.berkeley.edu/>

The NCEDC hosts a web page that allows users to easily query the NCEDC waveform inventory, and generate and submit *NetDC* requests to the NCEDC. The NCEDC currently supports both the *BREQ_FAST* and *NetDC* request formats. As part of our collaboration with SCEDC, the NCEDC provided its *BREQ_FAST* interface code to SCEDC, and has worked with them to implement *BREQ_FAST* requests at the SCEDC.

The various earthquake catalogs (including phase and earthquake mechanism) can be searched using NCEDC web interfaces that allow users to select the catalog, attributes such as geographical region, time and magnitude. The GPS data is available to all users via anonymous ftp. Research accounts are available to any qualified researcher who needs access to the other datasets that currently are not available via the Web.

The GPS data archived at the NCEDC is available over the Internet through the GSAC retailer system, which became publicly available in late 2002, as well as by anonymous FTP.

8.1 Web Pages

The NCEDC developed its Web pages in the early days of the Web. Unfortunately, time constraints have kept the pages somewhat static and limited in their use. In June of 2002, the NCEDC began a project to update and expand their Web offerings. This project was completed in October 2002, and provides the NCEDC with a uniform look-and-feel for all web pages.

9. Acknowledgements

The NCEDC is a joint project of the BSL and the USGS Menlo Park and is partially funded by the USGS.

Doug Neuhauser is the manager of the NCEDC. Stephane Zuzlewski, Rick McKenzie, Mark Murray, André Basset, and Lind Gee of the BSL and David Oppenheimer, Hal Macbeth, and Fred Klein of the USGS Menlo Park contribute to the operation of the NCEDC. Doug Neuhauser, Lind Gee, and Stephane Zuzlewski contributed to the preparation of this chapter.

Chapter 11

Outreach and Educational Activities

1. Introduction

The BSL is involved in a variety of outreach activities, ranging from lectures and lab tours to educational displays and the development of classroom materials for K-12 teachers. We maintain an earthquake information tape (510-642-2160) and an extensive set of Web pages, providing basic earthquake and seismic hazard information for northern and central California.

2. Outreach Overview

The BSL has several on-going outreach programs, such as the educational displays, WWW development, and the Earthquake Research Affiliates Program.

2.1 Educational Displays

As part of the BSL's outreach activities, we have made REDI earthquake data available to a number of universities, colleges, and museums as educational displays. As noted above, this year marked the expansion of this program to the K-12 environment. Participating organizations receive a REDI pager and the Qpager software to display the earthquake information. The Qpager program maps the previous seven days of seismicity, with earthquake shown as a dot. The size of the dot indicates the magnitude of the event, while the color of the dot indicates its age. These educational displays have been installed at UC Berkeley (McCone Hall, Earthquake Engineering Research Center, LHS), California Academy of Sciences, CSU Fresno, CSU Northridge, CSU Sacramento, Caltech, College of the Redwoods, Fresno City College, Humboldt State University, San Diego State University, Sonoma State University, Stanford University (Blume Engineering Center, Department of Geophysics), UC Davis, UC Santa Cruz, UC San Diego, and USC. In a pilot project initiated two years ago, the San Francisco Unified School District has been given two pager systems for use in middle school classrooms.

In addition to the seismicity displays, the BSL provides local waveform feeds for helicorders at several visitor centers associated with BDSN stations (CMB and

MHC). Organizations such as LHS, KRON, and KPIX receive feeds from BKS via dedicated phone lines for display, while the USGS Menlo Park uses data from CMB for display in the lobby of the seismology building. The BSL has also loaned a seismometer and helicorder display to the San Leandro Unified School District for their use in science classes.

2.2 WWW

Over the last year, we have continued to expand our presence on the WWW. Our primary goal has been to provide a source of earthquake information for the public, although we also provide information about the networks, such as station profiles, which benefits the research community as well. We provide such information as seminar schedules, course advertisements, descriptions of operations and research, updates on recent earthquake activity, details on Bay Area seismicity and hazards, and links to other earthquake and earth science servers. We also use the WWW server for our own information distribution, with such details as the computing and operational resources, rosters, and schedules for various purposes. Last year, we began an effort to update and revamp our Web pages, as described below.

2.3 Earthquake Research Affiliates Program

The UC Berkeley Earthquake Research Affiliates (ERA) Program is an outreach project of the BSL, the Department of Geology and Geophysics, and the Earthquake Engineering Research Center. The purpose is to promote the support of earthquake research while involving corporations and governmental agencies in academic investigation and education activities such as conferences and field trips. The ERA program provides an interface between the academic investigation and practical application of earthquake studies.

3. 2003-2004 Activities

3.1 Tours and Presentations

BSL staff spent considerable time with public relations activities during the past year. Several tours are given each month, with audiences ranging from middle-school students to scientists and engineers from China and Japan.

The BSL hosted several special groups during 2003-2004. Several large groups visited, including classes from Ecole Normale Superieure (Paris, France), Sixth Form College (Colchester, England) and the Coast Guard.

In addition to the tours, Drs. Romanowicz, Dreger, Gee, Hellweg, and Uhrhammer, presented talks on earthquakes and related phenomena to public groups. Dr. Gee gave a lecture during Homecoming Weekend.

3.2 Open Houses

The BSL participated in *Take Your Child to Work Day* this year. The attendance for the open house was quite good - visitors showed up before we opened the doors! The visitors learned about UC Berkeley's role in earthquake monitoring, watched a streaming feed of earthquake data, jumped up and down to "make a quake", played with the earthquake machine, made P and S-waves with springs, learned about earthquake preparedness, and were given sample seismograms.

3.3 1906 Centennial

The centennial of the great 1906 San Francisco earthquake is rapidly approaching! A number of Bay Area organizations are participating in the '06 Earthquake Centennial Alliance and beginning to plan activities commemorating the event and celebrating the progress we've made in reducing earthquake losses.

Although UC Berkeley was spared major damage, the 1906 earthquake did have a significant impact on the campus community. These effects were documented in an issue of the Chronicle of the University of California in 1998 which describes the refugee camps established on the campus and the dispatch of University cadets to help maintain order in San Francisco. Professor Andrew Lawson chaired the State Earthquake Investigation Commission which produced the first comprehensive government-commissioned report on an earthquake.

Given the many ties between the 1906 earthquake and fire and the University, many UC Berkeley units are beginning to coordinate plans for centennial activities. Ideas for centennial activities include new classes, public lecture series, symposia, displays on the progress of the SAFER program, exhibits of 1906 artifacts and photographs, film series, walking tours, and many others. A small group of people are meeting quarterly at the BSL to

plan activities. Information about their plans is available at <http://www.seismo.berkeley.edu/seismo/1906/>.

Lawson Lecture

As part of centennial activities, the BSL established an annual lecture in 2003. The public lecture is held each April and focus on issues of earthquakes and society. This year was the second Lawson Lecture and Dr. Ross Stein of the USGS, Menlo Park, gave an excellent presentation on *Earthquake Conversations*, that is, how earthquakes interact through the transfer of stress, such as the progression of mainshocks along a fault, aftershocks, seismic quiescence, and earthquake clustering. If you missed the lecture, don't despair! A Web cast of the talk is available at http://www.seismo.berkeley.edu/seismo/news/lawson_lecture.html.

SSA 2006

The BSL will co-host the annual meeting of the Seismological Society of America (SSA), scheduled for 4/18/2006 - 4/22/2006, with the USGS. Plans are moving ahead to hold the *100th Anniversary Earthquake Conference* as a co-convened meeting by the SSA, the Earthquake Engineering Research Institute, and California Governor's Office of Emergency Services. The joint conference, which will be held in the Moscone convention center in San Francisco, will focus on what has been accomplished during the last century, showcasing best practices and research results in science, engineering, and emergency management.

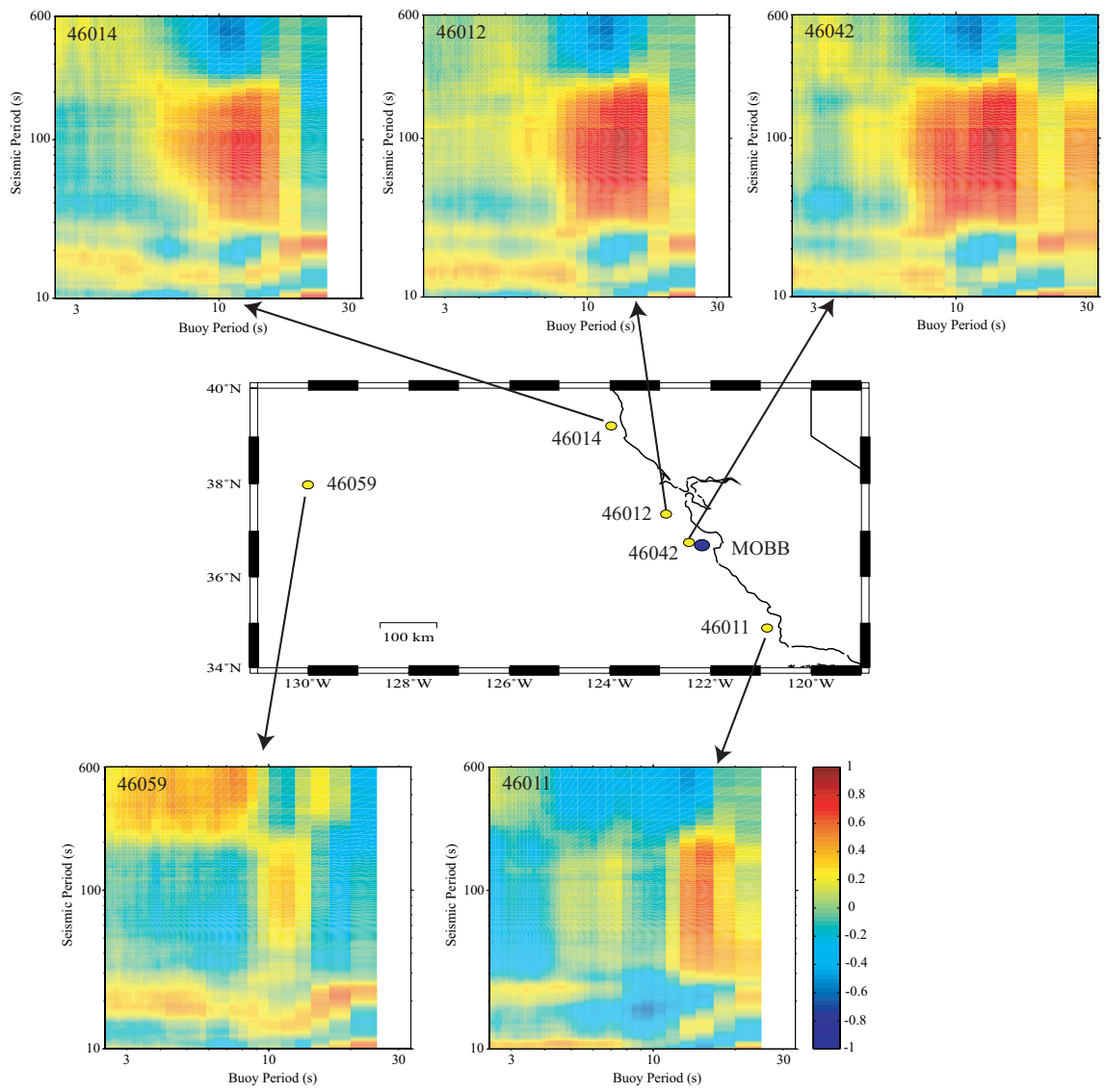
Lind Gee is on the Steering Committee for the anniversary conference and has been participating in monthly conference calls to plan for the meeting. In particular, there is much activity related to setting up the program, developing a realistic budget, and planning for special events such as a banquet celebrating the centennial of SSA. The development of the program is particularly exciting, as the conference is a unique gathering of people in earthquake-related fields. A plenary session is planned for each day, with presentations designed to cross disciplinary boundaries.

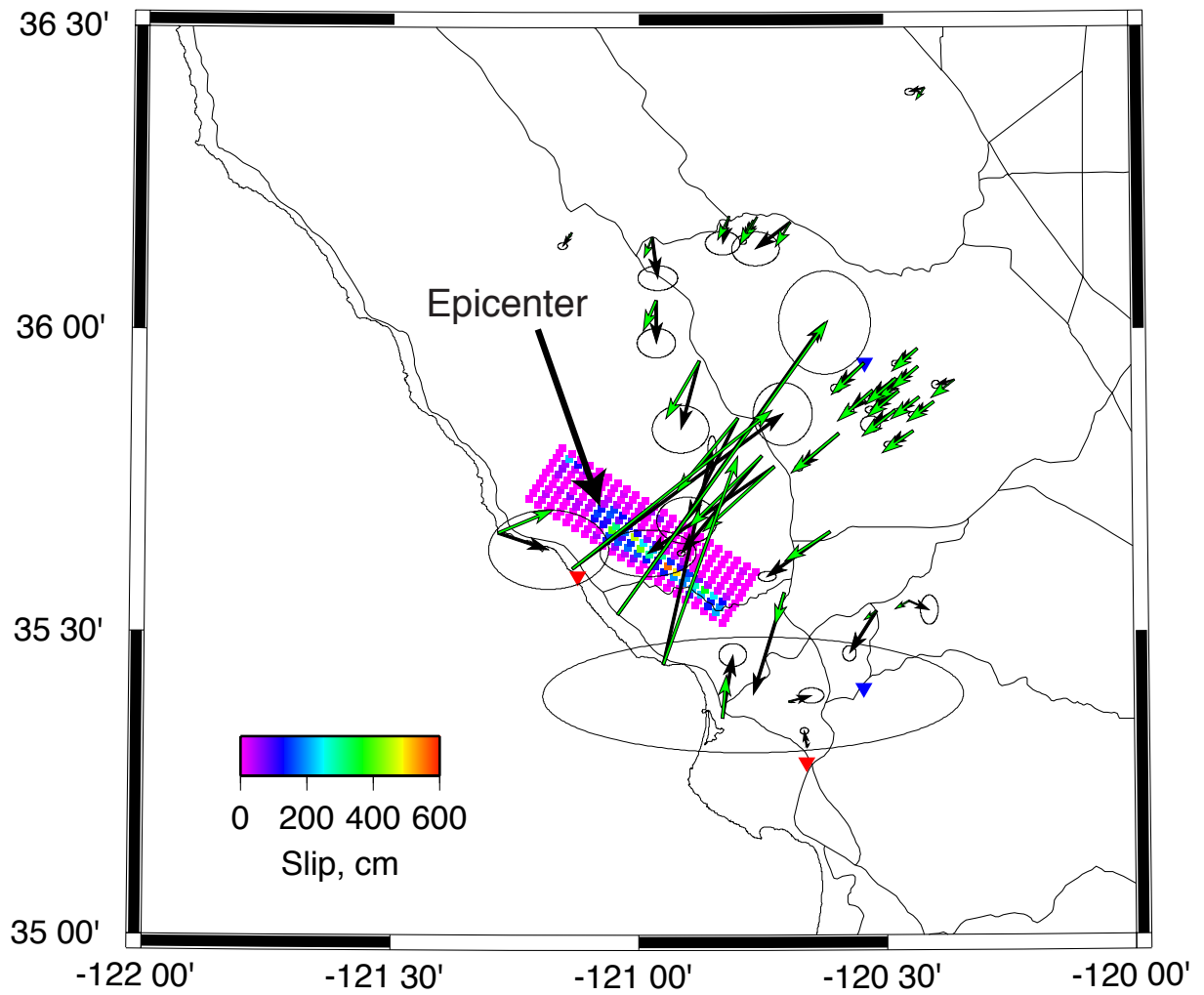
4. Acknowledgements

Lind Gee oversees the outreach activities at the BSL. Barbara Romanowicz, Peggy Hellweg, Bob Uhrhammer, Rick McKenzie, and many other faculty, staff, and students at the BSL contribute to the outreach activities. Lind Gee contributed to the preparation of this chapter.

Chapter 12

Research Studies





1. Periodic Earthquake Rate Variations on the San Andreas Fault

Robert M. Nadeau

1.1 Slip Rates from Micro-quakes

A characteristically repeating micro-earthquake sequence (CS) is a sequence of small earthquakes ($M \sim < 3.5$) whose seismograms, locations and magnitudes are nearly identical. Each earthquake in the sequence represents a repeated rupture of the same patch of fault, and the times between the ruptures (i.e., their recurrence intervals) are, in general, inversely proportional to the average tectonic loading rate on the fault (*Nadeau and McEvilly, 1999; Bürgmann et al., 2000; Igarashi et al., 2003*). Their unique properties allow CS to be used to infer fault slip rates at depth on faults, and this capability has been proven to be particularly useful in regions where geodetic measurements are limited in spatial coverage and frequency.

1.2 Repeating Quake Analysis

Along much of the 175 km stretch of the San Andreas Fault (SAF) separating the rupture zones of California's two great earthquakes (i.e., the \sim M8 1906 San Francisco and 1857 Fort Tejon events), geodetic measurements have been done relatively infrequently in campaign mode. Along this stretch, however, over 500 CS have been identified with events occurring between 1984 and 1999 (inclusive). And, analysis of these sequences reveal: 1) that the recurrence intervals within any given CS vary significantly, 2) that among different CS on a given fault segment the recurrence variations are coherent through time and 3) that in many cases the coherent variations recurred quasi-periodically (*Nadeau and McEvilly, 2004*).

1.3 Correlation with Larger Earthquakes

Recurrence variation information was used to construct a profile of deep fault slip rate histories along the 175 km study zone for the 1984-1999 study period (*Nadeau and McEvilly, 2004*). The profile reveals that along the northwestern-most 80 km segment of the study zone (Figure 12.1), deep fault slip rates commonly vary by over 100% and their variation patterns (i.e., pulse patterns) recur with a periodicity of ~ 3 years. Shown at the right in Figure 12.1 is a comparison of this large-scale periodic deep slip pattern with the occurrence times of M3.5 to M7.1 earthquakes (i.e., magnitudes larger than those of the CS events) and with the occurrence times of three known slow slip events in the area (*Linde et al., 1996; Gwyther et al., 2000*). The comparison reveals a significant correlation between the onset periods of the repeating deep slip signals and the occurrence rates of

the larger events.

To the resolution of the characteristic microearthquake slip rate data, the M7.1 Loma Prieta mainshock occurred coincident with the onset of the P2 timed pulse (Figure 12.1, right). The times of the next two largest non-aftershock events in the area and study period (i.e., M5.4 San Juan Bautista mainshock in 1998 and a M4.7 event in 1986) are also coincident with the onset of pulses P5 and P1, respectively, and the P3, P4, and P5 pulse onsets correspond closely to the times of the three slow slip events in the area whose aseismic moment magnitudes were estimated to be $\sim 5M_w$ (*Linde et al., 1996; Gwyther et al., 2000*).

Excluding Loma Prieta aftershocks, 45 earthquakes with $M > 3.5$ occurred in region during the 1984-1999 study period, and a general correlation is also observed between the occurrence times of these events and the 1-year onset periods of the pulses (i.e. the time interval where pulse slip velocities transition from low to high values). Thirty-three of the 45 events were found to occur during the onset periods, this represents an occurrence rate that is 6 times larger than the rate observed during the non-onset periods. When Loma Prieta aftershocks are included into the analysis the onset period rate increased to 7 times that of the non-onset period rate (Figure 12.1, right).

1.4 Implications

Earthquake triggering induced by velocity weakening effects (*Dietrich, 1986; Scholz, 1990*) associated with increasing fault slip velocities may provide an explanation for the increased rates of the larger earthquakes during the pulse onsets. It is also possible that the increased rates occur quasi-periodically due to some other mechanism, such as the accelerated accumulation of failure during quasi-periodic tectonic loading.

Continued monitoring of the $M > 3.5$ earthquake activity occurring since the 1984-1999 analysis period along the 80 km SAF segment shows that the quasi-periodic occurrence rate pattern for larger quakes is continuing and that the timing of the rate increases remains consistent with the projected pulse onset times based on the 1984-1999 pulsing statistics (Figure 12.1, right-top). As a consequence analysis of the post-1999 CS seismicity has now been initiated in order to confirm the continuance of the deep slip rate pulsing that the larger magnitude seismicity patterns suggest may be taking place.

Regardless of the outcome of this subsequent analysis, however, the the ongoing quasi-periodic patterns of

the larger earthquake rates holds the potential for refinement of time-dependent earthquake forecasts models for this area (WGCEP, 1999; Matthews *et al.*, 2002) to time scales comparable to the average pulse cycle duration of ~ 3 years that is observed.

1.5 Acknowledgements

Thanks are given to Roland Bürgmann and Mark H. Murray for stimulating conversations and inciteful comments regarding this work. This research was supported by the U.S. Geological Survey through awards 02HQGR0067 and 03HQGR0065 and by the National Science Foundation through award 9814605.

1.6 References

Bürgmann, R., D. Schmidt, R.M. Nadeau, M. d'Alessio, E. Fielding, D. Manaker, T.V. McEvilly, and M.H. Murray, Earthquake Potential along the Northern Hayward Fault, California, *Science*, 289, 1178-1182, 2000.

Dieterich, J.H., A model for the nucleation of earthquake slip, in *Earthquake Source Mechanics*, S. Das, J. Boatwright, and C.H. Scholz (Editors), *American Geophysical Monograph 37*, American Geophysical Union, Washington, D.C., 37-47, 1986.

Gwyther, R.L., C.H. Thurber, M.T. Gladwin, and M. Mee, Seismic and Aseismic Observations of the 12th August 1998 San Juan Bautista, California, M5.3 Earthquake, in *Proceedings of the 3rd Conference on tectonic problems of the San Andreas Fault system*, G. Bokermann and R. Kovach, Eds., *Stanford California School of Earth Sciences*, Stanford University, 2000.

Igarashi, T., T. Matsuzawa, and A. Hasegawa, Repeating earthquakes and interplate aseismic slip in the northeastern Japan subduction zone, *J. Geophys. Res.*, 108, 2249, doi:10.1029/2002JB001920, 2003.

Linde, A.T., M.T. Gladwin, M.J.S. Johnston, R.L. Gwyther, and R. Bilham, A slow earthquake near San Juan Bautista, California, in December, 1992, *Nature*, 383, 65-68, 1996.

Matthews, M.V., W.L. Ellsworth and P.A. Reasenberg, A Brownian Model for Recurrent Earthquakes, *Bull. Seism. Soc. Am.*, 92, 2233-2250, 2002.

Nadeau, R.M., and T.V. McEvilly, Fault slip rates at depth from recurrence intervals of repeating microearthquakes. *Science*, 285, 718-721, 1999.

Nadeau, R. M. and T. V. McEvilly, Periodic Pulsing of Characteristic Microearthquakes on the San Andreas Fault, *Science*, 303, 220-222, 2004.

Scholz, C. H., The mechanics of earthquakes and faulting, *Cambridge Univ. Press, Cambridge*, 439 pp., 1990.

Working Group on California earthquake Probabilities (WGCEP). Earthquake probabilities in the San Francisco Bay Region: 2000 to 2030—a summary of findings, *U.S. Geol. Surv. Open-File Rept. 99-517*, 36 pp., 1999.

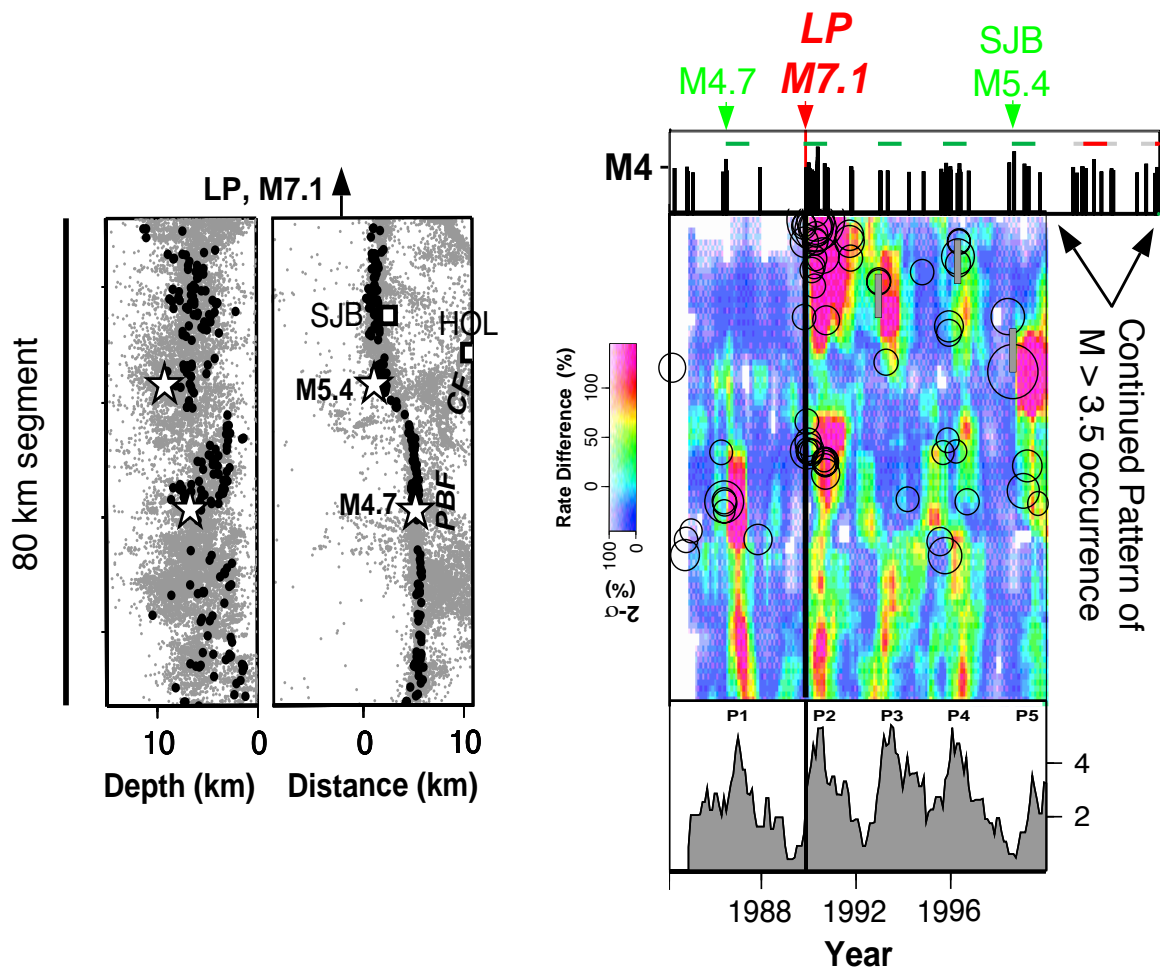


Figure 12.1: (Left) Background Seismicity (gray points) and CS locations (black circles) in depth section and map view along the northwestern 80 km segment. Horizontal scales are exaggerated by x2. White stars are locations of the two largest non-aftershock events (M5.4 and M4.7) occurring in the region and study period. Squares labeled SJB and HOL are the cities of San Juan Bautista and Hollister, CA. Calaveras and Paicines-San Benito fault seismicity are labeled CF and PBF, respectively. CS locations in map view outline the trend of the SAF. The 1989, M7.1 Loma Prieta earthquake occurred adjacent to the northwest of this 80 km segment. (Right, center) Profile of the 1984-1999 (inclusive) deep slip rate history for the segment inferred from the CS data. Rates (in color) are given in percent difference from the 1984-1999 average rate and color intensity are 95% confidence bounds. Open circles are along fault positions and times of the $M > 3.5$ earthquakes occurring in the region and study period. Sizes of these circles are keyed to their relative magnitudes. Vertical black line indicates the time of the Loma Prieta earthquake. (Right, bottom) Deep slip rates as a function of time for a representative 15 km sub-segment showing the P1 through P5 pulses discussed in the text. Vertical scale is in cm/yr. (Right, top) Occurrence times and magnitudes of the $M > 3.5$ earthquakes occurring in the study zone and for the period between 1984 and 2004.73 (inclusive). The times of the Loma Prieta and two largest non-aftershock events are labeled at the top. Horizontal green bars are the pulse onset periods discussed in the text. Horizontal red bars are the projected pulse onset times based on the 1984-1999 CS slip patterns. Gray extensions of the red bars show uncertainties in these projections based on the variance of the 1984-1999 pulse recurrence intervals. Analysis of the CS data for deep slip estimation has yet to be carried out for the 2000-2004.73 time period, but the ongoing pattern of occurrence of $M > 3.5$ earthquakes suggests that the quasi-periodic deep slip pattern may also continue.

2. Finite-Source Modeling of the 22 December 2003 San Simeon Earthquake

Douglas Dreger

2.1 Introduction

The M_w 6.5 San Simeon earthquake, which occurred in the central California Coast Ranges on December 22, 2003 was analyzed with our automated finite-source procedure the day of the earthquake. The derived source information was used to incorporate rupture finiteness into the ShakeMap greatly improving its representation of near-fault ground motions as well as those in the heavily struck community of Paso Robles, about 35 km to the SE of the earthquake.

In this report the initial line-source modeling, and its application toward improving published ShakeMaps is described. In addition, the current preferred model that combines GPS and seismic waveform data is presented, and the implications of the model in terms of central Coast Range ground motion hazard is discussed.

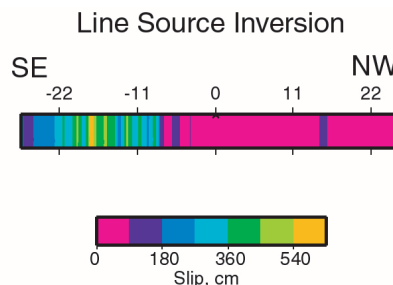
2.2 Line Source Modeling and ShakeMap

The seismic moment tensor was obtained automatically and the reviewed results were emailed within an hour after the event. The moment tensor result upward revised the magnitude from M_L 6.4 to M_w 6.5. The ShakeMap was updated with the new value automatically.

Subsequent analysis focussed on inverting broadband waveform data from the BDSN to test the two moment tensor nodal planes to determine the orientation of the causative fault. The method employed is based on *Hartzell and Heaton's* (1983) inverse scheme for kinematic rupture parameters such as slip distribution, slip rise time and rupture velocity. *Dreger and Kaverina* (2000) showed that it was possible to use a similar approach to determine key finite-source parameters quickly after an earthquake using the near-realtime broadband data stream. The *Dreger and Kaverina* (2000) method was developed by modeling the 1992 M_w 7.3 Landers and M_w 6.7 Northridge earthquakes. Although the system was not yet automated its application at the time of the Hector Mine earthquake, M_w 7.1, showed that the approach was feasible in the short time frame required for emergency response applications. The application of this method in the 2003 San Simeon earthquake is the first "live fire" test of the system, and the first time that near-realtime finite-source information was used to update ShakeMap (see *Hardebeck et al.*, 2004).

The first stage of the *Dreger and Kaverina* (2000) method is to test line-source models with the orientations of the two moment tensor nodal planes. In this analy-

sis the east dipping plane (strike=290, dip=56, rake=74) was found to fit the broadband data slightly better, though it could not be shown to be a statistically significant improvement in fit. Aftershocks, however, confirmed that the east dipping nodal plane was the causative structure. The line-source inversion results for both planes indicated that the main slip was located substantially SE of the hypocenter, extending as much as 20 km to the SE. Figure 12.2 shows the analyst reviewed line-source model for the east-dipping mechanism.



A line source inversion of broadband displacement waveforms shows that the bulk of slip is located south of the epicenter (0 on the above plot). This model assumes a rupture velocity of 2.7 km/s, and the focal parameters: strike=290, dip=56, rake=74.

Figure 12.2: Analyst reviewed line-source model of the 2003 San Simeon earthquake

The line-source information was used to incorporate source finiteness into the ShakeMap (Figure 12.3). In this calculation the distance used to model the ground motion attenuation, in areas where actual ground motion data was not available, was the closest distance to the extended fault rupture rather than to the epicenter as is typically done. The effect of this modification is an extension of the near-fault area of strongest shaking to the SE, elevating estimated ground motions in the Paso Robles region to instrumental intensity VII-VIII. This intensity is more consistent with the observed damage in the region. (e.g. *Hardebeck et al.*, 2004).

In Figure 12.3 it is shown how the ShakeMaps vary as additional information is added. Figure 12.3a shows the original ShakeMap. This map has only a few contributing stations, which are located far from the event and the afflicted region. The distribution of instrumental intensity therefore tends to be centered on the epicenter with radial decay. Estimated intensity in the vicinity of

Paso Robles is only V-VI. Figure 12.3b shows the map after adjustment by adding the finite-source information. Several days after the event as additional near-fault, non-realtime, ground motion recordings became available the ShakeMap was updated. Figure 12.3c shows the map obtained with the additional ground motion information. Note how the maps in Figures 12.3b and 12.3c agree. The former has no near-fault data, but does have the finite-rupture information obtained by inverting regional data for the rupture process, and the latter includes only the additional near-fault recordings. This comparison demonstrates the utility of incorporating either rupture finiteness or even directivity information in ShakeMaps to improve performance in regions where there may be few strong motion records or cases in which the near-fault data may not be immediately available. Finally, Figure 12.3d shows the final ShakeMap that includes all available near-fault observations as well as the finite extent of the rupture.

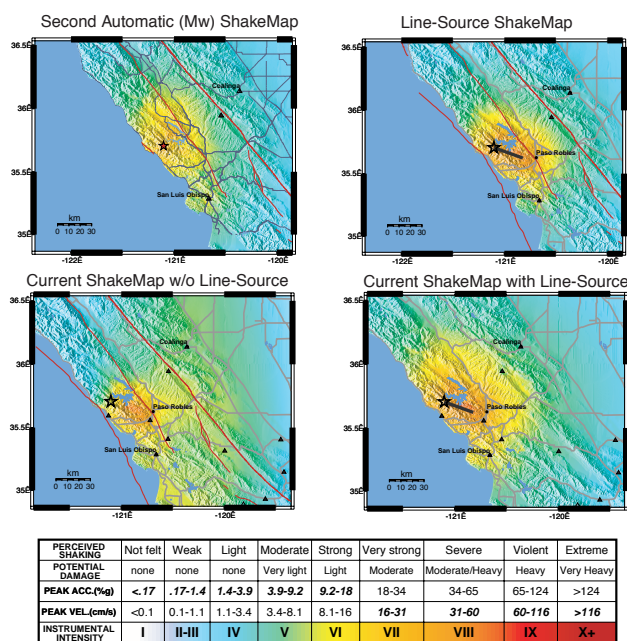


Figure 12.3: Evolution of instrumental intensity ShakeMaps (Wald et al., 1999) for the 2003 San Simeon earthquake. The star shows the epicenter, triangles the stations used, and thick line the finite extent of rupture. A), upper left, initial map based on M_w and realtime data. B), upper right, modification accounting for rupture finiteness. C), lower left, map with all available data including non realtime data. D), lower right, preferred map that combines available data and rupture finiteness.

2.3 Combined Slip Model and Ground Motion Simulation

Three-component displacement data at 8 regional and local stations, and three-component velocity records at the Parkfield site (PKD) were combined with 36 GPS permanent ground deformation vectors to invert for the detailed kinematic rupture process. This data is described in detail in Chapter 12. Figure 12.7 shows the fit to the seismic waveform data, and Figure 12.8 shows the fit to the GPS vectors. The fit to both data sets is very good. Figure 12.4. shows the slip distribution that was obtained.

The slip in the San Simeon earthquake is unusual in three respects. First, the distribution is elongated along strike, extending as much as 20 to 25 km SE of the hypocenter. This is in contrast to the primarily updip rupture of other reverse mechanism events such as the 1971 San Fernando (Heaton, 1982) and 1994 Northridge (Dreger, 1997) earthquakes. The San Simeon earthquake is similar to the much larger 1999 M_w 7.6 Chi-Chi, Taiwan earthquake in terms of the extensive along strike rupture. Secondly for a M_w 6.5 event the peak and average slip is high. Although, the peak slip is dependent upon the weight of the smoothing that is applied, all of the models show that over much of the fault the slip is between 1-3 m. Empirical relationships for average slip as a function of moment indicate that on average M_w 6.5 events have about 70 cm of average slip (e.g. Somerville et al., 1999). Third the event also has a relatively long slip rise time function that is variable over the rupture surface with an average of about 3 seconds. On average M_w 6.5 events have an average rise time of about 0.8 seconds (Somerville et al., 1999).

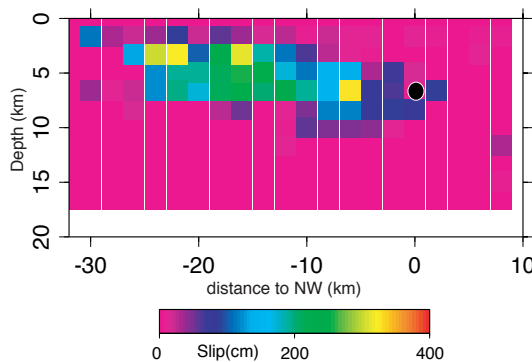


Figure 12.4: Fault normal projection of slip distribution. The black circle marks position of the hypocenter. The Fault orientation and slip vector are the same as obtained from the moment tensor analysis and used in the line-source calculation.

2.4 Central Coast Ground Motion Hazard Implications

From the derived kinematic source description it is possible to spatially and temporally integrate the slip using near-fault Green's functions to predict the distribution of near-fault strong shaking (Dreger and Kaverina, 2000). Figure 12.5a shows the results of such a calculation. The plot clearly shows the southeastward extension of ground motion contours due to the source finiteness and directivity. The two lobes of elevated ground velocity extending due east and due south of the earthquake are the directivity-amplified SH lobes of the reverse mechanism.

Whether the observed ground motions from the 2003 M_w 6.5 event are representative of all central Coast Range magnitude 6.5 earthquakes is an important question. There are strike-slip faults in the region, and the last large nearby earthquake, the 1952 Bryson event, was predominantly strike-slip (Dehlinger and Bolt, 1987). In order to address this question the kinematic source description that was obtained for the 2003 San Simeon earthquake was used to simulate near-fault ground motions for a hypothetical vertically dipping right-lateral strike-slip fault. The results of the calculation shows that for the vertical strike-slip fault the effect of directivity is greatly enhanced. In some areas the peak ground velocity can be three times greater, and the area receiving greater than 10 cm/s is four times larger than the reverse slip case. Fortunately in the 2003 San Simeon earthquake the slip direction was perpendicular to the rupture direction producing a relatively mild directivity effect. These calculations show however that while the recorded ground motions from the 2003 San Simeon earthquake are useful for characterizing earthquake hazard in the central Coast Ranges similar sized strike-slip earthquakes could be significantly more damaging.

2.5 References

Dehlinger, P., and B. Bolt, Earthquakes and associated tectonics in a part of coastal central California, *Bull. Seis. Soc. Am.*, 77, 2056-2073, 1987.

Dreger, D. S. The large aftershocks of the Northridge earthquake and their relationship to mainshock slip and fault-zone complexity, *Bull. Seism. Soc. Am.*, 87, 1259-1266, 1997.

Dreger, D., and A. Kaverina, Seismic remote sensing for the earthquake source process and near-source strong shaking: A case study of the October 16, 1999 Hector mine earthquake, *Geophys. Res. Lett.*, 27, 1941-1944, 2000.

Hardebeck, J.L., J. Boatwright, D. Dreger, R. Goel, V. Graizer, K. Hudnut, C. Ji, L. Jones, J. Langbein, J. Lin, E. Roeloffs, R. Simpson, K. Stark, R. Stein, J.C. Tinsley, Preliminary report on the 22 December 2003, M 6.5 San Simeon, California earthquake *Seism. Res. Lett.*, 75, 155-172, 2004.

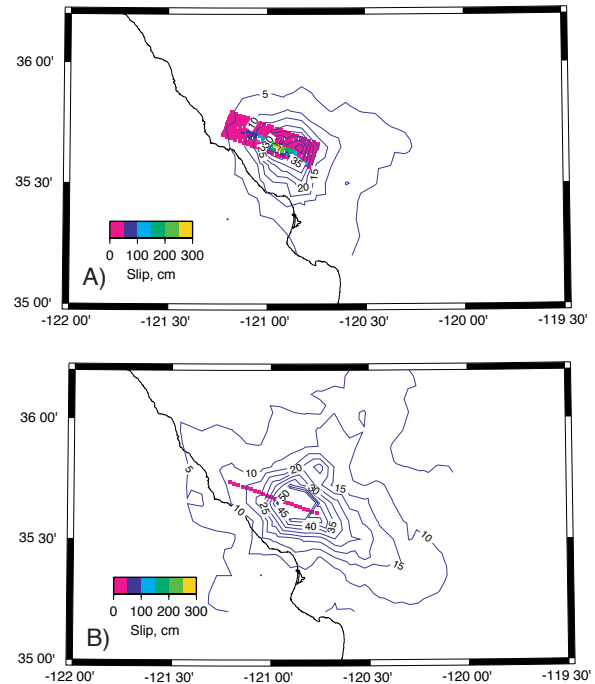


Figure 12.5: Simulated peak ground velocity assuming the obtained kinematic source description. Contours are in intervals of 5 cm/s beginning with 5 cm/s. The surface projection of slip is shown. A) Simulated PGV for the actual reverse slip mechanism. B) Simulated PGV for a vertical right-lateral strike-slip mechanism.

Hartzell, S. H., and T. H. Heaton, Inversion of strong ground motion and teleseismic waveform data for the fault rupture history of the 1979 Imperial Valley, California, earthquake, *Bull. Seism. Soc. Am.*, 73, 1553-1583, 1983.

Heaton, Y. H. The 1971 San Fernando earthquake: a double event?, *Bull. Seism. Soc. Am.*, 72, 2037-2062, 1982.

Somerville, P. G., K. Irikura, R. Graves, S. Sawada, D. Wald, N. Abrahamson, Y. Iwasaki, T. Kagawa, N. Smith, and A. Kowada. Characterizing crustal earthquake slip models for the prediction of strong ground motion, *Seism. Res. Lett.*, 70, 59-80, 1999.

Wald, D. J., V. Quitoriano, T. H. Heaton, H. Kanamori, C. W. Scrivner, and C. B. Worden. TriNet ShakeMaps: Rapid generation of instrumental ground motion and intensity maps for earthquakes in southern California, *Earthquake Spectra*, 15, 537-555, 1999.

3. Coseismic Slip Distribution of the 22 December 2003 San Simeon Earthquake

Frédérique Rolandone, Roland Bürgmann, Doug Dreger, and Mark Murray

3.1 Introduction

The M_w 6.5 San Simeon earthquake struck the central California coast on December 22 2003, 50 km west of the San Andreas fault. The San Simeon earthquake is one of several destructive blind-thrust earthquakes to have hit the central California Coast Range during the past two decades. This thrust earthquake accommodates a compressional component of the Pacific-North America plate motion. The mainshock nucleated at a depth of 8 km and was followed by a vigorous aftershock sequence primarily southeast of the hypocenter, consistent with the mainshock directivity (Hardebeck *et al.*, 2004). The strong directivity of the rupture resulted in a concentration of damage to the southeast, with high levels of damage in Paso Robles.

We combine geodetic and seismic data sets to constrain the coseismic slip distribution of the San Simeon earthquake. We use continuous and survey-mode GPS observations along with seismic waveform data from the Berkeley Digital Seismic Network (BDSN/CISN). We invert both data sets for fault slip model. Seismic and geodetic data sample ground deformation at different time scales and combining them provide more stable results than the inversion from individual data sets. The inversion results for this event indicate that the slip extend to the southeast of the epicenter approximately 25 km and in a depth range between 1.3 and 8 km.

3.2 GPS Data and Analysis

We use data from 36 GPS sites in this study. The San Simeon earthquake produced static displacements at 14 continuously operating GPS stations located within 70 km of the epicentral region. These stations are located northeast of the rupture near the Parkfield segment. The cluster of stations near Parkfield were displaced southwest by about 15 mm. One station 35 km northwest of the rupture moved about 60 mm southwest. In addition, one continuous station south of the rupture and 4 continuous stations north of it (operated by the University of Wisconsin since January 2003) recorded small (less than 12 mm) displacements.

Many of the 17 survey-mode GPS sites are located within 40 km of the rupture and provide useful coseismic deformation signals. Following the San Simeon earthquake, we resurveyed 6 GPS stations northeast of the mainshock. The USGS began continuously occupying 3 stations west of the epicenter one day after the event and another site southeast of the mainshock one week

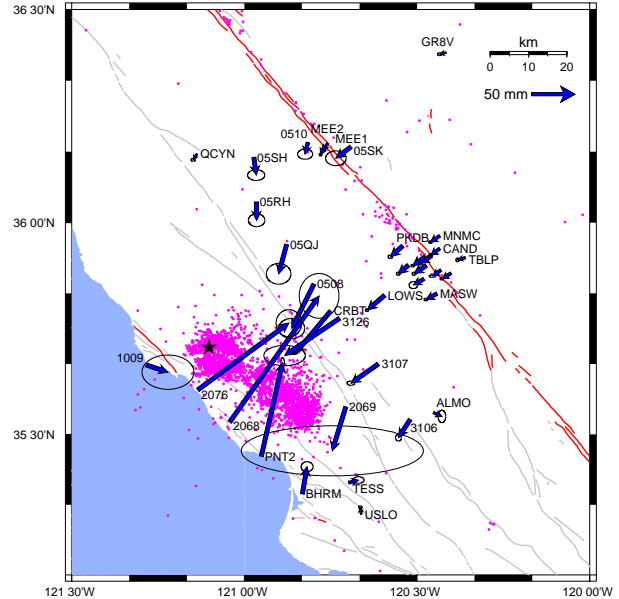


Figure 12.6: GPS sites and coseismic displacements from the M_w 6.5 San Simeon earthquake with 95% confidence ellipses. The black star shows the epicenter, the pink dots show relocated aftershocks (Hardebeck *et al.*, 2004). Surface fault traces are shown as red and grey lines.

later. Three sites east of the rupture were occupied by JPL within 3 days of the event. A survey of 4 additional sites south of the rupture was done 2 months after San Simeon.

For the campaign GPS sites, we have pre-existing GPS observations collected since the mid-1980's. Some of the sites have multiple years of measurements prior to the earthquake and have precise velocities. For the sites with less than 3 campaigns of data, we use interseismic velocities from the SCEC Crustal Motion Map (CMM). The CMM velocities indicate that the epicentral region had a well-constrained secular deformation field, which allows coseismic displacements to be reliably estimated from pre- and post-event measurements. We use the GAMIT/GLOBK GPS processing software to analyze the GPS data and combine our daily solutions and an appropriate set of global and regional solutions from SOPAC. We estimated the coseismic offsets at each site from these time series assuming that the interseismic velocity is the same before and after the earthquake. The southwest sites, closest to the rupture, recorded larger

coseismic offsets than the northeast sites (Figure 12.6). The largest measured horizontal displacement was 179 ± 14 mm.

3.3 Geodetic and Seismic Data Inversion for Fault Slip Model

We use the geodetic data to constrain the rupture geometry. We model the observed coseismic displacements using rectangular dislocations in an elastic, homogeneous and isotropic half-space (Okada, 1985). We use a constrained, nonlinear optimization algorithm (Bürgmann *et al.*, 1997), which allows us to estimate the geometry (parameterized by length, depth, width, dip, strike, and location) and the strike-slip and dip-slip offsets of one fault that best fit the GPS data. The optimal fault model has a strike of 303° and dips 56° to the northeast.

We use the results of our geometry inversion to construct the north-dipping fault plane to determine the distribution of fault slip. Our best-fitting single-fault model is enlarged at the down-dip and lateral edges and discretized into 2 by 2 km elements for the distributed slip inversions. We find that the optimal uniform-slip dislocation is consistent with seismological evidence. The San Simeon focal mechanism and the aftershock distribution suggest the Oceanic fault as the main rupture zone (Hardebeck *et al.*, 2004). The oceanic fault has a strike of about 292° near the epicenter and changes direction to the south with a more northern strike similar to the one given by our geometry inversion. Our measure of misfit, the reduced χ^2 value, is not improved if we allow for a second dislocation in the geometry inversion.

We combined displacement and velocity waveform data from 9, three-component BDSN/CISN strong motion stations with 36 observations of GPS deformation to simultaneously invert for the distribution of fault slip. The waveform data was processed by deconvolving the instrument response, double integrating the recorded acceleration to displacement (PKD was integrated only to velocity), and high pass filtering above 0.01 Hz to remove long-period noise.

The seismic waveform data may be generally characterized as low-frequency (Figure 12.7) and in order to model this characteristic a multiple time window approach (e.g. Hartzell and Heaton, 1983; Dreger and Kaverina, 2000; Kaverina *et al.*, 2001) was used to resolve the slip rise time distribution of the rupture. The results of the inversions indicate that the rise time was relatively long for a M_w 6.5 event with an average of about 3 seconds. The rupture velocity, though not well resolved, was found to be 2.6 km/s. Consistent with the non-linear GPS inversions for fault orientation the combined inversion favors a more northerly striking fault plane (strike=303, dip=56). The resulting slip model is shown in Figure 12.8. The slip is found to be shallow in depth (1.3 to 8 km) and extends approximately 25 km to the southeast of the epi-

center. This unusual aspect ratio for reverse fault rupture is consistent with the results of separate GPS and seismic waveform inversions, and leads to a moderate horizontal directivity effect as compared to a more typical updip directivity as was observed in the 1994 Northridge, California earthquake. The spatially concentrated peak slip was found to be 5.5 m, which is unusually high for a M_w 6.5 event, and it does depend on the applied smoothing. Over much of the fault, however the slip is between 1 to 3 m. The level of fit to the GPS and seismic waveform data is excellent as shown in Figure 12.7 and 12.8.

The extension of slip to the southeast of the epicenter indicates that this event ruptured unilaterally to the southeast producing a pronounced directivity effect in that direction. Elevated ground motions in the Paso Robles region, about 35 km to the southeast, resulted in two deaths from collapsed unreinforced masonry (URM) buildings, and numerous damaged red-tagged URM buildings in Paso Robles.

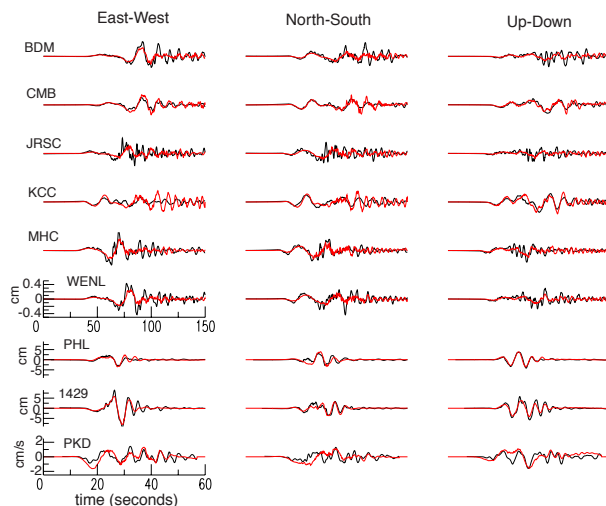


Figure 12.7: Comparison of observed (black) and simulated (red) displacement waveforms (velocity for PKD) for the combined seismic waveform and GPS model. Quantitatively the fit to the data was found to be excellent with a 72% variance reduction.

3.4 References

- Bürgmann, R., P. Segall, M. Lisowski, and J. Svarc, Postseismic strain following the 1989 Loma Prieta earthquake from GPS and leveling measurements, *J. Geophys. Res.*, 102, 4933-4955, 1997.
- Dreger, D., and A. Kaverina, Seismic remote sensing for the earthquake source process and near-source strong shaking: A case study of the October 16, 1999 Hector mine earthquake, *Geophys. Res. Lett.*, 27, 1941-1944, 2000.

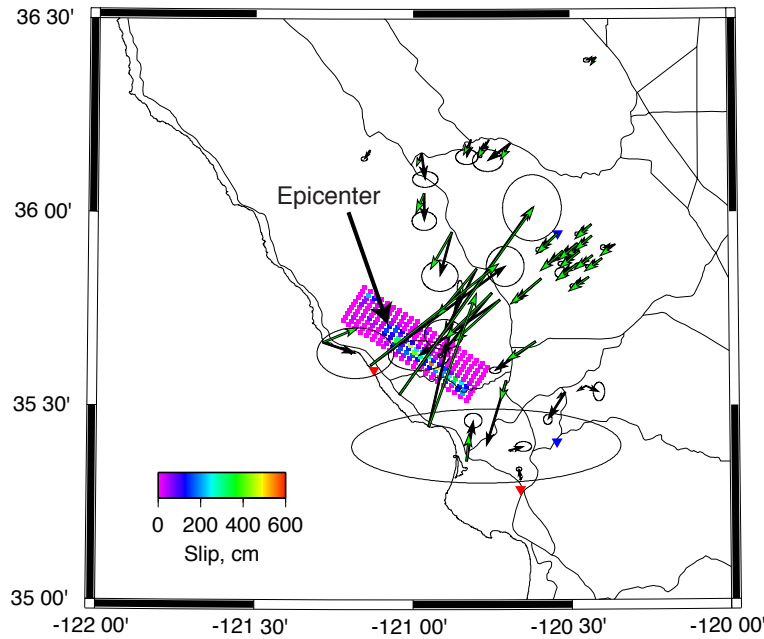


Figure 12.8: Map showing the surface projection of slip from the combined inversion. The epicenter is located at the northwestern edge of the slip distribution. Observed (black) and predicted (green) gps vectors are also shown. For reference major highways are also plotted. Quantitatively the fit to the GPS data was found to be excellent with a 94% variance reduction. A color version of this figure may be found on page 104.

Hardebeck, J.L., J. Boatwright, D. Dreger, R. Goel, V. Graizer, K. Hudnut, C. Ji, L. Jones, J. Langbein, J. Lin, E. Roeloffs, R. Simpson, K. Stark, R. Stein, J.C. Tinsley, Preliminary report on the 22 December 2003, M 6.5 San Simeon, California earthquake *Seism. Res. Lett.*, 75, 155-172, 2004.

Hartzell, S. H., and T. H. Heaton, Inversion of strong ground motion and teleseismic waveform data for the fault rupture history of the 1979 Imperial Valley, California, earthquake, *Bull. Seism. Soc. Am.*, 73, 1553-1583, 1983.

Ji, C., K.M. Larson, Y. Tan, K.W. Hudnut, and K. Choi, Slip history of the 2003 San Simeon Earthquake constrained by combining 1-Hz GPS, strong motion, and teleseismic data, submitted, 2004.

Kaverina, A., D. Dreger and E. Price. The combined inversion of seismic and geodetic data for the source process of the 16 October 1999 M_w 7.1 Hector Mine, California, earthquake, *Bull. Seism. Soc. Am.*, 92, 1266-1280, 2002.

Okada, Y., Surface deformation due to shear and tensile faults in a half-space, *Bull. Seism. Soc. Am.*, 75, 1135-1154, 1985.

4. Measuring and Modeling Fluid Movements in Volcanoes: Insights from Continuous Broadband Seismic Monitoring at Galeras Volcano, Colombia

Margaret Hellweg, Leigh House (Los Alamos National Laboratory) and Douglas Dreger

4.1 Introduction

One important goal of volcano monitoring is to be able to reliably identify significant changes in a volcano's activity, in order to minimize the threat to the local population and infrastructure. Seismic signals are often the most immediate indicators of such changes (*McNutt, 1996*), and to interpret them, we must understand the processes which produce them. At volcanoes, we observe two basic types of seismic signals. Volcano-tectonic events are earthquakes, usually small ones, resulting from slip across fault planes. The second type of events are non-tectonic and are unique to volcanoes. They include volcanic tremor, long period (LP) events, and less commonly, tornillos. In seismic recordings, non-tectonic signals are often emergent, may continue for a long time, and have highly variable amplitudes. Very often their spectra contain one or a few distinct, sharp peaks. They are assumed to be associated with the movement of fluids in the volcanic system (for a review, see *Konstantinova and Schlindwein, 2002*).

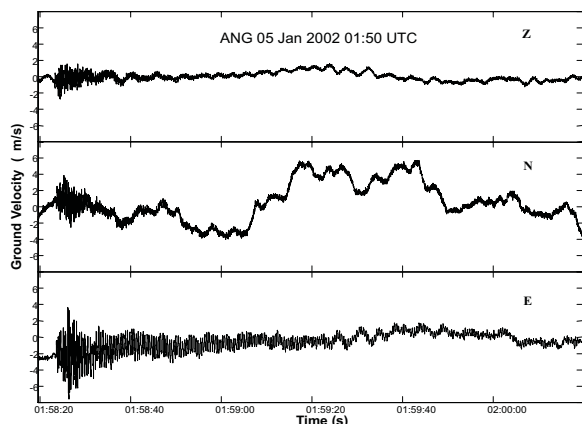


Figure 12.9: Unfiltered three-component record of a tornillo recorded at the crater rim seismic station ANG. The coda of the E component bears the most resemblance to a screw. The very long period noise particularly apparent on the N component is most likely due to wind.

4.2 Tornillos

At Galeras Volcano, Colombia, ‘tornillos’ occurred prior to explosive eruptions in 1992 and 1993 (*Narvez et al, 1997*). These distinctive seismic events have identifiable onsets and relatively long, gradually decaying event tails (codas) and their name comes from the resemblance of their shape on the seismic record to a screw (Spanish: tornillo. Figure 12.9). Their spectra have one or a few narrow peaks. That is, they are monochromatic or multi-chromatic (Figure 12.10). From December 1999 to December 2002, ninety tornillos occurred at Galeras Volcano, Colombia, and were recorded with broadband, three-component seismometers (*Seidl et al, 2003*). These tornillos have between 1 and 15 spectral peaks. To characterize the tornillos and learn what causes them, we are investigating the coda which gives them their name. The analysis of the coda follows the procedure described by *Seidl and Hellweg (2003)*, where each spectral peak in each tornillo is treated separately. Based on the azimuth Az_n , inclination In_n and rectilinearity Re_n for each spectral peak, the seismograms are rotated from the Z-N-E coordinate system of the seismometer into a coordinate system of the wavefield, X1-X2-X3. From these records, the frequency of the peak's maximum, f_{Pn} , and its amplitude, AP_n , are measured in the frequency domain, while the maximum velocity amplitude, v_n , damping factor, Q_n and the signal energy, EP_n , are measured in the time domain.

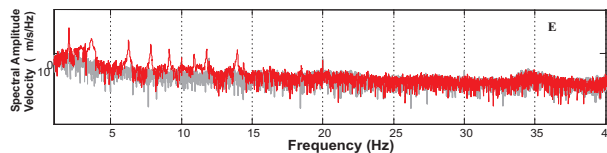


Figure 12.10: Linear-logarithmic spectrum of the E component for the tornillo shown in Figure 12.9. The spectrum during the tornillo is superimposed on the spectrum of the seismic noise before the tornillo (gray). Note the extremely narrow spectral peaks between 1 and 15 Hz.

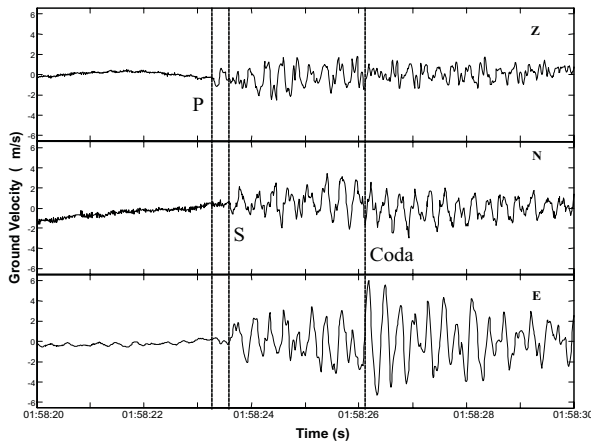


Figure 12.11: Expanded seismograms for the beginning of the tornillo shown in Figure 12.9. These data have been bandpass filtered between 1 and 40 Hz to suppress long-period noise. Note the clear onset on the vertical component marked P and the onsets on the horizontal components 0.25 s later marked S. It takes a little over 2 s for the characteristic coda of the tornillo to develop.

4.3 Interpretation

For the characteristic coda of the tornillos, it is clear that the frequencies of the spectral peaks present, which may range from 1 Hz to 40 Hz, are related to the source, but we have not yet found a pattern allowing us to predict precisely which frequencies or families of frequencies will be present in any particular tornillo. For the spectral peaks below 5 Hz, the polarization both remains constant during an individual tornillo and varies little from one tornillo to the next. This suggests that tornillos are all generated within a limited volume of the volcanic edifice. The variation in the polarization at higher frequencies should allow us to constrain the size of this volume (Hellweg, 2003). With the high resolution data from broadband instruments, we can see that the onset of the tornillo is small but clearly impulsive (Figure 12.11). The initial P-pulse on the vertical component is followed 0.25 s later by S-waves on the horizontal components. A transition of about two seconds follows before the characteristic coda develops. As we determine details about the tornillo onset and this intermediate wavepacket, and their relationships to the characteristics of the tornillo coda, we shall be able to derive a more thorough picture relating the triggering mechanism to its effect on the coda.

4.4 Acknowledgements

This project is funded by U.C. Berkeley - Los Alamos National Laboratory collaborative Institute for Geo-

physics and Planetary Physics Project number 04-1407. Tornillo data have been acquired as part of a cooperative project between the Bundesanstalt für Geowissenschaften und Rohstoffe (Germany) and the Instituto de Investigación e Información Geocientífica Minero-Ambiental y Nuclear (Colombia) on Multiparameter Monitoring of Volcanoes.

4.5 References

- Hellweg, M., The Polarization of Volcanic Seismic Signals: Medium or Source?, *J. Volc. Geotherm. Res.*, *128*, 159-176, 2003.
- Konstantinou, K.I. and V. Schlindwein, Nature, wavefield properties and source mechanism of volcanic tremor: a review. *J. Volcanol. Geotherm. Res.*, *119*, 161-187, 2002.
- McNutt, S.R., Seismic monitoring and eruption forecasting of volcanoes: A review of the state-of-the-art and case histories. In: *Monitoring and Mitigation of Volcano Hazards* (Eds. Scarpa, R. and Tilling, R.I.), Springer, Berlin-Heidelberg, 100-146, 1996.
- Narváez, M.L., R.A. Torres, D.M. Gómez, G.P.J. Cortés, H.V. Cepeda, and J. Stix, Tornillo-type seismic signals at Galeras volcano, Colombia, 1992-1993. *J. Volcanol. Geotherm. Res.*, *77*, 159-171, 1997.
- Seidl, D., M. Hellweg, M. Calvache, D. Gómez, A. Ortega, R. Torres, F. Böker, B. Buttkus, E. Faber and S. Greinwald, The multiparameter-station at Galeras Volcano (Colombia): Concept and realization, *J. Volc. Geotherm. Res.*, *25*, 1-12, 2003.
- Seidl, D. and M. Hellweg, Parametrization of multichromatic tornillo signals observed at Galeras Volcano (Colombia), *J. Volc. Geotherm. Res.*, *125*, 171-189, 2003.

5. The Orinda Earthquake Sequence

Margaret Hellweg

5.1 Introduction

On October 19 and 20, 2003, two earthquakes with M_L 3.5 and M_L 3.4 occurred ENE of Orinda, CA. Fortuitously, their hypocenters were located almost directly below Berkeley Seismological Laboratory’s station at Russell Reservation Field Station, BRIB (37.92 N, 122.15 W). This station is equipped at the surface with a Guralp CMG-3T in a 35 m posthole installation and a FBA-23 accelerometer. In addition, the station has a 3-component Oyo HS-1 geophone and a 3-component Wilcoxon 731A accelerometer in a borehole at a depth of 119 m.

5.2 The Seismicity

Since it is a short-period instrument, the Oyo HS-1 geophone in the borehole at BRIB usually only records local events. In the days, leading up to October 19, 2003, there were several small earthquakes, but they belonged to a sequence in Danville/Alamo, CA, further to the south and east. The Orinda sequence began on October 19, 2003 at 14:35 UTC (07:35 PDT) with an earthquake with M_d 2.5. This event was followed by more than 15 smaller events, the largest of which, at 15:12 UTC with M_d 1.67, was also located. Just under one hour later, a larger earthquake occurred, the M_L 3.5 mainshock of the sequence.

The two largest earthquakes, the mainshock at 15:32 UTC on October 19 with M_L 3.5, and the aftershock at 17:50 on October 20 with M_L 3.4, were clipped on one of the horizontal components of both the surface and the borehole seismometers. Fortunately, the clipped component of the borehole seismometer coincides with the single functioning component of the borehole accelerometer. When the instrument response is removed from the accelerometer recording and the trace is integrated, it matches the corresponding component of the velocity sensor. Figure 12.12 shows the three component recording of the mainshock, with the vertical trace at the top and the two orthogonal horizontal traces (H1 and H2) below. The bottom trace (H2) was clipped in the velocity recording and has been replaced by the integrated accelerometer trace. The offset traces between 15:32:50 and 15:32:53 are scaled 100,000 times the traces for the mainshock. There is clearly a very small event 1.5 s before the mainshock onset showing the range of sizes of the events in this sequence and the similarities in the waveform of both large and small events.

Of the many events which occurred during the first 24 hours of the sequence, only 14 appear in the catalog of the Northern California Seismic Network (NCSN)

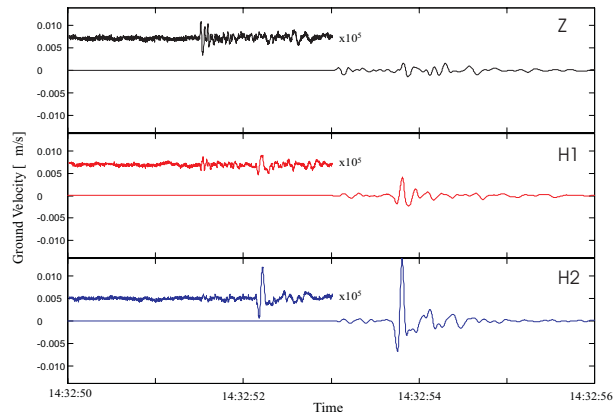


Figure 12.12: Three-component recording of the mainshock on the borehole instruments. H1 and H2 are the two orthogonal horizontal components. For this figure, the H2 recording has been replaced by the instrument-corrected and integrated record from the borehole accelerometer. The offset traces in the first 3 s of the figure have been scaled by a factor of 100,000 to show the “pre-event noise”, in this case a very small foreshock.

with locations and magnitudes. While the catalog reports depths of approximately 10 km for the two largest quakes, the S-P times at the station BRIB for all the events in the sequence range from 0.58 to 0.7 s. They must therefore be located less than 6 km below the station. The borehole instrument recorded more than 4000 fore- and aftershocks in the first week of the sequence. At the beginning of December aftershocks continued at a rate of 6 or more per day, with a M_d 2.9 aftershock recorded January 1, 2004.

Standard magnitudes cannot be determined for most of the earthquakes in the sequence: the events are too small to be recorded at other stations and, strictly speaking, the local magnitude scale is not defined for events as close as 6 km. To determine the magnitude threshold for the events, I calibrated a “manual magnitude” scale using the 14 events from the catalog. Following the definition of local magnitude (*Richter*, 1935), I measured the peak-to-peak amplitudes in the instrument-corrected velocity seismograms of the two horizontal components of the borehole velocity sensor and multiplied by the period and by the magnification of a Wood-Anderson instru-

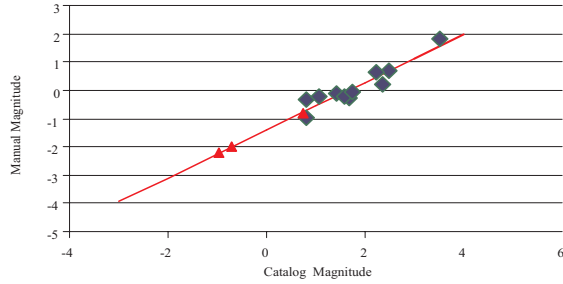


Figure 12.13: Calibration of “manual magnitude” to catalog magnitude (M_L or M_d). Diamonds denote events for which the NCSN catalog gives magnitudes. Triangles show how events for which only manual magnitudes exist. They have been placed on the regression line to determine their corresponding catalog magnitude.

ment at that period. The manual magnitude is defined as $M_m = \log_{10}[(N_{max} + E_{max})/2]$. This numerical result is comparable to the measurement used to determine M_L . As the distances of these events from the station BRIB are all nearly the same, no distance correction is necessary. Figure 12.13 shows a comparison between the catalog and manual magnitudes (diamonds). The line shows the regression using of the catalog magnitudes and manual magnitudes and allows me to project manual magnitudes to a corresponding catalog magnitude (triangles). The sequence includes still smaller events for which I have not yet determined manual magnitudes, thus the earthquakes in the sequence recorded at station BRIB range over more than 5 magnitudes in size.

5.3 Perspectives

This sequence provides a well-recorded multitude of tightly clustered, small events ranging over 5 magnitude units in size. It thus offers an excellent opportunity to investigate various aspects of event scaling and aftershock statistics.

5.4 References

Richter, C.F., An instrumental earthquake magnitude scale, *Bull. Seismol. Soc. Am.*, 25, 1-32, 1935.

6. Non-Double-Couple Earthquakes in the Long Valley Volcanic Region

Dennise C. Templeton and Douglas Dreger

6.1 Introduction

We study the extent of fluid-influenced faulting in the Long Valley volcanic region to better understand the connection between earthquake production and the geothermal and magmatic system. In the analysis of earthquake data, most events are assumed to follow the double-couple (DC) model of faulting characterized by shear along a linear fault plane induced by tectonic stresses. Earthquakes with coseismic volume changes indicate that tectonic forces were not the only factor contributing to failure. In geothermal or volcanic areas, such events are thought to be influenced by fluid migration, in either liquid or gas form, or a change in the state of matter of a fluid (Ross *et al.*, 1999 ; Dreger *et al.*, 2000).

In this study, we focus on a 100 km wide circular area centered at Long Valley caldera which encompassed the Mono-Inyo craters to the north and the Sierra Nevada mountain block to the south. A comprehensive search was performed for events greater than M3.5 since 1993 with significant non-DC components, specifically compensated-linear-vector-dipole (CLVD) and isotropic components.

6.2 Method

We model the waveforms of 128 events recorded in the NCSN catalog greater than M3.5 using four different source models: DC, DC+CLVD, DC+isotropic, and DC+CLVD+isotropic. For the DC and DC+isotropic models, a grid search method iterating over strike, dip, rake, DC moment and isotropic moment, which is equal to zero in the pure DC case, was used to find the solution which best fit the observed three-component waveforms. For the deviatoric and full moment tensor models, the second rank symmetric seismic moment tensor was solved by linearly inverting complete three-component broadband seismograms in the time domain using a weighted least squares approach. Green's functions for all four models were computed utilizing a frequency wavenumber integration method and the SoCal velocity model (Dreger and Helmberger, 1993). A set of seven BDSN stations (BKS, CMB, KCC, MHC, ORV, PKD, and SAO) providing the best azimuthal coverage and data quality were used in this investigation. In practice, however, a solution would usually have a subset of these stations in its inversion depending on station availability and data quality issues. Both data and synthetics were bandpass filtered between 0.02 and 0.05 Hz.

Using the F test as a statistical aid, we determine which of the four models was most appropriate for each

individual earthquake. Statistically significant isotropic components were determined if the improvement in fit to the data when using a more complex model was at or above the 90% significance level. We also performed several analyses to determine the stability of the solution, the depth sensitivity of the isotropic component, the recoverability of isotropic components, and the possibility of obtaining a spurious isotropic component.

6.3 Results

Within the chosen space and time constraints, 33 events were identified that had solutions with three or more stations in their inversion (Figure 12.14). Of these 33 events, 28 had statistically insignificant non-DC components. The remaining five events had statistically significant positive volumetric components. Two of these five also had statistically significant CLVD components. All of the non-DC events were located either in the south moat of the caldera or in the Sierra Nevada block. We were not able to analyze the source process of earthquakes in or near the vicinity of the Mono-Inyo volcanic chain because events greater than M3.5 were not recorded during the time interval investigated by this study.

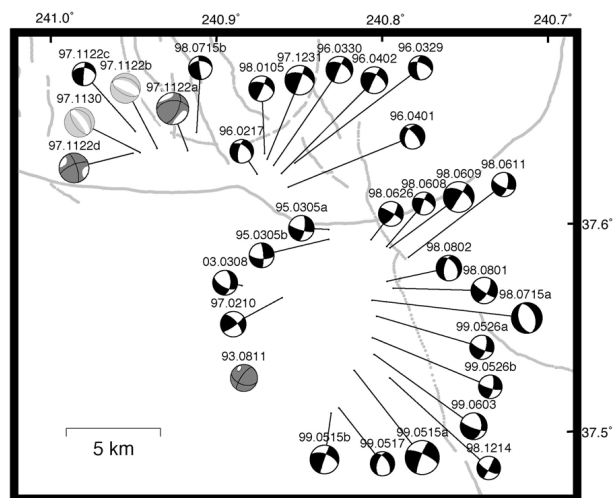


Figure 12.14: DC solutions shown in black. DC+isotropic solutions shown as dark gray. Full moment tensor solutions shown as light gray. Date of event shown as YY.MM.DD.

To test the stability of the focal mechanism solutions, we performed Jackknife tests on three events: DC event 97.12.31, DC+isotropic event 97.11.22b, and full moment

tensor event 97.11.30. Each event originally had six stations in its solution. We solve for all permutations of three, four, and five station combinations and compare these results with the six station solution for each event. DC and DC+isotropic solutions are remarkably stable for solutions with four or more stations in their inversion. Solutions with three stations in the inversion are seen to be slightly more variable. The full moment tensor event showed that the P-wave radiation pattern was stable but that the orientation of the faulting planes was unstable even when using as many as five stations. However it is important to note that the DC component of this event produced only 5% of the total moment released and that the CLVD and isotropic components dominated the inversion. Thus, inversions with four or more stations can be treated with confidence. Three station inversions, while often consistent with solutions with more stations, should be understood to have more uncertainty in the solution.

Most moment tensor inversions in this study did not have good depth control. In some cases, changes in depth may produce statistically significant isotropic components. For eight events, we test for spurious isotropic components due to depth mislocation using the station combination which yielded the best solution in each case. Solutions for source depths between 2 - 11 km are calculated for the five events with significant isotropic events and three DC events (events 97.12.31, 98.06.09, and 98.07.15a). These tests illustrate the importance of accurately knowing the depth of events when attempting to identify earthquakes with significant isotropic components. For the DC events, we can see that for depths deeper than the independently determined NCSN catalog depths, the improvement in fit to the data between the DC and DC+isotropic model is statistically significant. However, the overall fit to the data decreases with depth which indicates that the isotropic components are not modeling the true source behavior. For the DC+isotropic and full moment tensor events, solutions at depths shallower than the catalog depths sometimes do not recover the significant isotropic component. For some events depths outside the allowable range can fit the data better, however, it is important to remember that with the long wavelength data used in this study, the depth of the source is not well constrained which is why NCSN catalog depths are used as an independent constraint.

To determine the stability of the isotropic component with station combination, we performed Jackknife tests on the four events with significant isotropic components that had four or more stations in their inversion. For each event, for all station combinations of three or more, we determined the statistical significance of the volumetric component. For all events, all combinations of four or more stations recovered the statistically significant

isotropic component. For solutions with three station in the inversion, only four permutations out of 70 failed to recover the isotropic component. It is reasonable to assume that significant isotropic components can be recovered with as few as three, but preferably with at least four, stations in the inversion. Thus, we can be confident that there are no false negative occurrences within my set of 33 events.

We also investigate the possibility of obtaining a spurious isotropic component due to poor data coverage. For this test, we take three high quality DC inversions (events 97.12.31, 98.06.09, and 98.07.15a) and perform Jackknife tests to see if any combination of three or more stations would result in a statistically significant isotropic component at or above the 90% significance level. For their best solutions, events 97.12.31 and 98.06.09 had six stations in their inversions and event 98.07.15a had seven stations in its inversion. Of 65 four station inversions, four returned a false positive. Of 75 three station inversions, six returned a false positive. Five and six station inversions did not return false positives. Thus, from these tests, events with significant isotropic components that have four or fewer stations in their inversion should be treated with caution. This test casts doubt as to the validity of event 93.08.11 which has only three stations in its inversion.

6.4 Acknowledgements

We appreciate support for this project by NSF through contracts EAR-0087147 and EAR-0105998.

6.5 References

- Dreger, D.S. and D.V. Helmberger, Determination of source parameters at regional distances with three-component sparse network data, *J. Geophys. Res.*, *98*, 8,107 - 8,125, 1993.
- Dreger, D. S., H. Tkalic, and M. Johnston, Dilational processes accompanying earthquakes in the Long Valley Caldera, *Science*, *288*, 122 - 125, 2000.
- Ross, A., G. R. Foulger, and B.R. Julian, Source processes of industrially-induced earthquakes at The Geysers geothermal area, California, *Geophysics*, *64*, 1,877 - 1,889, 1999.

7. Observations of Infragravity Waves at the Monterey Ocean Bottom Broadband Station (MOBB)

David Dolenc and Barbara Romanowicz

7.1 Introduction

Ocean bottom broadband seismic observations show increased noise level when compared to land recordings. Infragravity waves are an important source of background noise at periods longer than 20 seconds. Long-period background noise can partially be removed by post-processing (Crawford and Webb, 2000; Stutzmann *et al.*, 2001). At the same time, observations of infragravity waves can help us better understand their generation from short-period waves. We investigated correlations between the infragravity waves recorded at MOBB and the short-period ocean wave data recorded at nearby ocean buoys. MOBB was installed 40 km offshore in the Monterey Bay at a water depth of 1000 m in April 2002 in collaboration between Berkeley Seismo Lab and Monterey Bay Aquarium Research Institute (MBARI) (McGill *et al.*, 2002; Uhrhammer *et al.*, 2002). It comprises a three-component broadband seismometer with a temperature sensor, a water current meter measuring current speed and direction, and a differential pressure gauge (DPG). The station is continuously recording data which are retrieved, on average, every three months.

7.2 Results

We calculated power spectral density (PSD) of the MOBB vertical component for 1-hour long periods for all the data recorded until February 2004. The results were compared to the spectral wave density (SWD) of the ocean waves as recorded on the eight NOAA buoys located from offshore Southern California to Alaska. The results clearly showed that the width of the infragravity wave band recorded on MOBB was best correlated with the energy of the ocean waves recorded at the local NOAA buoy 46042, located just 23 km W of MOBB. To further explore observed correlation between the MOBB PSD and the buoy SWD, we focused on a 7-day period and included 6 more buoys that were closest to MOBB, and had data available. We calculated correlation coefficient between 1-hour long MOBB PSD and buoy SWD values. Results for 5 of the buoys are presented in Figure 12.15. The highest correlation can be observed for the closest buoy (46042). The result also shows that the 7-17 sec ocean waves are best correlated with seismic waves with 30-200 sec period. A weaker correlation can be observed with the other two buoys located over the continental shelf to the north (46012 and 46014). Correlation with the buoy located to the south (46011) and the one further offshore (46059) is much smaller. We plan to

further investigate these observations as well as include pressure and tides data to better understand where and how the energy is transferred from the ocean to the seismic waves. Once the reliable DPG data from the MOBB are available we will also use them to remove the long-period noise from the MOBB vertical channel to improve the seismic data quality.

7.3 References

Crawford, W.C., and S.C. Webb, Identifying and removing tilt noise from low-frequency (<0.1 Hz) seafloor vertical seismic data, *Bull. Seism. Soc. Am.*, 90, 952-963, 2000.

McGill, P., D. Neuhauser, D. Stakes, B. Romanowicz, T. Ramirez, and R. Uhrhammer, Deployment of a long-term broadband seafloor observatory in Monterey Bay, *EOS Trans. Amer. Geophys. Un.*, 83, F1008, 2002.

Stutzmann, E., J.-P. Montagner, A. Sebai, W.C. Crawford, J.-L. Thiot, P. Tarits, D. Stakes, B. Romanowicz, J.-F. Karczewski, J.-C. Koenig, J. Savary, D. Neuhauser, and S. Etchemendy, MOISE: A prototype multiparameter ocean-bottom station, *Bull. Seism. Soc. Am.*, 91, 885-892, 2001.

Uhrhammer, R., B. Romanowicz, D. Neuhauser, D. Stakes, P. McGill, and T. Ramirez, Instrument testing and first results from the MOBB Observatory, *EOS Trans. Amer. Geophys. Un.*, 83, F1008, 2002.

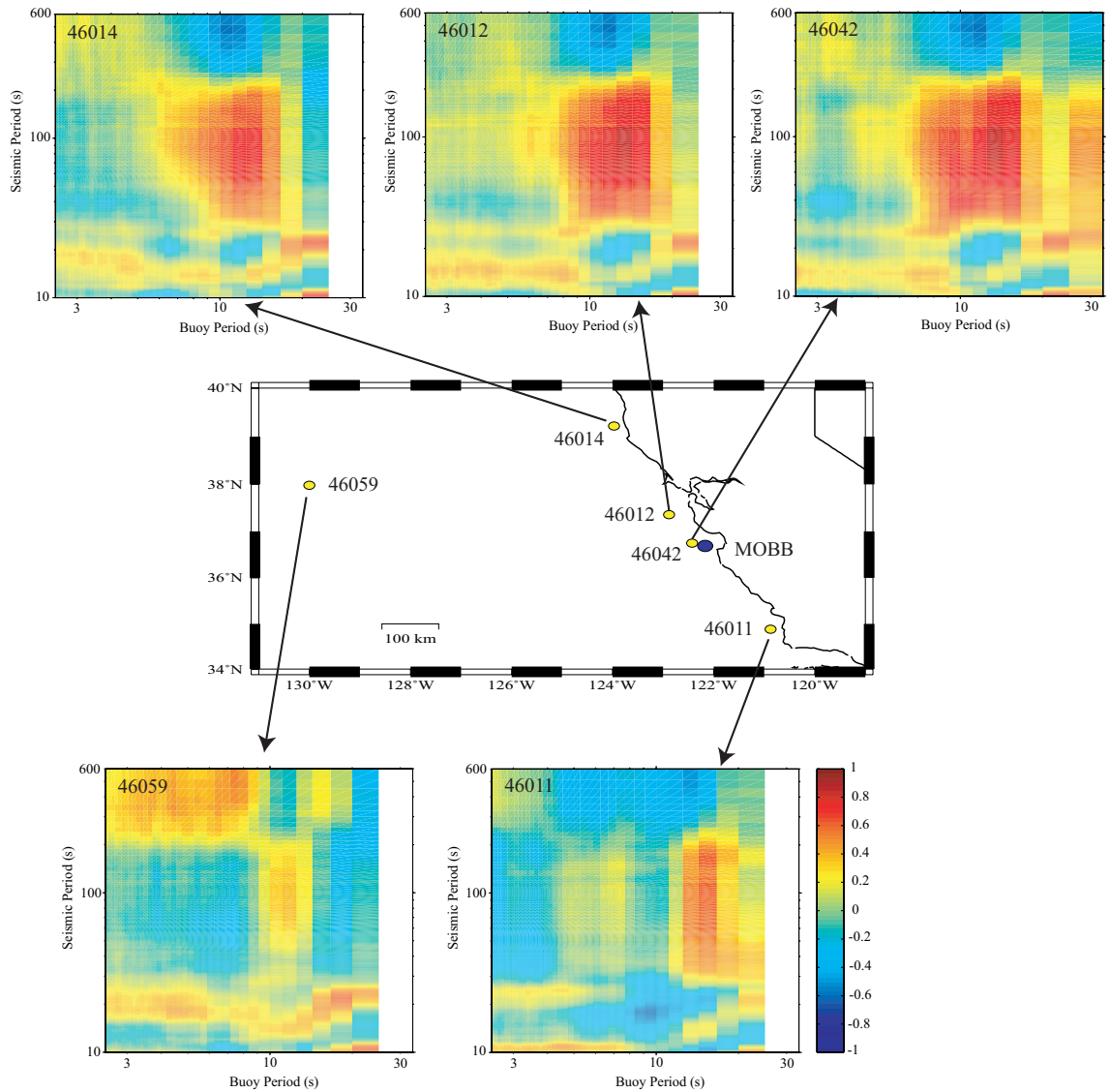


Figure 12.15: Correlations between power spectral density for the MOBB vertical channel and spectral wave densities measured on the closest buoys. Results for a 7-day period are shown. A color version of this figure is on page 103.

8. Slicing up the San Francisco Bay Area: Block Kinematics from GPS-derived Surface Velocities

Matthew A. d’Alessio, Ingrid A. Johanson, Roland Bürgmann, David A. Schmidt, and Mark H. Murray

The Berkeley Seismological Laboratory has collected and compiled interseismic velocities at over 200 Bay Area stations. This data set, the Bay Area Velocity Unification (BÄVÜ, pronounced “Bay View”) is the most comprehensive picture of crustal deformation in the region compiled to date. We use a block modeling approach to interpret these velocities at an unprecedented range of spatial scales. In this approach, we solve for the motion of fault bounded blocks that is most consistent with the observed surface velocities.

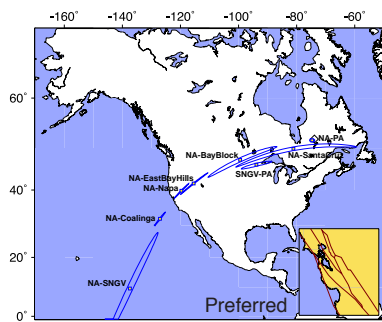


Figure 12.16: Calculated poles of rotation and 95% confidence limits for blocks in the Bay Area. Other than the Pacific-SNGV pole, all poles are relative to North America (NA). The diamond near Hudson Bay indicates the PA-NA from a two plate model that excludes stations near the plate boundary.

8.1 The Global Picture

Using the block model, we constrain the motion of blocks in the Bay Area relative to adjacent global plates (North America and Pacific), as well as the SNGV microplate. Individual blocks within the Bay Area do not move about identical poles of rotation of any of these major blocks as a “perfect transform” system, but instead have poles at intermediate locations. The poles transition systematically from west to east (Fig. 12.16). This systematic pattern may have implications for the development of the fault system.

8.2 Slip Rates on Bay Area Faults

We show a comparison between data and model velocities in (Fig. 12.17). Looking at the Bay Area region itself, we focus on quantifying the slip rates of individual

faults. We use precise relocations of earthquakes to determine the maximum depth of seismicity as a proxy for the local seismic/aseismic transition. We find slip rates that are typically within the uncertainty of geologic estimates (Table 12.1). We also document substantial slip on segments that have not been emphasized in previous studies. Models that include up to $4 \text{ mm} \cdot \text{yr}^{-1}$ of strike-slip on the West Napa fault north of San Pablo Bay provide almost identical model fit to those that exclude this fault. In our preferred model, we favor this geometry because it is consistent with geologic evidence showing that the some slip from the Calaveras fault is transferred westward, eventually connecting to the West Napa fault system. Adding a fault along the eastern margin of the Coast Range in our preferred model produces lower misfit and a geologically reasonable slip sense (right-lateral) on the Greenville – a notable improvement over models that exclude this “Valley Margin” deformation zone. This fault, running parallel to the San Andreas through central California carries $\sim 5 \text{ mm} \cdot \text{yr}^{-1}$ of right-lateral slip and $3 \text{ mm} \cdot \text{yr}^{-1}$ of fault-normal convergence. Poor data coverage near the model fault segment prevent us from determining if the deformation is accommodated by a single structure or a broad zone with many structures as might be implied by the distribution of moderate thrust earthquakes within the Diablo and Coast Ranges. We find that a similar magnitude of convergence is preferred along the entire eastern front of the Coast Range, but that an equal and opposite extension is observed west of the Bay in our models. Our block modeling approach provides the first strong geodetic constraints on the slip rates of several other faults because we include global GPS data from the Pacific plate and the physical constraint of coherent block motion. These faults include the San Gregorio fault ($2.4 \pm 0.5 \text{ mm} \cdot \text{yr}^{-1}$ right-lateral slip rate) and the Mount Diablo thrust ($3.9 \pm 0.5 \text{ mm} \cdot \text{yr}^{-1}$ reverse slip and an almost equal magnitude of right-lateral strike-slip). Overall, we find that the slip rates we determine fit GPS data substantially better than the slip rates defined in Working Group on California Earthquake Probabilities.

8.3 Fault Connectivity

Locally, block modeling allows us to test the connectivity of faults. Faults that are connected can transfer slip, so these connections have implications for slip rates and seismic hazard assessment. We show that shallow creep on Paicines fault is important, but that deep slip is best

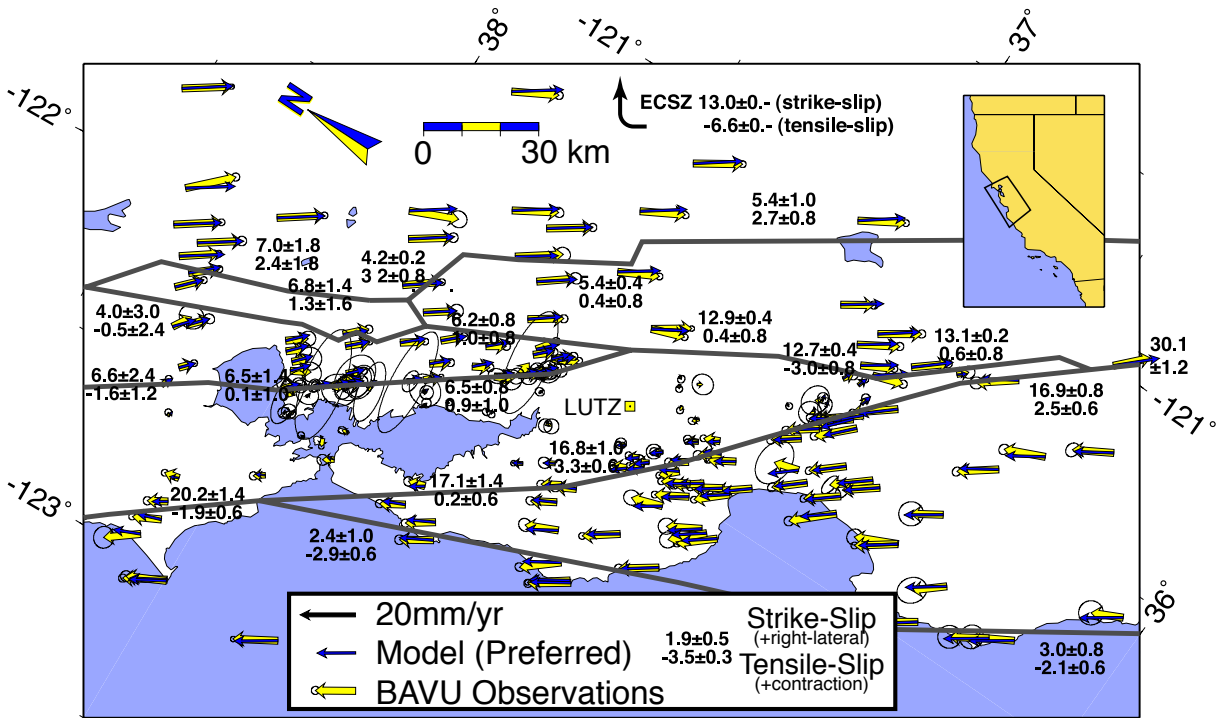


Figure 12.17: Observations (wider vectors with error ellipses) compared with model results (narrow, darker vectors) for our preferred model. Dotted grey lines represent the simplified geometry of faults in our model. Numbers indicate strike-slip and tensile-slip rates and 95% (2σ) uncertainties for select fault segments. Positive strike-slip indicates right-lateral slip. Positive tensile-slip indicates contraction while negative tensile-slip indicates extension.

modeled when the Calaveras fault is directly connected to both the Paicines and San Andreas faults. East of the Bay, we explore the possibility that the northern Calaveras fault transfers its slip east to the Concord/Green Valley fault, west to the West Napa fault system, or a combination of the two. The data slightly favor the eastern step over the western step alone, but we prefer models where both connections are included because they most closely reproduce the geologically inferred slip rate on the Green Valley fault and the lowest total model misfit.

In block modeling, three-dimensional fault geometry and connectivity have a very strong impact on the interpretation of surface deformation. While we systematically explored an extremely wide range of model geometries in this work, we look forward to further geologic constraints on fault geometry in 3-D to improve the reliability of block models. The ability to iteratively explore these different block geometries and test their consistency with geodetic data make the block modeling approach an excellent tool for understanding fault kinematics in the Bay Area.

Table 12.1: Comparison of strike-slip rates for geologic estimates (Working Group on California Earthquake Probabilities, WG03) and this study. Fault system names from top row: SG, San Gregorio; SA, San Andreas; RC, Rodgers Creek; H, Hayward; C, Calaveras; GV, Green Valley; Gr, Greenville. Fault segments from second row: N, North; C, Central; S, South; Mr, Marin; SF, San Francisco; SCM, Santa Cruz Mountains; RC, Rodgers Creek; H, Hayward; WN, West Napa; Cn, Concord; Gr, Greenville. Total for the northern section includes the sum of SA-Mrn + RC + WN + GV. Southern total is sum of SG-S + SA-SCM + C-C + Gr. We show 95% confidence bounds ($\pm 2\sigma$) for the three main models. Bounds for other models are similar in magnitude.

Study	SG		SA			RC/H			C			GV/Gr			Total	
	N	S	Mr	SF	SCM	RC	H	WN	N	C	S	GV	Cn	Gr	N	S
WG03	7	3	24	17	17	9	9	–	6	15	15	5	4	2	38	37
This Study	2.4	3.0	20.2	17.1	16.4	6.6	6.5	4.0	6.2	12.9	12.7	7.0	6.7	5.4	37.8	37.7
\pm	1.0	0.8	1.4	1.4	1.0	2.4	1.4	3.0	0.8	0.6	0.4	1.8	1.4	0.6	4.5	1.5

9. Active Tectonics of Northeast Asia: Using GPS Velocities and Block Modeling to Test Okhotsk Plate Motion Independent from North America

Edwin (Trey) Apel and Roland Bürgmann

9.1 Introduction

Horizontal surface velocities of 96 GPS sites (41 from the Eurasian, North American and Pacific plate and 55 from NE Asia) constrain the plate kinematics of NE Asia and allow for a rigorous test of the possibility of Okhotsk plate motion independent of the North American plate. A block modeling approach is used to incorporate both rigid block rotation and near-boundary elastic strain accumulation effects in a formal inversion of the GPS velocities. Considered models include scenarios with and without independent Okhotsk plate motion and a number of different plate boundary locations and locking depths. We are also considering the possible influence of an independent Amurian plate that may also affect the determination of Okhotsk plate existence and motion.

9.2 Background

The current plate kinematics of Northeast Asia are somewhat enigmatic due to subduction dominated deformation in the east and little to no differential plate motion in the west which results in diffuse and sparse seismicity. An Okhotsk plate that rotates independently of North America is not a particularly new idea (*Seno et al.*, 1996). However, it is important for defining the plate boundary geometry and constraining the relative motion of the major and minor plate in Northeast Asia and provides a rigorous framework for interpreting seismicity and the surface deformation observed by geodesy. Because the increasingly dense GPS networks in this region are in such close proximity to plate boundaries a sophisticated plate motion model that includes both rigid block rotations and elastic plate boundary strain effects is required to discriminate independent Okhotsk plate motion.

9.3 GPS Velocities

The GPS velocities used in our inversion are an updated subset of the 151 global stations processed for the final solution by *Steblov et al.* (2003). The data were processed using GAMIT/GLOBK by Bob King at MIT and Misha Kogan at Columbia. Processing details can be found in *Steblov et al.* (2003). Before our inversion the GPS sites were weighted according to site stability, distance from plate boundaries, and a simple declustering routine.

9.4 Blocks

In order to test for independent Okhotsk plate motion we tested two block configurations. In our 3-plate system we assumed that the Okhotsk region was part of the North American plate (Figure 12.18). Our 4-plate model (Figure 12.19) allows the Okhotsk plate to rotate independently. We then compared the misfit of the inversion to the data to test for significance. The segments that bound the blocks represent uniformly slipping elastic dislocations locked to some specified depth. Because our inversion combined rigid block rotation with elastic strain accumulation effects, the parameterization of the block boundary geometry is critical. Geometry of the plate boundaries was based heavily on seismicity. However, topography, geodetic gradients, and other modeling (such as single distributed slip inversions) were used to constrain the location and strike and dip of some of our elastic dislocations. Diffuse boundaries surrounding the Okhotsk region like the northern and western edges are not manifested as discrete structures in any geological or geophysical data set. These plate boundary deformation zones are represented in our model by vertical dislocations locked to optimal depths of approximately 75 km that are allowed both strike-slip and tensile motions. These deeply locked elastic dislocations generate diffuse surface deformation consistent with observed patterns of surface deformation. The kinematics of subduction zones are represented by dipping dislocations, locked to 40 km depth and allowed to accommodate both strike slip and dip slip motion.

9.5 Inversion

The GPS data and pre-defined block boundary geometry were used as inputs in our block modeling inversion code (*Meade and Hager*, 2004). We used all of these data (96 sites) to invert for predicted horizontal surface velocities at each GPS station while simultaneously considering rigid block rotation and elastic strain effects for both block configurations. Our 3-plate model shows a clear, systematic pattern of residual velocities that suggests independent Okhotsk plate motion (Figure 12.18). Euler vectors, calculated from our optimized 4-plate inversion, suggest the Okhotsk plate rotates 0.206 deg/Myr clockwise, with respect to North America, about a pole located north of Sakhalin (Figure 12.19 inset).

9.6 Discussion and Conclusions

Our inversion favors a scenario with independent Okhotsk plate motion but does not require it, based on the application of F-test statistics, which indicate that the improved fit is significant only at 87% confidence. The plate-motion parameters of the Okhotsk plate are consistent with right-lateral motion in northern Sakhalin and contraction in southern Sakhalin, inferred from focal mechanism solutions. However, subtle changes in block and segment geometry can cause significant changes in the estimated pole of rotation of the Okhotsk plate. This is due, in large part, to the close proximity of most GPS stations in northeast Asia to plate boundaries, such as the Kamchatka-Kurile subduction zone and the Sakhalin Island contraction and strike-slip shear zone. GPS velocities on the Kamchatka peninsula capture a complex pattern associated with the locked subduction zone. This locked subduction zone may require a more complex model than a simple elastic dislocation for the rotational signal to be resolvable. Additional blocks may also affect the determination of an independently rotating Okhotsk plate. Our continued work includes formally examining the potential role of adjacent blocks such as the Amurian, northern Hokkaido, and Magadan blocks.

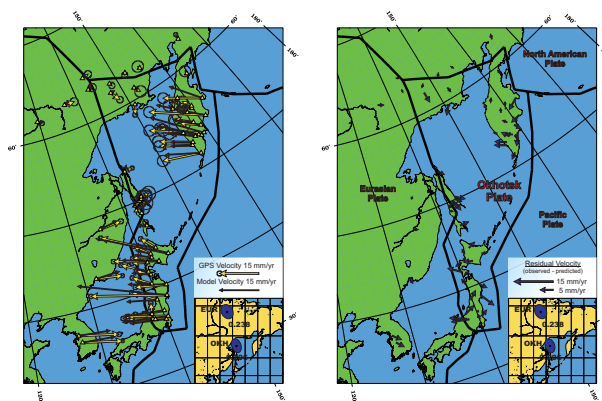


Figure 12.19: Observed, predicted, and residual velocities for the 4-plate model. The inset map shows the position of the Eurasian and Okhotsk poles of rotation (2-sigma error ellipses) with respect to North America and are labeled in degrees per million years.

American plate in Siberia revealed by GPS, *Geo. Res. Let.*, **30(18)**, 2003.

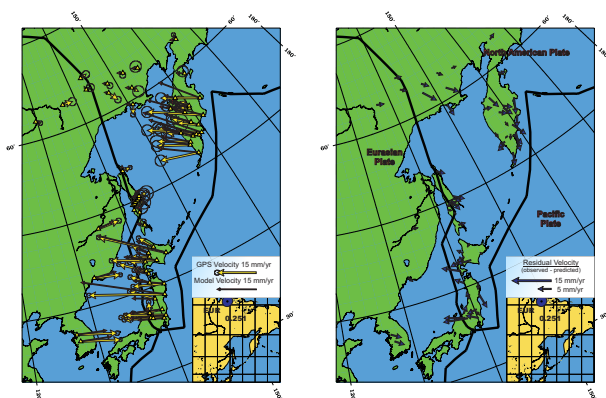


Figure 12.18: Observed, predicted, and residual velocities for the 3-plate model. The inset map shows the position of the Eurasian pole of rotation (2-sigma error ellipses) with respect to North America and is labeled in degrees per million years.

9.7 References

Meade, B.J. and B.H. Hager, Block Models of Crustal Motion in Southern California Constrained by GPS Measurements, *J. Geophys. Res.* (**IN PRESS**), 2004.

Seno, T., T. Sakurai, and S. Stein, Can the Okhotsk plate be discriminated from the North American plate?, *J. Geophys. Res.*, **101**, 11305-11315, 1996.

Steblov, G.M., M.G. Kogan, R.W. King, C.H. Scholz, R. Bürgmann, and D.I. Frolov, Imprint of the North

10. The Spatial Pattern of Active Uplift in Eastern Taiwan

Leslie Hsu and Roland Bürgmann

10.1 Introduction

The eastern coast of Taiwan is one of the most actively deforming regions in the world, with present-day convergence at 8 cm/year where the Luzon Arc is colliding with the Eurasian Plate (Yu *et al.*, 1997). The Eastern Coastal Range is thrust upwards along the east-dipping Longitudinal Valley Fault (LVF), accommodating about 3 cm/yr of the convergence (Yu *et al.*, 1997). Present-day active uplift along the fault is constrained by a GPS network and leveling measurements, showing along-strike variation in rates of slip (Yu and Kuo, 2001). In addition, the marine terrace record indicates that some segments of the LVF have been uplifting more rapidly than others over the timescale of the Holocene (Hsieh *et al.*, 2004). We are using InSAR to improve our knowledge of present-day vertical movement and strain accumulation along the Longitudinal Valley Fault.

The new InSAR data, yielding an improved velocity field, will be used to both reevaluate previous dislocation models and formulate new models. These improvements may help to explore currently unresolved issues such as the location of strain accommodation near in the northern half of the LVF within the Coastal Range or on proposed offshore faults (Bos *et al.*, 2003; Yamaguchi and Ota, 2004). We will also investigate the uplift patterns perpendicular and parallel to the faults strike. The former will tell us to what extent the Coastal Range is uplifting like a rigid block and the latter will illustrate transitions between locked and creeping sections of the fault.

10.2 Results

From 9 SAR scenes, we created 13 unwrapped interferograms from pairs spanning one month to 2.5 years. We made three stacks of 3-4 interferograms in an attempt to average out atmospheric effects. In some stacks, the recent mapped fault trace correlates well with an offset in the phase signal. Near Chishang, we measured a maximum offset across the fault that gave 14-26 mm/yr movements in the slip direction (Figure 12.20), agreeing well with the nearby creepmeter data (Lee *et al.*, 2003). However, this signal is not present everywhere along the fault.

We are developing an interseismic model that will be used as the basis for estimating and removing an orbital ramp from each interferogram. The interseismic model is produced from a simple fault geometry in an elastic half-space. We have also compiled horizontal and vertical GPS measurements, creepmeter data, leveling data, and current fault traces for comparison with the interfer-

ometry. Combining these different measures of deformation, we hope to achieve a better understanding of the nature and origin of spatial variation of movement along the Longitudinal Valley Fault.

10.3 Acknowledgements

This research is made possible by the Francis Turner Fellowship and a University Fellowship granted by the Taiwanese-American Foundation of Boston.

10.4 References

Bos, A.G., W. Spakman, and M.C.J. Nyst, Surface deformation and tectonic setting of Taiwan inferred from a GPS velocity field, *J. Geophys. Res.*, 108(B10), 2458, doi:10.1029/2002JB002336, 2003.

Hsieh, M.L., P.M. Liew, and M.Y. Hsu, Holocene tectonic uplift on the Hua-tung coast, eastern Taiwan, *Quatern. Int.*, 115, 47-70, 2004.

Lee, J.C., J. Angelier, H.T. Chu, J.C. Hu, F.S. Jeng, and R.J. Rau, Active fault creep variations at Chihshang, Taiwan, revealed by creep meter monitoring, 1998-2001, *J. Geophys. Res.*, 108(B11), 2528, doi:10.1029/2003JB002394, 2004.

Yamaguchi, M., and Y. Ota, Tectonic implications of Holocene marine terraces, east coast of Coastal Range, Taiwan, *Quatern. Int.*, 115, 71-81, 2004.

Yu, S.B., H.T. Chen, and L.C. Kuo, L.C., Velocity field of GPS stations in the Taiwan area, *Tectonophysics*, 274, 41-59, 1997.

Yu, S.B., and L.C. Kuo, Present-day crustal motion along the Longitudinal Valley Fault, eastern Taiwan, *Tectonophysics*, 333, 199-217, 2001.

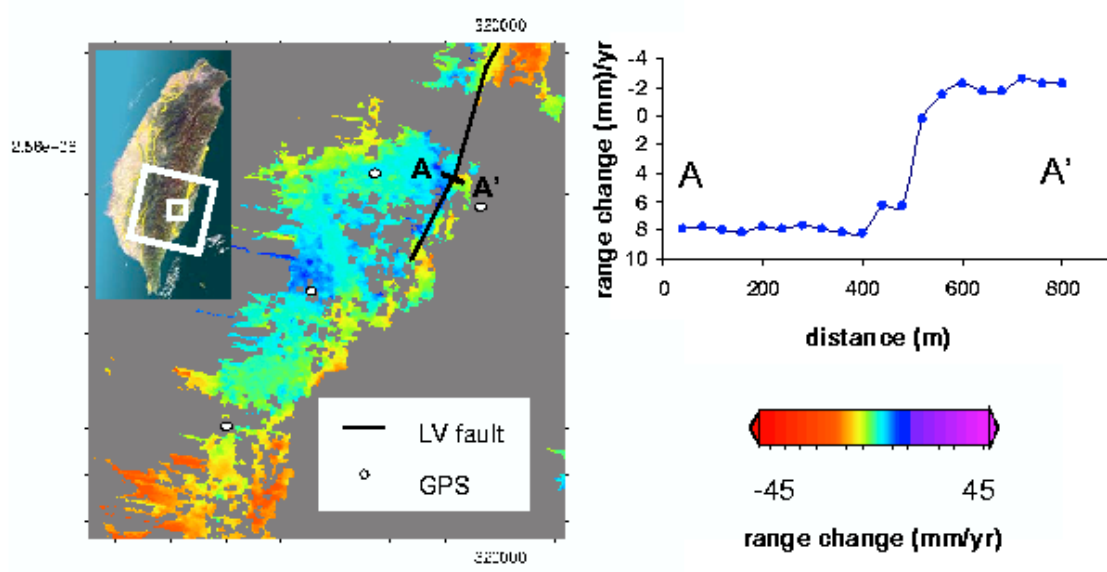


Figure 12.20: Location map, unwrapped interferometry, and offset on the Longitudinal Valley Fault, near Chishang. The interferogram is produced from a stack of three pairs spanning 1997 to 2000 (970517-980502, 970726-980815, 980815-000122). We calculated 14-26 mm/yr offset in the slip direction across the fault from A to A'.

11. Crustal Deformation Along the Northern San Andreas Fault System

Mark H. Murray

11.1 Introduction

The San Andreas fault system in northern California includes three sub-parallel right-lateral faults: the San Andreas, Ma'acama, and Bartlett Springs. This northernmost segment is the youngest portion of the fault system, forming in the wake of the northwestwardly propagating Mendocino triple junction where the Pacific, North America, and Gorda (southern Juan de Fuca) plates meet. The Pacific plate moves about 35-40 mm/yr relative to central California across a broad ~100-km zone in northern California. Additional deformation in eastern California and the Basin and Range province contribute to the total relative Pacific-North America motion of ~50 mm/yr. The San Andreas fault itself has been essentially aseismic and accumulating strain since it last ruptured in the great 1906 San Francisco earthquake, and no major earthquakes have occurred during the historical record on the more seismically active Ma'acama, and Bartlett Springs faults, which are northern extensions of the Hayward-Rodgers Creek and Calaveras-Concord-Green Valley faults in the San Francisco Bay area.

In *Frey Mueller et al.* (1999), we used GPS data collected in 1991-1995 along two fault-crossing profiles near Ukiah and Willits (Figure 12.21). The total deep slip rate on the San Andreas fault system inferred from the GPS data is $39.6^{+1.5}_{-0.6}$ mm/yr (68.6% confidence interval). Although deep slip rates on the individual faults are more poorly resolved due to high correlations between estimated slip rates and locking depths, and between slip rates on adjacent faults, the inferred slip rate on the Ma'acama fault ($13.9^{+4.1}_{-2.8}$ mm/yr) implies that it has accumulated a slip deficit large enough to generate a magnitude 7 earthquake, posing a significant seismic hazard.

In this ongoing study, we are resurveying the original profiles, adding new profiles to the north (near Covelo) and south (near Healdsburg), and surveying nearly 40 additional stations in the southern portion of the network to provide better monitoring along the Rodgers Creek and Ma'acama faults (Figure 12.21). The survey of the 4 primary profiles was conducted during 2003. Altogether, 43 site positions were measured during 94 session occupations lasting 6.5–8 hours, with the assistance of students and staff of the BSL. We are currently surveying about 40 monuments in the southern portion of network and are planning to install new profiles in special focus areas along the Bartlett Springs fault, whose long-term slip rate, locking depth and surface creep are poorly resolved. Most of the monuments were last observed in 1993–1995,

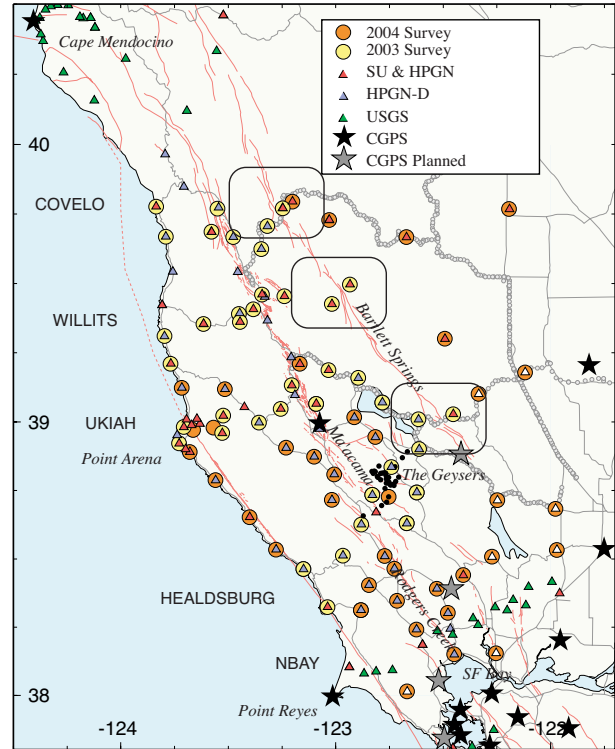


Figure 12.21: GPS sites along the northern San Andreas fault system. Light circles, sites that were observed in early 2003. Dark circles, 2004 surveyed or planned stations. Profile names are capitalized. USGS conduct surveys along the NBAY profile and near Cape Mendocino. Only one continuous GPS station (HOPB) currently operates in this region, with at least 5 planned PBO stations to be installed in Summer and Fall 2004. Rounded boxes, special focus areas along the Bartlett Springs fault where we will establish new profiles in Fall 2004.

so the new observations significantly improve the velocity estimates and models of average interseismic strain accumulation, including possible spatial variations along the fault system. The 10-station profiles from Pt. Reyes to Cape Mendocino together with planned PBO stations form a primary monitoring network for future observations to detect temporal variations in deformation.

11.2 Deformation

Figure 12.22 shows site velocities for the 1994-2004 period relative to stable North America, as defined by a set of 20 fiducial stations. The data are processed using

GAMIT/GLOBK software using many of the same techniques used to process the BARD observations described in Chapter 6 that provide a well-defined velocity reference frame with respect to the stable North America. Most of the velocities were derived from data spanning 8-10 years, whereas those with the largest error ellipses include data from only a 4 year span (most of these stations will be reoccupied in 2004). The easternmost stations exhibit motions typically associated with Sierran-Great Valley block (ORLA: 12.5 mm/yr NW). The westernmost sites are moving close to the Pacific plate rate (PTAR: 45.9 mm/yr NW). Fault-normal contraction is observed east of the Ma'acama fault, in the region of the Coast Ranges near the Central Valley where similar contraction has been observed elsewhere (e.g., *Murray and Segall, 2001*).

We apply angular velocity-fault backslip modeling techniques (e.g., *Murray and Segall, 2001*) to account for both far-field plate motions and interseismic strain accumulation. We are currently using a set of algorithms provided by Brendan Meade of MIT that extend this simple 2D methods to complex, 3D fault systems (including subduction zones and extensional provinces) by summing backslip on rectangular dislocations. We have successfully used the algorithms in a study of block motions in the Adriatic region and in the the BAVU block modeling efforts for the San Francisco Bay Area, both of which are described in other research chapters.

Preliminary results from our block modeling efforts are shown in Figure 12.22. We assume a simple fault geometry with 2 blocks between the 3 major faults in the San Andreas fault system. We also include the Pacific and North America plates, with sufficient numbers of stations to resolve their relative motions, and a Sierran-Great Valley block to provide better constraints on motions just east of the Bartlett Springs fault. The agreement between observed and predicted velocities is typically less than the 2 mm/yr level. Misfits are larger in a few areas close to faults, such as along the central Ma'acama and near the MTJ, that should be decreased with further refinement of the fault geometry. Total deformation across the San Andreas fault system is 38 mm/yr, in agreement with previous studies, but deep slip is concentrated on the Ma'acama fault (24 mm/yr) and on the Bartlett Springs fault (10 mm/yr), with only 4 mm/yr on the San Andreas. We are currently investigating this result, which is due in part to the high-degree of correlation between the slip rates on the 3 faults, and will test methods for adding geologic and other information using Bayesian techniques, which should reduce the correlations on slip rates and provide better resolution on other parameters such as locking depths. Fault normal contraction of about 3 mm/yr is estimated due to the impingement of the Sierran-Great Valley on the fault system, but more sophisticated error analysis is required to

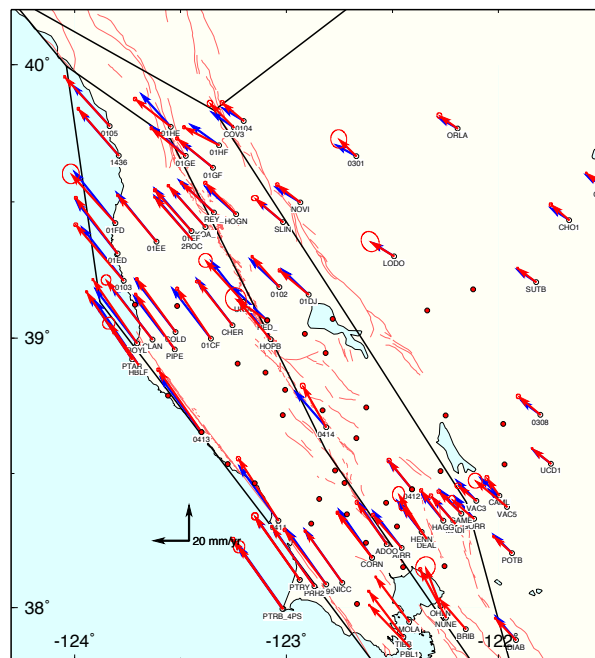


Figure 12.22: Velocities of sites in the Coast Ranges relative to North America, with 95% confidence regions assuming white-noise process only. Included are sites from this study plus sites from the BARD continuous network and the USGS North Bay profile. Red, observed velocities. Blue, velocities predicted from angular velocity-fault backslip block model assuming block boundaries (heavy black lines). We assume Pacific, North America, and Sierran-Great Valley blocks, plus 2 small blocks between the San Andreas, Ma'acama, and Bartlett Springs faults. The most significant misfits, such as near Cape Mendocino, can be reduced by refining the fault geometry.

assess whether this result is significant.

11.3 Acknowledgements

We appreciate support for this project by the USGS NEHRP through grant numbers 02HQGR0064 and 03HQGR0074. We thank André Basset, Maurizio Battaglia, Dennise Templeton, and especially Todd Williams for assistance conducting the survey.

11.4 References

Freymueller, J. T., M. H. Murray, P. Segall, and D. Castillo, Kinematics of the Pacific-North America plate boundary zone, northern California, *J. Geophys. Res.*, *104*, 7419–7442, 1999.

Murray, M. H., and P. Segall, Modeling broadscale deformation in northern California and Nevada from plate motions and elastic strain accumulation, *Geophys. Res. Lett.*, *28*, 4315–4318, 2001.

12. The Adriatic Region: An Independent Microplate within the Africa-Eurasia Collision Zone

Maurizio Battaglia, Mark H. Murray, Enrico Serpelloni (INGV) and Roland Bürgmann

12.1 Introduction

The tectonics of the Mediterranean is shaped by deformation related to the collision between the Nubia (Africa), Eurasia, and Anatolia plates. In this study, we use block modeling of surface velocities recorded by GPS measurements (Battaglia *et al.*, 2004) to investigate the present-day deformation of the Adriatic (Figure 12.23).

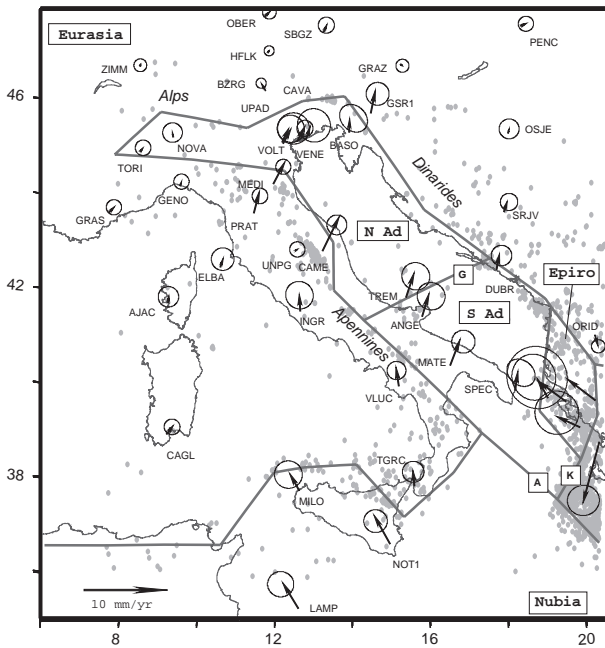


Figure 12.23: Location of the segments (solid lines) and blocks used to model the Adriatic region. [N Ad] North Adria, [S Ad] South Adria. [G] Gargano-Dubrovnik fault zone; [K] Kefallinia fault zone; [A] Apulia escarpment. GPS velocities and their 95% confidence ellipses. The grey dots indicate the location of the shallow seismicity from 1975 to 2000 ($M > 3.5$).

The tectonics of the Adriatic is not well constrained and remains controversial. Given the lack of significant seismic activity along the southern margin of the Adriatic Sea, the boundary with the Nubia plate, if it exists, is not well defined. Geomagnetic data averaged over several Myr and S_n shear wave propagation observations suggest that Nubia extends as a promontory into the Adriatic region (Mele, 2001), whereas historic geodetic and seismic evidence suggest that the Adriatic is an independent microplate (Adria) within the Nubia-Eurasia plate bound-

ary zone (Nocquet and Calais, 2003). Oldow *et al.* (2002) propose that Adria is divided by the Gargano-Dubrovnik fault into two blocks. Northwestern Adria has little or no motion relative to Europe and is part of the Alpine collage of southern Europe. Southeastern Adria is moving together with Nubia and is continuous from Sicily to Apulia. Other studies suggest that the Adriatic is an area of distributed deformation (Nocquet *et al.*, 2001).

To test different tectonic models for the Adriatic region, we develop a block model of regional deformation (Figure 12.23). This approach incorporates secular velocity and fault geometry estimates, as well as elastic strain accumulation. With this model we can assess whether different hypotheses are compatible with geodetic data, estimates of fault slip rates and locking depths, areas of rigid block rotation, and regions of anomalous strain accumulation (Meade *et al.*, 2002; Battaglia *et al.*, 2004).

12.2 GPS Measurements of Deformation

We use publicly available observations made at 30 continuous GPS stations of the European Reference Permanent Network (EUREF) and Italian Space Agency networks to estimate deformation in the Adriatic region (Figure 12.23). To improve the realization of a stable reference frame for the velocity solution, additional sites from the International GPS Service and EUREF networks are included as loosely constrained solutions provided by the Scripps Orbit and Permanent Array Center. Our solution includes data spanning 4 years from 102 stations, including 50 in the Mediterranean area. We incorporate velocities from 38 episodic GPS (EGPS) sites from McClusky *et al.* (2000) and 10 EGSP sites from Serpelloni *et al.* (2001) to better constrain deformation in the Eastern Mediterranean (Aegean and Anatolian plates) and southern Adriatic regions.

12.3 Block Model

Our block model of the Adriatic includes the interaction between the Eurasia, Nubia, Adria, Anatolia, Aegea, and Arabia plates. The plate boundaries are based on the description of the tectonic settings of the Mediterranean after van Dijk and Scheepers (1995), and seismicity distribution in the in the Mediterranean basin (International Seismological Center, 2001).

Plate boundary strain is determined from single continuous faults along the Calabrian coast, the Apennines, the Alps, the Dinarides, and the Hellenic Arc (Figure 12.23). This approach provides a first-order kinematic

description in areas with more broadly distributed deformation, where the station distribution is insufficient for detailed study.

We evaluate several possible representations of Adria and the Adria-Nubia margin: (1) the Adriatic is a region of continuous deformation within the Eurasian plate; (2) Northwestern Adria is part of the Alpine collage of southern Europe with the southern boundary with Nubia being the Gargano-Dubrovnik fault; (3) Nubia extends as a promontory into the Adriatic region; (4) Adria is divided from Nubia by the Gargano-Dubrovnik fault; (5) Adria is divided from Nubia and Aegea by the Apulia Escarpment and the Kefallinia fault; (6) Adria consists of two blocks separated by the Gargano-Dubrovnik fault in the middle and divided from Nubia and Aegea by the Apulia Escarpment and the Kefallinia fault.

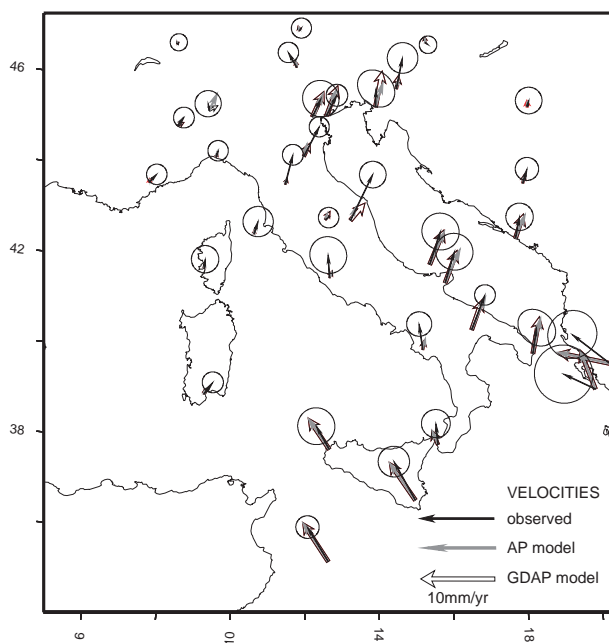


Figure 12.24: Observed and modeled GPS velocities for the single block (AP) and the two blocks (GDAP) model of Adria.

12.4 Results

The geodetic data and the models presented here (Figure 12.24) indicate that the Adriatic block is neither part of the Eurasia nor the Nubia plate. Geodetic data show that the Nubia plate is moving NW with respect to Eurasia with a velocity of 6 mm/yr, while the Adriatic microplate moves NE at a rate of 4-5 mm/yr (McClusky *et al.*, 2000). Our results show that independent microplate models of Adria offer a better fit to GPS velocities than models considering Adria as continuous with the Nubia or Eurasia plate. Geodetic data alone can-

not discriminate between a single block (AP) or a two block (GDAP) description of Adria (Figure 12.24), but the GDAP model predicts boundary slip rates that are in better agreement with observations from previous studies. Modeling results suggest that a possible location of the southern Adriatic/Nubia boundary could be the Apulia Escarpment lineament.

12.5 Acknowledgements

We acknowledge the GEODAF data archive of the Italian Space Agency (ASI) for providing GPS data. B. Meade (MIT) kindly allowed the use of his block model code. This work was supported by the Berkeley Seismological Laboratory and the Istituto Nazionale di Oceanografia e Geofisica Sperimentale (CRS-INOGS).

12.6 References

- Battaglia M., Murray M.H., Serpelloni E., and R. Bürgmann. The Adriatic region: an independent microplate within the Africa-Eurasia collision zone. *Geophys. Res. Lett.*, 31(9), L09605, 10.1029/2004GL019723, 2004.
- McClusky, S., et al., Global Positioning System constraints on plate kinematics and dynamics in the eastern Mediterranean and Caucasus, *J. Geophys. Res.*, 105, 5695-5719, 2000.
- Meade, B.J. et al., Estimates of seismic potential in the Marmara Sea region from block models of secular deformation constrained by Global Positioning System measurements, *Bull. Seism. Soc. Am.*, 92, 208-215, 2002.
- Mele, G., The Adriatic lithosphere is a promontory of the Africa Plate; evidence of a continuous mantle lid in the Ionian Sea from efficient S_n propagation, *Geophys. Res. Lett.*, 28, 431-434, 2001.
- Nocquet, J.M., and E. Calais, Crustal velocity field of Western Europe from permanent GPS array solutions, 1996-2001, *Geophys. J. Int.*, 154, 72-88, 2003.
- Nocquet, J.M., E. Calais, Z. Altamini, P. Sillard, and C. Boucher, Intraplate deformation in Western Europe deduced from an analysis of the International Terrestrial Reference Frame 1997 (ITRF97) velocity field, *J. Geophys. Res.*, 106, 11,239-11,257, 2001.
- Oldow, J.S. et al., Active fragmentation of Adria, the north Africa promontory, central Mediterranean orogen, *Geology*, 30; 779-782, 2002.
- Serpelloni, E., et al., Combination of permanent and non-permanent GPS networks for the evaluation of the strain-rate field in the central Mediterranean area. *Boll. Geof. Teor. Appl.*, 43, 195-219, 2002.
- van Dijk, J.P., and P.J.J. Scheepers, Neotectonic rotations in the Calabrian Arc; implications for a Pliocene-Recent geodynamic scenario for the Central Mediterranean, *Earth-Science Rev.*, 39, 207-246, 1995.

13. Bayesian Inference of Lower-Crustal Viscosity Near the Kunlun Fault Based on Geologic, Geomorphic, and Geodetic Data

George E. Hilley, Roland Bürgmann, Pei-Zhen Zhang (State Key Laboratory of Earthquake Dynamics, Beijing, China), and Peter Molnar (University of Colorado, Boulder, USA)

13.1 Introduction

Bayesian methods provide the means of integrating geologic, paleoseismic, seismic, and geodetic data to improve estimates of fault zone and lower-crustal properties (e.g., Segall, 2002) that are important for predicting the long-term deformation of plate boundary zones (e.g., Shen et al., 2001), understanding deformation and stress transfer following earthquakes, and estimating future seismic hazard (e.g., Hardebeck, 2004). Herein, we develop a Bayesian methodology that integrates geologic, geomorphic, and geodetic data to provide probabilistic estimates of fault-zone and lower-crustal properties.

We will apply this methodology to the Kunlun Fault in northern Tibet (Figure 12.25), where estimates of lower-crustal viscosity are generally lacking. Here, geologic and geomorphic information constrain the range of permissible long-term slip rates and coseismically generated offsets. We combined these a priori estimates with GPS velocities using a Bayesian implementation of an elastic-viscoelastic earthquake cycle model (Savage and Prescott, 1978) to estimate fault-zone and lower crustal properties in the area. The probabilistic nature of these models allows straightforward assessments of the uncertainties within, and covariance between model parameters. Our example shows that these methods may aid in elucidating the active tectonics of other areas, and improve seismic hazard assessments by formally assimilating disparate data types (e.g., geologic, geomorphic, seismic, or geodetic datasets) into crustal deformation studies.

13.2 Bayesian Modeling Framework

The Bayesian approach that we use to analyze data from northern Tibet uses geologic and geomorphic estimates of fault slip rates and observed offsets in conjunction with geodetic data to refine estimates of fault slip rate, schizosphere thickness, recurrence time of events, and viscous relaxation time of the plastosphere (“chizosphere” refers to the portion of the upper crust that deforms elastically, while “plastosphere” refers to areas that deform elastically over short time-scales but undergo viscous stress relaxation over longer time-scales; Scholz, 1988). Our method is based on Bayes’ Rule (Bayes, 1763), which allows quantitative refinement of initial estimates of model parameters (in this case, fault zone and lower crustal properties) given the information provided by the geodetic observations (Segall, 2002; Johnson and Segall, 2004):

$$P(m_i|x) = \frac{P(x|m_i) \times P(m_i)}{\sum_{i=1}^n P(x|m_i) \times P(m_i)} \quad (12.1)$$

In the context of this paper, m_i denotes a vector of model parameters, x is a vector of the observed geodetic velocities, $P(m_i|x)$ denotes the probability that the set of model parameters explains the geodetic velocities, $P(x|m_i)$ is the probability of observing the geodetic velocities given a combination of model parameters m_i , $P(m_i)$ is the probability that the chosen combination of model parameters actually occur, and the denominator normalizes the probability to all possible combinations of model parameters. In this context, $P(x|m_i)$ encapsulates the goodness of fit between observed geodetic velocities and those that would be expected based on the physical model that relates the surface velocity distribution to fault-zone and lower crustal properties (described below). Geodetic inversions that find the set of model parameters that best explain the observed data maximize $P(x|m_i)$. In contrast, the Bayesian approach not only considers the goodness of fit of the velocity to model predictions, but also $P(m_i)$, which describes in a probabilistic sense, some prior knowledge about what sets of model parameters are likely to occur. This term may be used to incorporate information such as slip rates along faults and recurrence times of earthquakes whose range may be estimated based on geologic and geomorphic considerations (e.g., Buck et al., 1996; Biasi et al., 2002; Segall, 2002). Therefore, the Bayesian modeling strategy has a two-fold advantage to conventional geodetic inversions: 1) Uncertainties in model parameters and covariance between model parameters may be straightforwardly obtained for complicated models (e.g., Hargreaves and Annan, 2002); and 2) Other types of data (e.g., geologic, geomorphic, and paleoseismic) may be used in conjunction with the geodetic data to improve estimates of model parameters. Explicit evaluation of Equation 12.1 may be untenable for potentially large, multidimensional parameter spaces that may arise even in simple physical models such as the model described below. Therefore, we solve Equation 1 using the Metropolis-Hastings variant of the Markov-Chain Monte Carlo (MCMC) simulation methods that allows approximation of the joint distribution $P(m_i|x)$ without an exhaustive search of the parameter space (Metropolis et al., 1953).

The mechanical model we employ (evaluated through $P(x|m_i)$) idealizes earthquake-cycle deformation as resulting from elastic strain release during rupturing events

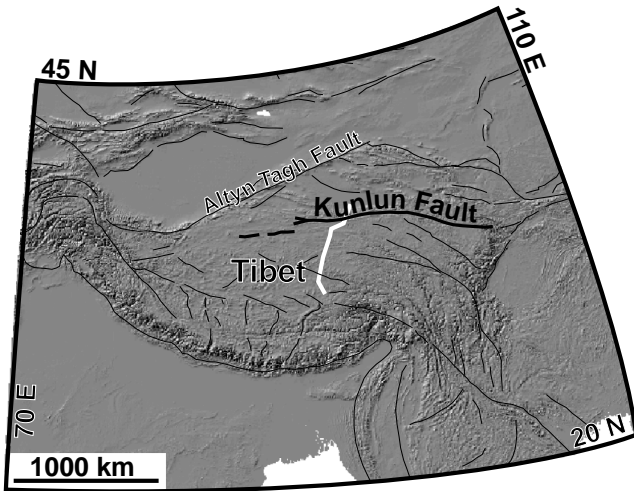


Figure 12.25: Location of the Kunlun Fault in central Asia. The Kunlun fault is one of a series of strike-slip faults that may accommodate a portion of the Indo-Eurasian collision. White line shows approximate location of GPS profile used in this study.

followed by viscoelastic relaxation of the lower crust and upper mantle (e.g., Savage and Prescott, 1978). The crust is idealized as two-dimensional in cross-section, and so movement along the major strike-slip faults occurs in the out-of-plane dimension. The rheology of the crust is treated as a two-layered medium in which an elastically deforming schizosphere overlies a linear, visco-elastically deforming plastosphere (e.g., Savage and Prescott, 1978; Savage, 2000; Segall, 2002; Dixon et al., 2003). The deformation during the earthquake cycle is defined by the long-term, average strike-slip velocity of the modeled fault (s), the Maxwell relaxation time of the plastosphere ($\tau = 2\nu/\mu$, where ν is the viscosity and μ is the shear modulus), the thickness of the schizosphere (H), the time since the last earthquake (t), and the average recurrence interval (T). Following Savage and Prescott (1978) and Segall (2002), we non-dimensionalize the model by introducing four groups: $t^* = t/T$, $\tau^* = \tau/T$, $s^* = s/s_{ref}$, and $H^* = H/x_{ref}$, where s_{ref} and x_{ref} are arbitrary velocity and length scales set to 1 mm/yr and 1 km, respectively. Although this is a simple representation of the earthquake cycle, this model is appropriate for inferring slip rates along the Kunlun Fault (and active strike-slip faults in Tibet in general) because: 1) The model captures the basic observation that the crustal deformation during the seismic cycle consists of coseismic, elastic, deformation followed by postseismic viscoelastic adjustment of the lower crust (e.g., Savage and Prescott, 1978; Segall, 2002); and 2) Several previous studies have successfully employed these types of simple models to provide first-order estimates of fault zone and lower-crustal

properties. Given the density of geodetic measurements from this portion of Tibet, the earthquake cycle modeling we employ allows us to consider velocity variations during the earthquake cycle that cannot be assessed using the types of dislocation models currently employed to interpret interseismic geodetic velocities from this area (i.e., Wallace et al., 2004; Zhang et al., 2004).

13.3 Application to the Kunlun Fault

Along the Kunlun Fault, numerous studies show consistency in estimated slip rates over a variety of different time-scales (10-100 kyr time-scales), and so the primary goal of the specific example is to estimate lower-crustal properties beneath the Kunlun fault based on geologic, geomorphic, and geodetic datasets. Along the Kunlun fault, 1) Geologic and geomorphic studies indicate that long-term slip rates are between 9-16 mm/yr (Kidd and Molnar, 1988; van der Woerd et al., 2001); 2) Geomorphic studies and historic ruptures suggest that the slip during each event is approximately 10 m (van der Woerd et al., 2001); and 3) The lack of historic seismicity places a minimum bound on the recurrence time of earthquakes along the fault. Using this information, we will construct prior joint probability densities and apply our Bayesian methodology to refine estimates of each of these parameters and the Maxwell relaxation time of the lower crust.

13.4 References

- Bayes, T., An essay towards solving a problem in the doctrine of chances, *Phil. Trans. R. Soc. Lond.*, 53, 370-418, 1763.
- Biasi, G. P., R. J. Weldon II, T. E. Fumal, and G. G. Seitz, Paleoseismic event dating and the conditional probability of large earthquakes on the southern San Andreas Fault, California, *Bull. Seism. Soc. Am.*, 92, 2761-2781, 2002.
- Buck, C. E., W. G. Cavanagh, and C. D. Litton, *The Bayesian Approach to Interpreting Archaeological Data*, Wiley, Chichester, 382 pp, 1996.
- Dixon, T. H., E. Norabuena, and L. Hotaling, Paleoseismology and Global Positioning System: Earthquake-cycle effects and geodetic versus geologic fault slip rates in the Eastern California shear zone, *Geology*, 31, 55-58, 2003.
- Hardebeck, J. L., Stress triggering and earthquake probability estimates, *J. Geophys. Res.*, B109, B04310, doi:10.1029/2003JB002437, 2004.
- Hargreaves, J. C., and J. D. Annan, Assimilation of paleo-data in a simple Earth system model, *Clim. Dynam.*, 19, 371-381, 2002.
- Johnson, K. M., and P. Segall, Viscoelastic earthquake cycle models of deep stress-driven creep along the San Andreas Fault system, *J. Geophys. Res.*, B, in press, 2004.

Kidd, W. S. F. and P. Molnar, Quaternary and active faulting observed on the 1985 Academia Sinica-Royal Society Geotraverse of Tibet, *Phil. Trans. R. Soc. Lond.*, *327*, 337-363, 1988.

Metropolis, N., A. W. Rosenbluth, M. N. Rosenbluth, A. H. Teller, and E. Teller, Equations of state calculations by fast computing machines, *J. Chem. Phys.*, *21*, 1087-1091, 1953.

Savage, J. C., Viscoelastic-coupling model for the earthquake cycle driven from below, *J. Geophys. Res.*, *B105*, 25,525-25,532, 2000.

Savage, J. C. and W. H. Prescott, Asthenosphere readjustment and the earthquake cycle, *J. Geophys. Res.*, *83*, 3369-3376, 1978.

Scholz, C.H., *The mechanics of earthquakes and faulting*, Cambridge University Press, Cambridge, 439 pp, 1988.

Segall, P., Integrating geologic and geodetic estimates of slip rate on the San Andreas fault system, *Int. Geol. Rev.*, *44*, 62-82, 2002.

Shen, F., L. H. Royden, and B. C. Burchfiel, Large-scale crustal deformation of the Tibetan Plateau, *J. Geophys. Res.*, *B106*, 6793-6816, 2001.

van der Woerd, J., P. Tapponnier, F. J. Ryerson, A.-S. Meriaux, B. Meyer, Y. Gaudemer, R. C. Finkel, M. W. Caffee, G.h. Zhao, and Z.q. Xu, Uniform postglacial slip-rate along the central 600 km of the Kunlun Fault (Tibet), from ²⁶Al, ¹⁰Be, and ¹⁴C dating of riser offsets, and climatic origin of the regional morphology, *Geophys. J. Int.*, *148*, 356-388, 2001.

Wallace, K., G.h. Yin, and R. Bilham, Inescapable slow slip on the Altyn Tagh fault, *Geophys. Res. Lett.*, *31*, L09613, doi:10.1029/2004GH019724, 2004.

Zhang, P.-Z., Z. Shen, M. Wang, W. Gan, R. Brgmann, P. Molnar, Z. Niu, J. Sun, Q. Wang, J. Wu, H. Sun, and X. You, Continuous deformation of the Tibetan Plateau from GPS, *Geology*, in press, 2004.

14. Observations and Modeling of Microseisms in the Santa Clara Valley, California

David Dolenc, Doug Dreger, and Shawn Larsen (LLNL)

14.1 Introduction

Previous studies of the 3D velocity structure in the Santa Clara Valley (SCV) showed that teleseismic, local, and microseism data recorded by the 41-station Santa Clara Valley Seismic Experiment (SCVSE) are all sensitive to basin structure and that they may be used to refine the velocity model of the basins (Dolenc *et al.*, 2004; Dolenc and Dreger, 2004). In our recent work we focused on constraining the source of the microseisms and used this for modeling the microseism observations in the SCV.

14.2 Results

A recent study by Schulte-Pelkum *et al.* (2004) showed that seismic noise in Southern California is highly monodirectional and that the microseisms source can be localized. We have performed a similar analysis by using f-k array method for the data recorded during the SCVSE. Our results show that at low frequencies (0.1 to 0.3 Hz), wavefield observations in the SCV also display directionality (Figure 12.26). At higher frequencies (0.3 to 0.5 Hz), wavefield directionality is lost, which may be due to scattering of the waves by the 3D structure in the SCV basins. The important result of these observations is that the source can be localized and can therefore be used in numerical simulations. We used the 3D finite-difference code E3D (Larsen and Schultz, 1995) and the UCB velocity model (Stidham, 1999; Stidham *et al.*, 1999) to simulate the microseism wavefield. A vertically oriented CLVD source located about 27 km offshore was used to generate isotropic Rayleigh waves. We used the source time function that was a superposition of sine waves at discrete periods over the observed microseismic band. Results for the observed and simulated microseisms are presented in Figure 12.27; both display directionality and source localization for low frequencies.

14.3 Conclusions

The analysis of the observed microseisms in the SCV shows directionality and source localization for low frequencies which enables us to simulate the microseism wavefield. Analysis of simulated waveforms shows agreement with observations in terms of directionality at low frequencies. We plan to refine the method to simulate microseism wavefield by including the source spectrum derived from the ocean wave data recorded at the Santa Cruz buoy. Obtained results will further be used to de-

velop a simultaneous inversion of the teleseismic, local, and microseism observations to constrain the velocity structure of the SCV basins.

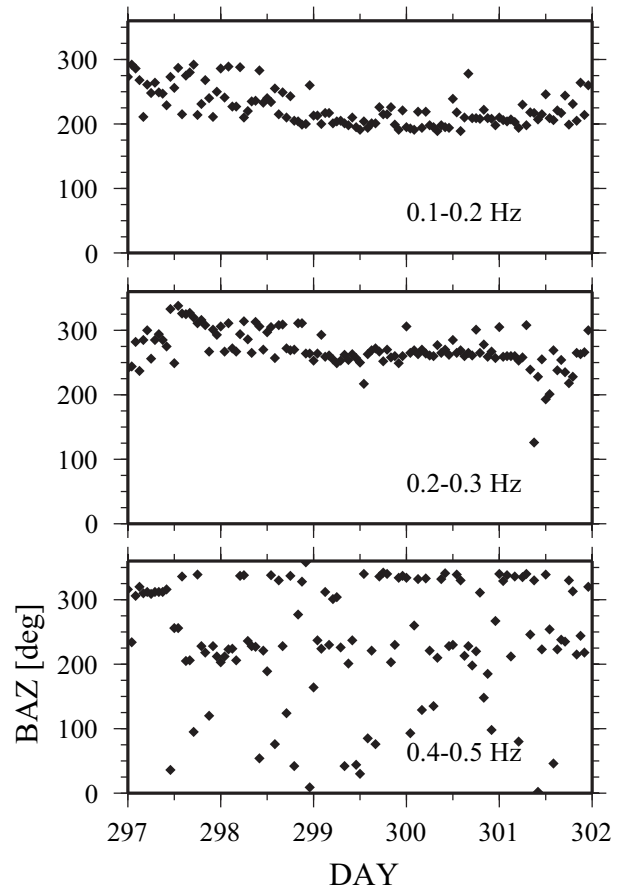


Figure 12.26: Backazimuth of the microseism wavefield over the 5-day period in 1998 determined with the f-k analysis. Results for the three frequency bands are presented.

14.4 Acknowledgements

This research was supported by the USGS grants 03HQGR0003 and 04HQGR0062.

14.5 References

Dolenc, D., D. Dreger, and S. Larsen (2004). Basin structure influences on the propagation of teleseismic

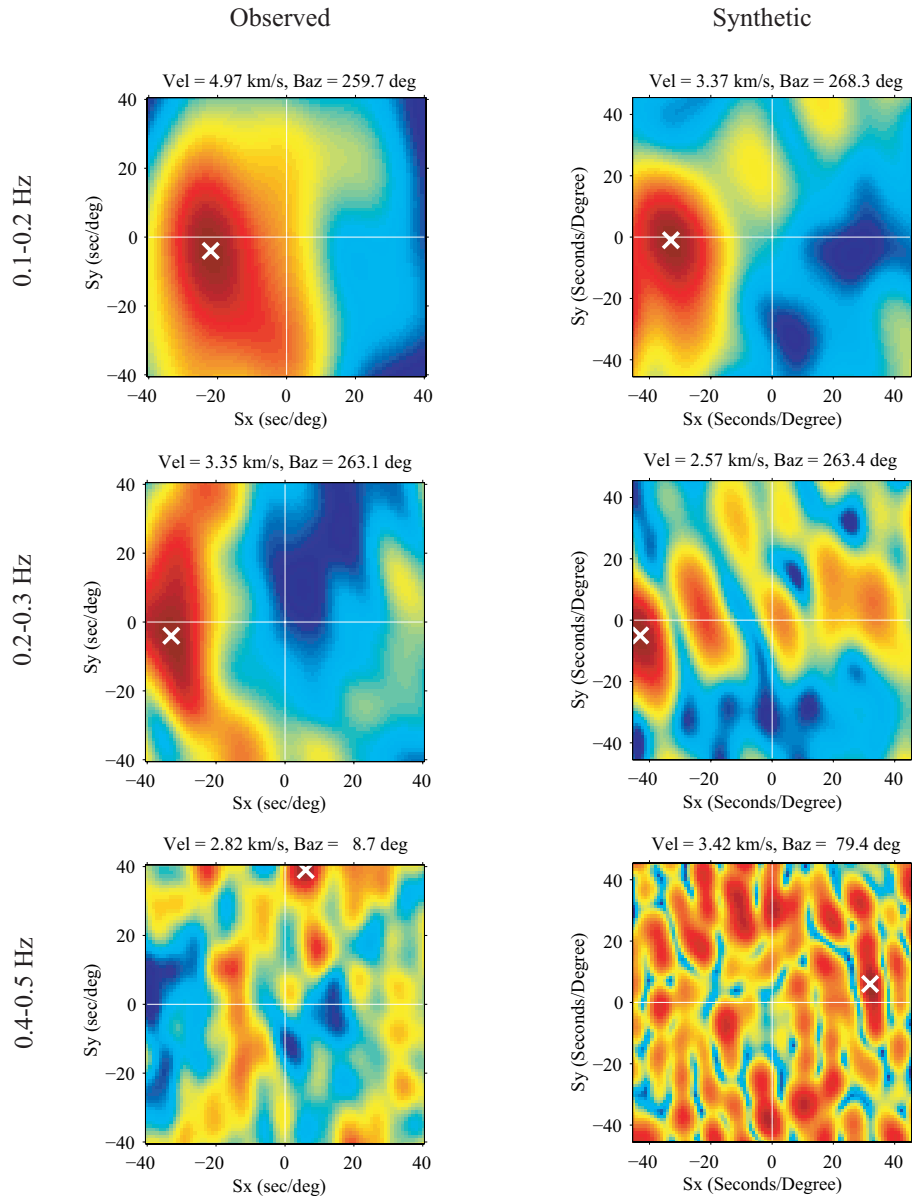


Figure 12.27: Observed (298.1998, 23 UTC) and simulated microseisms in the f-k slowness domain. Crosses indicate maximum power. In both cases, directionality and source localization is observed for low frequencies (0.1 to 0.3 Hz). A color version of this figure may be found on page 154.

waves in the Santa Clara Valley, California, *Bull. Seism. Soc. Am.*, in revision.

Dolenc, D. and D. Dreger (2004). Microseisms observations in the Santa Clara Valley, California, *Bull. Seism. Soc. Am.*, in revision.

Larsen, S. and C.A. Schultz (1995). ELAS3D: 2D/3D elastic finite-difference wave propagation code, Technical Report No. UCRL-MA-121792, 19 pp.

Schulte-Pelkum, V., P.S. Earle, and F.L. Vernon (2004). Strong directivity of ocean-generated seismic noise, *Geochem. Geophys. Geosys.*, 5, Q03004,

doi:10.1029/2003GC000520, 13pp.

Stidham, C., M. Antolik, D. Dreger, S. Larsen, and B. Romanowicz (1999). Three-dimensional structure influences on the strong-motion wavefield of the 1989 Loma Prieta earthquake, *Bull. Seism. Soc. Am.*, 89, 1184-1202.

Stidham, C. (1999). Three-dimensional crustal structure influences on wave propagation and generation of strong ground motion in the greater San Francisco Bay region, *Ph.D. Thesis*, University of California, Berkeley.

15. Excitation of Earth’s Incessant Free Oscillations by Atmosphere-Ocean-Seafloor Coupling

Junkee Rhie and Barbara Romanowicz

15.1 Introduction

The "hum" of the earth is well observed on broadband vertical seismic records on days without large earthquakes (*Suda et al.*, 1998). In other words, fundamental mode Rayleigh waves continuously propagate over the whole globe even if there are no significant earthquakes or volcanic eruptions. Its excitation level is similar to the level due to continuous occurrence of events with M_w 5.75 to 6.00. (*Ekström*, 2001). Since first observation, two competing models for sources of the hum have been proposed; atmospheric random perturbations (*Kobayashi and Nishida*, 1998) and processes in ocean (*Tanimoto*, 2003; *Rhie and Romanowicz*, 2004).

We are here concerned with developing an array-based method to detect and locate the sources of the hum. The array-based method is designed to measure the propagating direction of Rayleigh waves. By using two different arrays in the globe, we can get locations of the energy sources which generate continuous Rayleigh waves propagating through the solid earth. Our results show that Rayleigh wave originates primarily in the northern Pacific Ocean, during northern hemispheric winter, and in the southern oceans during the summer. The location of the sources shift seasonally and have a correlation with the maxima in significant wave height associated with winter storms. Considering our observation, we infer that atmosphere-ocean-seafloor coupling plays a crucial role in generating the "hum" of the Earth. The energy is transferring from storm to solid earth through infragravity waves.

15.2 Method and Observation

As the amplitude of waveform due to the hum is too weak to be detected at any individual recording, amplitude stacking in frequency domain or full great circle anti-dispersion filtering (*Ekström*, 2001) are used to enhance the signal. Both methods are good to detect the hum but inherently impossible to locate the sources because they are not sensitive to propagating direction of Rayleigh waves at all. To resolve the ambiguity in two competing models, we need to develop the method which is able to locate the sources by taking advantage of propagating properties of Rayleigh waves. An array-based method is a combined method of a traditional beam forming and an anti-dispersion filtering technique. By combining two methods, we can develop an optimal method to detect and measure the propagating direction of the long period (around 240s) surface wave. We used two regional

arrays in Northern California (BDSN) and Japan (F-net). More than 10 quiet stations in each array are selected and then an array-based method is applied on vertical velocity seismograms recorded at those stations. Before applying an array-based method, we need to remove waveforms affected by significant earthquakes because we are only interested in non-earthquake sources. We removed all time windows, which can be affected by events of $M_w > 5.5$. As small events cannot significantly contribute to Rayleigh wave energy above 150s, events with $M_w < 5.5$ are ignored. An array-based method allows us to estimate the distribution of background energy levels of long period Rayleigh waves as a function of time and back azimuth. As we are interested in the long-term average of energy levels, non-symmetric shape of the array can distort the average levels with respect to back azimuth. To overcome this unwanted effect, we just look at the Fourier spectrum of the stack amplitudes as a function of azimuth. If we compare this spectrum to one from synthetic experiment by assuming uniform distribution of sources, we can find that a synthetic spectrum has a negligible "degree one" component, but our observation has a strong degree one component. It indicates that the sources are not uniformly distributed. Here "degree one" means the Fourier component with period of 360 deg.

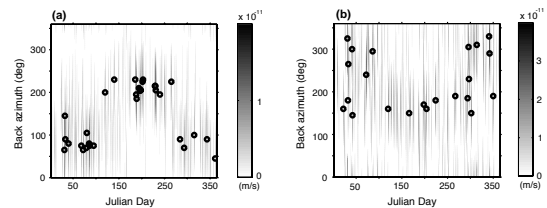


Figure 12.28: Amplitude of degree one as a function of time and back-azimuth for quiet days between 2000 and 2002. A "quiet day" contains at least 12 hours uncontaminated by earthquakes. The quiet day with larger amplitude was selected when we have more than 2 quiet days at same Julian day. (a) Back-azimuth corresponding to the maximum in the degree 1 component of stack amplitude for F-net as a function of time. Black circles indicate maxima with amplitude larger than 1.0×10^{-11} (m/s). (b) same as (a) for BDSN. Amplitude criteria for black circles is 3.0×10^{-11} (m/s)

We considered 3 years of data starting from 2000. One of our final observations is a variation of degree one com-

ponents of average stacks over one day for different Julian days and arrays. Time variation of maximum amplitudes and maximum directions of degree one components of averaged stacks show significant seasonal variation for each season and two arrays point to different regions for summer and winter (Fig. 12.28a,b). Here summer and winter are defined by 6 months from March through September and other 6 months, respectively. By using two maxima directions of degree one components averaged over each season, we can determine the probable regions where the hum originated during each season in 2000 (see Fig. 12.29a,b). We can get similar results for other years.

Two given regions show strong correlation with maxima of significant wave height for summer and winter (Fig. 12.29c,d) and it infers that energy transfer from ocean to solid earth is happening in these regions. However, there is still a possibility that we failed to locate other source regions because the distribution of arrays are too sparse and we are utilizing only first order information of direction to the sources.

15.3 Discussion

Our result implies that the ocean takes an important part in the excitation of the hum. A highly probable scenario of energy transfer from atmosphere to solid earth through oceans is as follows: 1) a significant winter storm generates ocean waves over the mid-latitude oceans; 2) some of the energy leaks out and propagate as free waves into the ocean basins; 3) They interact with the topography of the ocean basin and transfer energy to the solid earth. But the efficiency of generating elastic waves seems to depend on various factors, such as the depth of sea floor, the shape of the continental shelves bounding the ocean basin, and the strength and persistence of storms. For example, the strengths of storms in northern Pacific and northern Atlantic are comparable during northern hemispheric winter, but only northern Pacific seems to generate significant elastic waves, which is in agreement with differences of 20-30dB in pressure noise on the ocean basin between these oceans in the infragravity wave bands (*Webb et al.*, 1999).

15.4 References

Ekström, G., Time domain analysis of Earth's long-period background seismic radiation, *J. Geophys. Res.*, *106*, 26,483-26,493, 2001.

Kobayashi, N., and N. Nishida, Continuous excitation of planetary free oscillations by atmospheric disturbances, *Nature*, *395*, 357-360, 1998.

Rhie, J., and B. Romanowicz, Excitation of earth's incessant free oscillations by atmosphere-ocean-seafloor coupling, *Nature*, **431**, 552-556. 2004.

Suda, N., K. Nawa, and Y. Fukao, Earth's background free oscillations, *Science*, *279*, 2089-2091, 1998.

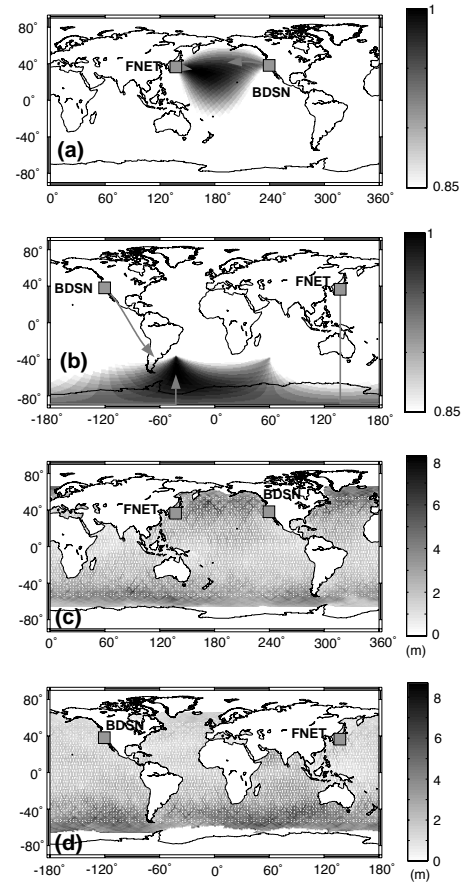


Figure 12.29: Comparison of seasonal variations in the distribution of hum-related noise (degree 1 only) and significant wave height in the year 2000. The directions corresponding to mean amplitudes that are larger than 85 percent of the maximum are combined for the two arrays in winter (a) and in summer (b) to obtain the region of predominant sources in each season. Arrows indicate the direction of maxima. Both arrays are pointing to the Northern Pacific Ocean in the winter and to the southern ocean in the summer. Global distribution of significant wave height, in the winter (c) and in the summer (d), averaged from TOPEX/Poseidon images for the months of January and July, 2000, respectively

Tanimoto, J., Jet stream, roaming ocean waves, and ringing earth, *EOS Trans. AGU* *84*(46), Fall Meet. Suppl., Abstract S12F-04, 2003.

Webb, S., X. Zhang, and W. Crawford, Infragravity waves in the deep ocean, *J. Geophys. Res.*, *96*, 2723-2736, 1991.

16. Episodic Tremor and Slip in the Southern Cascadia Subduction Zone

Mark H. Murray and Bob Uhrhammer

16.1 Introduction

Continuous GPS stations operating over the last decade have begun to detect transient deformation signals from aseismic processes that can occur over hours to days. Deviations from uniform motion of GPS stations in Washington and British Columbia led to the detection of an aseismic 1–2 week slip event on the deeper (25- to 45-km) northern Cascadia subduction zone interface (Dragert *et al.*, 2001). Similar events repeat at 13- to 16-month intervals (Miller *et al.*, 2002), and are also spatially and temporally correlated with pulsating, tremorlike seismic signals with 1–5 Hz frequency content that do not have impulsive onsets (Rogers and Dragert, 2003). One possible explanation for these episodic tremor and slip (ETS) events is that fluids generated by dehydration processes from the slab are playing an important role in regulating the deep slip on the interface (Obara, 2002).

Recent evidence suggest that ETS activity may be occurring along the entire Cascadia subduction zone (Szeliga *et al.*, 2004). We are assessing our GPS and seismic observations to provide better constraints on this behavior in northern California.

16.2 Results

The daily position time series at Yreka (YBHB) (Figure 12.30) shows evidence for cm-level transient deformation lasting 1–2 weeks that is similar to the behavior detected in northern Cascadia. We have developed a detection algorithm, based on a smoothed, 10-day running median of hourly power spectral density estimates in the 1–5 Hz range, and have applied this algorithm to Yreka (YBH) seismic data from 2000–2004. The high peaks (Figure 12.30) correspond to periods when the tremor noise dominates the signals, and these peaks are highly correlated with the episodic westward GPS displacements. The peaks have a 10.9 ± 2.0 month period (shorter than the 14 month period found near Puget Sound). The correlations are less clear on the north GPS component. Episodic displacements at these frequencies have not been observed on the coastal continuous GPS stations, so currently the YBHB GPS observations and the corresponding tremors observed at YBH and other northern California stations provide the only evidence for episodic slow earthquakes in the southern Cascadia subduction zone. We are currently studying tremors detected on other seismic instruments and improving our GPS regional filtering techniques to better characterize the possible deformation signals.

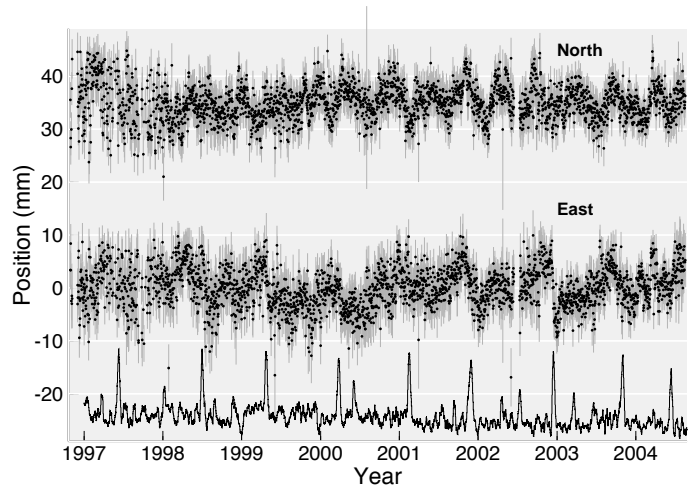


Figure 12.30: Timeseries of YBHB daily north and east positions, with standard errors, estimated using GAMIT. Long-term average motion and annual sinusoidal signals have been removed. Black lines are the smoothed hourly median power spectral density estimates in the 1–5 Hz pass band at the YBH BDSN station, with higher values during periods of strong seismic tremor. The episodic GPS deformation, particularly on the east component, is strongly correlated with tremor periods, suggesting that episodic slow earthquakes may be occurring along the southern Cascadia subduction zone.

16.3 References

- Dragert, H., K. Wang, and T. S. James, A silent slip event on the deeper Cascadia subduction interface, *Science*, 292, 1525–1528, 2001.
- Miller, M. M., T. Melbourne, D. J. Johnson, W. Q. Sumner, Periodic slow earthquakes from the Cascadia subduction zone, *Science*, 295, 2423, 2002.
- Obara, K., Nonvolcanic deep tremor associated with subduction in southwest Japan, *Science*, 296, 1679–1681, 2002.
- Rogers, G., and H. Dragert, Episodic tremor and slip: The chatter of slow earthquakes, *Science*, 300, 1942–1944, 2003.
- Szeliga, W., T. I. Melbourne, M. M. Miller, and V. M. Santillan, Southern Cascadia episodic slow earthquakes, *Geophys. Res. Lett.*, 31, L16602, doi:10.1029/2004GL020824, 2004.

17. A Three Dimensional Radially Anisotropic Model of Shear Velocity in the Whole Mantle

Mark Panning and Barbara Romanowicz

17.1 Introduction

The 3D seismic velocity structure of the Earth’s mantle represents a snapshot of its current thermal and chemical state. As tomographic models of the isotropic seismic velocity converge in their main features (*Masters et al., 2000; Mégnin and Romanowicz, 2000; Ritsema and van Heijst, 2000; Gu et al., 2001*), geodynamicists use them to infer the density structure, and thus the buoyancy contrasts which drive mantle convection (*Hager, 1984; Ricard and Vigny, 1993; Daradich et al., 2003*). This process, however, is complicated by the difficulty of separating thermal and chemical contrasts, and the lack of direct sensitivity of seismic velocities to the density contrasts which drive the convection.

In many regions of the mantle, analyzing the anisotropy of seismic velocities can give us another type of constraint on mantle dynamics. Nearly all the constituent minerals of the mantle have strongly anisotropic elastic properties on the microscopic scale. Random orientations of these crystals, though, tend to cancel out this anisotropy on the macroscopic scale observable by seismic waves, unless crystals or materials with strongly contrasting elastic properties are aligned through deformation processes. While in the relatively cold regions of the lithosphere these anisotropic signatures can remain frozen in over geologic time-scales (*Silver, 1996*), observed anisotropy at greater depths likely requires dynamic support (*Vinnik et al., 1992*). Thus, the anisotropy observed at sub-lithospheric depths is most likely a function of the current mantle strain field, and these observations can help us map out mantle flow.

17.2 Model Results

We have developed a degree 16 3D radially anisotropic shear velocity model of the whole mantle using a large three component surface and body waveform dataset and an iterative inversion for structure and source parameters based on Nonlinear Asymptotic Coupling Theory (NACT) (*Li and Romanowicz, 1995*). The model is parameterized in terms of isotropic V_S and an anisotropic parameter, ξ , which is defined by $\xi = V_{SH}^2/V_{SV}^2$. The model shows a link between mantle flow and anisotropy in a variety of depth ranges.

The common features of S tomographic models are present in the isotropic V_S model. The uppermost 200 km is dominated by tectonic features, with fast continents and slower oceans that show an age-dependent increase in velocity away from the slow velocities near ridges. Re-

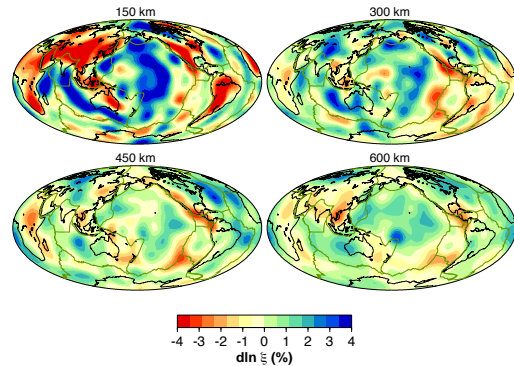


Figure 12.31: ξ structure at four depths in the upper mantle and transition zone.

gions of active tectonic processes are, in general, slower, such as western North America, the major circum-Pacific subduction zones, and the East African rifting. In the transition zone depth range, the most prominent features are the fast velocities of subducted slabs, while the slow ridges are no longer present. Mid-mantle velocity anomalies are low in amplitude, and more white in spectrum. Finally, in the lowermost 500 km, the amplitudes of heterogeneity increase again, and become dominated by a degree 2 pattern with rings of higher velocities surrounding two lower velocity regions under the central Pacific and Africa, commonly referred to as superplumes.

In the ξ model of the upper mantle (Figure 12.31), we confirm observations of regions with positive ξ anomalies ($V_{SH} > V_{SV}$) starting at ~ 80 km under oceanic regions and ~ 250 km under old continental lithosphere, suggesting horizontal flow beneath the lithosphere (*Gung et al., 2003*). We also observe a $V_{SV} > V_{SH}$ signature at ~ 200 - 300 km depth beneath major ridge systems with amplitude correlated with spreading rate. In the transition zone (400-700 km depth), regions of subducted slab material are associated with negative ξ anomalies ($V_{SV} > V_{SH}$) (Figure 12.31), while the ridge signal decreases except under the East Pacific Rise.

We also confirm the observation of strong radially symmetric $V_{SH} > V_{SV}$ in the lowermost 300 km (Figure 12.32) (*Panning and Romanowicz, 2004*). The 3D deviations from this degree 0 signature are associated with

the transition to the large-scale superplumes under the central Pacific and Africa, suggesting that $V_{SH} > V_{SV}$ is generated in the predominant horizontal flow of a mechanical boundary layer, with a change in signature related to transition to upwelling at the superplumes.

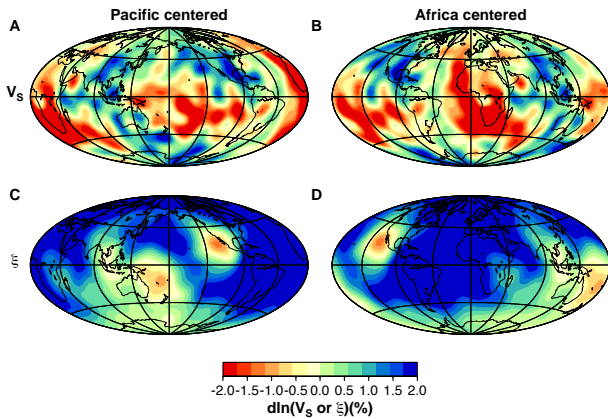


Figure 12.32: Isotropic V_S (top) and ξ (bottom) structure at 2800 km depth, centered under the Pacific (left) and Africa (right).

17.3 Source Inversions

In the process of developing the anisotropic model, we also invert for source parameters for the events in our dataset, starting from published Harvard CMT solutions, which are developed in a simpler mantle velocity model. We performed an iterative inversion, with scalar seismic moment fixed. 964 of the 1191 events in our dataset had sufficient data coverage for a stable inversion which showed an improvement in fit. While changes in mechanism and location were quite small (horizontal location shifts averaged 0.015°), there was evidence for systematic relocation due to the improved structural model, particularly in the circum-Pacific subduction zones (Figure 12.33).

17.4 References

Daradich, A., J.X. Mitrovica, R.N. Pysklywec, S.D. Willett and A.M. Forte, Mantle flow, dynamic topography, and rift-flank uplift of Arabia, *Geology*, **30**, 901-904, 2003.

Gu, Y.J., A.M. Dziewonski, W. Su, and G Ekström, Models of the mantle shear velocity and discontinuities in the pattern of lateral heterogeneities, *J. Geophys. Res.*, **106**, 11,169-11,199, 2001.

Gung, Y., M. Panning and B. Romanowicz, Global anisotropy and the thickness of continents, *Nature*, **422**, 707-711, 2003.

Hager, B.H., Subducted slabs and the geoid - constraints on mantle rheology and flow, *J. Geophys. Res.*,

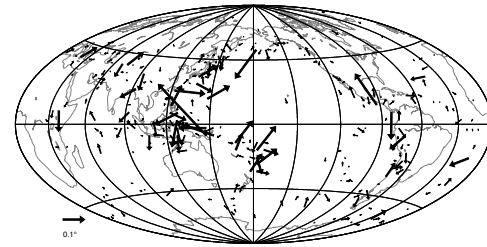


Figure 12.33: Vector-summed event relocations in $5^\circ \times 5^\circ$ cells.

89, 6003-6015, 1984.

Li, X.D. and B. Romanowicz, Comparison of global waveform inversions with and without considering cross-branch modal coupling, *Geophys. J. Int.*, **121**, 695-709, 1995.

Masters, G., G. Laske, H. Bolton and A. Dziewonski, The relative behavior of shear velocity, bulk sound speed, and compressional velocity in the mantle: implications for chemical and thermal structure, in *Earth's Deep Interior*, AGU Monograph 117, pp. 63-86, eds. Karato, S., A.M. Forte, R.C. Liebermann, G. Masters and L. Stixrude, Amer. Geophys. Union, Washington, D.C., 2000.

Mégnin, C., and B. Romanowicz, The 3D shear velocity of the mantle from the inversion of body, surface, and higher mode waveforms, *Geophys. J. Int.*, **143**, 709-728, 2000.

Panning, M.P. and B. Romanowicz, Inferences on flow at the base of Earth's mantle based on seismic anisotropy, *Science*, **303**, 351-353, 2004a.

Ricard, Y. and C. Vigny, Mantle dynamics with induced plate tectonics, *J. Geophys. Res.*, **94**, 17,543-17,560, 1989.

Ritsema, J. and H.-J. van Heijst, Seismic imaging of structural heterogeneity in Earth's mantle: evidence for large-scale mantle flow, *Science Progress*, **83**, 243-259, 2000.

Silver, P.G., Seismic anisotropy beneath the continents: probing the depths of geology, *Annu. Rev. Earth Planet. Sci.*, **24**, 385-432, 1996.

Vinnik, L.P., L.I. Makeyeva, A. Milev and Y. Usenko, Global patterns of azimuthal anisotropy and deformations in the continental mantle, *Geophys. J. Int.*, **111**, 433-447, 1992.

18. High Resolution Anisotropic Structure of the North American Upper Mantle from Inversion of Body and Surface Waveform Data

Federica Marone, Yuancheng Gung and Barbara Romanowicz

18.1 Introduction

Seismic anisotropy is required for a correct interpretation of the retrieved S -velocity structure in tomographic studies at least in the first 400 km of the upper mantle (Gung *et al.*, 2003). A detailed knowledge of the seismic anisotropic structure of the earth's mantle also provides insight into debated geophysical issues, such as the nature and strength of lithosphere/asthenosphere coupling, the depth extent of continental sub-regions and the relation of imaged seismic anisotropy to present-day asthenospheric flow and/or past tectonic events recorded in the lithosphere.

To date, our knowledge of the North American anisotropic structure arises mainly from global tomographic models (e.g. Ritsema *et al.*, 1999; Gung *et al.*, 2003) or SKS splitting studies (e.g. Fouch *et al.*, 2000; Savage and Sheehan, 2000), which lack horizontal and vertical resolution respectively, and are limited to either radial or azimuthal anisotropy.

Our goal is a new high resolution model for the North American upper mantle incorporating both radial and azimuthal anisotropy. We aim at unprecedented lateral and depth resolution by improving both data coverage and methodology.

18.2 Dataset

We have collected and processed 3 component body, fundamental and higher mode surface waveforms to complement the BSL database and improve the data coverage for North America. In particular, we focused our attention to broad band seismograms recorded at the numerous permanent seismic stations deployed throughout North America (Figure 12.34), from events at teleseismic and far regional distances. From each deconvolved and filtered seismogram, individual body and surface wave energy packets have been extracted using an automated selection algorithm and subsequently checked by hand, to ensure a high quality dataset. The compiled data collection consists of more than 100,000 3 component body, fundamental and higher mode surface waveforms and provides a fairly homogeneous path (Figure 12.34) and azimuthal coverage.

We plan to use independent information from SKS splitting measurements as additional constraints on the anisotropic model.



Figure 12.34: Data coverage - Paths of teleseismic events with $M_w \geq 6$ recorded at North American stations (indicated by white triangles), for which high quality fundamental mode Rayleigh wavepackets have been selected.

18.3 Methodology Improvements

We invert seismic long period waveform data in the framework of normal mode asymptotic theory (NACT - Li and Romanowicz, 1996). The resulting broad band sensitivity kernels allow us to exploit the information contained in long period seismograms for body, fundamental and higher mode surface waves simultaneously.

Until now, this approach has only been applied at the global scale with lateral parametrization in terms of spherical harmonics (Li and Romanowicz, 1996; Mégnin and Romanowicz, 2000). We have adapted the procedure to the regional case by implementing a lateral parametrization in terms of spherical splines on an inhomogeneous triangular grid of knots (e.g. Wang and Dahlen, 1995), with the finest mesh for the region of interest, where the data coverage is densest, and a coarser grid outside the studied region (Figure 12.35).

Body and surface wave datasets used in mantle seismic tomography are sensitive to crustal structure, but cannot resolve details within the crust. Accurate crustal corrections are therefore essential for the quality of high resolution regional tomographic studies. The effect of shallow-layer features is often removed from the data by assuming an a priori crustal model (e.g. CRUST2.0) and applying

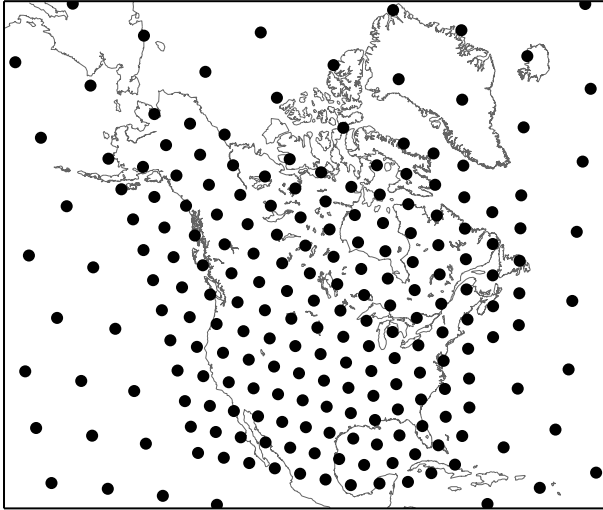


Figure 12.35: Example of irregular grid with a finer mesh for North America

linear perturbation corrections. However, lateral variations in Moho depth can be fairly large even over short distances, as for instance at ocean/continent transitions and the adequacy of linear corrections is questionable. In fact, *Montagner and Jobert (1988)* showed that the non-linearity of shallow-layer corrections is often non negligible even at long periods. In high resolution upper mantle regional tomographic studies, it is therefore important to take the crustal structure into account in a more accurate way. Going beyond the linear perturbation approximation, we follow the approach proposed by *Montagner and Jobert (1988)* and split the correction into a linear and non-linear part. At each point along a path, we assign a 1D reference model according to the local crustal structure (e.g. extended crust, orogen, ocean, ...). We then correct for the difference between the discontinuities in the chosen a priori crustal model (e.g. CRUST2.0) and the selected 1D local reference model assuming a linear perturbation, and exactly for the difference, if any, between the local reference model and PREM (our global reference model).

18.4 Future of the Project

Preliminary inversions of the compiled dataset using the improved NACT algorithm resulted in a radial anisotropic upper mantle structure reproducing the major features shared by all recent models (e.g. *Ritsema et al., 1999*; *Gung et al., 2003*), such as high velocities beneath cratons between 100 and 250 km depth and negative velocity anomalies in back arc regions. While refining this preliminary model, we will work on the next step and implement a more complete anisotropic parametrization. Our final goal is a model incorporating both radial and

azimuthal anisotropy. Such a model can be parametrized in terms of radial anisotropy with a symmetry axis of arbitrary orientation, corresponding to the 5 Love parameters plus two angles defining the axis orientation. The backbone permanent network component of USArray, complemented by temporary Big Foot deployments, will provide an unprecedented density of recordings. This unique dataset will guarantee the resolution of this increased number of parameters.

18.5 Acknowledgements

This work has been financially supported by the Swiss foundation “Stefano Franscini”.

We are grateful to the IRIS Data Management Center (DMC) as well as to the Geological Survey of Canada for providing waveform data used in this study.

18.6 References

- Fouch, M.J., K.M. Fischer, E.M. Parmentier, M.E. Wysession and T.J. Clarke, Shear-wave splitting, continental keels, and patterns of mantle flow, *J. Geophys. Res.*, *105*, 6255-6275, 2000.
- Gung, Y., M. Panning and B. Romanowicz, Global anisotropy and the thickness of continents, *Nature*, *422*, 707-711, 2003.
- Li, X.D. and B. Romanowicz, Global mantle shear-velocity model developed using nonlinear asymptotic coupling theory, *Geophys. J. R. Astr. Soc.*, *101*, 22,245-22,272, 1996.
- Mégnin, C. and B. Romanowicz, The 3D shear velocity structure of the mantle from the inversion of body, surface and higher mode waveforms, *Geophys. J. Int.*, *143*, 709-728, 2000.
- Montagner, J.-P. and N. Jobert, Vectorial tomography; II. Application to the Indian Ocean, *Geophys. J.*, *94*, 309-344, 1988.
- Ritsema, J., H. van Heijst and J. Woodhouse, Complex shear wave velocity structure imaged beneath Africa and Iceland, *Science*, *286*, 1925-1928, 1999.
- Savage, M.K. and A.F. Sheehan, Seismic anisotropy and mantle flow from the Great Basin to the Great Plains, western United States, *J. Geophys. Res.*, *105*, 13,715-13,734, 2000.
- Wang, Z. and F. Dahlen, Spherical-spline parametrization of three-dimensional Earth models, *Geophys. Res. Lett.*, *22*, 3099-3102, 1995.

19. Tests of Normal Mode Asymptotic Approximations against Computation Using the Spectral Element Method

Yuancheng Gung, Barbara Romanowicz and Yann Capdeville

19.1 Introduction

We evaluate normal mode asymptotic methods by comparing the corresponding 3D synthetics with those computed using the coupled spectral element/normal mode method (CSEM) (Capdeville *et al.*, 2003). Three normal mode based asymptotic approaches are compared: (1) path average approximation (PAVA) (Woodhouse and Dziewonski, 1984), in which only along-branch mode coupling effects are considered; (2) Non-linear asymptotic coupling theory (NACT) (Li and Romanowicz, 1995), which includes the across-branch mode coupling effects; and (3) NACT+F, an extension of NACT with focusing terms computed using higher order asymptotic theory (Romanowicz, 1987; Romanowicz *et al.*, 2004). Systematic waveform comparisons are implemented. We find that NACT and NACT+F provide much better fit, and the off-great-circle effects, which result in focusing/defocusing and not seen by PAVA or NACT, are well explained by NACT+F.

19.2 Experiments and Results

Two 3-D synthetic Earth models are used to test the validity of three normal mode based analytical approaches, PAVA, NACT and NACT+F. The CSEM is used to provide the accurate reference synthetics in the 3-D test models.

The synthetic models are parameterized laterally using spherical harmonics up to degree 16, and radially using cubic splines. To examine more closely the small perturbation of the seismograms caused by the 3-D heterogeneities, the differential waveforms (i.e. $\mathbf{u}_{3D \text{ model}} - \mathbf{u}_{\text{reference model}}$) for CSEM and normal mode techniques are compared. Two representative results are shown here. Figure 12.36 shows the results for an isotropic source in a 3-D model with an ellipsoidal anomaly centered at the 220 km depth, and Figure 12.37 shows the results for a dip-slip source in a 3-D model with two opposite ellipsoidal anomalies centered at 150 km depth.

From the above results, we find that (1) when the path just grazes the anomaly, both PAVA and NACT fail to match CSEM synthetics, since they are insensitive to off-path structure, while NACT+F predicts the expected focusing effects fairly well; and (2) when the path passes through two anomalies with opposite signs, the effects of heterogeneities are cancelled out in the PAVA formalism (there is nearly no perturbation in PAVA differential waveform, as seen in Figure 12.37), and they are well

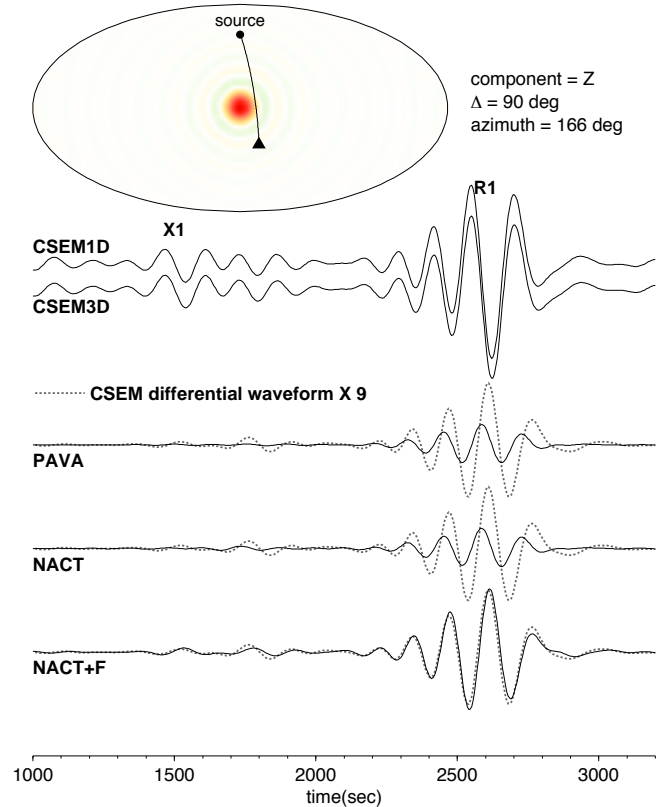


Figure 12.36: Top map: the geometrical relation of the isotropic source (black dark circle), the surface receiver (triangle) and lateral variations of hypothetical 3-D model, a slow velocity anomaly of maximum amplitude -5% at 220 km depth. Top trace: CSEM synthetics for the reference model (CSEM1D) and for the 3-D model (CSEM). In the bottom panels, the differential waveforms of CSEM (dashed line) and three normal mode based asymptotic approaches (solid line) are compared. Note that in this particular case, the great circle path just grazes the anomaly.

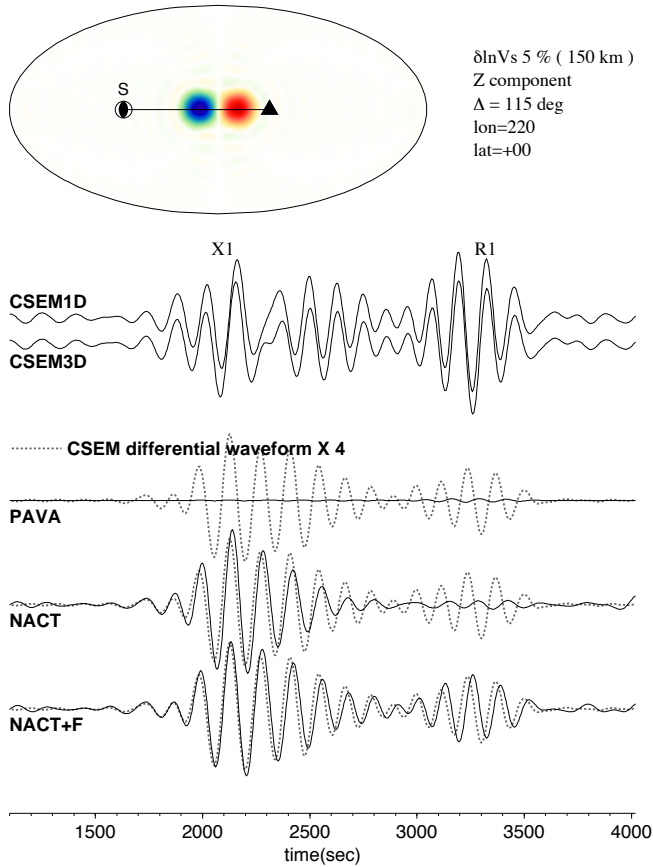


Figure 12.37: The geometrical relation of the dip-slip source, the surface receiver and lateral variations of the hypothetical 3D model at 150 km depth. The 3D model consists of two equal anomalies of opposite signs (fast and slow), with maximum velocity contrast of 5%. In the bottom panels, the differential waveforms of CSEM and three normal mode based asymptotic approaches are compared. Note that in this case, the great circle path passes the surface center of two anomalies.

explained in NACT and NACT+F, particularly for the overtone phases.

In summary, we have confirmed, through a series of synthetic experiments, that NACT and NACT+F are much better than PAVA in explaining waveform perturbations in a 3D heterogeneous Earth model. We also verified that the focusing effects are predicted well by the higher order asymptotic approximation, NACT+F.

19.3 Future Work

NACT+F is potentially very important in Q tomography, in which the major technical difficulty encountered is how to discriminate anelastic signals from elastic effects on the amplitude of seismic data. It has been shown that while the elastic focusing/defocusing effects are not significant at low degrees (8) (Selby and Woodhouse, 2002), they need to be included to achieve a higher resolution Q model.

With NACT+F, we propose a two-step iterative waveform inversion procedure for a next generation of Q model. In the first step, 3D elastic models are inverted with the radial anisotropy and focusing effects taken into account. In the second step, anelastic 3D models are inverted, and 3D elastic models from step one are used to correct the phase shift and focusing effects due to elastic anomalies prior to anelastic tomography.

19.4 References

- Capdeville Y., E. Chaljub, J.P. Vilotte and J.P. Montagner, Coupling the spectral element method with a modal solution for elastic wave propagation in global Earth models, *Geophys. J. Int.*, 152, 34-66, 2003.
- Li, X.-D. and B. Romanowicz, Comparison of global waveform inversions with and without considering cross-branch modal coupling, *Geophys. J. Int.*, 121, 695-709, 1995.
- Romanowicz, B., Multiplet-multiplet coupling due to lateral heterogeneity: asymptotic effects on the amplitude and frequency of Earth's normal modes, *Geophys. J. R. Astr. Soc.*, 90, 75-100, 1987.
- Romanowicz, B., Y. Gung and Y. Capdeville, Long period seismograms in a 3D earth: tests of normal mode asymptotic approximations against computations using the Spectral Element Method, *in preparation*, 2004.
- Selby, N.D. and J.H. Woodhouse, The Q structure of the upper mantle: constraints from Rayleigh wave amplitudes, *J. Geophys. Res.*, 107, 933-940, 2002, doi:10.1029/2001JB000257, 2002.
- Woodhouse, J.H. and A.M. Dziewonski, Mapping the upper mantle: Three dimensional modeling of Earth's structure by inversion of seismic waveforms, *J. Geophys. Res.*, 89, 5,953-5,986, 1984.

20. Finite Boundary Perturbation Theory for the Elastic Equation of Motion

Nozomu Takeuchi

20.1 Introduction

The crust is the most heterogeneous region of the Earth, and accurate crustal correction (i.e., accurate computation of the perturbation of synthetic seismograms caused by the crustal heterogeneities) is critical for obtaining accurate mantle structure models. The heterogeneities are usually represented by the summation of (i) the perturbation of physical properties (such as density and elastic constants) in the internal regions and (ii) the perturbation of the location of the boundaries (such as Moho and the surface), and the principal difficulty is how to compute the effect of the latter perturbation.

The computational method applied to the actual waveform inversion studies for global 3-D Earth structure thus far has been either the modal summation method (e.g., *Li and Tanimoto, 1993*) or the Direct Solution Method (e.g., *Takeuchi et al., 2000*). Both methods solve the weak form equation of motion (or its equivalence) and use vector spherical harmonics as the laterally dependent part of the trial functions. For those global trial functions, severe limitations still exist in computing the perturbation of synthetic seismograms caused by the perturbation in the location of the boundaries, because previous solutions rely on the first order perturbation theory of the free oscillation (hereafter referred as 1DT; *Woodhouse, 1980*). Thus, this method breaks down for strongly heterogeneous medium or for higher frequencies.

In this study, we derive the exact weak form equation of motion for the medium with finite boundary perturbations. This method can be applied to arbitrary trial functions; that is, to both global and local trial functions. We can solve the derived equation of motion by either direct solution or higher order perturbation approximations, which allows highly accurate synthetic seismograms. Hereafter we refer this solution as the finite boundary perturbation theory or FPT.

20.2 Numerical Examples

We show that in the simulations of realistic problems, a breakdown can be observed in 1DT synthetic seismograms. We consider a plane of a great circle including the path shown by the solid line in Figure 12.38a, and simulate SH waves propagating on this plane.

We compute synthetic seismograms for the initial model (isotropic PREM) and the perturbed model (Figure 12.38b), and show the record sections in Figure 12.39. For the perturbed model, we compute by using FPT and 1DT, respectively. We apply a band pass filter with the

corner frequencies of 1/1000 and 1/50 Hz. In the record section for the initial model (Figure 12.39 left), as well as the body waves observed at the first motion part, we observe the Love waves traveling at a speed of about 4.4 km/s (aligning almost straight in the record section). Their waveforms are almost one wave packet and do not clearly show dispersion. On the other hand, in the record section computed for the perturbed model by using FPT (Figure 12.39 middle), we observe Love waves with clear dispersion. This is a well-known feature of Love waves traveling through a continent. However, in the record section computed for the perturbed model by using 1DT (Figure 12.39 right), we cannot clearly see dispersion, an indication that 1DT breaks down for this frequency range.

20.3 Discussion

In the numerical examples we showed that 1DT breaks down for surface waves with a period of 50 seconds in a realistic problem. In recent waveform inversion studies (e.g., *Mégnin and Romanowicz, 2000*; *Takeuchi and Kobayashi, 2004*), the body waves for this frequency range are used as a data set, but the surface waves for this frequency range are excluded. This is mainly due to the insufficient accuracy of 1DT for computing the effect of crustal heterogeneities. Our method can compute accurate synthetic seismograms for arbitrary frequency ranges, and should be better able to retrieve the information in the surface waves of higher frequencies.

20.4 Acknowledgements

This research was partly supported by grants from the Japanese Ministry of Education, Culture, Sports, Science, and Technology (No. 16740249).

20.5 References

- Bassin, C., G. Laske, and G. Masters, The current limits of resolution for surface wave tomography in North America, *EOS Trans. Amer. Geophys. Un.*, 81, F897, 2000.
- Li, X.D. and T. Tanimoto, Waveforms of long-period body waves in a slightly aspherical Earth model, *Geophys. J. Int.*, 112, 92-102, 1993.
- Mégnin, C. and B. Romanowicz, The three-dimensional shear velocity structure of the mantle from the inversion of body, surface and higher-mode waveforms, *Geophys. J. Int.*, 143, 709-728, 2000.

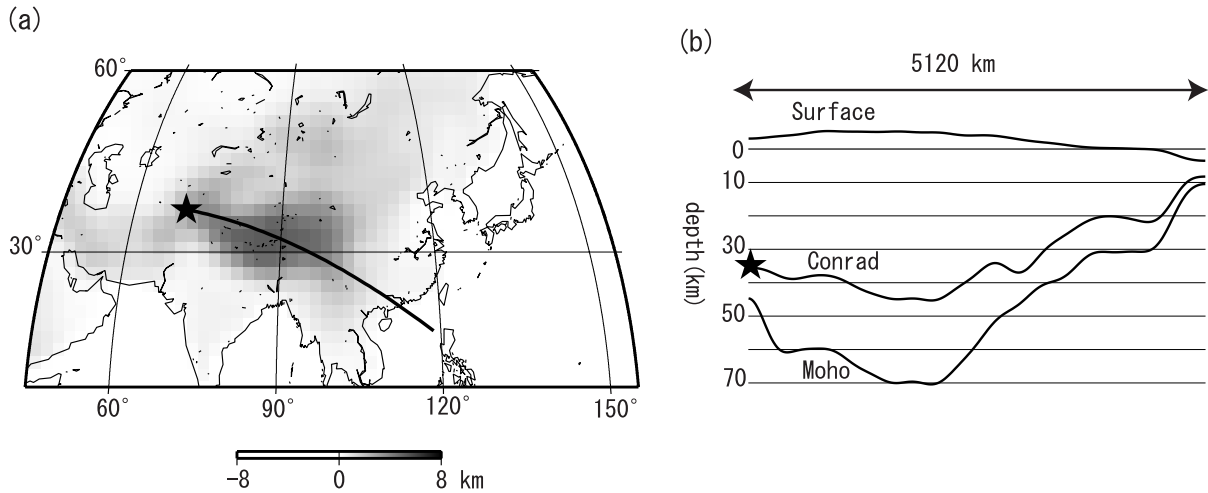


Figure 12.38: (a) The path on which the SH wave propagations are simulated (thick solid line). The star shows the location of the source. Surface (or bathymetry) topography of Crust 2.0 model (*Bassin et al.*, 2000) are overlapped by black-and-white color scale. (b) The crustal topography model used as the perturbed model in this simulation to represent the Crust 2.0 model on the thick solid line in Figure 12.38a. The star shows the location of the source used with this perturbed model.

Takeuchi, N., R.J. Geller and P.R. Cummins, Complete synthetic seismograms for 3-D heterogeneous Earth models computed using modified DSM operators and their applicability to inversion for Earth structure, *Phys. Earth and Plan. Int.*, 119, 25-36, 2000.

Takeuchi, N. and M. Kobayashi, Improvement of Seismological Earth Models by Using Data Weighting in Waveform Inversion, *Geophys. J. Int.*, 158, 681-694, 2004.

Woodhouse, J.H., The coupling and attenuation of nearly resonant multiplets in the Earth's free oscillation spectrum, *Geophys. J. R. Astr. Soc.*, 61, 261-283, 1980.

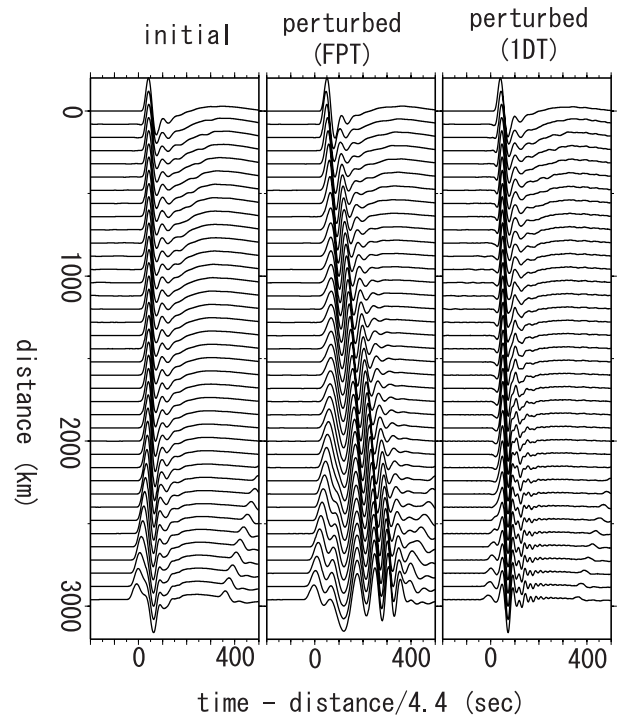


Figure 12.39: The record section computed for the initial model (left), for the perturbed model by using FPT (middle), and for the perturbed model by using 1DT (right). The vertical axis shows the distance from the epicenter, and the horizontal axis shows the reduced time by 4.4^{-1} s/km. The amplitude is normalized by the maximum amplitude of each trace.

21. Sharp lateral Boundaries in the D'' Region

Akiko To and Barbara Romanowicz

21.1 Introduction

Global shear velocity tomographic models show the existence of two superplumes lying in the lower mantle. The large-scale low velocity structures are observed under southern Africa and the mid-Pacific (*Romanowicz*, 2003). Recently, sharp lateral transitions in the velocity structure have been reported at the borders of the African superplume (*Ni et al.*, 2002) and Northeast side of the Pacific superplume (*Bréger and Romanowicz*, 1998). Here we report that a sharp lateral boundary also exists at the southern edge of the Pacific superplume. The set of SHdiff waveforms, which graze the South Pacific, have similar features to those observed at the southeastern edge of the African superplume. The arrival time shifts rapidly, with the emergence of multiple pulses, depending on the azimuth. The coupled mode/spectral element method (CSEM in what follow) (*Capdeville et al.*, 2003) is used to construct synthetic waveforms. We show the first order features of these waveforms from Africa and the South Pacific can be produced by a very simple structure model with strong, sharp lateral heterogeneity lying almost parallel to the ray paths.

21.2 Data and Modeling

Figure 12.40(a) shows the locations of the events and stations. Only deep earthquakes (depth > 450 km) are used. Figure 12.40(b) left panel shows the the SHdiff waveforms which graze southeastern edge of African anomaly (hereafter AFA) recorded at the Tanzanian array. They are also shown in other studies (*Wen*, 2001; *Ni and Helmberger*, 2004). Figure 12.40(b) right panel shows the SHdiff records of Fiji-Tonga events recorded at the station BDFB Brazil. They graze the Southern part of Pacific slow velocity anomaly region (hereafter PSA). These two sets of SHdiff waveform, are very similar in the following ways. First of all, the onset times of the first arrivals show large delay as the raypath enter the slow region that lies on the northern part. The first arrivals shift about 20 seconds and 12 seconds in the case of AFA and SPA respectively. Second, the waveforms, which graze the transition show an additional pulse indicated with red lines in Figure 12.40(b). This later phase is the feature we model in the following section. The travel time shift observed in PSA is due to a heterogeneity at the base of the mantle, because the differential travel times measurements of Sdiff-SKKS increase steeply for 8 seconds with respect to the back azimuth.

We used a coupled mode and spectral element method for the waveform modeling. The spectral element method

is most appropriate technique at present, because it can handle 1) the propagation of seismic waves in 3D models with strong lateral variations and in spherical geometry and 2) diffracted waves along the core mantle boundary. The drawback of the method is the large numerical cost. The CSEM is a hybrid method that couples spectral element computations with a normal mode solution, so that the spectral element method is used only in the target strongly heterogeneous regions, which is the bottom 370km of the mantle in this study. We compute the synthetic waveforms down to 12 seconds with a corner frequency at 18 seconds. The model has the 1D structure of PREM (*Dziewonski and Anderson*, 1981) down to a depth of 2591 km, and the 3D model below 2591km, down to the CMB. The model of the 3D part is shown in Figure 12.40(c). The boundaries are displaced 15 degrees from the great circle (shown by a yellow line) that goes through the source.

Figure 12.40(d) shows the synthetic waveforms constructed by CSEM. Each trace is normalized by its maximum amplitude. The source is located on the fast side in Figure 12.40(d) left panel and slow side in the right panel. Multiple pulses are observed in both cases. The possible explanation for each pulse is shown in the caption.

According to the tomographic models, the configurations of the raypaths and the interface of the observed cases are likely to be those of Figure 12.40(d) left panel. The synthetic waveforms capture the following features of the observations: 1) they consist of multiple pulses in the transition region 2) when moving from the fast to the slow region, the arrival of the first and last pulses become closer and finally merge for the stations located in the slow region. This features is observed more clearly in AFA case, but can only be suggested in PSA case.

The observed and synthetic waveforms are presented in different time scale and frequency ranges, to show the qualitative similarity between the waveforms. The time scale of the synthetics is much larger than that of the observed waveforms. However, this is because of the frequency limitation of the present SEM calculations, which is dictated by the computer power available to us. Calculations of the CSEM synthetics to higher frequencies would allow a better separation of these pulses for paths close to the vertical boundary, as seen in the observations. We also note that only a 3% velocity jump is sufficient to explain the observed time shift of 20 sec in AFA. A large contrast of 6% at the boundary is chosen in the models in order to observe each pulse clearly, since a smaller velocity contrast makes the amplitude of the second pulse

much smaller.

neath the Indian Ocean. *Earth Planet. Sci. Lett.*, **194**, pp.,2002

21.3 Discussion and Conclusion

When the wavepath in the D" is quasi-parallel to a sharp vertical boundary, the Sdiff waveforms are accompanied by secondary phases (red lines in Figure 12.40(b) and Figure 12.40(d)). The synthetic tests from the models of Figure 12.40(c) give only a qualitative constraint on the model, which is the existence of a sharp lateral boundary in the D" region. However, because SEM includes the 3D effects from strong heterogeneous structures, the order of magnitude of the effects to the waveforms is well captured with the simple model.

We show that sharp lateral boundaries, which rise almost like a vertical wall, exist not only in the border of the African plume but also under the south Pacific. This indicates that the low velocity region in the lower mantle under Pacific and Africa, observed as the strong degree-2 pattern in shear velocity tomographic models, have the similar nature also in the finer scales. Unlike the African superplume where the shape and the location of much of the boundaries are revealed, large uncertainty remains in the shape of the Pacific superplume.

21.4 Acknowledgements

We thank the National Science Foundation for support of this research.

21.5 References

Bréger L. and B. Romanowicz, Three-dimensional structure at the base of the mantle beneath the central Pacific. *Science*, **282**, pp. 718-720,1998.

Capdeville, Y., A. To and B. Romanowicz, Coupling spectral elements and modes in a spherical earth: an extension to the "sandwich" case, *Geophys. J. Int.*, **154**, 44-57, 2003

Dziewonski A.M. and D.L. Anderson, Preliminary reference Earth model. *Phys. Earth Planet. Inter.*, **25**, pp. 297-356,1981.

Mégnin C. and B. Romanowicz, The three-dimensional shear velocity structure of the mantle from the inversion of body, surface and higher-mode waveforms. *Geophys. J. Int.*, **143**, pp. 709-728,2000.

Ni S. and D. Helmberger, Seismic Modeling Constraints on the South African Superplume *draft* 2004

Ni S., E. Tan, M. Gurnis and D.V. Helmberger, Sharp sides to the African super plume. *Science* **296**, pp. 1850-1852,2002.

Romanowicz B, Global Mantle Tomography: Progress Status in the Past 10 Years *Annu. Rev. Earth Planet. Sci.*, **31** 303-328, 2003

Wen L., Seismic evidence for a rapidly varying compositional anomaly at the base of the Earth's mantle be-

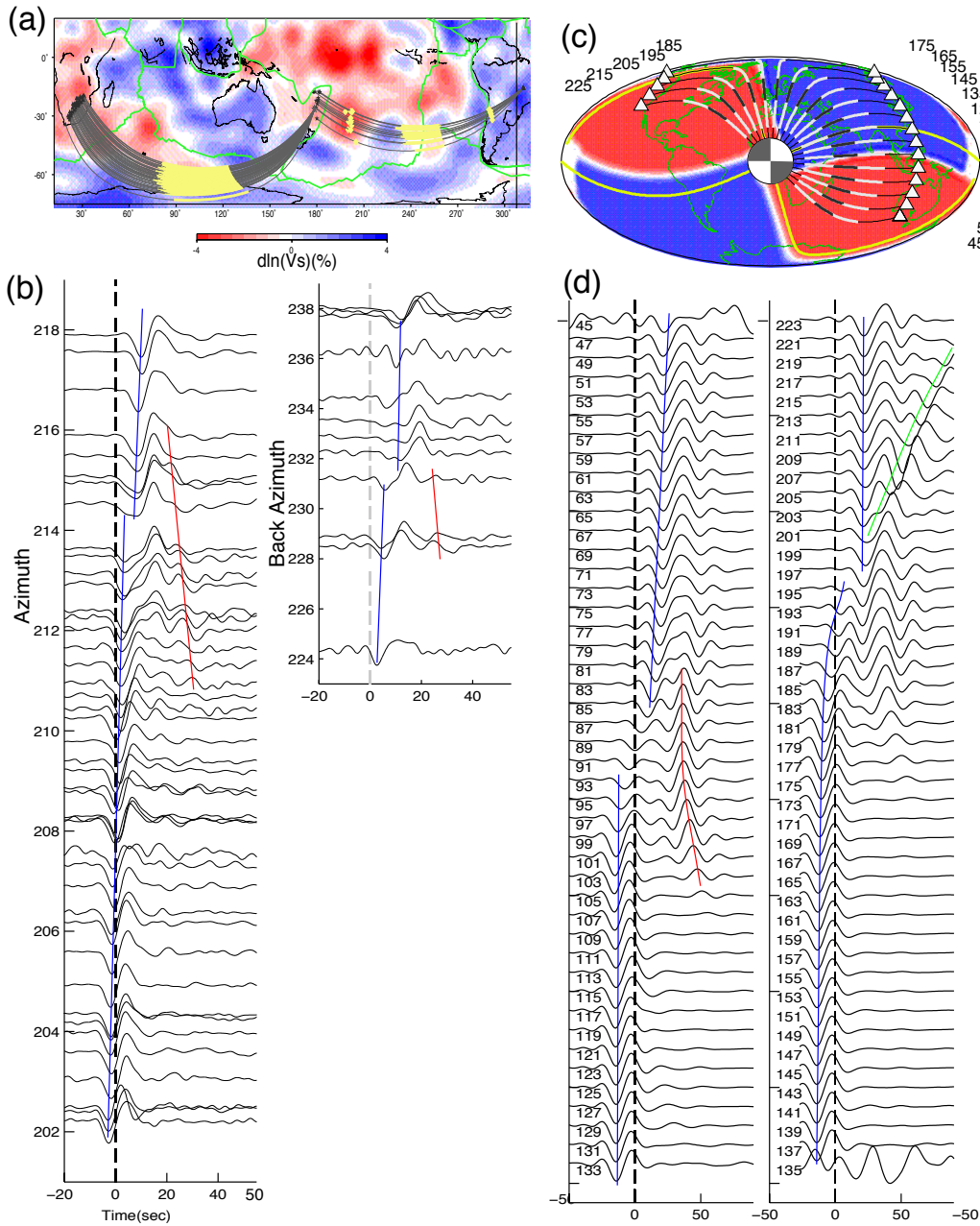


Figure 12.40: (a) Earthquakes (stars), stations (triangles), and projections of the raypaths. Background model is the shear velocity model SAW24b16 (*Mégnin and Romanowicz, 2000*) at the CMB. The thick yellow lines show the diffracting portion of the paths on the CMB. (b) Observed velocity waveforms. A bandpass filter with corner frequency at 0.01 to 0.125 (Hz) is applied. Left; Waveforms from the event 19970904 in Fiji-Tonga region recorded at South Africa. Right; Waveforms from 12 events in Fiji-Tonga region recorded at the station BDFB in Brazil. (c) The shear velocity model used in the CSEM synthetic waveform calculation. Each quadrant has either -3% or +3% constant anomaly with respect to PREM. (d) Synthetic waveforms calculated using CSEM for the model shown in (c). The numbers on the left side of each trace indicates the station number. Left; the source is located on the fast side of the interface. Right; the source is located on the slow side of the interface. The blue lines follow the trough of the first arrivals. When the source is located in the slow anomaly region (Right panel), large postcursors (green lines) are observed at the receivers located in the slow regions. They correspond to paths turning within the velocity gradient. They are observed at stations 221-203. When the source is located in the fast region (Left panel), a reflected wave is observed at the stations in the fast regions and refracted wave, which first enters the fast region and then enters the slow region by refraction, is observed at stations in slow regions. Both waves are shown by red lines. They are observed at stations 81-105.

22. Hemispherical Transition of Seismic Attenuation at the Top of the Earth’s Inner Core

Aimin Cao and Barbara Romanowicz

22.1 Introduction

The Earth’s inner core is formed by a freezing process of iron as the liquid outer core gradually cools (*Jacobs, 1953; Stacey, 1980*). Because the outer core material is not pure iron, some of the light elements are excluded from the inner core during this dynamic process, to power the geodynamo, while the residual is likely kept within a mushy layer at the top of the inner core (*Fearn et al., 1981*). Thus, constraining the characteristics of the mushy layer at the top of the inner core, as revealed by seismic velocity and attenuation measurements, should give us important insights into the dynamics of the Earth’s core.

The outer core Q_α is usually regarded as infinite ($\geq 10,000$) (*Cormier and Richards, 1976*), but the estimated Q_α in the inner core is constrained to be less than 450. This huge contrast indicates that a zone of decreasing Q_α with depth must exist beneath the ICB. However, this zone of decreasing Q_α should be confined to the top of the inner core, because multiple seismic observations confirm that Q_α increases with depth below a depth of approximately 100 km beneath the ICB (e.g., *Souriau and Roudil, 1995*). Therefore, the existence of a transition zone at the top of the inner core, where Q_α turns from decreasing to increasing with depth, seems likely.

In order to study the seismic structure at the top of the inner core, the most suitable body wave phases are PKIKP and PKiKP in the epicentral distance range from 120° to 144° (Figure 12.41). In this distance range, PKIKP samples the top 0-110 km of the inner core and PKiKP is reflected from ICB. The two phases have almost the same ray paths in the mantle and very close ray paths in the outer core. Hence the assumption that they experience almost the same heterogeneities in the mantle and outer core is valid in a first approximation. The differences in travel times and amplitudes can therefore be attributed to the vicinity of the ICB.

Unfortunately, these two phases present a great challenge. The separation of PKIKP and PKiKP is very small. For example, it is less than 1.3 seconds when the epicentral distance is less than 135° (when referred to the seismic reference model PREM (*Dziewonski and Anderson, 1981*)). On the other hand, the source time functions are usually longer than 3.0 seconds for events of $m_b \geq 5.5$ (*Cormier and Choy, 1986*). Interference between the two phases seems inevitable. We have developed a direct, but arguably effective, approach to circumvent the complex issue of event source time functions and directivities.

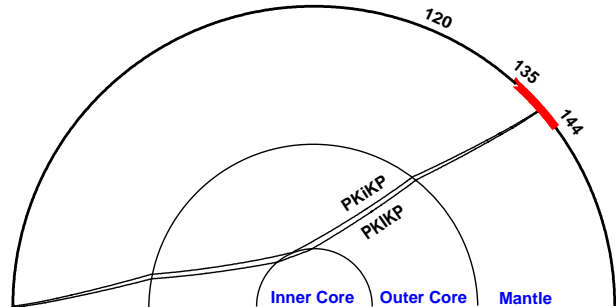


Figure 12.41: Ray paths of PKiKP (reflected P wave from the ICB) and PKIKP (P wave passing through the inner core). The two phases may appear simultaneously as early as 120° , but we can only obtain well-separated PKIKP and PKiKP phases in the epicentral distance range from 135° to 144° .

22.2 Data, Method, and Results

We systematically downloaded both broadband and short-period vertical component seismograms from IRIS DMC, GRF, GRSN, Jarray, and F-net seismic networks corresponding to recordings in the epicentral distance range of $134^\circ - 144^\circ$, for intermediate and deep earthquakes (focal depth >70 km, $M_w \geq 5.5$). These deeper events have shorter source time functions and higher signal-to-noise ratios than shallow events. To preprocess the seismograms, we employed a strictly narrow band-pass filter with corner frequencies of 0.7 and 2.0 Hz (corresponding to 1.5 and 0.5 seconds in period). The goal is to try to retrieve events whose 1.0 Hz energy was released in a short time and impulsively (within about 1.0 second), no matter how long their overall source time functions were. For this kind of events, we expect to observe pairs of well-separated PKIKP and PKiKP phases. In this paper, we directly measure amplitude ratios of PKIKP versus PKiKP in the time domain in order to estimate Q_α at the top of the inner core.

Our method requires to account for the phase shift of PKiKP with respect to PKIKP. Because PKiKP is a post-critically reflected wave at the ICB, the phase shift between PKiKP and PKIKP is approximately in the range of 142° to 163° (arguably close to 180°) in the epicentral distance range of our study. This means that if we reverse (that is multiplying the corresponding portion of the seismogram by -1) the PKiKP phase, the two phases should be very similar, as we verified using

synthetic seismograms.

After data preprocessing, our data-picking criteria are as follows: (1) the signal-to-noise ratio before the identified PKiKP is ~ 6 or more; (2) the signal-to-noise ratio within about one duration of the waveform after the identified PKiKP is ~ 3 or more; (3) the identified PKiKP and PKiKP phases are well-separated; (4) the reversed PKiKP waveform is similar to the PKiKP waveform. Following the above criteria, we successfully selected 280 pairs of high-quality PKiKP and PKiKP phases.

This large dataset of well-separated and similar PKiKP and reversed PKiKP waveforms provides us a unique opportunity to explore the seismic structure at the top of the inner core. In order to study the P-wave velocity structure, we first measure the differential travel time between PKiKP and PKiKP by means of cross-correlation, and then calculate the differential travel time residuals between PKiKP and PKiKP with respect to the reference seismic model PREM. In order to study the Q_α structure, we first measure the peak-to-peak amplitude ratios of PKiKP to PKiKP, and then estimate Q_α from these amplitude ratios after applying corrections for geometrical spreading, transmission, and reflection.

For differential travel time residuals, our results show a striking hemispherical pattern in the epicentral distance range 135° to 142° (corresponding to depths of approximately 32 to 85 km beneath the ICB) (Figure 12.42a), in agreement with the observations of *Niu and Wen* (2001) and *Garcia* (2002). Beyond 142° , the robust hemispherical pattern is not as clear.

For quality factor Q_α , our results also show a reliable hemispherical pattern almost in the same epicentral distance range (135° - 141.5°) (Figure 12.42b). In the western hemisphere Q_α decreases as a function of distance. In the eastern hemisphere, Q_α increases as a function of distance. Beyond an epicentral distance of 141.5° , the hemispherical pattern in Q_α disappears, as does that in the differential travel time residuals.

The P velocity and Q_α variations are compatible with an interpretation in terms of small hemispherical variations of temperature at the top of the inner core (*Sumita and Olson*, 1999) and their influence on the morphology of porosity and connectivity of liquid inclusions in the mushy zone. The disappearance of the differences in Q_α beneath 85 km provide constraints on the likely depth extent of the mushy zone.

22.3 Acknowledgements

We thank the following networks and data centers for providing the high quality data used in this study: IRIS-DMC, GRF, GRSN, J-array, and Fnet.

22.4 References

Cormier, F., Choy, G.L., A search for lateral heterogeneity in the inner core from differential travel times

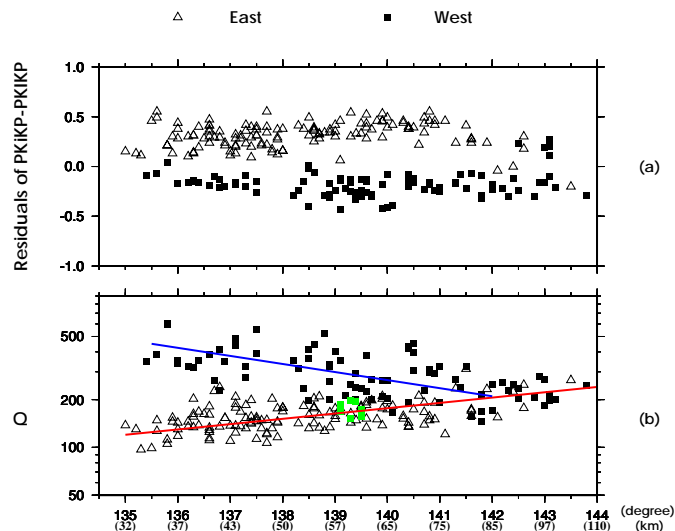


Figure 12.42: (a) Differential travel time residuals (referring to PREM). (b) Q_α with respect to the epicentral distance and depth beneath the ICB. High-lighted green squares show the data sampling offshore northwest of Africa. The event epicentral distances were all calibrated with a reference focal depth 100 km.

near PKP-D and PKP-C, *Geophys. Res. Lett.*, 13, 1553-1556, 1986.

Cormier, V.F., Richards, P.G., Comments on 'The damping of the core waves' by Antony Qammar and Alfredo Eisenberg, *J. geophys. Res.*, 981, 3066-3068, 1976.

Dziewonski, A.M., Anderson, D.L., Preliminary reference Earth model, *Phys. Earth Planet. Inter.*, 25, 297-356, 1981.

Fearn, D.R., Loper, D.E., Roberts, P.H., Structure of the Earth's inner core, *Nature*, 292, 232-233, 1981.

Jacobs, J.A., The earth's inner core, *Nature* 172, 297, 1953.

Garcia, R., Constraints on upper inner-core structure from waveform inversion of core phases, *Geophys. J. Int.*, 150, 651-664, 2002.

Niu, F., Wen, L., Hemispherical variations in seismic velocity at the top of the Earth's inner core, *Nature*, 410, 1081-1084, 2001.

Souriau, A., Roudil, P., Attenuation in the uppermost inner core from broad-band GEOSCOPE PKP data, *Geophys. J. Int.*, 123, 572-587, 1995.

Stacey, F.D., The cooling earth: A reappraisal, *Phys. Earth Planet. Inter.*, 22, 89-96, 1980.

Sumita, I., Olson, P., A laboratory model for convection in Earth's core driven by a thermally heterogeneous mantle, *Science*, 286, 1547-1549, 1999.

Chapter 13

Appendices

